Prostanoid-mediated Inhibition of IL-6 *Trans*-Signalling in Pulmonary Arterial Hypertension: a Role for Suppressor of Cytokine Signalling 3?

Gillian Anne DURHAM

Submitted for the Degree of

Doctor of Philosophy

School of Pharmacy and Medical Sciences

Faculty of Life Sciences

University of Bradford

2019

I. Abstract

Gillian Anne Durham

Prostanoid-mediated Inhibition of IL-6 *Trans*-Signalling in Pulmonary Arterial Hypertension: a Role for EPAC1 Mediated Induction of Suppressor of Cytokine Signalling 3?

Keywords: Pulmonary arterial hypertension, SOCS3, IL-6, JAK/STAT signalling, endothelial cells.

Pulmonary arterial hypertension (PAH) is a rare, devastating disease with no cure. Current treatment consists of a cocktail of vasodilators which relieve symptoms of PAH but do not treat the cause. Thus, there is a need for novel drugs that target the underlying pathological causes of PAH.

PAH is a multi-factorial, but one key contributor is the pro-inflammatory cytokine IL-6 which stimulates pro-inflammatory and pro-angiogenic signalling mediated by the JAK/STAT pathway. One way in which IL-6 signalling via JAK/STAT is inhibited is via SOCS3 in a type of negative feedback loop whereby IL-6 induces transcription of SOCS3, which then attenuates further JAK/STAT signalling.

SOCS3 can also be induced by cAMP. This is interesting as prostanoids, a type of drug used in the treatment of PAH due to its vasodilator effects and the only type to show any efficacy improving the life expectancy of PAH patients, acts by mobilising cAMP. Thus, prostanoid stimulation of cAMP could potentially limit IL-6 signalling via the induction of SOCS3. This is a novel mechanism of prostanoids which has not previously been considered.

This study investigated the capability of prostanoids to limit the pro-inflammatory/pro-angiogenic effects of IL-6 that enable PAH to develop. Initial experiments confirmed that vascular endothelial cells responded to prostanoids which increased SOCS3 and limited IL-6 signalling activity. Further experiments utilising SOCS3 KO endothelial cell models demonstrated prostanoid inhibition of IL-6 signalling was due in part to SOCS3.

In conclusion, this project has confirmed that prostanoids do limit the pro-inflammatory effects induced by IL-6 and that this is in part due to SOCS3. Although the exact mechanism is yet to be discovered, it will be beneficial in the treatment of PAH as it provides currently unexploited drug targets which can be considered for future PAH therapies.

II. Acknowledgement

I would like to thank Prof. Tim Palmer for his supervision, expertise and support throughout my PhD, Dr Jamie Williams for his support in the technical aspects of my experiments and my other supervisors, Dr Talat Nasim and Dr Jacobo Ellies-Gomez, for their help and feedback throughout my studies. I would like to give a special mention to other staff members within the School of Pharmacy and Medical Sciences, particularly within the PET research group, the academic skills department and those from the School of Chemistry and Biosciences who have offered support and advice in moments of need.

Also, a special acknowledgement and thanks to the BHF for funding the project.

III. Authors Declaration

I hereby declare that this thesis which follows is my own, original composition and that all work has been performed by me unless otherwise acknowledged. Furthermore, none of this work has been previously presented as part of an application for a higher degree.

Gillian A. Durham

June 2019

IV. **Contents**

V. Figures

VI. Tables

VII. Abbreviations

Please find non-standard abbreviation detailed below. Standard abbreviations, as defined by the Journal of Biological Chemistry (2017), have not been included.

5-HT	5-Hydroxytryptamine (serotonin)
6-Bnz	N^6-Benzoyladenosine-3',5'-cyclic monophosphate sodium salt
6-MWD	6 minute walk distance
6-MWT	6 minute walk test
8-CPT	8-(4-chlorophenylthio)-2′-O-methyladenosine-3′,5′-cyclic monophosphate sodium salt
8-pCPT	8-(4-chlorophenylthio)-2'-O-methyladenosine-3',5'-cyclic monophosphate acetoxymethyl ester
αSMA	α smooth muscle actin
AC	Adenylyl cyclase
ACT-333679	[4-((5,6-diphenylpyrazin-2-yl)(propan-2-yl)amino)butoxy] acetic acid
ADAM	A disintegrin and metalloprotease
AKAP	A-kinase anchoring protein
ALK	Activin receptor-like kinase
ANA	Anti-nuclear antibody

APS	Ammonium persulphate
APVT	Acute pulmonary vasoreactivity test
AS-M.5	Angiosarcoma derived endothelial cell line
BAEC	Bovine aortic endothelial cells
BCA	Bicinchoninic acid
Bcl	B-cell lymphoma
BLMVECs	Bovine lung microvascular endothelial cells
BMP	Bone morphogenetic protein
BMPR2	Bone morphogenetic protein receptor type II gene (human)
Bmpr2	Bone morphogenetic protein receptor type II gene (murine)
BMPR-II	Bone morphogenetic protein receptor type II protein
BNP	Brain natriuretic peptide
BPAEC	Bovine pulmonary arterial endothelial celld
BPS	Beraprost sodium salt
BRD4	Bromodomain protein 4
BrdU	Bromodeoxyuridine / 5-bromo-2'-deoxyuridine
bw	Body weight
CAV-1	Caveolin-1 protein
CAV-1	Caveolin-1 gene (human)
CCL2	C-C Motif Chemokine Ligand 2

C/EBP	CCAAT/enhancer binding protein
CHD	Coronary heart disease
CIS	Cytokine-inducible SH2 domain protein
CMRI	Cardiac magnetic resonance imaging
COMPERA	Comparative, Prospective Registry of Newly Initiated Therapies for Pulmonary Hypertension
CNB	cAMP-nucleotide binding domain
Co-SMAD	Common-SMAD
COX	Cyclooxygenase
CREB	CRE-binding protein
CTCF	Corrected total cell fluorescence
CTD	Connective tissue disease
CX3CRI	CX3 chemokine receptor 1
DEP	Dishevelled/EgI-10/pleckstrin
DP	Prostaglandin D_2 receptor
DMEM	Dulbecco's Modified Eagle Medium
DUSP 10	Dual specificity protein phosphatase 10
EBM-2	Endothelial basal medium
EC	Endothelial cell
ECE-1	Endothelin converting enzyme 1

ECG	Electrocardiogram
ECM	Extracellular matrix
EGF	Epidermal growth factor
eGFR	Estimated glomerular filtration rate
EGM-2	Endothelial cell growth medium-2
EMT	Endothelial to mesenchymal transition
ENG	Endoglin
eng	Endodlin gene (murine)
eNOS	Endothelial nitric oxide synthesis
EP	Prostaglandin E_2 receptor
EPAC	Exchange protein directly activated by cAMP
EPO	Erythropoietin
ERA	Endothelin receptor antagonist
ERK	Extracellular signal-regulated kinase
FBS	Foetal bovine serum
FERM	4.1, ezrin, radixin and moesin
FKBP12	FK506-binding protein 12
FOXM1	Forkhead box M1
FPAH	Familial pulmonary arterial hypertension
Fsk	Forskolin

FP	Prostaglandin F receptor
GAPDH	Glyceraldehyde-3-phosphate dehydrogenase
GF	Growth factor
GPCR	G-protein-coupled receptor
Grb2	Growth factor receptor-bound protein 2
HBSS	Hanks' Balanced Salt Solution
HEK	Human embryonic kidney
HIF	Hypoxia-inducible factor
HPAH	Hereditary pulmonary arterial hypertension
HPAEC	Human pulmonary arterial endothelial cell
HPMEC	Human pulmonary microvascular endothelial cell
HPASMC	Human pulmonary arterial smooth muscle cell
HRP	Horseradish peroxidase
HSVEC	Human saphenous vein endothelial cell
HUVEC	Human umbilical vein endothelial cell
I942	N-(2,4-dimethylbenzenesulfonyl)-2-(naphthalen-2-yloxy)acetamide
ICAM1	Intercellular adhesion molecule
Id-1	DNA-binding protein inhibitor
IFN	Interferon

IL	Interleukin
IL-1R1	Interleukin-1 receptor 1
IL-13Rα	Interleukin-13 receptor α
IL-6Rα	Interleukin-6 receptor α
IL-6/sIL-6Rα	IL-6 (5 ng/ml) and sIL-6Rα (25 ng/ml)
IP	Prostaglandin I_2 receptor
IPAH	Idiopathic pulmonary arterial hypertension
I-SMAD	Inhibitory SMAD
JAK	Janus kinase
KCNK3	Potassium channel subfamily K member 3
KIR	Kinase inhibitory region
LB	Luria Bertani
L-NAME	NG-nitro-L-arginine methyl ester
LPS	Lipopolysaccharide
MAPK	Mitogen-activated protein kinase
mbIL-6Rα	Membrane-bound IL-6 receptor-α
Mcl-1	Induced myeloid leukemia cell differentiation protein
MCT	Monocrotaline
MEF	Mouse embryonic fibroblast
miRNA	Micro-RNA

MH	Mad homology
mPAP	Mean pulmonary arterial pressure
NF-κB	Nuclear factor – kappa B
NICD	Notch intracellular domain
NTproBNP	N-terminal proBNP
NYHA	New York Heart Association
PI3K	Phosphoinositide 3-kinase
p27/^{KIP1}	Cyclin-dependent kinase inhibitor 1B
PA	Pulmonary arterial
PAH	Pulmonary arterial hypertension
PAEC	Pulmonary arterial endothelial cell
PASMC	Pulmonary arterial smooth muscle cell
PAOP	Pulmonary artery occlusion pressure
PASP	Pulmonary artery systemic pressure
PCNA	Proliferating cell nuclear antigen
PCWP	Pulmonary capillary wedge pressure
PDGF	Platelet-derived growth factor
PDGFR	Platelet derived growth factor receptor
PDE-5	Phosphodiesterase-5
PEC	Pulmonary endothelial cell

PEST	Proline (P), glutamic acid (E), serine (S), and threonine (T)
PGE2	Prostaglandin E_2
PGH2	Hydroxyl endoperoxide
PGI_2	Prostacyclin
PGI_2S	Prostacyclin synthase
PH	Pulmonary hypertension
PIAS	Protein inhibitor of activated STAT
PKA	Protein kinase A (cAMP-dependent protein kinase)
PKI	PKI 14-22 amide, myristoylated (PKA inhibitor)
PKG	Protein kinase G (cGMP-dependent protein kinase)
PPH	Primary pulmonary hypertension
P-STAT3	Tyrosine 705 phosphorylated signal transducer and activator of transcription 3
PTP	Protein tyrosine phosphatase
PVR	Pulmonary vascular resistance
QOL	Quality of life
qPCR	Quantitative PCR
RANTES	Regulated on activation, normal T cell expressed and secreted
REVEAL	Registry to Evaluate Early and Long-term PAH Disease Management

RHC	Right heart catheterisation
R-SMAD	Receptor-regulated SMAD
RA	Ras association
REM	Ras-exchange motif
R-smad	Receptor-smad
RV	Right ventricle
RVH	Right ventricle hypertrophy
RVSP	Right ventricle systolic pressure
sGC	Soluble guanylyl cyclase
SF-36	Short form health surveys
SFK	Src family kinase
sFlT1	Soluble fms-like tyrosine kinase-1
SH2	Src homology 2
SHP2	Src homology 2-containing protein tyrosine phosphatase 2
sIL-6Rα	Soluble interleukin-6 receptor α
SMC	Smooth muscle cell
SOCS	Suppressor of cytokine signalling
SUMO	Small ubiquitin-like modifier
SPECT	Single proton emission computed tomography
SSc	Systemic sclerosis

ST2	Streptozotocin
STAT	Signal transducer and activator of transcription
Su5416	Sugen 5416 (2-undecyl-thiazolidine-4-carboxylic acid)
Su/Hx	Sugen 5416 injection plus hypoxia animal model of PAH
T1R	Type I receptor
T2R	Type II receptor
TALEN	Transcription activator-like effector nucleases
TBS	Tris-buffered saline pH 7.6
TBST	TBS containing 0.1% (v/v) Tween 20
TBST-M	5% (w/v) non-fat milk powder in TBST
TEER	Trans-endothelial electrical resistance
TEMED	N,N,N',N' tetramethylethylenediamine
TGF-β	Transforming growth factor-β
TNF-α	Tumour necrosis factor-α
TREP	Treprostinil
TRCP	Transient receptor potential channel
TUB	Tubulin
TUNEL	Terminal deoxynucleotidyl transferase (TdT) dUTP nick-end labeling
VASP	Vasodilator-stimulated phosphoprotein

VCAM-1	Vascular cell adhesion molecule-1
VEC	Vascular endothelial cell
VEGF	Vascular endothelial growth factor
VEGFR	Vascular endothelial growth factor receptor
VSMC	Vascular smooth muscle cell
YAP	Yes-associated protein

1. Introduction

1.1 Pulmonary Arterial Hypertension

Pulmonary arterial hypertension (PAH) is a rare progressive disorder characterised by a remodelling of the small to medium sized (5 to 100 μm in diameter (Pappano and Gil Wier 2013)) pulmonary arterioles in the lungs resulting in increased pulmonary vascular resistance (PVR) and mean pulmonary artery pressure (mPAP). This causes sheer stress on the right ventricle (RV) of the heart which initially responds via maladaptive hypertrophy through upregulating protein synthesis and cardiomyocyte size (reviewed by Ryan and Archer 2014). However, this hypertrophy is not sustainable and eventually leads to dilation of the RV reducing its contractility. This results in a longer contraction time and reduced RV stroke volume. The RV and left ventricle (LV) become unsynchronized causing under filling of the LV and the reduced cardiac output characteristic of PAH (Voelkel et al. 2006; Marcus et al. 2008). RV function has been suggested as the most important predictive factor regarding PAH prognosis and RV failure is the common cause of death in PAH (Tonelli et al. 2013; reviewed by Ryan and Archer 2014).

The pulmonary hypertension (PH) registry of the UK and Ireland published an estimated PAH prevalence of 6.6/million and an incidence of 1.1/million in 2009, with survival rates of 92.7%, 73.3%, and 61.1% for 1-, 3-, and 5-years respectively (Ling et al. 2012). A number of registries have published data regarding PAH epidemiology in the last 10 years (Table 1.1), which highlights

Place	Time Period	Age of diagnosis (years±SD)	Female: male ratio (%)	1 year survival (%)
Czech (Jansa et al. 2014)	2000-2007	52±17	65:35	89
US (REVEAL) (Benza et al. 2010)	2006-2009	50±15	80:20	91
UK and Ireland (Ling et al. 2012)	2001-2009	50±17	70:30	93
China (Jiang et al. 2012)	2008-2011	38±13	70:30	92
Europe (COMPERA) (Hoeper et al. 2013c)	2007-2011	65±15	60:40	92
Germany (Gall et al. 2017)	1993-2011	51±16	65:35	88
Japan (Ogawa et al. 2017)	1992-2012	33.3±14.4	74:26	98
Spain (Quezada Loaiza et al. 2017)	1984-2014	44±14	67:33	92
Australia/New Zealand (Strange et al. 2018)	2012-2016	57±19	70:30	96

Table 1.1: **A summary of findings from registries published in the past 10 years**

REVEAL: Registry to Evaluate Early and Long-term PAH Disease Management; PH: pulmonary hypertension; COMPERA: Comparative, Prospective Registry of Newly Initiated Therapies for Pulmonary Hypertension. Adapted from Hoeper and Simon (2014).

diagnosis generally occurs during middle age at approximately 50 years of age, earlier in Eastern Asian cultures, with females being more susceptible to the disorder than males, and 1-year survival rates of 88% – 96%. Average 5-year survival rates are 65.4% (Farber et al. 2015), which is much improved compared to over 30 years ago with 1-year, 3-year and 5-year survival rates in 1981 - 1988 published as 68%, 48% and 34% respectively (D'Alonzo et al. 1991), however there has been little improvement in the past 20 years.

1.1.1 Classification of PAH

PAH is currently classified according to two systems; the New York Heart Association (NYHA) functional class classification, used to classify the severity of PAH, and the Dana Point clinical classification which categorises PH according to similar pathologies.

DANA POINT Clinical Classification

The Dana Point clinical classification identifies five categories of PH according to pathological findings, haemodynamic characteristics and appropriate management; (1) PAH, (2) pulmonary heart disease due to left heart disease, (3) PH due to chronic lung disease and/or hypoxia, (4) chronic thromboembolic PH, and (5) PH due to unclear multifactorial mechanisms. PAH, and relevant sub-categories, are category group 1 (Table 1.2). The prevalence of different PAH subgroups are not equal with idiopathic PAH (IPAH) identified as the most common form, followed by connective tissue disease (CTD)–associated PAH (Hoeper et al. 2017; Strange et al. 2018). HIV-associated PAH and familial (f)PAH are the least common forms of PAH (Benza et al. 2010; Quezada Loaiza et al. 2017).

Sub-Categories of Dana Point Group 1 Classification for Pulmonary Hypertension	
1	**Pulmonary arterial hypertension**
1.1	Idiopathic PAH
1.2	Hereditable PAH
1.2.1	BMPR-II
1.2.2	ALK-1,ENG,SMAD9,CAV1,KCNK3
1.2.3	Unknown
1.3	Drug and toxin Induced
1.4	Associated with;
1.4.1	Connective tissue disease
1.4.2	HIV infection
1.4.3	Portal hypertension
1.4.4	Congenital heart disease
1.4.5	Schistosomiasis
1’	Pulmonary veno-occlusive disease and/or pulmonary capillary hemangiomatosis
1’’	Persistent pulmonary hypertension of the new-born (PPHN)

Table 1.2: DANA POINT subgroups of PAH

The subcategories of group 1 PH, PAH, according to the updated DANA POINT clinical classifications. ALK-1; activin receptor-like kinase 1, BMPR-II; bone morphogenetic protein receptor type II protein, CAV1; caveolin 1, ENG, Endoglin, KCNK3; potassium channel subfamily K member 3. Adapted from Simonneau et al. (2013).

NYHA Functional Class Classification

Also known as the World Health Organisation (WHO) system, this categorises PAH into four functional severity classes based on a patient's ability to perform physical activity (Table 1.3). These classifications are used clinically to predict prognosis, monitor disease progression and identify the most effective course of treatment (Galie et al. 2015).

1.2 Diagnosis and Monitoring Progression of PAH

1.2.1 Diagnosis

Survival analysis has shown that early detection of PAH results in a better prognosis and long term outcome (Humbert et al. 2010). Due to a number of challenges associated with PAH diagnosis, early diagnosis is not always achievable, with an average delay of 27 months between the patient presenting with symptoms and diagnosis reported in a French national registry (Humbert et al. 2006) and no improvement reported over the following 15 years (Frost et al. 2019). Unfortunately, in this time PAH has often progressed and prognosis worsens. A diagnostic algorithm devised by Galie et al. (2009b), summarising the different stages involved in the diagnosis of PAH (Figure 1.1), demonstrates the complexity involved. Initial PAH symptoms (fatigue, shortness of breath, angina) are non-specific and often confused with more common disorders such as asthma and coronary heart disease (CHD), therefore these must be eliminated first. The patient's history is then explored and a physical examination carried out, followed by a number of additional tests, such as a chest X-ray and electrocardiogram (ECG) to identify any

NYHA/WHO functional classifications of PAH.	
Class I	Patients with pulmonary hypertension without limitation of physical activity. Ordinary physical activity does not cause dyspnea, fatigue, chest pain, or near syncope
Class II	Patients with pulmonary hypertension with slight limitation of physical activity.
Class III	Patients with pulmonary hypertension with marked limitation of physical activity.
Class IV	Patients with pulmonary hypertension with inability to perform any physical activity without symptoms. These patients manifest signs of right-heart failure. Dyspnea and/or fatigue are present at rest.

Table 1.3: NYHA/WHO functional classifications of PAH

NYHA/WHO functional classifications of PAH increasing in severity from Class I to Class IV. NYHA; New York Heart Association, WHO; World Health Organisation. Adapted from Patel et al. (2012).

abnormalities or alterations within the heart, lungs or circulation (Galie et al. 2015). For absolute confirmation of PAH, a right heart catheterisation (RHC) is required to measure the mPAP and pulmonary capillary wedge pressure (PCWP), also referred to as the pulmonary artery occlusion pressure (PAOP). PAH is defined by mPAP of greater than or equal to 25 mmHg and PCWP of less than or equal to 15 mmHg (Galie et al. 2015). PVR values used to be considered for the diagnosis of PAH but were excluded to ensure a simpler diagnosis (Badesch et al. 2009; Hoeper et al. 2013b).

Current biomarkers for PAH are not very successful in terms of accuracy or predictive value as they are not specific to PAH. Currently, only brain natriuretic peptide (BNP), a biomarker for right ventricular dysfunction, and N-terminal (NT)proBNP are approved for clinical use (Andreassen et al. 2006; Mauritz et al. 2011; Takatsuki et al. 2012). As they are increased only in late stages of disease, they are not informative with regards to early stages of PAH. In addition, BNP and NTproBNP are both reduced in obesity (McCord et al. 2004; Fox et al. 2013), which would undermine any prognostic or diagnostic value of these biomarkers in obese PAH patients. Thus, there is an apparent need for novel biomarkers such as the anti-apoptotic B-cell lymphoma (Bcl)-xL (Chowdhury et al. 2019), or anti-nuclear antibodies (ANAs) which have been advised to differentiate CTD- and HIV-associated PAH from IPAH (Pagan et al. 2014). Currently, neither of these have been adopted in the clinic. Similarly, increased plasma concentrations of the pro-inflammatory cytokine tumour necrosis factor (TNF)-α have been suggested as a way to differentiate PAH from other types of PH (Saleby et al. 2017), but this is yet to be incorporated into the diagnosis process.

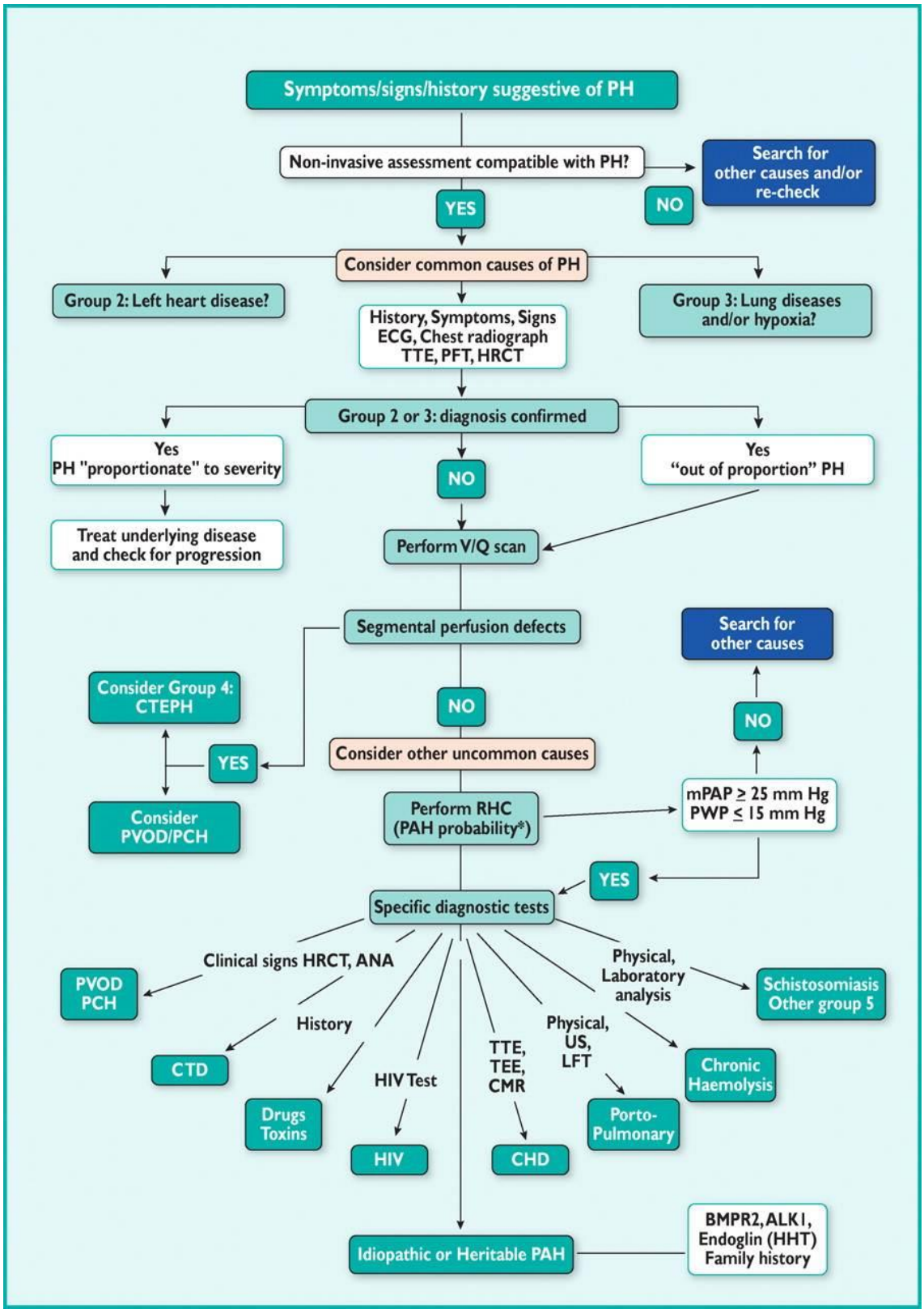
Symptoms/signs/history suggestive of PH
Non-invasive assessment compatible with PH?
Search for other causes and/or re-check
NO
YES
Consider common causes of PH
Group 2: Left heart disease?
History, Symptoms, Signs
ECG, Chest radiograph
TTE, PFT, HRCT
Group 3: Lung diseases and/or hypoxia?
Group 2 or 3: diagnosis confirmed
Yes
PH "proportionate" to severity
Treat underlying disease and check for progression
NO
Yes
"out of proportion" PH
Perform V/Q scan
Segmental perfusion defects
Search for other causes
Consider Group 4: CTEPH
NO
YES
Consider other uncommon causes
NO
Consider PVOD/PCH
Perform RHC (PAH probability*)
mPAP ≥ 25 mm Hg
PWP ≤ 15 mm Hg
YES
Specific diagnostic tests
Clinical signs HRCT, ANA
PVOD PCH
History
CTD
Drugs Toxins
HIV Test
HIV
TTE, TEE, CMR
CHD
Physical, US, LFT
Porto-Pulmonary
Physical, Laboratory analysis
Schistosomiasis Other group 5
Chronic Haemolysis
Idiopathic or Heritable PAH
BMPR2, ALK1, Endoglin (HHT) Family history

Figure 1.1: Diagnostic algorithm for the diagnosis of pulmonary arterial hypertension

ALK-1; activin-receptor-like kinase 1, ANA; anti-nuclear antibodies, BMPR2; bone morphogenetic protein receptor 2, CHD; congenital heart disease, CMR; cardiac magnetic resonance, CTD; connective tissue disease, Group; clinical group, HHT; hereditary haemorrhagic telangiectasia, HIV; human immunodeficiency virus, HRCT; high-resolution computed tomography, LFT; liver function tests, mPAP; mean pulmonary arterial pressure, PAH; pulmonary arterial hypertension, PCH; pulmonary capillary haemangiomatosis, PFT; pulmonary function test, PH; pulmonary hypertension, PVOD; pulmonary veno-occlusive disease, PWP; pulmonary wedge pressure, RHC; right heart catheterization, TEE; transoesophageal echocardiography; TTE; transthoracic echocardiography, US; ultrasonography, V/Q scan; ventilation/perfusion lung scan. Taken from Galie et al. (2009b).

1.2.3 Monitoring PAH Progression and Patient Prognosis

It is important to be able to monitor PAH and assess a patient's response to therapy. Although RHC would be ideal with regards to the accuracy and reliability of the results, its invasiveness means it is often not practical and other clinical markers and non-invasive measures must be utilised instead.

The 6 minute walk test (MWT) is one way in which this can be done. A healthy 6 minute walk distance (MWD) is 600 - 700metres. Less than 350 metres would be considered a poor outcome and less than 165 metres would be associated with somebody with extreme physical limitations (Miyamoto et al. 2000). Research has found that improving the 6MWD by just 33 metres correlates with a better quality of life (QOL) (Mathai et al. 2012). Further to this, calculating the heart rate recovery by measuring the heart rate of the patient immediately after the 6MWD test and then one minute after enables a better assessment of patient's response to therapy and prognosis than just completing the 6MWT alone (Minai et al. 2012). The 6MWT is easy to perform, reproducible and, due to minimum special training or equipment required, it is inexpensive. Therefore, it is often used in clinical trials as a method to measure response to therapy. This is limited as 6MWD results alone are not sufficient to predict long-term disease progression (Gaine and Simonneau 2013; reviewed by Demir and Kucukoglu 2015). However, the 6MWT is considered useful in assessing and managing PAH when used alongside other tests such as measuring RV function (van Wolferen et al. 2007; Gaine and Simonneau 2013; reviewed by Demir and Kucukoglu 2015).

ECGs allow for non-invasive assessment of the RV structure and function including estimation of RV performance index, RV systolic pressure (RVSP),

and right atrial pressure (reviewed by Bossone et al. 2013). However, there are limitations with ECG. Haemodynamic measurements such as PA systolic pressure (PASP) are often underestimated when determined this way, therefore resulting in possible misclassification of the severity of PAH (Fisher et al. 2009). Thus, although useful in assessing RV function, ECG alone should not be used to monitor the disease, nor should it be considered as a replacement for RHC in definitive RV assessment.

Cardiac magnetic resonance imaging (CMRI) is an alternative non-invasive method currently used to evaluate changes in RV function and morphology in PAH patients (Peacock et al. 2014). Although CMRI provides detailed anatomic, functional and haemodynamic information that is considered to be more accurate and reproducible than measurements taken via echocardiograms (Bottini et al. 1995), it is still advised that both methods are used in a complementary manner (Crowe et al. 2018). Novel imaging methods such as V/Q single proton emission computed tomography (SPECT) have also been used to identify global perfusion defects, which correlated with increased mPAP in PAH patients (Chan et al. 2018).

Novel methods for monitoring PAH development and prognosis indicators have been explored. Numerous angiogenic and inflammatory biomarkers have been suggested as potential tools to assess PAH severity. Soluble fms-like tyrosine kinase-1 (sFlT1), also known as soluble vascular endothelial growth factor (VEGF) receptor (VEGFR)1, is an angiogenesis inhibitor found to be elevated in PAH in parallel with VEGF-A (Saleby et al. 2017). Increased levels of sFlT1 were found to correlate with reduced hemodynamic performance and thus, increased PAH severity (Saleby et al. 2017).

Pulmonary vasoreactivity, measured via an acute pulmonary vasoreactivity test (APVT), has been suggested as an accurate predictor of clinical deterioration, measured via NYHA functional class and the 6MWD (Hernandez-Oropeza et al. 2018). Those with improved AVPT experienced clinical deterioration nearly two years later than those with no improvement in pulmonary vasoreactivity (Hernandez-Oropeza et al. 2018). This study only recruited CTD-PAH patients from one tertiary care unit producing a relatively small, biased sample. However, this still offers a potential non-invasive method to measure response to therapy and clinical prognosis in PAH patients.

Renal dysfunction has also been associated with poor-survival in PAH patients (reviewed by Nickel et al. 2017), prompting research into potential biomarkers of PAH that reflect that reflect renal function. A 10% decline in estimated glomerular filtration rate (eGFR) over a year period predicted poor survival in PAH patients independently of 6MWD in over 2000 PAH patients with chronic kidney disease (Chakinala et al. 2018). eGFR is calculated using serum creatinine levels measured via a blood test. Thus, this is a potential non-invasive, simple biomarker that could be used for monitoring PAH progression.

For the most up-to-date guidelines regarding the diagnosis and monitoring of PAH the reader is referred to the 2015 ESC/ERS Guidelines for the Diagnosis and Treatment of Pulmonary Hypertension (Galie et al. 2015) and Diagnosis of Pulmonary Hypertension (Frost et al. 2019).

1.3 Pathophysiology of PAH

PAH is characterised by the remodelling of the PA and the formation of plexiform lesions, defined as glomeruloid structures consisting of numerous small vessels which form branches in the pulmonary artery and occur due to sustained proliferation and activation of local endothelial cells (ECs) and smooth muscle cells (SMCs) (Tuder et al. 1994; Jonigk et al. 2011). These occur due to an accumulation of molecular alterations within the immediate area, including cellular dysfunction, genetic mutations, dysregulation of vascular tone, growth factor (GF) signalling and inflammation.

Much of the research regarding PAH pathophysiology has utilised animal models of PAH. Numerous animal models of PAH have been developed (reviewed by Sztuka and Jasinska-Stroschein 2017) but two of the most commonly used are chronic hypoxia and treatment with monocrotaline (MCT). Chronic hypoxia, or exposure of animals to hypoxia for between two and six weeks (Stenmark et al. 2006; Burke et al. 2009; Savale et al. 2009; Maston et al. 2018), triggers a sustained thickening of pulmonary vascular walls as a result of increased pulmonary arterial (PA)SMC hypertrophy and proliferation, and increased extracellular matrix (ECM) deposition (Stenmark et al. 2006). PAECs also undergo hypertrophy and hyperplasia, resulting in intimal thickening (Stenmark et al. 2006). The chronic hypoxia model has been further developed by co-injection with Sugen 5416 (Su5416) (20mg/kg) at the onset of hypoxia, resulting in a more sustained phenotype of PAH which reproduces more of the pathological features observed in human PAH than chronic hypoxia alone (Vitali et al. 2014; Penumatsa et al. 2019). Su5416 is a VEGFR-

2 kinase inhibitor originally developed for the treatment of cancer (Fong et al. 1999) but clinical trials were not successful and further use of the drug for this purpose was not explored (Hoff et al. 2006).

MCT is a more severe model of PAH with a strong inflammatory component that develops three to four weeks after a single intraperitoneal or subcutaneous dose (60 mg/kg bodyweight) of MCT (Nogueira-Ferreira et al. 2015; Sztuka and Jasinska-Stroschein 2017). This is sufficient to modulate PAEC and PASMC behaviour resulting in thickening of the PA medial hypertrophy and RV hypertrophy (Ghodsi and Will 1981). Although the mechanisms responsible for MCT-induced PAH remain unclear (Gomez-Arroyo et al. 2012), there is evidence to show a role for transforming growth factor (TGF)-β (Zakrzewicz et al. 2007; Zaiman et al. 2008).

Animal models of PAH have come under some criticism due to the differences in elevated plasma cytokine levels observed in animal models compared to PAH patients (Schlosser et al. 2017). However, many of the changes in cell behaviour that contribute to vascular remodelling in human PAH are observed in animal models.

1.3.1 Cellular Dysfunction in PAH

Cellular dysfunction within pulmonary arterioles is a major contributor to PAH development as increased proliferation and migration of PAECs and PASMCs results in vascular remodelling and the formation of plexiform lesions (Tuder et al. 1994; Cool et al. 1999) causing narrowing of the blood vessels and increased mPAP and PVR. PAECs isolated from IPAH patients demonstrate increased proliferation and migration *in vivo* due to an increased sensitivity to

GFs and a pro-survival phenotype, as well as altered tube formation, which contribute to the formation of plexiform lesions (Masri et al. 2007). Numerous pro-survival factors have been implicated in this phenomenon.

PAECs isolated from IPAH PA were less apoptotic than the healthy controls due to increased levels of myeloid cell leukaemia (Mcl-1), an anti-apoptotic factor, mediated in this case by IL-15 (Masri et al. 2007). ECs in a plexiform lesion are exposed to greater concentrations of pro-growth and pro-angiogenic factors such as vascular endothelial growth factor (VEGF), VEGF receptor-2 (VEGFR2), and hypoxia-inducible factor (HIF)-1α and HIF-1β, and reduced levels of pro-apoptotic molecules such as cyclin-dependent kinase inhibitor ($p27/^{kip1}$) (Cool et al. 1999; Tuder et al. 2001). Forkhead box M1 (FOXM1), a transcription factor that regulates genes important for cell-cycle progression and cell survival, was upregulated in PASMCs from lung tissue isolated from PAH patients and in MCT and Su5416/chronic hypoxia (Su/Hx) rat models of PAH (Bourgeois et al. 2018). Caspase-3 protein expression, terminal deoxynucleotidyl transferase (TdT) dUTP nick-end labeling (TUNEL) assays and annexin V labelling all confirmed that inhibition of FOXM1 with thiostrepton reduced PAH-PASMC survival. This was due to inhibition of FOXM1-mediated DNA repair and expression of pro-survival factor survivin (Bourgeois et al. 2018). Thiostrepton also improved RVSP, mPAP and PVR in MCT and Su/Hx rat models of PAH (Bourgeois et al. 2018). Rat pulmonary vascular (V)ECs cultured in a hypoxic environment developed apoptotic resistance which was not demonstrated by VSMCs under the same conditions (Zeng et al. 2018). A luciferase-based assay identified micro (mi)RNA-195-5p to be a key factor in a mechanism involving SMAD7 and HIF1-α. Finally, human pulmonary

microvascular (HPM)ECs exposed to pulsatile shear stress, a model of blood flow, developed an apoptosis-resistant hyperproliferative phenotype (Sakao et al. 2005). This was confirmed via increased caspase-3, proliferating cell nuclear antigen (PCNA), annexin-V and bromodeoxyuridine / 5-bromo-2'-deoxyuridine (BrdU) labelling demonstrated by immunohistochemical analysis and flow cytometry (Sakao et al. 2005).

Dysfunctional ECs also produce factors that stimulate aberrant SMC proliferation (Dewachter et al. 2006), or do not produce the factors that inhibit SMC proliferation (Alastalo et al. 2011), enabling PASMC hyperplasia and hypertrophy. Control HPASMCs exposed to medium derived from control HPAECs underwent increased proliferation. This effect was exacerbated when PAECs isolated from PAH patients were used. In addition, endothelin-1 (ET-1) and serotonin (5-hydroxytrytamine; 5-HT) levels were increased in the media of PAH-PAECs compared to control PAECs, but not in PASMC (Eddahibi et al. 2006). The significance of ET-1 and 5-HT is discussed in Sections 1.3.4.3 and 1.3.4.4 respectively. Pulmonary (P)ECs isolated from IPAH patients secreted increased levels of C-C Motif Chemokine Ligand 2 (CCL2), also known as monocyte chemoattractant protein-1, which is potentially responsible for the increased levels of CCL2 in lung tissue of plasma of IPAH patients compared to control tissue and plasma, resulting in increased monocyte attraction compared to control PECs (Sanchez et al. 2007). In addition, PASMCs isolated from iPAH patients were more responsive to CCL2 than control PASMCs, as determined by their increased migration (Sanchez et al. 2007). Thus, abnormally high CCL2 production by ECs in PAH may contribute to vascular remodelling by promoting SMC migration and

increased inflammation, as CCL2 stimulates inflammatory cell recruitment and infiltration (Fuentes et al. 1995; Takahashi et al. 2009).

Hypoxia-PAH and MCT-PAH mice models have demonstrated increased small ubiquitin-like modifier (SUMO)1 expression associated with an increased autophagy in mice aortic SMCs (Yao et al. 2019). SUMO1 is part of an ubiquitin system that targets proteins for degradation (reviewed by Grillari et al. 2010). Increased SUMO1 expression in mouse VSMCs resulted in a greater sensitivity to hypoxia-induced proliferation and migration, as well as exacerbating the anti-apoptotic signalling, whereas siRNA-mediated silencing of SUMO1 expression in human (H)PASMCs was sufficient to reverse hypoxia-induced proliferation and migration, and reduce autophagy (Yao et al. 2019).

A key consequence of EC dysfunction is increased endothelial permeability, which has also been associated with PAH. Although the exact impact of endothelial permeability on PAH is unknown, it is thought that impaired barrier function may enable permeation of GFs and inflammatory mediators through the EC monolayer where they can then exert their effects on underlying SMCs (reviewed by Zhou et al. 2018). Treatment with thapsigargin, which increases calcium levels via the inhibition of calcium uptake by the endoplasmic reticulum has been shown to increase EC permeability via the transient receptor potential channel (TRPC)4 (reviewed by Ahmmed and Malik 2005), which is exacerbated in Su/Hx animal models of PAH (Francis et al. 2016; Zhou et al. 2016). In addition, bone morphogenetic protein (BMP) receptor type II (BMPRII) and caveolin also impact cell permeability (Long et al. 2015; Prewitt et al. 2015). This is interesting because *bone morphogenetic protein receptor*

type 2 (BMPR2) and *caveolin (CAV)-1* genetic mutations, which will be discussed in greater detail (Sections 1.3.3.1 and 1.3.3.2), are associated with sensitivity to PAH (Table 1.2; group 1.2.1 and group 1.2.2 respectively).

In human (H)PAECs, downregulating *BMPR2* via siRNA resulted in impaired barrier function as measured via a FITC permeability assay (Anderl et al. 2012) and increased TNF-α induced neutrophil transmigration though the EC monolayer (Burton et al. 2011). In addition, conditional pulmonary vasculature *Bmpr2* KO mice displayed increased pulmonary vascular leakage compared to their WT counterparts (Burton et al. 2011). PECs isolated from mice containing a heterozygous *Bmpr2* KO mutation also demonstrated reduced endothelial barrier function as measured by transendothelial electrical resistance (TEER) (reviewed by Srinivasan et al. 2015) and FITC-permeability assays (Prewitt et al. 2015). This could be because *Bmpr2*$^{+/-}$ PECs exhibited altered caveolin (CAV)-1 localisation (Prewitt et al. 2015). CAV-1 expression has been shown to reduce microvascular permeability in endothelial-specific CAV-1 transgenic mice (Bauer et al. 2005). Alternatively, it could be a result of increased EMT, as siRNA-mediated *BMPR2* silencing in PAECs and PEC knockdown of *Bmpr2* in mice resulted in the upregulation of EMT markers such as α smooth muscle actin (αSMA) (Good et al. 2015).

Endothelial to mesenchymal transition (EMT), in which ECs sustain a number of molecular changes resulting in their transition to a phenotype similar to mesenchymal cells (e.g., fibroblasts), also impairs barrier function (Good et al. 2015). EMT-ECs are present in the vasculature of systemic sclerosis (SSc)-PAH patients and in Su/Hx animal models of PAH, where they are thought to display increased migration but reduced proliferation, and to initiate a pro-

inflammatory response due to increased secretion of numerous interleukins (IL) such as IL-4, IL-6, IL-13, and IL-18 and TNF-α compared to control PAECs (Good et al. 2015).

To summarise, vascular cells local to PAH pathogenesis undergo clear phenotypical alterations that contribute to the vascular remodelling characteristic of PAH. Angiogenesis is another crucial event that contributes to the vascular remodelling characteristic of PAH (Voelkel and Gomez-Arroyo 2014). The main driver of angiogenesis is VEGF, a GF whose expression levels are increased in plexiform lesions (Tuder et al. 2001). VEGF is one of many GFs with an altered expression in PAH.

1.3.2 Growth Factors in PAH

Genotyping of nearly 600 PAH patients identified a SNP (rs833061T>C) increased in PAH patients compared to controls. Luciferase assays determined that rs833061C, a VEGF promoter SNP, promoted VEGF gene transcription and protein expression (Zhuo et al. 2017). Thus, increased VEGF activity is a potential risk factor for PAH. On the other hand, Su5416 PAH models work via the inhibition of VEGFR2 to rapidly initiate EC apoptosis, resulting in an accumulation of apoptosis-resistant EC clones that increase proliferation resulting in severe plexiform lesions comparable to those characteristic of PAH (Mizuno et al. 2012; Nicolls et al. 2012). This suggests a complex mechanism where both upregulating and downregulating VEGF signalling results in apoptotic resistance and vascular remodelling.

In the distal pulmonary arteries of PAH patients, expression of platelet derived GF (PDGF) and its two receptors, PDGF receptor (PDGFR)α and PDGFRβ,

are increased (Perros et al. 2008). This is supported by Humbert et al. (1998) who also found increased levels of PDGF in lung biopsies from PH patients compared to healthy controls and suggested it may contribute to the initiation and progression of PH. *In vitro*, PDGF can also be utilised as a chemoattractant for SMCs (Grotendorst et al. 1982) and stimulates SMC proliferation (Ross et al. 1974) suggesting that in the case of vascular injury, PDGF may contribute to vascular remodelling by altering normal SMC behaviour.

Similar findings can be seen in animal models of PAH. Treatment with the selective PDGF-B blocker NX1975 (2 mg/day) in sheep models of chronic intrauterine PH reduced vascular remodelling and RV hypertrophy (RVH) (Balasubramaniam et al. 2003). Although there was no significant difference in PDGF-A or -B mRNA expression in whole lung homogenates from PH sheep compared to healthy control homogenates, increased PDGFR protein was present in hypertensive sheep (Balasubramaniam et al. 2003). Unfortunately, the effect of selective PDGF-A inhibition was not investigated. In PASMCs isolated from rat hypoxia models of PH, thickening of pulmonary artery medial walls occurs as a result of PASMC proliferation and is accompanied by the upregulation of PDGFRα and PDGFRβ (Jankov et al. 2005). PDGF-BB, a major PDGF-betaR ligand,in particular was found to induce DNA synthesis and hyperplasia in SMCs, contributing to vascular remodelling (Jankov et al. 2005).

Treatment with imatinib, a PDGFR inhibitor currently approved for the treatment of numerous cancers (Ben Ami and Demetri 2016; Suttorp et al. 2018), in MCT rats and hypoxic mice models of PAH, reduced pulmonary remodelling and RVH (Schermuly et al., 2005). Imatinib has also shown some

limited success in the treatment of one human PAH case, a 61 year old male, when used alongside normal PAH therapy. Three months of imatinib treatment resulted in improved exercise capacity, as measured via the 6MWT, mPAP, RV performance and PVR which were sustained 6 months after treatment was initiated with no obvious side effects (Ghofrani et al. 2005). This led to a clinical trial of imatinib for the treatment of PAH which has now been successfully completed [Clinical trial identifier; NCT00902174]. Unfortunately, although treatment of human PAH with imatinab was beneficial with regards to improved haemodynamics and increased exercise capacity for those who were not responding to their current treatment regime, it also caused more severe side effects and was associated with increased morbidity (Hoeper et al. 2013a). However, this may be a promising therapeutic strategy worth developing in the future.

MCT-PAH rat models were treated with PKI166, a selective epidermal (E)GF receptor (EGFR) (HER1 in humans) tyrosine kinase inhibitor, 21 days post MCT injection resulting in reduced mPAP and RVH, and increased rat survival compared to control MCT-PAH rats (Merklinger et al. 2005). In addition, PASMCs isolated from pulmonary arteries of PKI166-treated rats were found to have higher rates of apoptosis than controls (Merklinger et al. 2005), which suggests blocking EGF signalling has a potential therapeutic benefit in PAH.

This is supported by research from Dahal et al. (2010) who also treated MCT-PAH rat models with EGFR inhibitors but in this case they used gefitinib, erlotinib, and lapatinib which are currently approved for the treatment of cancers (Segovia-Mendoza et al. 2015; Yang et al. 2017). Treatment with each drug alone was sufficient to inhibit EGF-induced proliferation of PASMCs

isolated from MCT-PAH rats and reduce RVH and RVSP, although not cardiac index or systemic atrial pressure, in MCT-PAH rat models (Dahal et al. 2010). Only gefitinib reduced vascular remodelling at all doses administered (30 mg/kg body weight (bw) and 10 mg/kg bw), whereas erlotinib had an effect at 10 mg/kg bw but not 5 mg/kg bw, and lapatinib had no effect at either 10 mg/kg bw or 5 mg/kg bw doses (Dahal et al. 2010). Interestingly, none of the inhibitors reduced RVSP, systemic atrial pressure, or vascular remodelling in hypoxia-PAH rat models (Dahal et al. 2010).

TGF-β signals through numerous receptors, one of which is endoglin (ENG)-1 (Chaouat et al. 2004). Mice with a heterozygous ENG-1 mutation (*eng*$^{+/-}$) have been used to measure the effect of reducing TGF-β signalling (Gore et al. 2014). In normoxic conditions, neither WT nor *eng*$^{+/-}$ mice suffered from increased RVSP or PA muscularisation, although *eng*$^{+/-}$ mice did have increased macrophage infiltration in the lung. However, post-hypoxia exposure *eng*$^{+/-}$ mice demonstrated reduced RVSP, PA muscularisation and macrophage infiltration compared to WT mice (Gore et al. 2014).

Finally, increased TGF-β mRNA and protein expression have been reported in the serum and lung tissue of IPAH patients compared to control samples, and in isolated PECs and PASMCs (Gore et al. 2014). Increased TGF-β receptor expression was evident in PECs but not in PASMC or lung tissue, although this was dependent on the receptor subtype. Conditioned medium from cultured PECs was added to PASMCs, resulting in increased PASMC proliferation. This effect was exacerbated by treatment of the PECs with TGF-β (Gore et al. 2014). Taken together, these findings suggest increased TGF-β expression in PAH patients, particularly by PECs, results in upregulated

PASMC proliferation which contributes to vascular remodelling and the development of PAH. This is unsurprising considering associated signalling molecules such as BMPR-II are heavily involved in PAH development, with BMPR-II mutations the most common of all hereditary (H)PAH cases.

1.3.3 Genetic Mutations associated with PAH

HPAH is PAH caused by a genetic mutation and includes familial (F)PAH (PAH that occurs in two or more family members) and simplex PAH (one occurrence of HPAH in a family) . FPAH is the cause of ≤ 4% of PAH cases (Jansa et al. 2014; Benza et al. 2015) and shows genetic anticipation but low penetrance (Austin et al. 1993). To classify as FPAH, patients must demonstrate the following criteria; a mutation in *BMPR2* or another PAH-associated gene, exclusion of other causes and two or more family members with PAH. Generally, the mutations seen in FPAH are germ-line mutations in genes that encode proteins of the TGF-β superfamily including *BMPR2* (Deng et al. 2000), *activing-receptor-like kinase-1 (ALK1)* (Harrison et al. 2003), *SMAD1*, *4*, and *9* (Nasim et al. 2011), and *eng* (Chaouat et al. 2004). A rare mutation in *potassium channel subfamily K member 3* (*KCNK3)* (Ma et al. 2013) and a *CAV-1* mutation (Han et al. 2016) have also been associated with FPAH. These and other important PAH-related genetic mutations are discussed in reviews by Ma and Chung (2017) and Morrell et al. (2019).

1.3.3.1 BMPR-II signalling and mutations in PAH

70% of FPAH patients have a heterozygous mutation in *BMPR2* (Cogan et al. 2006), a 190kb gene that encodes a mature protein containing four functional domains; an N-terminal extracellular ligand binding domain, a single pass transmembrane domain, an intracellular serine/threonine kinase domain and

a C-terminal cytoplasmic domain (Machado et al. 2006). More than 300 mutations have been identified within all four functional domains of *BMPR2* but the majority (approximately 73%) are within the serine/threonine kinase domain. 70% of identified mutations are nonsense or missense mutations that cause premature truncation of the BMPR-II mRNA which is then degraded via nonsense-mediated decay (Machado et al. 2006).

In the presence of a functional receptor, BMPs act as paracrine, autocrine and endocrine regulators in numerous systems including the cardiovascular system where they regulate cell differentiation, proliferation/apoptosis and inflammation (reviewed by Yu et al. 2008; Morrell et al. 2016). BMPs are members of the TGF-β superfamily, which also includes growth differentiation factors, TGF-β, inhibins and activins. There are over 30 BMP ligands that signal via receptor complexes consisting of a type I receptor (T1R) and a type II receptor (T2R).

BMPR-II is a T2R which, when activated by ligand binding, forms a complex with specific TGF-β T1Rs including activin-like kinase (ALK)1, ALK-2, BMPR-IA (ALK-3) and BMPRIB (ALK-6) (ten Dijke et al. 1994a; ten Dijke et al. 1994b; reviewed by Horbelt et al. 2012). As previously mentioned, BMPR-II contains an intracellular kinase domain which phosphorylates the GS domain, a glycine and serine-rich intracellular region of the T1R, upon agonist-stimulated formation of the receptor complex (reviewed by David et al. 2007; Heldin and Moustakas 2016). This initiates signal transduction via phosphorylation of receptor (R)-SMADs (Zhang et al. 2003).

There are three types of SMAD; R-SMADs, collaborating (co)-SMADs and inhibitory (i)-SMADs (Macias et al. 2015). R-SMADs and co-SMADS contain conserved Mad homology (MH)1 and MH2 domains which mediate the interaction between themselves and other protein such as T1Rs and transcription factors (reviewed by Heldin et al. 1997). R-SMADs 1, 5 and 8 are specific to BMP signalling (Hoodless et al. 1996; Chen et al. 1997; Nishimura et al. 1998; reviewed by Nishimura et al. 2003) and bind to the T1R via their MH2 domain. Upon doing so, R-SMADs are activated via T1R mediated phosphorylation of serine residues within the C-terminal SSxS region of the MH1 domain (reviewed by Heldin and Moustakas 2016). Once activated, R-SMADs form a complex with co-SMAD4 which is mediated by the MH domains (Zhang et al. 1997; Qin et al. 2001), triggering the translocation of the R-SMAD/co-SMAD complex to the nucleus where it is able to regulate the transcription of target genes (Figure 1.2) (reviewed by Liu et al. 1996; Massague et al. 2005).

TGF-β competes with BMP to bind to TGF-β T1R and together they regulate numerous functions such as cell growth, differentiation, migration and cytoskeletal organisation in a cell-type specific manner. TGF-β signalling stimulates cell proliferation and increases inflammation, whereas BMP signalling promotes a more pro-apoptotic, anti-proliferative phenotype (Zhang et al. 2003; Yu et al. 2008). Thus, a loss of BMPR-II results in imbalanced TGF-β/BMP signalling that favours TGF-β and enables PAH (reviewed by Morrell et al. 2009).

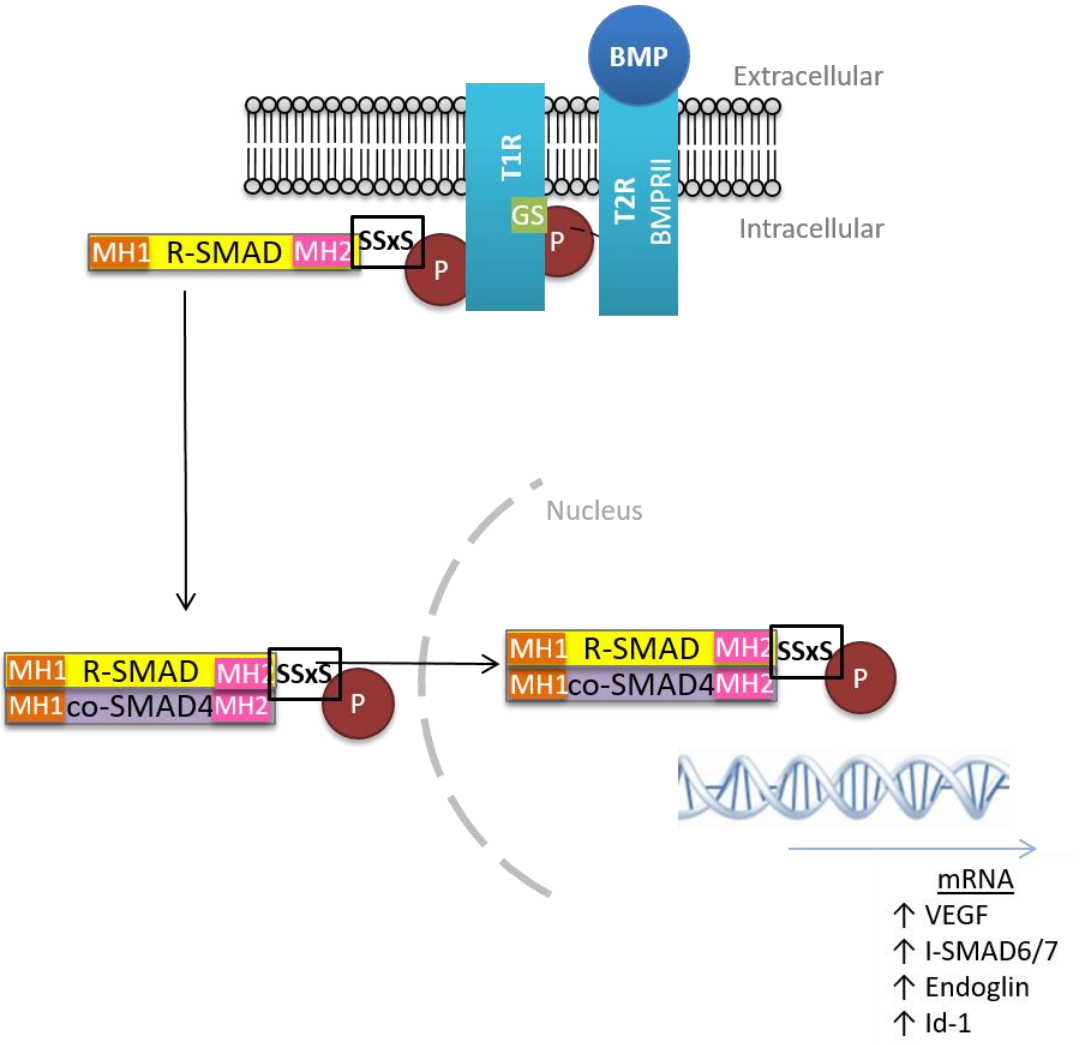

Figure 1.2: The bone morphogenetic protein signalling pathway.

BMP mediated activation of BMPR-II, resulting in phosphorylation of the T1R and consequential phosphorylation of R-SMAD within its SSxS domain. Activated R-SMADs form a complex which co-SMAD4 which then translocates to the nucleus to initiate transcription of target genes. BMP; bone morphogenetic protein, BMPR-II; BMP receptor II, co-SMAD; collaborating SMAD, GS; intracellular glycine and serine-rich domain, Id-1; DNA-binding protein inhibitor, I-SMAD; inhibitor SMAD MH; mad homology, P; phosphorylated residue, R- SMAD; receptor-SMAD, T1R; type 1 receptor, T2R; type 2 receptor, VEGF; vascular endothelial growth factor.

Immunohistochemistry of lung sections isolated from PAH patients has revealed significantly lower BMPR-II, SMAD1 and SMAD 5 expression compared to control lung sections, especially in tissue from patients carrying *BMPR2* mutations (Atkinson et al. 2002). This is supported by RNA sequencing of PAECs isolated from IPAH patients that identified numerous BMPR-II associated genes were downregulated in IPAH-PAECs compared to control PAECs, even in the absence of a BMPR-II mutation (Rhodes et al. 2015).

In ECs, BMP4 binding to BMPR-II results in increased EC proliferation and migration, and reduced EC apoptosis, thus enabling PA remodelling and the progression of PAH (Teichert-Kuliszewska et al. 2006). Conversely, in the main and lobar arteries BMP inhibits cell growth, whereas in the smaller PA involved in PAH, BMP2 and BMP4 stimulate proliferation via extracellular signal-regulated kinase (ERK)1/2-and p38 mitogen-activated protein kinase (MAPK)-dependent (Yang et al. 2005) and SMAD-independent pathway (Nasim et al. 2012). This is most likely due to the expression of different SMAD subtypes. Further to this, BMP-2 and BMP-7 were shown to induce apoptosis via downregulating B-cell lymphoma-2 in control PAMSCs (Zhang et al. 2003). PASMCs isolated from primary (P)PH patients undergoing lung transplantation expressed less BMPR-II than control cells and were more resistant to BMP-mediated apoptosis (Zhang et al. 2003). This supports the theory that apoptotic-resistance in ECs and SMCs results from downregulated BMPR-II signalling.

There is a body of work in rodent models of PAH examining the impact of *bmpr2* mutations. Reduced levels of BMPR-II mRNA and protein expression

have been found in the lungs of rodents with hypoxia-induced PH (Takahashi et al., 2006). Mice with a *bmpr*2 mutation resulting in a dominant loss of BMPR-II in SMCs developed PAH with PA wall remodelling (West et al., 2004), while EC-specific *bmpr*2 KO in mice results in elevated RVSP, RVH and vascular remodelling determined via αSMA staining in the small arteries (30-70 μm in diameter) compared to WT mice (Hong et al., 2008). Conversely, adenoviral delivery of a *bmpr*2 transgene to the pulmonary vascular endothelium improved RVH and PVR, and slowed down pulmonary arterial muscularisation in rat MCT models of PAH compared to a control adenovirus (Reynolds et al. 2012). In contrast, other research has shown adenoviral delivery of *bmpr2* in MCT-induced PAH in rats was found to have no effect (McMurtry et al., 2007).

Mice with a *Bmpr2*$^{+}$/^{R899X} mutation, which mimics the p.R899X premature stop *BMPR2* mutation seen in human disease, demonstrated greater TGF-β activity in both normoxic and hypoxic conditions (Nasim et al., 2012). This resulted in increased cell proliferation of mouse PASMCs via TGF-β-mediated modulation of the MAPK signalling cascade (Nasim et al. 2012). In addition, *Bmpr2*$^{+}$/^{R899X} mice developed an age-associated increase in RVSP that was not present in control mice (Long et al. 2015). Neither *Bmpr2*$^{+}$/^{R899X} mice or control mice experienced RVH, but *Bmpr2*$^{+}$/^{R899X} mice did demonstrate increased muscularisation of peripheral lung pulmonary arteries (Long et al. 2015). These effects were reversed by treatment with BMP9, which was found to restore BMPR-II downstream signalling and to limit increased RVSP and RVH in MCT-PAH rat models (Long et al. 2015). Finally, PASMCs isolated from PAH patients carrying the p.R899X mutation demonstrated an anti-apoptotic, pro-survival phenotype due to increased Bcl-xL resulting from impaired BMPR-II

signalling (Chowdhury et al. 2019), although interestingly, PAECs isolated from the same patients demonstrated increased EC apoptosis resulting from reduced Bcl-xL expression. This suggests a cell-specific effect of BMPR-II dysfunction which results in the preferential expression of Bcl-xL, as opposed to the pro-apoptotic Bcl-xS, in PASMCs but not PAECs (Chowdhury et al. 2019).

In summary, it is clear that loss-of-function *BMPR2* mutations enable PAH development. However, although heterozygous *Bmpr2* mutations in mice exacerbate the effects of lipopolysaccharide (LPS) and 5-HT on PASP, RVH and vascular remodelling, *Bmpr2* mutations alone are insufficient to produce a PAH phenotype (Long et al. 2006; Soon et al. 2015) suggesting a *BMPR2* mutation may just increase a person's susceptibility to the disorder.

1.3.3.2 CAV-1 mutation

CAV-1 mutations have been considered in this research due to the identification of a novel SOCS3-Cavin-1 interaction (Williams et al. 2018) which will be further explored in the context of PAH in Chapter 6.

Two frameshift heterozygous mutations, c.474delA (p.P158PfsX22) and c.473delC (p.P158HfsX22), in *CAV-1* have been associated with PAH (Austin et al. 2012; Han et al. 2016). *CAV-1* codes for the CAV-1 protein which is required for the synthesis and stability of caveolae. Caveolae are small invaginations within the plasma membrane that have numerous roles including mechanoprotection, signal transduction, transcytosis, and lipid homeostasis (reviewed by Cheng and Nichols 2016). In ECs, caveolae have been shown to protect cells from membrane damage resulting from increased cardiac output

via caveolar disassembly, which involves ATP- and actin-independent flattening of caveolae (Sinha et al. 2011; Cheng et al. 2015), triggering a dissociation of cavin proteins from the caveolar complex (Sinha et al. 2011). Cavins are a family of four key proteins (cavin-1-4) which, in conjunction with caveolins, form the core structure of caveolae and regulate their stability and function (Liu and Pilch 2008; McMahon et al. 2009; Hayer et al. 2010; reviewed by Lamaze et al. 2017).

Therefore, loss of caveolin-1 expression in VECs results in a loss of caveolae which increases vulnerability to mechanical damage. As EC dysfunction is a key factor in PAH, this may at least partly explain why a *CAV-1* mutation results in susceptibility to PAH. SMCs, fibroblasts and microvascular ECs isolated from *CAV-1 KO* mice displayed no morphologically distinct caveolae invaginations (Zhao et al. 2002) and, although viable, *CAV-1 KO* exhibited spontaneous dilated cardiomyopathy, RV hypertrophy and increased mPAP compared to WT mice (Zhao et al. 2002).

In patient cases of *CAV-1*-associated PAH, caveolin-1 and caveolae appear to be expressed at normal levels in patient cells, and to co-localise as expected (Han et al. 2016). The key difference between cells isolated from *CAV-1*-associated PAH patients and healthy controls is reduced co-localisation between caveolin-1 and cavin-1 (Han et al. 2016). The key effects of this are yet to be determined but it is most likely to increase susceptibility to mechanical damage due to reduced caveolae stability.

In *CAV-1* KO mice, exposure to hypoxia results in RV failure associated with increased RVH consistent with interstitial fibrosis and elevated endothelial

nitric oxide synthase (eNOS) activity, but interestingly not increased RVSP (Cruz et al. 2012). In VEC and VSMC-specific *CAV-1* KO mice and SMC-specific *CAV-1* KO mice displayed reduced contraction in response to high-potassium-induced cell contraction and increased cardiac hypotrophy in both ventricles in comparison to WT cells, with EC-*CAV-1* KO mice affected more than SMC-*CAV-1* KO mice (Murata et al. 2007). In addition, EC-*CAV-1* KO mice demonstrated increased eNOS activity compared to SMC-*CAV-1* KO mice and control mice (Murata et al. 2007). The significance of eNOS activity will be discussed in Section 1.3.4.2.

In NIH-3T3 fibroblasts, 293T cells, a derivative of human embryonic kidney (HEK) 293 cells which is highly transfectable, and COS-7 cells, caveolin-1 was shown to negatively regulate the TGF-β/SMAD signalling pathway (Razani et al. 2000; Razani et al. 2001). This provides a potential alternative mechanism in which a *CAV-1* mutation enables the development of PAH.

BMPR2 and caveolin have both been linked with mediators of vascular tone, in particular NO and ET-1 which are considered key for PAH development and are targets for treatment.

1.3.4 Mediators of Vascular Tone in PAH

There are three main mediators of vascular tone that primarily contribute to the increased vessel constriction seen in PAH; prostacyclin (PGI_2), NO and ET-1. These are also the target of current PAH therapy (Section 1.6) (reviewed by Badlam and Bull 2017). The effect of 5-HT, another key vasodilator, s also discussed.

1.3.4.1 Prostacyclin

PGI_2 is part of the prostaglandin family of lipid mediators and induces vasodilation via paracrine signalling. An unstable 20-carbon unsaturated carboxylic acid with a cyclo-pentane ring (Vane and Botting 1995), PGI_2 is the main product of arachidonic acid metabolism in ECs (reviewed by Vane et al., 1990). Arachidonic acid is oxidised to form hydroperoxy endoperoxide which is then reduced to hydroxyl endoperoxide (PGH_2). Both of these reactions are catalysed by cyclooxygenase (COX)1 and COX2 (reviewed by Gryglewski 2008). PGH_2 is then converted to PGI_2 by prostacyclin synthase (PGI_2S) (Vane and Corin 2003). Prostaglandins binds to one of nine prostaglandin receptors (prostaglandin D_2 receptor $(DP)_1$, DP_2, prostaglandin E_2 (PGE_2) receptor $(EP)_1$, EP_2, EP_3, EP_4, prostaglandin F receptor (FP), prostaglandin I_2 receptor (IP), and the thromboxane receptor (TP) which are all rhodopsin-like G-protein coupled receptors (GPCRs) (reviewed by Tsuboi et al. 2002). PGI_2 binds to and activates the IP subtype of prostaglandin receptors (Woodward et al. 2011).

GPCRs have three extracellular N-terminal loops, seven transmembrane α-helical domains, three intracellular loops and a C-terminal intracellular tail (Midgett et al. 2011). It is within the seven transmembrane helices that ligand binding occurs, upon which a G protein is activated which in turn binds and activates adenylyl cyclase (AC). AC catalyses the formation of cAMP from ATP which then activates protein kinase A (PKA) (Figure 1.3) (Namba et al. 1994) resulting in SMC vasodilation, as well as inducing anti-thrombotic and anti-inflammatory effects (Figure 1,3) (Moncada et al. 1976; Haynes et al. 1992; Murata et al. 1997). When released by ECs, PGI_2 either binds to the IP on the

surface of SMCs to induce vasodilation, or it is quickly degraded into the inactive metabolite 6-ketoprostaglandin Fα (Vane et al. 1990). At physiological temperature and pH, PGI_2 has a half-life of three - four minutes (reviewed by Whittle and Moncada 1984; Gryglewski 2008). Prostacyclin also acts via IP and cAMP to inhibit SMC proliferation (Clapp et al. 2002).

PGI_2, IP and PGI_2S are reduced in PAH patients (Christman et al. 1992; Tuder et al. 1999). Stearman et al. (2014) utilised PCR to genotype PGI_2S gene promoters in over 300 individuals and identified a number of gene variants that resulted in a range of transcriptional activity including promoting gene expression and inhibiting it. Healthy individuals, in this case those not suffering from PAH, were found to have more active versions of the PGI_2S promoter compared to PAH patients.

In mice, PGI_2S over-expression has been found to protect against hypoxia induced PAH (Geraci et al. 1999) and disrupting the PGI_2S gene results in the thickening of vascular walls in the kidney and lungs contributing to the development of vascular disorders (Yokoyama et al. 2002). IP KO mice exposed to chronic hypoxia developed more severe PAH compared to WT mice as evidenced by increased RVSP values and RV hypertrophy (Hoshikawa et al. 2001). IP KO mice also developed significant medial wall thickening post-hypoxia, versus WT mice (Hoshikawa et al. 2001).

Taking all these findings into account, reduced PGI_2 signalling, either as a result of alterations to PGI_2S expression or PGI_2 signalling, can result in a vulnerability to the development of PAH.

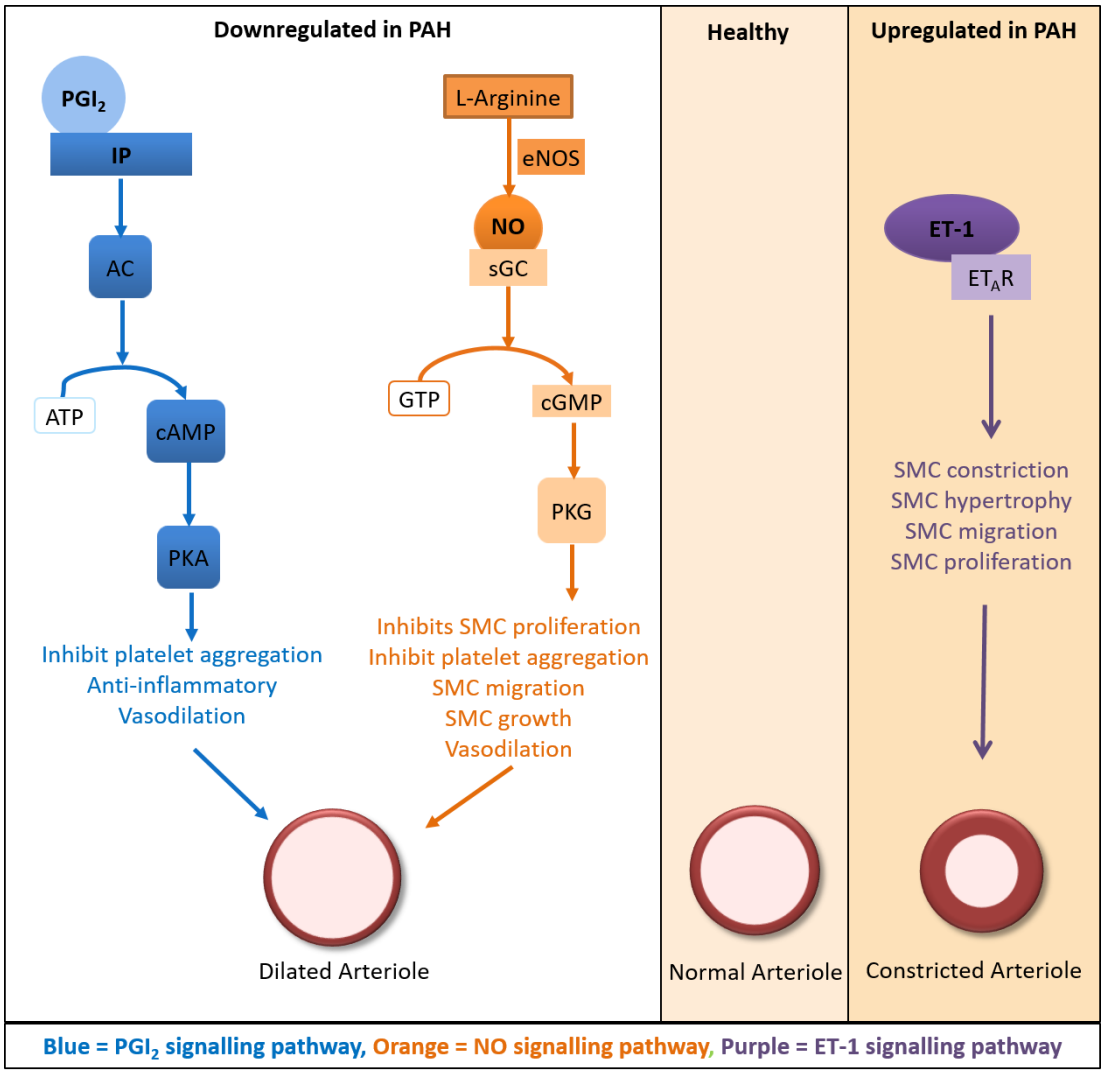
Downregulated in PAH
Healthy
Upregulated in PAH
PGI2
IP
AC
ATP
cAMP
PKA
Inhibit platelet aggregation
Anti-inflammatory
Vasodilation
L-Arginine
eNOS
NO
sGC
GTP
cGMP
PKG
Inhibits SMC proliferation
Inhibit platelet aggregation
SMC migration
SMC growth
Vasodilation
Dilated Arteriole
Normal Arteriole
ET-1
ETAR
SMC constriction
SMC hypertrophy
SMC migration
SMC proliferation
Constricted Arteriole
Blue = PGI2 signalling pathway, Orange = NO signalling pathway, Purple = ET-1 signalling pathway

Figure 1.3: A summary of the prostacyclin, nitric oxide and endothelin-1 signalling pathways in pulmonary arterial hypertension

PGI_2 binds to the IP activating AC which converts ATP to cAMP. cAMP induces PKA-mediated effects (vessel dilation). L-arginine is converted to NO by eNOS. NO binds to sGC which converts GTP to cGMP. cGMP induces PKG-mediated effects (vessel dilation). ET-1 binds to ET_AR to induce it's effects resulting in vessel constriction. AC; adenylyl cyclase, eNOS; endothelial nitric oxide synthase, ET; endothelin, IP; prostaglandin I2 receptor, NO; nitic oxide, PAH; pulmonary arterial hypertension, PGI2; prostacylin, PKA; protein kinase A (cAMP-dependent protein kinase, PKG; protein kinase G (cGMP-dependent protein kinase) sGC; soluble guanylyl cyclase, SMC; smooth muscle cell.

PGI_2 also binds to peroxisome proliferator-activated receptors (PPARs), and it is via PPARα (Biscetti et al. 2009) and PPARβ (Piqueras et al. 2007) that PGI_2 stimulates production of VEGF, encouraging the vascular remodelling characteristic of PAH. Conversely, activation of PPARγ in rat MCT-PAH inhibits PASMC proliferation, therefore reducing vascular remodelling, right ventricle systolic pressure (RVSP) and RV hypertrophy, thereby inhibiting PAH development (Zhang et al. 2014). This suggests an alternative PGI_2 mechanism that could be either protective or detrimental in the context of PAH depending on the subtype of PPAR activated.

1.3.4.2 Nitric Oxide

In EC, eNOS catalyses the oxidation of L-arginine to form NO and L-citrulline in the presence of oxygen, NAPDH and co-factors such as tetrahydrobiopterin. NO is a vasodilator that binds to soluble guanylyl cyclase (sGC) in SMCs. sGC converts GTP into 3',5'-cyclic GMP (cGMP) which activates cGMP-dependent protein kinase, PKG (Figure 1.3) (reviewed by Zuckerbraun et al. 2011).

PKG is a serine/threonine-directed protein kinase predominantly found in the lung, cerebellum, platelets and SMCs which acts via phosphorylation of target proteins to regulate their activity (reviewed by Carvajal et al. 2000). One such protein is myosin light chain phosphatase which, alongside myosin kinase, modulates the level of active myosin. Myosins are motor proteins important in cell contraction and migration (Matsumura and Hartshorne 2008). PKG also regulates vascular SMC proliferation via phosphorylation and activation of vasodilator-stimulated phosphoprotein (VASP) (Chen et al. 2004). Interestingly, PKG mediates NO-induced inhibition of VSMC growth via phosphorylation of VASP at serine 239, however VASP serine 157

phosphorylation by PKA stimulates DNA synthesis and cell proliferation (Chen et al. 2004). NO also inhibits SMC proliferation by inactivating RhoA, a small GTPase involved in the ERK1/2 pathway. Whether SMCs are pro- or anti-proliferative depends on the activation state of RhoA, with GTP-bound active RhoA stimulating cell proliferation (Zuckerbraun et al. 2007).

Reduced expression of eNOS, and therefore impaired NO production, in the lungs is characteristic of PAH (Giaid and Saleh 1995). PAECs isolated from lung tissue of PAH patients were also found to produce less NO than cells from healthy controls (Xu et al. 2004), contributing to pulmonary vasoconstriction and increased PASMC proliferation. Conversely, eNOS was upregulated in ECs within plexiform lesions and PA present in lung tissue of PPH patients compared to control lung tissue (Mason et al. 1998). This was supported by (Nickel et al. 2011), who also found increased eNOS mRNA expression in plexiform lesions compared to expression levels in healthy PAs. Although, expression of eNOS does not necessarily correlate with increased NO signalling, modulating eNOS expression has been shown to have an effect in animal models of PAH.

Homozygous eNOS-deficient ($eNOS^{-/-}$) mice were more sensitive to 2 weeks exposure to hypoxia than WT mice, according to RVSP values (Fagan et al. 1999). Although end-point RVSP was the same in $eNOS^{-/-}$ and WT mice after 4 weeks exposure to hypoxia (Fagan et al. 1999). $eNOS^{-/-}$ mice were also more susceptible to vascular remodelling with a two-fold increase in vessel wall thickness after 4 weeks of hypoxia exposure versus $eNOS^{-/-}$ mice maintained in normoxic conditions, whereas WT mice showed no change in vessel wall

thickness when exposed to normoxic conditions, 2 weeks of hypoxia or 4 weeks of hypoxia (Fagan et al. 1999).

Interestingly, eNOS activation has also been linked to both BMPR-II and caveolin-1 signalling. In bovine (B)PAECs, BMP-induced cell migration was found to be via PKA-mediated phosphorylation of eNOS at serine 1179 (human; serine 1177) (Gangopahyay et al. 2011). In BPAECs and HPAECs, *BMPR2* mutations attenuated eNOS phosphorylation, whereas PAECs from healthy controls still demonstrated eNOS activity under the same conditions, suggesting BMP is activating PKA and eNOS via BMPR-II in these cells (Gangopahyay et al. 2011).

With respect to caveolins, eNOS was found to co-localise with caveolin-1 in bovine aortic ECs (BAECs) but with caveolin-3 in rat cardiac myocytes (Feron et al. 1996). Also in BAECs, tyrosine phosphorylation of eNOS as a result of oxidative stress resulted in reduced catalytic activity of eNOS (Garcia-Cardena et al. 1996). Interestingly, phosphorylated eNOS was found to co-localise with caveolin-1 (Garcia-Cardena et al. 1996), and a potential regulatory relationship in which caveolin-1 provides negative allosteric regulation of tyrosine phosphorylated eNOS specifically within the oxygenase domain of eNOS, but not the reductase domain, was also identified (Ju et al. 1997). As discussed, *CAV-1* KO mice are viable but develop PH (Zhao et al. 2002) (Section 1.3.3.2), however these mice also exhibit a significant increase in systemic NO levels resulting from an increase in eNOS activity (Zhao et al. 2002). Although, these experiments do not define whether increased eNOS activity is a cause of the cardiac changes observed or a result of them, further experiments utilising CAV-1$^{-/-}$, eNOS$^{-/-}$ mice showed silencing eNOS activity was sufficient to

prevent the increased RVSP and medial thickening demonstrated by CAV-1 KO mice (Zhao et al. 2009). In another study, *CAV-1* KO mice display an altered lung phenotype, smaller alveoli and wide septa, which was rescued via treatment with the NO synthase inhibiter, NG-nitro-l-arginine methyl ester (L-NAME) (Wunderlich et al. 2008). L-NAME also improved lung function, measured via oxygen saturation, haemoglobin and haematocrit levels, RVH, systolic pulmonary artery pressure, and exercise capacity in *CAV-1* KO mice (Wunderlich et al. 2008).

Combined, this research demonstrates a complex role for NO, with eNOS KO or inhibition protecting from the development of spontaneous PH in mice due to *CAV-1* KO, whilst also enabling PAH in hypoxia-induced mice models. Potentially, eNOS will have different effects depending on its localisation in the cell and how it is activated.

1.3.4.3 Endothelin-1

ET-1 is a vasoactive peptide 21 amino acids in length formed from 'big ET-1', a 39 amino acid long peptide which is converted to ET-1 by endothelin converting enzyme-1 (ECE-1) (Yanagisawa et al. 1988). ET-1 binds and activates G protein-coupled receptors ET_AR and ET_BR. ET_AR is predominantly found on VSMCs and myocytes whereas ET_BR is found on SMCs and ECs (reviewed by Chester and Yacoub 2014). In SMC cells, ET-1 binding to both ET_AR and ET_BR stimulates vasoconstriction as well as mediating SMC proliferation, migration and hypertrophy (Figure 1.3) whereas in ECs, ET-1 appears to have an opposing effect, acting via ET_BR to increase NO and PGI_2 production and stimulate vasodilation (Migneault et al. 2005; Sauvageau et al. 2007). Thus, although vasodilatory drugs are non-selective antagonists of both

ET_AR and ET_BR, they inhibit ET-1 mediated vasodilation in ECs due to their greater affinity for ET_AR (reviewed by Rubin and Roux 2002; reviewed by Cheng 2008).

Increased levels of ET-1 have been found in PAH lungs, circulation and plasma versus healthy controls (Rubens et al. 2001) and is correlated with greater PVR and structural abnormalities (Giaid and Saleh 1995; Bressollette et al. 2001). Compared to control cells, PAH PASMCs also demonstrate a greater response to ET-1 with regards to Ca^{2+} influx, a marker of SMC contraction and a critical second messenger involved in the regulation of cell proliferation and gene expression (Berridge 1993; Landsberg and Yuan 2004), as well as cell constriction (Yu et al. 2013).

Like NO, ET-1 also has links with BMPR-II. In HMVECs, silencing of *BMPR2* via siRNA resulted in increased ET-1 mRNA and protein expression due to BMP signalling mediated by ALK2 as opposed to BMPR-II (Star et al. 2013).

1.3.4.4 Serotonin (5-HT)

Like ET-1, 5-HT stimulates vasoconstriction but, when not properly regulated, it also initiates abnormal EC-SMC interaction. In chronic-hypoxia induced PAH mice models, mice with inactive 5-HT receptors were resistant to hypoxia-induced increase in blood pressure and vascular remodelling (Launay et al. 2002). In addition, a 5-HT inhibitor, fluoxetine, was able to reduce PASMC growth resulting from incubation in EC derived medium, and tryptophan hydroxylase, an enzyme involved in 5-HT synthesis, was increased in ECs isolated from IPAH patients compared to control ECs (Eddahibi et al. 2006). Finally, the use of anorectic drugs such as fenfluramine, a selective serotonin

reuptake inhibitor (SSRI), is an established cause of PAH (reviewed by Montani et al. 2013).

To summarise, dysregulation of vascular tone contributes to the development of PAH and, aswill be discussed, form the basis of current PAH therapies. The role of inflammation in the development of PAH is becoming better understood (reviewed by Cohen-Kaminsky et al. 2014; reviewed by Groth et al. 2014), supported by the knowledge that auto-immune diseases or diseases that trigger an inflammatory response like CTD, HIV and schistosomiasis infection are associated with PAH (Table 1.2; subgroup 1.4.1, 1.4.2, and 1.4.5 respectively). Through this, potentially novel drug targets may be identified.

1.3.5 Inflammation and PAH

A number of inflammatory factors, such as interleukins, and immune cells, including B and T lymphocytes, macrophages, and dendritic cells, are present in human PAH and PAH animal models (Savai et al. 2012; Oguz et al. 2014; Kumar et al. 2015; Parpaleix et al. 2016).

Bromodomain protein 4 (BRD4), an epigenetic reader which enables transcriptional activity of target genes, in particular pro-inflammatory genes increased in PAH such as IL-6, TNF-α and CCL2, is overexpressed in distal pulmonary arteries and coronary arteries of human PAH tissue (Meloche et al. 2015), and in the coronary arteries of MCT-PAH rat models (Meloche et al. 2017). In human coronary artery SMCs isolated from PAH tissue, BRD4 overexpression triggered pro-proliferative/anti-apoptotic behaviour which was reversed by treatment with BRD4-inhibitor JQ1 (Meloche et al. 2017).

Downregulating BRD4 via treatment with miR-204 mimics, a negative regulator of BRD4, also reversed Su/Hx-induced PAH (Meloche et al. 2015).

In T-cells from PAH patients, fractalkine, a chemokine that promotes chemokine receptor 1 (Cx3CR1)-expressing leucocyte recruitment, is upregulated compared to control cells (Balabanian et al., 2002). Fractalkine and CX3XR1 are also overexpressed in the lungs and PA from an MCT-rat model of PAH (Perros et al. 2007), where they were found to induce proliferation of rat PASMCs, suggesting a complex role in disease progression.

The expression of cytokines regulated on activation, normal T cell expressed and secreted (RANTES) and CCL2, which are chemoattractants for monocytes and T-cells, are also increased in PAH lung compared to control tissue (Dorfmuller et al. 2002; Sanchez et al. 2007). They are thought to contribute to inflammation and remodelling by attracting monocytes to the pulmonary endothelium (Sanchez et al. 2007).

Inhibition of nuclear factor - kappa B (NF-κB), a family of transcription factor complexes that stimulate cytokine production, in the MCT-PAH rat model protected against vascular remodelling, as measured by medial wall thickness and elastin and collagen hyperplasia (Bai et al. 2017). It also limited inflammation, as evidenced by reduced levels of intercellular adhesion molecule (ICAM-1) and IL-6.

Interleukins are a group of cytokines that elicit a wide range of immune and inflammatory- responses (reviewed by Akdis et al. 2016). Several interleukins important in PAH progression have been identified. Overexpression of cardiac-specific IL-1α is sufficient to cause concentric left ventricle hypertrophy in mice

(Nishikawa et al. 2006), and a study by Parpaleix et al. (2016) identified that IL-1 receptor-1 (IL-1R1) is highly expressed in the lungs of hypoxic mice models of PAH and IPAH patients. In addition, treatment with an IL-1R1 antagonist was found to reverse MCT-induced PAH and inhibit IL-1β-induced PASMC growth (Parpaleix et al. 2016).

TNF-α has previously been mentioned as a pro-inflammatory cytokine increased in PAH that contributes to inflammatory cell infiltration and vascular remodelling (Burton et al. 2011; Good et al. 2015; Saleby et al. 2017). In PASMCs, TNF-α was found to reduce BMPR-II expression via downregulation of *BMPR2*, resulting in increased cell proliferation (Hurst et al. 2017). Additionally, in MCT and Su/Hx rat models of PAH, inhibiting TNF-α action with either a recombinant human TNF-α receptor antagonist or the clinically approved anti-TNF-α drug etanercept improved mPAP, RVSP and RVH (Wang et al. 2013; Hurst et al. 2017). In addition, increased plasma TNF-α levels in PAH patients correlated with increased body pain (Matura et al. 2015). Similar results were seen in patients with increased IL-6 plasma concentrations who also reported increased pain, fatigue, anxiety and depression (Matura et al. 2015). Interestingly, TNF-α had no effect on mental-wellbeing symptoms. This was measured via patients self-assessing their own physical and mental well-being and did not include data on other contributing factors such as alcohol intake and diet.

Chronically elevated levels of IL-4 have been shown to cause cardiac fibrotic and left ventricle remodelling and dysfunction in mice (Kanellakis et al. 2012; Peng et al. 2015). There is also evidence to suggest IL-4 has a causal role in the development of SSc-PAH, as IL-4/IL-13 knockout mice are protected

against SSc/(TGF)-β induced PH. However, this effect is only seen with a combined deficiency as neither IL-4 nor IL-13 knockout alone is sufficient to offer protection (Kumar et al. 2015).

IL-13 acts predominantly via the phosphorylation and nuclear translocation of signal transducer and activator of transcription (STAT)3 and STAT6 to inhibit PASMC proliferation and ET-1 production by PASMCs (Hecker et al. 2010). IL-13 receptor-α 2 (IL-13Rα2), a decoy receptor for IL-13, overexpression in PASMCs inhibits IL-13-mediated anti-proliferative effects, STAT phosphorylation and suppression of ET-1 production. This is reversed when IL-13Rα2 expression is reduced via siRNA-mediated knockdown (Hecker et al. 2010). Interestingly, IL-13Rα2 is highly expressed in the lungs of IPAH patients and in hypoxia-induced PAH mice where it has been shown to contribute to pulmonary vascular remodelling via the inhibition of IL-13 signalling (Hecker et al. 2010). This suggests that IL-13 is protective when acting via IL-13Rα1, but upregulation of IL-13Rα2 enables PAH progression due to the abrogation of IL-13/IL-13Rα1 signalling.

IL-10 also appears to provide protection against PAH. Four weeks of treatment with adeno-association virus-IL-10 vector in rat models of MCT-induced PAH was sufficient to ameliorate mPAP and RVH resulting from MCT treatment, and improved rat survival (Ito et al. 2007). It also inhibited MCT-induction of TGF-β and IL-6, reduced the accumulation of macrophages, inhibited vascular cell proliferation and improved survival. In addition, pre-treatment with IL-10 inhibited TGF-β induced PASMC proliferation, although not IL-6-induced proliferation (Ito et al. 2007).

This body of research make a clear case that inflammation may contribute to the development of PAH. Further evidence for this can be seen in numerous studies that link increased IL-6 signalling with the initiation and progression of PAH.

1.4 IL-6 signalling in PAH

1.4.1 IL-6 signalling via JAK/STAT

IL-6 family cytokines consist of four straight α-helices (A,B,C,D) which are joined by four loops (two large and two smaller) so that IL-6 helices reside in an ‘up, up, down, down’ formation (Figure 1.4) (reviewed by Somers et al. 1997; Bravo and Heath 2000). Specific ‘sites’ on the cytokine surface enable IL-6 association with the receptor complex (Figure 1.4). Site I, found within the C-terminal of the AB-loop, binds to the cytokine binding molecule (CBM) of the α-receptor unit. Site II, formed centrally between helices A and C, interacts with the first signal transducing receptor (gp130). Site III is recognised by the IgG-like domain of the second signal transducing receptor (gp130, LIFR or OSMR) which is then recruited to the complex (Savino et al. 1994; Clackson and Wells 1995; Paonessa et al. 1995; reviewed by Heinrich et al. 1998).

IL-6 binds to a receptor complex consisting of the α-receptor-subunit (IL-6Rα) and the signal transducing subunit, a gp130 homodimer (Murakami et al. 1993). IL-6Rα consists of an N-terminal IgG-like domain followed by a CBM made up of two fibronectin (FN)III-like domains which contain a membrane-proximal WSXWS motif and four cysteine residues (Bazan 1990). The CBM resides in loops within the hinge region of (FN)III-like domains which contain a

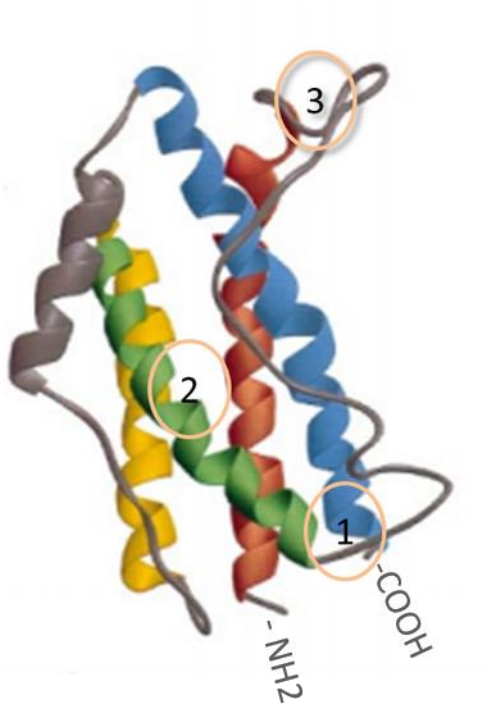

Figure 1.4: The crystal structure of IL-6

The structure of IL-6 showing the four α helices A (red), B (green) C (yellow), D (blue), and the connecting loops (grey). The positions of sites 1, 2 and 3 which are involved in the formation of a receptor complex with IL-6Rα and gp130 have also been highlighted. Adapted from Bravo and Heath (2000).

membrane-proximal WSXWS motif and four cysteine residues (Bazan 1990). The CBM resides in loops within the hinge region of the receptor and is involved in ligand recognition (Yawata et al., 1993). All of the functional domains of IL-6Rα are positioned extracellularly, with just a short cytoplasmic tail of 82 amino acids residing inside the cell (Figure 1.5) (reviewed by Heinrich et al. 2003).

Signalling via membrane-bound (mb)IL-6Rα is known as classic signalling; however IL-6 *trans*-signalling via a soluble form of the IL-6Rα (sIL-6Rα) also occurs. With the exception of some leucocytes and hepatocytes (Hirata et al. 1989; Wang and Fuller 1994; Rojkind et al. 1995), most cells do not express mbIL-6Rα. Thus, sIL-6Rα enables IL-6 *trans*-signalling to occur in cells such as vascular cells which do not express mbIL-6Rα. Interestingly, it has been shown that PASMCs from distal PAs of IPAH patients express significantly more mbIL-6R than healthy PASMCs suggesting that both classic and *trans*-signalling is active within the remodelled vascular of PAH (Tamura et al. 2018).

sIL-6Rα is produced mainly via proteolytic cleavage of mbIL-6Rα. A disintegrin and metalloprotease (ADAM)-10, ADAM-17 and the metalloproteases soluble meprin α and membrane-bound meprin β have all been shown to trigger ectodomain shedding of the receptor *in vitro* (Mullberg et al. 1993; Schumacher et al. 2015; Riethmueller et al. 2016; Arnold et al. 2017). Alternative splicing of IL-6Rα mRNA to produce sIL-6Rα can also occur (Holub et al. 1999), but its contribution to the generation of sIL-6Rα is relatively minor (Lust et al. 1992; Rose-John 2012). sIL-6Rα is comprised of the functional ectodomain of mbIL-6Rα but is not tethered to the plasma membrane (Figure 1.5). The sIL-6Rα/IL-6 complex forms in the extracellular space prior to

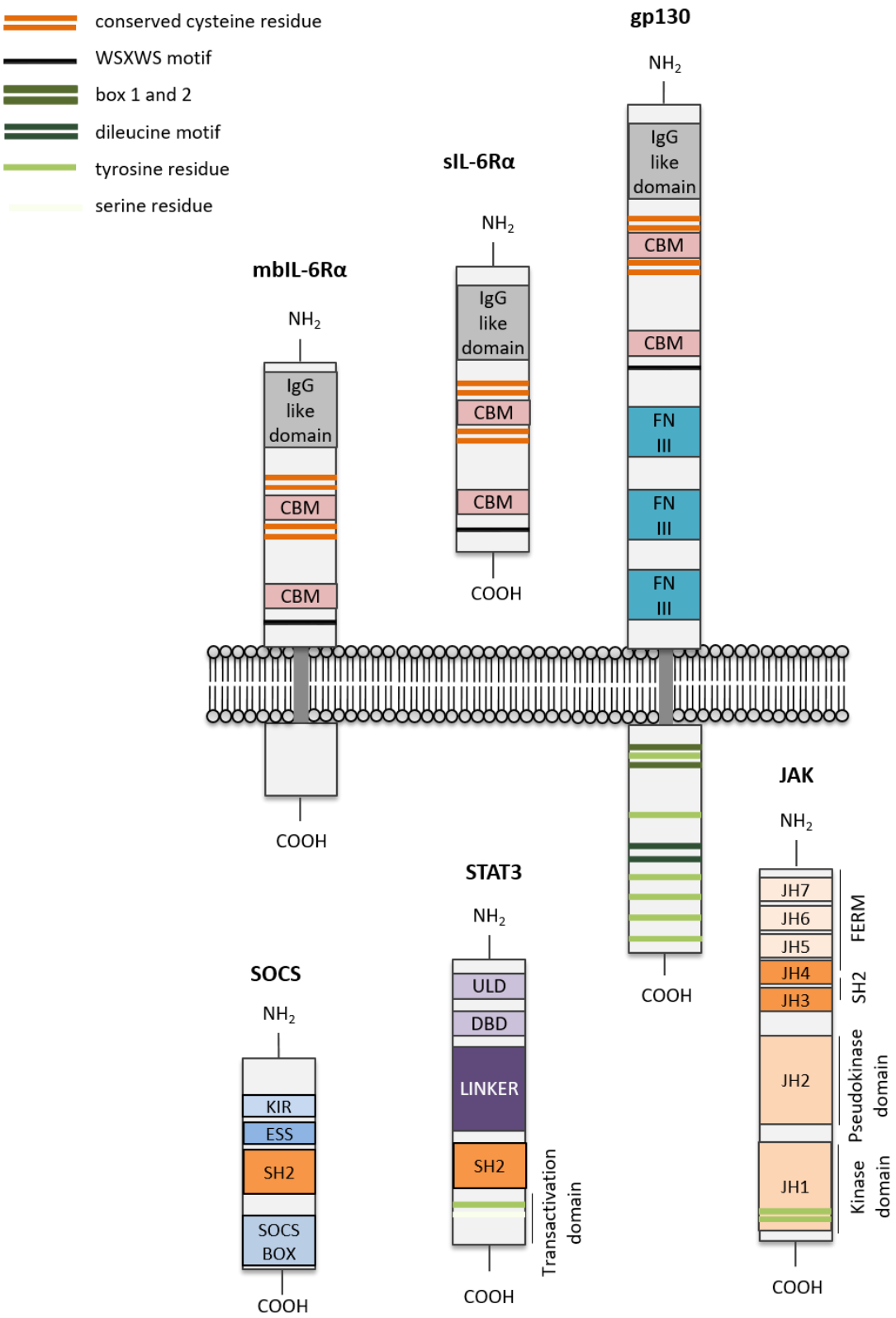
conserved cysteine residue
WSXWS motif
box 1 and 2
dileucine motif
tyrosine residue
serine residue
gp130
NH2
IgG like domain
CBM
CBM
FN III
FN III
FN III
COOH
sIL-6Rα
NH2
IgG like domain
CBM
CBM
COOH
mbIL-6Rα
NH2
IgG like domain
CBM
CBM
COOH
JAK
NH2
JH7
JH6
JH5
JH4
JH3
JH2
JH1
FERM
SH2
Pseudokinase domain
Kinase domain
COOH
STAT3
NH2
ULD
DBD
LINKER
SH2
Transactivation domain
COOH
SOCS
NH2
KIR
ESS
SH2
SOCS BOX
COOH

Figure 1.5: The structural domains of IL-6Rα, sIL-6Rα, gp130, STAT3 and SOCS3

Structural domains of mbIL-6Rα, sIL-6Rα, gp130, JAK, STAT and SOCS3. CBM; cytokine binding molecule, DBD; DNA-binding domain, ESS; extended SH2 domain, FERM; 4.1, ezrin/radixin/moesin, FN; fibronectin, gp130; glycoprotein 130, IgG; immunoglobulin, mbIL-6Rα; membrane bound IL-6 receptor α, JH; JAK homology, sIL-6Rα; soluble IL-6 receptor α, KIR; kinase inhibitory region, STAT; signal transducer and activator of transcription SOCS3; suppressor of cytokine 3, ULD; oligomerisation domain.

binding to ubiquitously expressed membrane-bound gp130 dimers. A short stalk region which resides in close proximity to the plasma membrane in mbIL-6Rα and in the COOH-terminal of sIL-6Rα has also been described which regulates IL-6 proteolysis by ADAM proteins, and enables the sIL-6Rα/IL-6 complex to bind to gp130 (Baran et al. 2013).

Gp130 shares a similar extracellular structure to IL-6Rα but with three addition FNIII domains (Figure 1.5) which are crucial for ligand binding and signal transduction (Horsten et al. 1995). Deletion of the three addition FNIII domains results in a receptor unable to signal (Kurth et al. 2000). In the intracellular region of gp130 are two box domains, a di-leucine motif and a number of relevant tyrosine residues (Figure 1.5), important for gp130/Janus kinase (JAK) association (reviewed by Heinrich et al., 1998). The box1 domain is a proline rich area of the protein essential for JAK binding (Haan et al. 2000). The box 2 domain contains a number of hydrophobic amino acids followed by positively charged amino acids. Although not critical for JAK binding, the box 2 domain does appear to stabilise the gp130/JAK association as in the absence of the box 2 domain, JAK will only bind when overexpressed (Haan et al. 2002).

JAK is comprised of an N-terminal FERM (four point-one, ezrin, radixin and moesin) domain which is important in associating with the receptor (Hamada et al. 2000), an SH2 domain, and a C-terminal kinase domain that is regulated by a pseudo-kinase domain which precedes it (Figure 1.5) (reviewed by Heinrich et al., 2003). JAKs are constitutively bound to the membrane in an inactive state as the pseudo-kinase domain on one JAK inhibits the other and vice versa. Upon formation of an IL-6/IL-6Rα complex, JAK undergoes a

conformational change which relieves this inhibition, enabling the tyrosine kinase domains of the receptor-bound JAKs to trans-phosphorylate adjacent key tyrosine residues at positions 1034 and 1035 of human JAK1 (Toms et al. 2013; Shan et al. 2014). This fully activates both JAKs, resulting in the phosphorylation of specific tyrosine residues at positions 767, 814, 905 and 915 within the cytoplasmic tail of human gp130 (Brooks et al. 2014), which act as docking sites for STATs to associate via their SH2 domains (Figure 1.6) (Stahl et al. 1995; Hemmann et al. 1996).

There are seven STAT family members in humans; 1, 2, 3, 4, 5a, 5b and 6 which share an N-terminal oligomerisation domain, followed by a DNA-binding domain, a linker domain, a SH2 domain and a C-terminal transactivation domain which contains relevant tyrosine and serine residues (Figure 1.5) (reviewed by Heinrich et al., 2003). IL-6/gp130 signalling mostly occurs via phosphorylation of STAT3 (Hemmann et al. 1996).

Two monomeric STAT3 molecules undergo a short-lived association with the YXXQ motif of gp130 which is mediated by the STAT SH2 domain and requires phosphorylation of tyrosine residues on gp130 (Stahl et al. 1995; Novak et al. 1998). Binding of STAT3 precedes STAT3 tyrosine 705 phosphorylation by JAK, which triggers dimerization of the two STAT3 molecules, a process which is also mediated by the STAT3 SH2 domain (Shuai et al. 1994), triggering the translocation of STAT3 to the nucleus (Milocco et al. 1999). Gp130-mediated phosphorylation of serine 727 in STAT3 also occurs, and is critical for the recruitment of transcriptional co-activators and target gene transcription (Kuppner et al. 1990; Wei et al. 2003b; Hazan-Halevy et al. 2010). However,

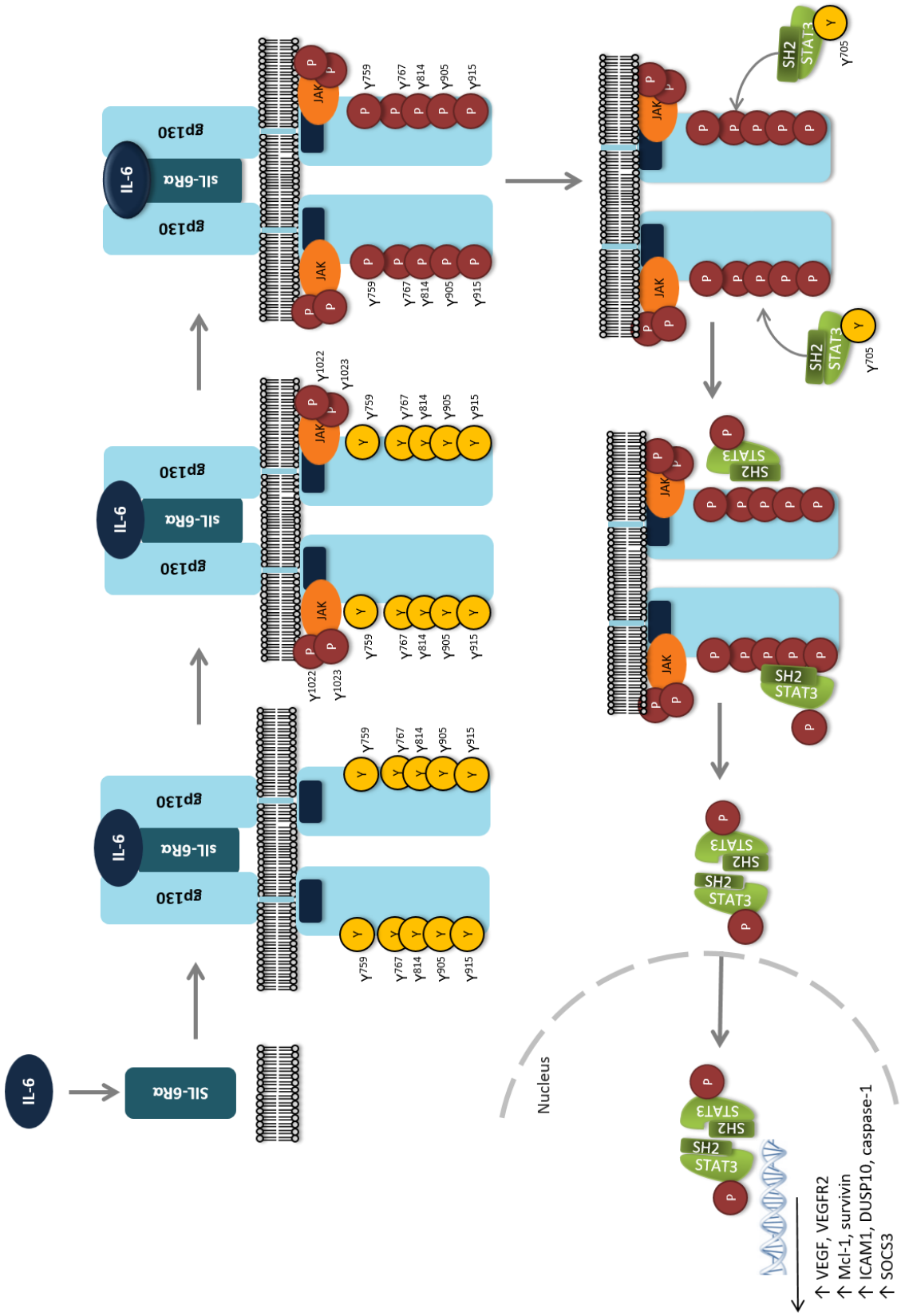
IL-6
sIL-6Rα
gp130
JAK
P
Y759
Y767
Y814
Y905
Y915
Y1022
Y1023
SH2
STAT3
Y705
Nucleus
↑ VEGF, VEGFR2
↑ Mcl-1, survivin
↑ ICAM1, DUSP10, caspase-1
↑ SOCS3

Figure 1.6: IL-6 induction of the gp130/JAK/STAT signalling pathway

IL-6 induction of the gp130/JAK/STAT signalling pathway via the trans-signalling pathway. IL-6 and sIL-6Rα form a complex extracellularly prior to binding to membrane- bound gp130. Local JAK molecules are activated and phosphorylate the gp130 cytoplasmic tail (relevant tyrosine residues have been highlighted). STAT3 binds to phosphorylated residues on the gp130 tail, triggering STAT3 phosphorylation and translocation to the nucleus where it initiates target gene transcription. DUSP10; dual specificity phosphatase 10, gp130; glycoprotein 130, ICAM1; intracellular adhesion molecule 1, IL-6; interleukin 6, JAK; janus kinase, P; phosphorylated tyrosine residue, sIL-6Rα; soluble IL-6 receptor α, SOCS3; suppressor of cytokine signalling 3, STAT; signal transducer and activator of transcription, VEGF; vascular endothelial growth factor, VEGFR2; VEGF receptor 2, Y; tyrosine residue.

non-phosphorylated stable STAT3 homodimers have also been found to exist in the absence of gp130/STAT activation (Braunstein et al. 2003).

STAT3 target genes tend to promote a pro-inflammatory and pro-survival environment, which is why STAT3 hyperactivity is associated with numerous cancers (reviewed by Carpenter and Lo 2014). For instance, the anti-apoptotic proteins Mcl-1 and survivin are upregulated as a result of JAK/STAT3 activity in human myeloma cells and human breast cancer cells respectively (Puthier et al. 1999; Gritsko et al. 2006). On the other hand, the well-established p53 gene, which is a key anti-oncogene that initiates apoptosis, is repressed by STAT3 in BALB/c 3T3 fibroblasts and mouse embryonic fibroblasts (MEFs). Transcription of the pro-inflammatory mediators, dual specificity phosphatase 10 and caspase-1 is mediated by STAT3 in human T-helper 17 cells (Tripathi et al. 2017), and the pro-inflammatory C-reactive protein (CRP) is upregulated as a result of IL-6 activation of STAT3 in human hepatoma Hep3B cells (Zhang et al. 1996). The adhesion molecules ICAM-1 and vascular cell adhesion molecule (VCAM-1) are also upregulated post-IL-6 treatment in human umbilical vein ECs (HUVEC). In addition, STAT3 has been shown to directly induce VEGF gene transcription in NIH3T3 fibroblasts, SCK mammary carcinoma, and B16 melanoma cell lines (Niu et al. 2002), as well as in gastric cancer cells where it was shown to enhance cell growth and invasion capacity (Zhao et al. 2016), thus enabling angiogenesis. Although, many of these findings have been found in cancer cells and not vascular cells, it still presents an idea of the overall pro-inflammatory and pro-survival consequence of IL-6 signalling.

SH2-containing protein tyrosine phosphatase 2 (SHP2) and Src family kinases (SFK) also bind to cytokine-activated gp130 (Kim et al. 1998; Taniguchi et al. 2015). SHP2 binds to JAK-phosphorylated tyrosine 759 (human; mouse tyrosine 757) of gp130 to activate the ERK1/2 and phosphatidylinositol 3-kinase (PI3K) pathways (Schaper and Rose-John 2015). ERK1/2 is also activated by PAH-associated *BMPR2* mutations and causes increased proliferation of PAECs (Awad et al. 2016). PI3K is associated with PA remodelling in animal models of PAH via PASMC proliferation and increased deposition of ECM proteins (Xia et al. 2016). In the intestinal epithelium, SFK binds to gp130 within amino acids 812-827 to activate Yes-associated protein (YAP) (Taniguchi et al. 2015). Although the IL-6/gp-130/SFK pathway has yet to be studied in vascular cells, YAP activation in PA adventitial fibroblasts can increase PAEC and PASMC proliferation via a self-amplifying, regulatory loop with miRNA-130/301, contributing to ECM remodelling in PAH (Bertero et al. 2015).

Thus, IL-6 signalling results in the transcription of pro-inflammatory, pro-angiogenic and pro-survival genes which, when not properly regulated, have the potential to cause cellular dysfunction and disease such as PAH.

1.4.2 Evidence of IL-6 signalling in the development of PAH

IL-6 is overexpressed in the serum and lungs of IPAH patients (Humbert et al. 1995; Soon et al. 2010). IL-6 *trans*-signalling activity in 26 PAH patients was compared to healthy controls via ELISA to quantify IL-6, sIL-6R and soluble (s)gp130 plasma concentrations. Sgp130 is a naturally occurring inhibitor found in human plasma that is generated by translation of alternately spliced gp130 mRNA and functions as a specific inhibitor of IL-6 *trans*-signalling as it

binds to IL-6/sIL-6Rα complexes to block binding to membrane-bound gp130 (Narazaki et al. 1993; Diamant et al. 1997; Jostock et al. 2001). Sgp130 levels did not differ between patients but IL-6 and sIL-6R levels were elevated in PAH patient plasma compared to controls (Jasiewicz et al. 2015). Thus, in the absence of increased levels of sgp130, there is a potential for increased *trans*-signalling.

Plasma IL-6 concentrations > 2.3 pg/ml correlated with clinical deterioration as measured by levels of BNP (Casserly and Klinger 2009), ventilator efficiency, the cardiopulmonary exercise test and the 6MWT (Jasiewicz et al. 2015). In contrast, levels of sIL-6R and sgp130 did not correlate with patient deterioration. Additionally, elevated serum levels of IL-6 are inversely correlated with RV function, cardiac index, and stroke volume (Prins et al. 2018). However, no correlation has been found between serum IL-6 levels and mPAP or PVR, which are key measurements used to diagnose PAH suggesting IL-6 may have a greater impact on RV dysfunction than the PA remodelling initially involved in disease development.

As previously mentioned, increased IL-6 plasma concentrations correlate negatively with QOL, with patients reporting increased pain, tiredness and mental health issues (Matura et al. 2015). Plasma IL-6 concentrations are also associated with patient survival, with IL-6 levels of > 9 pg/mL resulting in a 5-year survival of 30% compared with 63% 5-year survival for patients with levels ≤ 9 pg/mL (Soon et al. 2010). In this PAH cohort, cytokine levels were considered a more accurate measure of prognosis than traditional methods such as the 6MWD and haemodynamics. A major limitation of these studies is that they assess correlative relationships between IL-6 and specific outcomes.

As such, they cannot define a causative role for IL-6 in PAH progression. Regardless, evidence demonstrates IL-6 is a good biomarker for monitoring prognosis in PAH and thus its inclusion should be considered for current monitoring.

PAECs isolated from PAH patients demonstrated increased tyrosine 705 phosphorylation of STAT3 and increased STAT3 activity, measured via the expression of arginase-II, a STAT3 regulated gene essential for EC proliferation, compared to control cells (Masri et al. 2007). Likewise, in HUVECs IL-6 signalling induced STAT3 mediated induction of the pro-inflammatory CCL2 (Zegeye et al. 2018). This was found to be a result of IL-6 *trans*-signalling specifically as STAT3 tyrosine 705 phosphorylation only occurred post-treatment with IL-6/sIL-6Rα, not with IL-6 alone.

There is a bulk of animal research that provides more conclusive evidence for a causative role of IL-6. In mice subject to chronic hypoxia, IL-6 mRNA levels in the lung peak after 2 days and return to normal after 7 days, consistent with positive IL-6 immunostaining in the intima and medial layers of PAs and small arteries 2 days post-hypoxia (Hashimoto-Kataoka et al. 2015). Treatment with the monoclonal rat anti-IL-6R antibody MR16-1 post-hypoxia reduced medial wall thickness and RVSP compared to untreated mice (Hashimoto-Kataoka et al. 2015). Similar results have been shown in IL-$6^{-/-}$ mice exposed to 2 weeks chronic hypoxia which demonstrated significantly lower RVSP and RVH compared to WT mice (Savale et al. 2009). Distal pulmonary vessel muscularisation and macrophage recruitment were also reduced in IL-$6^{-/-}$ versus WT mice. However, these changes occurred in the absence of any

significant effects on the expression of pro-inflammatory markers such as ICAM-1 and VCAM-1 (Savale et al. 2009).

A mouse model in which an IL-6 transgene was specifically overexpressed in the lung (Tg^+) displayed spontaneous elevated RVSP versus WT mice which was exacerbated following chronic hypoxia, with the RVSP of Tg^+ mice more than double that of WT controls (Steiner et al. 2009). Under normoxic conditions, Tg^+ mice also displayed RVH compared to control mice, which was increased following chronic hypoxia. In contrast, there was no change in RVH for WT mice in hypoxic versus normoxic conditions (Steiner et al. 2009). This was due to an increased muscularisation of the pulmonary vascular bed in Tg^+ mice which was not apparent in WT animals. In addition, Tg^+ mice demonstrated partial or complete occlusion of the arterioles in normoxic conditions which was aggravated after exposure to hypoxia (Steiner et al. 2009). This was due in part to IL-6 stimulation of PAEC proliferation which was associated with an upregulation of VEGF in PA walls, causing the formation of occlusive and concentric plexiform lesions. Inflammatory cell infiltration, evidenced by the presence of CD3+ T cells, was also observed in normoxic Tg^+ mice, and which may have contributed to the observed vascular remodelling (Steiner et al. 2009). In contrast, no intimal thickening was detectable in WT mice under normoxic conditions, and inflammatory cell infiltration was only detectable after chronic hypoxia, albeit not to the same extent as Tg^+ mice (Steiner et al. 2009). Based on these findings, the authors concluded that increasing lung-specific expression of IL-6 was sufficient to replicate many pathological features seen in PAH patients (Steiner et al. 2009).

In rat-MCT models of PAH, treatment with SC 144 hydrochloride, a gp130 inhibitor which binds to gp130 causing gp130 serine 788 phosphorylation resulting in gp130 deglycosylation and preventing STAT3 phosphorylation (Xu et al. 2013), or with miR-125a-5p agomir, to target STAT3 activity, improved symptoms such as mPAP, RVSP and RV hypertrophy in a rat MCT model of PAH (Huang et al. 2016; Cai et al. 2018). VEGF and PCNA levels were also reduced in MCT-treated rats administered SC 144 hydrochloride compared to control rats. Similarly, limiting IL-6 signalling via treatment with the IL-6 inhibitor MR16-1, which blocks the IL-6R, or with the gp130 inhibitor sgp130Fc, in hypoxia-PAH mouse models protected rodents from hypoxia induced inflammatory cell infiltration into the lung and improved RVSP and RVH (Hashimoto-Kataoka et al. 2015; Maston et al. 2018).

Research by Brock et al. (2009) demonstrated that IL-6 also signals via STAT3 to control the miRNA-17/19 cluster in HPAECs to post-transcriptionally regulate BMPR-II protein expression. This may be one potential explanation for reduced BMPR-II expression in PAH even in the absence of a *BMPR2* mutation. A negative feedback loop between IL-6 and BMP signalling in human PASMCs and in mice has also been identified (Hagen et al. 2007). This is supported by a study in mice which illustrated that short term loss of BMP signalling alone was not sufficient to produce a pro-inflammatory environment, however when treated with LPS, PASMC from PAH patients and from *Bmpr2*$^{(+/-)}$ mice did exhibit increased IL-6 activity and a greater inflammatory response than that seen in the healthy/WT controls (Soon et al. 2015)

Combined, these studies demonstrate a crucial role for IL-6 in multiple PAH animal models and a potential link between IL-6 and BMP signalling, a key

signalling pathway affected by the majority of PAH-associated mutations (Section 1.3.3.1). This suggests therapeutically targeting the IL-6 pathway might be effective in reducing the inflammation and vascular remodelling characteristic of PAH. A review by Heinrich et al. (2003) discusses three factors involved in naturally terminating the IL-6 signalling pathway; protein tyrosine phosphatases (PTPs), protein inhibitor of activated STAT (PIAS) and suppressor of cytokines signalling (SOCS). PTPs phosphorylate key components in the signal transduction cascade. PIAS are co-transcriptional regulators of the JAK/STAT pathway; PIAS1 inhibits STAT1 and PIAS3 inhibits STAT3. The SOCS family comprises 8 different proteins (SOCS 1-7 and cytokine-inducible SH2 domain protein (CIS)) but SOCS3 is responsible for the inhibition of IL-6 signalling (reviewed by Croker et al. 2003; Babon et al. 2014). SOCS3 is of particular interest because as well as limiting IL-6 signalling, it has also been linked with downregulation of TGF-β (Kinjyo et al. 2006), improved caveolae stability (Williams et al. 2018), and cAMP signalling (Gasperini et al. 2002), which have all been associated with PAH (Sections 1.3.3.1, 1.3.3.2 and 1.3.4.1 respectively).

1.4.3 SOCS3 inhibition of JAK/STAT signalling

SOCS3 contains an N-terminal kinase inhibitory region (KIR) and a central SH2 domain which are common to all SOCS proteins (Figure 1.5) (Naka et al. 1997), plus an extended SH2 subdomain critical for binding to gp130 and JAK, and a C-terminal SOCS box responsible for targeting bound proteins for proteasomal degradation (Babon et al. 2006). SOCS3 is expressed at low concentrations in resting cells but is upregulated by IL-6 via the JAK-STAT pathway. It then inhibits further signalling by binding to phosphorylated tyrosine

759 within activated human gp130 (tyrosine 757 in mice). Whilst in this position the KIR region of SOCS3 is in close enough proximity to receptor-bound JAKs to inhibit tyrosine kinase activity, thus attenuating downstream activation of STAT3 (Figure 1.7) (Babon et al. 2012; reviewed by Babon et al. 2014).

In VSMCs, overexpression of SOCS3 attenuated IL-6/interferon (IFN)γ induced cell migration and proliferation via the inhibition of STAT3 phosphorylation and consequent STAT3-mediated transcription of inflammatory cytokines (Xiang et al. 2013). Thus, there is precedent to consider increasing SOCS3 expression to limit the effects of IL-6 signalling.

1.5 cAMP induction of SOCS3

As previously discussed, upon activation of a GPCR an active Gαs protein is released, activating membrane-bound enzyme AC which converts ATP in to cAMP (Section 1.3.4.1). cAMP acts through three effector proteins (PKA, exchange protein directly activated by cAMP (EPAC), and cyclic nucleotide gated (CNG) ion channels) to control a number of processes including endothelial barrier function and VSMC proliferation and vasodilation to maintain normal vascular function and suppress inflammation (Fukuhara et al. 2005; reviewed by Roberts and Dart 2014).

EPAC proteins are guanine nucleotide exchange factors specific for Rap that mediate a number of cell functions and signalling pathways such as endothelial barrier function, ERK1/2 signalling, SOCS3 induction and cardiac gap junction formation (reviewed by Holz et al. 2006). There are two EPAC isoforms.

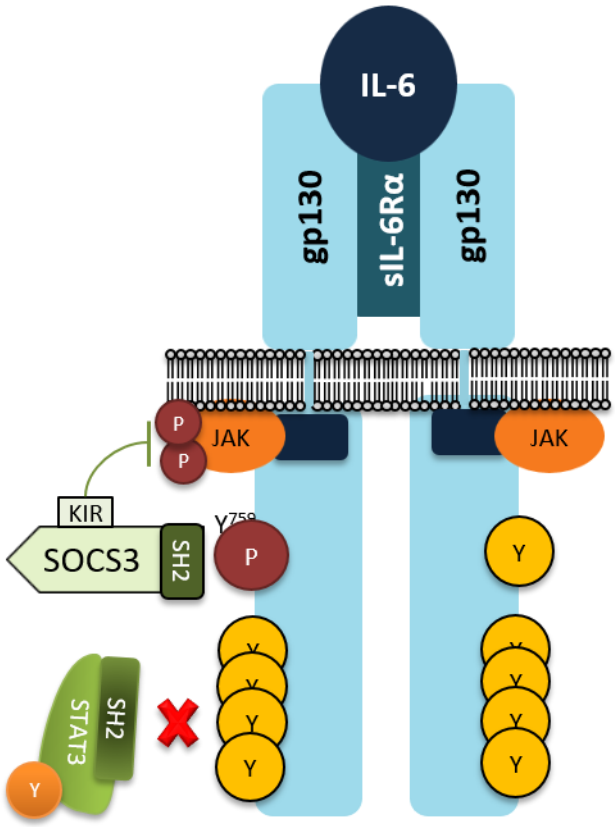

Figure 1.7: SOCS3 inhibition of JAK/STAT signalling

SOCS3, induced by IL-6 in a type of negative feedback loop, binds to tyrosine 759 on the gp130 tail. Once bound, the KIR region of SOCS3 is in close enough proximity to JAK to inhibit kinase activity, thus attenuating gp130 phosphorylation. As STAT3 molecules require phosphorylated tyrosine residues, they are no longer able to bind to gp130 thus further phosphorylation and activation of STAT is attenuated. gp130; glycoprotein 130, IL-6; interleukin 6, JAK; janus kinase, KIR; kinase inhibitory region, sIL-6Rα; soluble IL-6 receptor α, SOCS3; suppressor of cytokine 3, STAT; signal transducer and activator of transcription.

EPAC1 is widely expressed (de Rooij et al. 1998) while EPAC2 expression is restricted to the adrenal glands, pancreatic β-cells, liver and discrete areas of the brain (Ueno et al. 2001). Both EPAC isoforms contain an N- terminal regulatory domain consisting of a dishevelled/EgI-10/pleckstrin (DEP) domain responsible for targeting EPAC (Ponsioen et al. 2009), and either one or two cAMP-nucleotide binding domains (CNB) (Dao et al. 2006). The catalytic region consists of a Ras-exchange motif (REM) domain, a Ras-association (RA) domain, a CDC25-HD domain and the COOH terminus (Figure 1.8A). The CDC25-HD domain is responsible for binding to GDP-bound Rap1 and Rap2, which is then stabilised by the REM domain (Rehmann et al. 2003).

In the absence of cAMP, EPAC resides in an inactive state with the regulatory region preventing the catalytic region from binding to Rap1/2; however upon cAMP binding to the CNB, EPAC undergoes a conformational change resulting in the CDC25-HD domain of the catalytic region being able to bind Rap1 and Rap2 (Figure 1.8B) (Rehmann et al. 2006) which, with the help of the REM domain, activates Rap via the exchange of GDP for GTP (Rehmann et al. 2003).

EPAC is able to induce SOCS3 expression in MEFs via rapid mobilisation of the transcription factor CCAAT/enhancer binding proteins (C/EPB)β resulting in SOCS3 gene transcription independently of PKA (Yarwood et al. 2008). In COS-7 cells, cAMP mediated EPAC1 induction of SOCS3 in a PKA independent manner (Borland et al. 2009). PKC inhibitors, however, did significantly reduce cAMP mediated SOCS3 induction (Borland et al. 2009), suggesting EPAC1 induction of SOCS3 requires PKC and ERK activation.

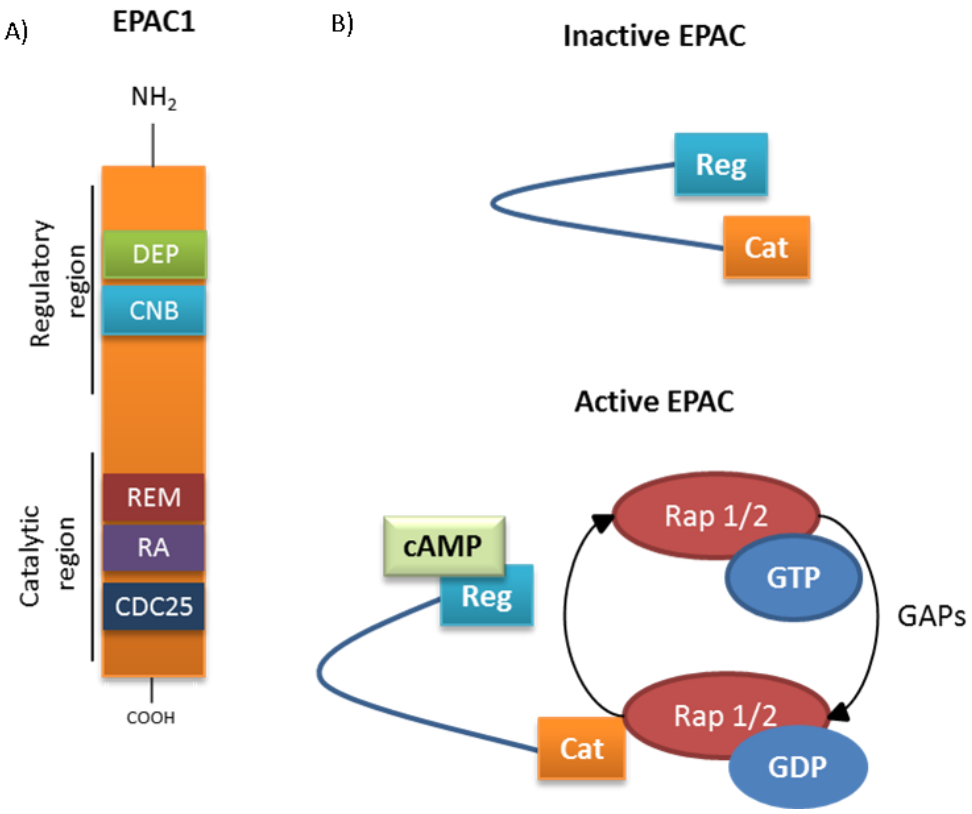

Figure 1.8: Structural domains of EPAC1 and EPAC activation by GTP

A) Structural domains of EPAC1. DEP; dishevelled/Egl-10/pleckstrin domain; CNB, cAMP-nucleotide binding domain, RA; ras-associated domain, REM; Ras-exchange motif (REM) domain. B) The conformational change of EPAC when activated. cAMP binds to the regulatory (Reg) domain to expose the catalytic (Cat) domain of EPAC which is then free to activate Rap1 and Rap2. This is reversed by GTPase-activating proteins (GAPs). (Roberts and Dart 2014).

In HUVECs, aortic ECs, and MEFs, forskolin (Fsk), which directly binds and activates AC, reduced IL-6-mediated STAT3 tyrosine 705 and ERK1/2 phosphorylation (Sands et al. 2006; Woolson et al. 2009). Treatment with 8-(4-chlorophenylthio)-2′-O-methyladenosine-3′,5′-cyclic monophosphate (8-pCPT), an EPAC-selective activator had the same effect (Sands et al. 2006), whereas a PKI inhibitor had no effect on Fsk-mediated inhibition of STAT3 or ERK1/2 activation (Woolson et al. 2009), suggesting this to be an EPAC-dependent mechanism. In support of this mechanism in HUVECs, treatment with the EPAC1 agonist N-(2,4-dimethylbenzenesulfonyl)-2-(naphthalen-2-yloxy)acetamide (I942) was sufficient to induce SOCS3 and limit IL-6-mediated STAT3 phosphorylation in an EPAC1-dependent manner (Wiejak et al. 2019).

cAMP has also been shown to inhibit IL-6 signalling via SOCS3-independent, PKA-dependent mechanisms. In rat ventricular myocytes, activation of PKA stimulated phosphorylation of SHP2 on threonine 73 and serine 189 to inhibit its activity (Burmeister et al. 2015). Activation of PKA in human dermal fibroblasts and MEFs has also been shown to rapidly inhibit IL-6 stimulation of ERK1/2 but not STAT3 (Sobota et al. 2008). This was measured via a reduction in ERK1/2 -mediated CCL2 expression, and was shown to occur via an EPAC1-independent mechanism that may involve rapid PKA-mediated phosphorylation of c-Raf (Sobota et al. 2008).

Thus, modulation of SOCS3 expression by cAMP may be one way in which to limit IL-6 signalling. This is interesting because epoprostenol, a type of prostanoid and one of a cocktail of drugs used in the treatment of PAH that acts via cAMP-mediated activation of PKA, is the only drug currently used in

the treatment of PAH to have any efficacy in improving survival rates (Sitbon et al. 2002).

1.6 Treatment of PAH

The primary aim of current PAH treatments such as prostanoids, phosphodiesterase-5 (PDE-5) inhibitors and endothelin receptor antagonists (ERAs) is to re-establish normal PGI_2, NO and ET-1 signalling respectively (Table 1.4). They are typically administered in combination to induce vasodilation and relieve symptom of PAH but have their drawbacks such as side effects and complex administration procedures (reviewed by Badlam and Bull 2017; Huang et al. 2019).

1.6.1 Prostanoids

Prostanoids are PGI_2 analogues that activate the IP to increase intracellular cAMP levels (reviewed by Gryglewski 2008). Their best characterised role is induction of vasodilation, however PGI_2 has also been shown to have anti-proliferative (Asada et al. 1994), anti-inflammatory (Aronoff et al. 2004; Takayama et al. 2006) and anti-thrombotic (Moncada et al. 1976; Zhang et al. 2016c) effects. Although all prostanoids have been shown to be beneficial in improving functional class, exercise tolerance and pulmonary haemodynamics (Waxman and Zamanian 2013), treatment with them is associated with side effects such as headaches, flushing, jaw pain and diarrhoea. In addition, like PGI_2, they have short half-lives and therefore require complex administration procedures that cause additional discomfort and complications (Zhang et al. 2016b).

Drug Type	Method of action	Drug	Information
Prostanoids	Re-establish normal PGI_2 levels	Eproprostenol	Administered via a continuous IV catheter, half-life < 5 min. Only drug to improve life expectancy of PAH patients (Rubin et al. 1990; Galie et al. 2013)
		Treprostinil	Usually administered subcutaneously via micro-infusion pump, also IV and inhaled. Oral administration shown to have no clinical benefit. Half-life = 4hrs. Results in haemodynamic improvement and increased exercise capacity (reviewed by Seferian and Simonneau 2013)
		Treprostinil Diolamine	Oral - two or three times daily. Improves 6MWD and dyspnea after 16 weeks. Additional adverse effects of extremity pain, hypokalaemia and abdominal discomfort (Jing et al. 2013; Enderby and Burger 2015).
		Beraprost	Oral, clinical effectiveness not sustained after 12 months. Only licenced in Japan and South Korea (Barst et al. 2003).
		Ilaprost	Inhaled, clinical benefit not sustained after 5 years, retrospective study showed no clinical benefits and a poor survival (Oudiz et al. 2009)
Non-prostanoids IP agonist	Bind to IP -> increased intracellular cAMP	Selexipag	17 weeks of treatments -> 30.0% reduction in PVR. Side effects - headache, jaw pain, nausea, nasopharyngitis (Simonneau et al. 2012)

PDE-5 inhibitor	Inhibit degradation of cGMP	Silidenafil	Improves 6MWD, pulmonary haemodynamics and WHO functional class after 1 year of treatment (Galie et al. 2005; Rubin et al. 2011).
		Tadalafil	Improves 6MWD and pulmonary haemodynamics after 16 weeks (Galie et al. 2009a).
sCG NO receptor agonist	Bind to sCG -> increased levels of cGMP	Riociguat	Oral - three times daily. Improves 6MWD, WHO functional class and pulmonary haemodynamics after 12 weeks of treatment. (Ghofrani and Grimminger 2009).
Non-selective ERA	Target ET_A and ET_B receptors to inhibit ET-1	Bosentan	Oral, reduces PVR, risk of hepatic damage (Rubin et al. 2002; Galie et al. 2008).
Selective ERA	Target ET_A receptors to inhibit ET-1	Sitaxentan	Moderate clinical efficacy but removed from market due to high risk of acute liver failure (Lavelle et al. 2009).
		Ambrisentan	Improves 6MWD and WHO functional class. Has lower hepatic toxicity compared to bosentan (McGoon et al. 2009; Oudiz et al. 2009).
Dual ERA	Target ET_A and ET_B receptors to inhibit ET-1	Macitenton	Better receptor binding, enhanced affinity and tissue penetration, and longest duration of receptor blocking compared to other ERAs. Reduced morbidity and mortality after 3.5 years of treatment in human trials at a 10mg daily dose (Oudiz et al. 2009; Gatfield et al. 2012)

Table 1.4: A summary of the drugs currently approved for the treatment of PAH

A summary of the different kind of drugs currently approved for the treatment of PAH with details of the method of action, specific examples of drugs and their clinical effectiveness. 6MWD; 6 minute walk distance, ERA; endothelin receptor antagonists IV; intravenous, NO; nitric oxide, PAH; pulmonary arterial hypertension, PDE-5; phosphodiesterase-5, sCG; soluble guanylyl cyclase, WHO; World Health Organisation.

A meta-analysis for total mortality identified the prostanoid epoprostenol as the only therapy to demonstrate some efficacy in improving survival rates, with a 70% mortality risk reduction (Galie et al. 2013). Unfortunately, due to its short half-life, epoprostenol must be administered via continuous IV administration resulting in additional risks associated with indwelling catheters such an infection or pump malfunctions. As a result of this, epoprostenol is only recommended for WHO functional class IV patients who have not responded to previous monotherapy or combination therapy (Greig et al. 2014). Epoprostenol was approved for use in the clinic in 1995 (Sitbon et al. 2002). Since then other prostanoids, such as beraprost sodium (BPS) and treprostinil, have been developed to try and overcome some of the limitations of epoprostenol administration.

Treprostinil, a worldwide approved synthetic prostanoid analogue, can be administered in numerous ways but the preferred method is subcutaneously via a micro-infusion pump. Intra-venous and inhaled forms of treprostinil have also shown some clinical success, however oral administration had no clinical benefit (reviewed by Kumar et al. 2016). Treatment with treprostinil has been shown to increase a patients exercise capacity, monitored via the 6MWT, and improve a patients hemodynamic capabilities and WHO functional class in adults and children (Jing et al. 2013; Levy et al. 2018). In 2017, a successful method of implanting an IV infusion system for treprostinil was developed (Waxman et al. 2017). Although, the long term benefits of this have yet to be established.

An oral version of treprostinil has also been developed. Treprostinil diolamine is administered orally at a dose of 0.25 mg twice daily or 0.125 mg three times

daily depending on how well the patient tolerates it (Tapson et al., 2012). In initial clinical trials, treprostinil diolamine improved 6MWD and dyspnea after 16 weeks of treatment (Tapson et al. 2012; Jing et al. 2013). However, although administering the drug in this manner is less complex, there were additional side effects associated including extremity pain, hypokalaemia and abdominal discomfort (Enderby and Burger, 2015).

BPS has a half-life of 30-45 minutes and was developed to provide an oral prostanoid option. In animal models, treatment with BPS appeared promising with regards to improving arterial lesions and inhibiting thrombosis (Murai et al. 1989), as well as inhibiting the production of cytokines such as IL-6, IL-1 and TNF-α by alveolar macrophages (Miyata et al. 1996). Although initially effective in reducing mPAP and PVR in WHO functional class I and II human patients, and improving a patient's 6MWD, these clinical benefits were not sustained after 12 months of treatment. BPS is currently only licenced for use in Japan and South Korea (reviewed by Melian and Goa 2002; Barst et al. 2003).

Selexipag, a non-prostanoid IP agonist has also been developed to address the challenges with the short life half of prostanoid analogues. Selexipag is a pro-drug which is metabolised to its active form [4-((5,6-diphenylpyrazin-2-yl)(isopropyl)amino)butoxy]acetic acid (ACT-333679) by carboxylesterase 1. In initial clinical trials, patients demonstrated improved mPAP, PVR and 6MWD after 17 weeks of treatment (Simonneau et al. 2012). Side effects were similar to those seen with traditional prostanoids, with headaches, jaw and extremity pain, nausea, and nasopharyngitis reported (Simonneau et al. 2012). Later clinical trials reported that although the risk of PAH-related complications was

significantly lower with selexipag than with placebo, there was no difference in mortality rates (Sitbon et al. 2015).

1.6.2 Emerging developments in PAH therapies

Despite the number of drugs approved for the treatment of PAH, the main target is vasodilation and there is little currently being done to target the numerous other factors that contribute to PAH progression. Thus, there is an opportunity to develop novel therapies that provide relief or prevention from other key abnormalities characteristic of PAH such as chronic inflammation, EC dysfunction and TGF-β/BMP signalling imbalances by reversing the pathological changes that occur.

1.6.2.1 Targeting the TGF-β/BMP signalling pathway

An imbalance in the TGF-β/BMP signalling pathway which favours proliferation is characteristic of PAH (Section 1.3.3.1), making it a potential therapeutic target. A high-throughput screen utilising a luciferase assay of genes in a mouse carcinoma cell line identified tacrolimus, also known as FK506, as an activator of BMPR-II signalling (Spiekerkoetter et al. 2013). Tacrolimus was able to induce DNA-binding protein inhibitor (Id-1), a measure of BMPR-II activity, in the absence and presence of BMP ligands. Tacrolimus is currently prescribed after organ transplantation for immune suppression via the inhibition of calcineurin. However, it was also found to bind to FK-binding protein-12 (FKBP12), thus limiting FKBP12-mediated inhibition of BMP signalling (Spiekerkoetter et al. 2013). In both animal models of PAH and cell culture experiments, tacrolimus was able to rescue EC dysfunction and tube formation, as well as reverse the development of pulmonary vascular lesions characterised by neointimal formations (Spiekerkoetter et al. 2013).

Tacrolimus is currently undergoing clinical trials to assess the benefit in PAH patients (Spiekerkoetter 2016), with low doses of tacrolimus appearing beneficial so far (Spiekerkoetter et al. 2015).

Numerous other potential therapeutic targets have been identified (reviewed by Badlam and Bull 2017; Satoh et al. 2018), however as we know epoprostenol to have shown the most efficacy in improving life expectancy we propose investigating potential targets of prostanoids. Prostanoids act via cAMP elevation, and as cAMP has been shown to induce SOCS3 and limit IL-6 signalling (Section 1.5), the potential of therapeutically targeting the IL-6 signalling pathway was investigated.

1.6.2.2 Targeting the IL-6 signalling pathway

As discussed, IL-6 signalling activity plays a crucial role in the development of PAH (Section 1.4.2). Although, IL-6 has been discussed as a therapeutic target in PAH (reviewed by Pullamsetti et al. 2018; reviewed by Durham et al. 2019), there are no current guidelines to target IL-6 signalling in the treatment of PAH. Clinically approved JAK inhibitors, such as tociluzimab, and anti-IL-6 therapies, such as tofacitinib and baracitinib, are currently used in the treatment of inflammatory diseases including rheumatoid arthritis and ulcerative colitis (Bonovas et al. 2018; Taylor 2019)

There has been one reported example of a patient suffering from PAH associated with Castleman's disease where the patient (31 year old, female) was treated with tocilizumab in addition to steroids and conventional PAH therapy and demonstrated significant clinical improvement compared to conventional therapy alone (Arita et al., 2010). This supports the potential of

larger re-purposing studies to test the efficacy of anti-IL-6 therapies in the treatment of PAH, but also supports that targeting IL-6 may be an additional mechanism of action in prostanoid treatment of IL-6 which should be further explored.

1.7 Hypothesis

Taking all this into consideration, we propose that an important mechanism by which cAMP-mobilising prostanoid drugs limit PAH is by inhibiting IL-6-mediated pulmonary inflammation and remodelling via cAMP-induced SOCS3 inhibition of IL-6 mediated JAK/STAT signalling (Figure 1.9). Therefore, this study aims to further characterise the role of prostanoid-mediated inhibition of IL-6 induced JAK-STAT signalling in PAH via the induction of SOCS3.

Prostanoid
IP
↑ cAMP
PKA
Epac1
SOCS3 mRNA
IL-6
sIL-6Rα
gp130
gp130
JAK
JAK
P
P
Y
Y
Y
Y
Y
Y
Y759
P
SH2
SOCS3
KIR
SH2
STAT3
Y
VEGF, VEGFR2
Mcl-1, survivin
ICAM1, DUSP10, caspase-1
SOCS3

Figure 1.9: Hypothetical inhibition of IL-6 *trans*-signalling activity by prostanoid-mediated cAMP induction of SOCS3.

We propose prostanoid drugs act via IP to elevate cAMP, inducing SOCS3 gene transcription via an EPAC1 dependent, PKA independent mechanism. SOCS3 then inhibits IL-6 signalling via binding to the phosphorylated tyrosine 759 residue of gp130, attenuating JAK activity and thus preventing further phosphorylation of gp130 and STAT3 molecules, thus reducing STAT3 gene transcription activity and the promotion of IL-6 mediated pro-inflammatory and pro-angiogenic genes that contribute to the development of PAH. cAMP; cyclic adenosine monophosphate, DUSP10; dual specificity phosphatase 10 EPAC1; exchange protein directly activated by cAMP 1, gp130; glycoprotein-130, ICAM1; intracellular adhesion molecule 1, IL-6; interleukin 6, IP; prostaglandin I2 receptor, JAK; janus kinase, KIR; kinase inhibitory region, PKA; protein kinase A (cAMP dependent protein kinase), SOCS3; suppressor of cytokine signalling 3, sIL-6Rα; soluble IL-6 receptor α, STAT3; signal transducer and activator of transcription 3, VEGF; vascular endothelial growth factor, VEGFR; vascular endothelial growth factor receptor.

2. Materials and Methods

2.1 Materials

Supplier	Cat. No.
Abcam, Cambridge, UK	
Anti-GAPDH antibody [6C5] - Loading Control	ab8245
Anti-SOCS3 antibody	ab16030
Anti-STAT3 antibody (EPR787Y)	ab68153
Anti-VE Cadherin antibody	ab33168
Applied Biosystems, California, USA	
GAPDH Taqman gene expression assay (Hs01000485_g1)	4331182
High-capacity cDNA reverse transcription kit	4368814
MicroAmp® Fast Optical 96-Well Reaction Plate with Barcode, 0.1 mL	4346906
MicroAmp® Optical Adhesive Film	4360954
RNase inhibitor (20 U/µL)	N8080119
SOCS Taqman gene expression assay (Hs99999905_m1)	4331182
TaqMan® Universal Master Mix II, no UNG	4440040
New England Biolabs, Massachusetts, USA	
Deoxynucleotide (dNTP) Solution Mix	N0447S

Cayman Chemicals, Cambridge, UK

Beraprost (sodium salt)	18230
Treprostinil	10162

Cell signalling technology, Massachusetts, USA

Phospho-Stat3 (Tyr705) Antibody	9131
VCAM-1 Antibody	12367

Clearsynth, Mumbai, India

Selexipag metabolite ACT-333679	CS-O-15166

Cyanegen Srl, Bologna, Italy

WESTAR Supernova HRP Detection Substrate	K1-0066

Development Studies Hybridoma Bank, Iowa, USA

Anti-alpha tubulin-s (deposited to the DSHB by Frankel, J. / Nelsen, E.M.)	12G10

Gibco laboratories, Maryland, USA

HBSS, calcium, magnesium, no phenol red	14025-050
Phosphate buffer solution	14190-094
Opti-mem	51985

Invitrogen, California, USA

F(ab')2-Goat anti-Rabbit IgG (H+L) Secondary Antibody, Alexa Fluor® 568 conjugate	A-21069
Hoechst 33342	H3570

Purelink DNase Set	12185010
SYBR Safe DNA Gel Stain	S33102
SYTOX™ Green Nucleic Acid Stain	S7020
VEGF Human ELISA Kit	KHG0111
Wheat Germ Agglutinin, Alexa Fluor™ 594 Conjugate	W11262

Lonza Ltd, Basal, Switzerland

Epithelial growth media (EGM) – 2 Bulletkit	CC-3162
Human pulmonary artery endothelial cells	CC-2530

Merck Biosciences, Nottingham, UK (formally Sigma Aldrich Company, UK)

Anti-Mouse IgG (whole molecule)–Peroxidase antibody produced in goat	A4416
Anti-Rabbit IgG (whole molecule)–Peroxidase antibody produced in goat	A6154
Anti-Goat IgG (Whole Molecule) – Peroxidase antibody produced in rabbit	A8919
Anti-VEGFR2 antibody produced in rabbit	SAB4501645
Ampicillin	A9393
Bovine serum albumin	A7030
Bromophenol blue	B7021
Corning Transwell –COL collagen coated membrane inserts	CLS3496
Corning cell culture flasks	CLS430825
Corning tissue-culture treated culture dishes	CLS430165

Dimethyl Sulfoxide (DMSO)	D2650
ESI-09	SML0814
Ethanol	32221
Forskolin	344270
High-capacity cDNA reverse transcription kit	43688
Lipopolysaccharides from Esherichia coli 0111:B4	L4391
L-Glutamine	G7513
Methanol	34860
Monoclonal ANTI-FLAG® M2 antibody produced in mouse	F3165
MG-132	474790
N,N,N′,N′-Tetramethylethylenediamine (TEMED)	T9281
Penicillin-Streptomycin	P0781
RNase inhibitor (20U/µl	N8080119
Trypsin-EDTA solution	T4299

Perkin-Elmer, Inc., Massachusetts, USA

Western Lighting Pus Enhanced chemiluminescence substrate	NEL 104

Promega Corporation, Wisconsin, USA

1 Kb DNA Ladder	G571A
100bp DNA Ladder	G210A
Blue/Orange 6x Loading Dye	G190A

Pfu DNA Polymerase (3u/µl)	M774A
Pfu 10X Reaction Buffer w/20mM $MgSO_4$	M776A
Wizard Plus SV Minipreps DNA Purification Systems	A1330

Promocell GmBH, Heidelberg, Germany

Endothelial cell growth medium MV (Ready-to-use)	C-22020
Human pulmonary microvascular endothelial cells	C-12281

Qiagen, Hilden, Germany

FlexiTube GeneSolution GS9021 for SOCS3	1027416
HiPerFect Transfection Reagent	301707
RNeasy micro kit	74004

R&D systems, Minnesota, USA

Recombinant human IL-6 protein	206-IL
Recombinant human IL-6 R alpha protein	227-SR-025

Roche Applied Science, West Sussex, UK

Complete, EDTA-free protease inhibitor cocktail tablets	11836170001

Santa Cruz Biotechnology, Texas, USA

Nurr1/Nur77 antibody (E-20)	sc-990
SOCS3 antibody (M-20)	sc-7009

Sarstedt, Nümbrecht, Germany

Tissue culture cell scraper 25cm	83.183

Severn Biotech Ltd, Worcestershire, UK

30% Acrylamide (w/v) Ratio 37.5:1 bis acrylamide	20-2100-10

Sino-Biological Inc., Beijing, China

Human VEGFA transcript variant 3 natural ORF mammalian expression plasmid	HG10009-UT

Tocris Bioscience, Bristol, UK

6-Bnz-cAMP sodium salt	5255
8-pCPT-2Me-cAMP, sodium salt	1645
PKI 14-22 amide, myristolyated	2546
PF 04418948	4818

VectorBuilder Inc., California, USA

pLV[Exp]-EGFP:T2A:Puro-EF1A>mCherry	VB160109-10005
pLV(Exp)-CMV>ORF_714bp* (Flag-SOCS3)	VB141125-10023
pLV[shRNA]-mCherry:T2A:Puro-U6>Scramble shRNA, polybrene (5 mg/ml)	VB151104-10082
pLV[shRNA]-mCherry:T2A:Puro-U6>hSOCS3, polybrene (5 mg/ml)	VB180808-1176mwy

FITC (Sigma Aldrich (Merck Biosciences, UK), Cat # FD40S) was kindly provided by Dr W. Roberts (School of Clinical & Applied Sciences, Leeds Beckett University).

Sheep polyclonal anti-GFP serum was generously provided by Professor G. Milligan (Institute of Molecular Cell & Systems Biology, University of Glasgow) and was used in a 1 in 2000 dilution.

2.2 Methods

2.2.1 Cell culture

All cells were cultured at 37ºC, in 5% (v/v) CO_2 in a humidified atmosphere using a cell culture incubator. HPAECs (cat. no. CC-2530) were purchased from Lonza. HPMECs (cat. no. C-12281) were purchased from Promocell. Both cell types originated from males aged 55 and 64 respectively. Angio-sarcoma derived endothelial (AS-M.5) cells and AS-M.5 SOCS3 knockout cells (Krump-Konvalinkova et al. 2003) were kindly provided by Dr J.J.L. Williams (Institute of Molecular, Cell and Systems Biology, University of Glasgow) and Mr N.A.S. Alotaiq (Institute of Cardiovascular Medical Sciences, University of Glasgow) (Williams et al. 2018).

2.2.1.1 Maintenance and passage of human pulmonary arterial endothelial cells

HPAECs were maintained as monolayers in Endothelial Cell Growth Medium (EGM-2) which was purchased as a bulletkit comprising Endothelial Basal Medium (EBM-2) and EGM-2 SingleQuot Kit Supplement & Growth Factors and made up as recommended by the supplier. Cells were maintained in T75

tissue culture flasks and media was replenished every 48 hours. Cells were sub-cultured at approximately 80-90% confluency.

For cell passage, medium was aspirated from the HPAEC monolayers which were then washed twice with 5 ml/flask of pre-warmed Dulbecco's PBS. PBS was discarded and HPAECS were treated with 2 ml trypsin-EDTA at room temperature until cells detached, this was aided with gentle tapping. Cell detachment was monitored under the microscope. The trypsin was then inactivated via dilution with 10 ml EGM-2 and HPAECs were re-suspended by gentle trituration using a sterile 10 ml disposable pipette and transferred to a 50 ml falcon tube. HPAECs were centrifuged at 500g for 5 minutes at room temperature to pellet cells and the supernatant was discarded. HPAECs were then re-suspended in 5–12 ml fresh EGM-2 and gently mixed using a sterile 5 ml disposable pipette. 10 µl of the cell suspension was counted using a haemocytometer and the total number of cells was calculated. The desired number of cells were then seeded in the required tissue flasks and fresh EGM-2 media was added to make a total volume of 12 ml, 3 ml or 2 ml in T75, 6 cm dish and 6-well plates respectively. HPAECs were not used past passage 10 as cells developed an elongated morphology and lost their characteristic cobblestone appearance. Additionally, at passages greater than 10 HPAECs demonstrated slower growth and a reluctance to reach confluency.

For cryogenic storage, cell pellets were prepared as previously described and then re-suspended in foetal bovine serum (FBS) supplemented with 10% (v/v) DMSO. Cells were immediately frozen at -80ºC overnight before being transferred to liquid nitrogen. To thaw frozen cells, cell stocks were rapidly defrosted at 37ºC and transferred in to a sterile T75 tissue culture flask

containing 12 ml of pre-warmed fresh media for incubation overnight to allow cells to attach. Media was replenished the following day and the cells were maintained as described above.

2.2.1.2 Maintenance and passage of human pulmonary microvascular endothelial cells

HPMECs were cultured and maintained in Endothelial Cell Growth Medium MV which was purchased as Endothelial Cell Growth Medium and Endothelial Cell Growth Medium supplement kit and made up as recommended by suppliers. Cells were maintained in sterile T25 tissue culture flasks in 10 ml media which was replenished every 3 - 4 days as required. Cells were sub-cultured at approximately 70% confluency. Cell passage and cryogenic storage of HPMECs was completed using the same protocol described for HPAECs apart from 1 ml trypsin-EDTA was used to detach the cells and 5 ml Endothelial Cell Growth Medium MV supplemented with 10% FBS was used to inactivate the trypsin. HPMECs were not used past passage 7 as at passages greater than this it was observed cells were less able to attach to the cell culture flasks or grow to confluency.

2.2.1.3 Cell culture of immortalised angiosarcoma derived endothelial cells

AS-M.5 cells (Krump-Konvalinkova et al. 2003) were cultured and maintained as described in section 2.2.1.1. The passage number of AS-M.5 cells was recorded but there was no upper limit of passage number used for experiments.

2.2.2 Transfection of cells

2.2.2.1 Lentiviral titres

Lentivirus titres of pLV[shRNA]-mCherry:T2A:Puro-U6>hSOCS3 and pLV[shRNA]-mCherry:T2A:Puro-U6>Scramble shRNA were performed by F. Moshapa (School of Pharmacy and Medical Sciences, University of Bradford) in human embryonic kidney (HEK) 293 cells to determine optimum transduction concentration. 6-well plates were seeded with HEK 293 cells at a density of $2x10^5$ cells per well in Dulbecco Modified Eagle Medium (DMEM)-high glucose containing 10% (v/v) FBS, 2 mM L-glutamine, 100 units penicillin and 0.18 mM streptomycin in 0.9% NaCl and incubated overnight in the cell culture incubator.

Serial dilutions of pLV[shRNA]-mCherry:T2A:Puro-U6>hSOCS3 and pLV[shRNA]-mCherry:T2A:Puro-U6>Scramble shRNA lentivirus were prepared ranging from $1x10^{-2}$ - $1x10^{-6}$ in polybrene (8 µg/ml)-containing media. Media was then gently aspirated from the cells and replaced by 1 ml of the relevant lentivirus dilutions. The 6-well plates were then gently rocked to mix the virus evenly and incubated overnight in the cell culture incubator, before replacing the lentiviral media with fresh media containing the relevant antibiotic. Cells were then maintained in antibiotic-supplemented media for 10 days before washing with PBS and adding 1 ml of crystal violet solution prior to incubation for 10 minutes at room temperature. The crystal violet solution was then removed and cells were washed 3 X with PBS prior to counting the blue stained colonies at 40x magnification. The lentiviral titre was then calculated by multiplying the number of colonies per well by the dilution factor, and expressed as transforming units per ml (TU/ml).

Lentiviral titre of pLV(Exp)-EGFP:T2A:puro-EFIA>mcherry ultra-purified and pLV(Exp)-Puro-CMV-0RF_705bp was performed by Dr J.J.L. Williams (Institute of Molecular, Cell and Systems Biology, University of Glasgow) in the same method described above.

2.2.2.2 Lentiviral infection

HPAECs were maintained in 6 cm dishes until reaching approximately 70% confluency. Polybrene (8 µg/ml)-containing DMEM was prepared and 1 ml was aliquoted in to sterile 1.5 ml tubes. The lentivirus was then thawed at room temperature and mixed via gentle tapping. Appropriate volume of virus particle was added to 1 ml polybrene-containing media and mixed by gentle pipetting with a 1000 µl pipette. Media was then aspirated from the cells and replaced with the virus/polybrene-containing DMEM. Cells were incubated overnight in the cell culture incubator before removal of media. Cells were then incubated in the cell culture incubator for a further 24 hours in 2 ml of fresh Endothelial Cell Growth Medium MV prior to any further treatments.

Transduction efficiency was monitored via imaging of GFP expression in cells. HPAECs were seeded in Nunc™ Lab-Tek™ Chambered Coverglass at a density of $2x10^5$ cells per chamber and left to incubate overnight. Cells were then infected with pLV(Exp)-EGFP:T2A:puro-EFIA>mcherry as described above prior to fixation via incubation in methanol for 10 minutes at -20ºC. Cells were then washed with 500 µl ice-cold 0.1% v/v triton/PBS for 5 minutes prior to 2 X 5 minute washes in 500 µl PBS at room temperature. HPAECs were counterstained via 20 minutes incubation with 500 µl 1 µM Hoechst 33342 in PBS at room temperature prior to 3 X 5 minutes washes in 500 µl PBS at room temperature. Cells were fluorescently imaged to visualise GFP expression

using a Nikon ECLIPSE TE2000-E confocal microscope. Images were taken at 400x magnification with a large pinhole, a pixel dwell of 20 millisecond and an average of 4 using EZ-C1 3.90 software. For representative figures, an image was taken from each chamber and a 5 cm x 5 cm section of the image was cropped from the centre of the image using EZ-C1 3.90 freeviewer software.

2.2.2.3 siRNA transfection

HPAECs were maintained in 6 cm dishes until reaching approximately 70% confluency. siRNAs were stored at -20°C at 10 µM. Appropriate volumes of siRNA and 3 µl HiPerFect were added to Opti-MEM media to make 100 µl total volume of 0.2 – 2 µM siRNA and left to incubate at room temperature for 10 minutes. A further 900 µl of OPTIMEM media was then added and mixed via pipetting before adding the mix to the cells. After 3 hours a further 1 ml of EGM-2 media was added to the cell culture dish. Further treatments were then applied after 48 hours.

2.2.2.4 Short hairpin (sh)RNA infection

For silencing of SOCS3, HPAECs were maintained in 6 cm dishes until reaching 50 - 70% confluency. Polybrene (8 µg/ml)-containing DMEM was prepared and 1 ml was aliquoted in to sterile 1.5 ml tubes. pLV[shRNA]-mCherry:T2A:Puro-U6>hSOCS3 and pLV[shRNA]-mCherry:T2A:Puro-U6>Scramble shRNA lentivirus were thawed at room temperature and mixed via gentle tapping. A full summary of the shRNA vectors can be found in Appendix 1 and Appendix 2 respectively. Appropriate volume of virus particle was added to 1 ml polybrene-containing media and mixed via vortexing for no longer than 1 second. Media was then aspirated from the cells and replaced

with the shRNA/polybrene-containing DMEM. Cells were incubated overnight in the cell culture incubator before replacing the shRNA-containing media with Endothelial Cell Growth Medium MV. Cells were then maintained in the cell culture incubator for 5 - 7 days prior to any further treatments.

To monitor shRNA infection, treated HPAECs were imaged for mCherry expression. Cells were seeded in Nunc™ Lab-Tek™ Chambered Coverglass at a density of 20,000 cells per chamber and left to incubate overnight. The lentivirus was then prepared at appropriate concentrations and applied to cells as previously described. Cells were incubated for 5 days prior to fixation via incubation in methanol for 10 minutes at -20ºC. Cells were then washed with 500 µl ice-cold 0.1% v/v triton/PBS for 5 minutes prior to two 5 minute washes in 500 µl PBS at room temperature. HPAECs were counterstained via 20 minutes incubation with 500 µl 1µM Hoechst 33342 in PBS at room temperature prior to three 5 minutes washes in 500 µl PBS at room temperature. Cells were fluorescently imaged to visualise mCherry expression using a Nikon ECLIPSE TE2000-E confocal microscope. Images were taken at 400x magnification with a medium pinhole, a pixel dwell of 20 millisecond and an average of 4 using EZ-C1 3.90 software. For representative figures, an image was taken from each chamber and a 5cm x 5cm section of the image was cropped from the centre of the image using EZ-C1 3.90 freeviewer software.

2.2.3 Protein analysis

2.2.3.1 Immunoblot analysis

Whole cell lysate preparation

HPAECs and AS-M.5 cells were seeded and maintained in 6 cm dishes, except for siRNA and shRNA experiments where cells were maintained in 6-well plates. HPMECs were seeded and maintained in 6-well plates only. Post-treatment, cell stimulations were stopped by transferring the cell dishes to an ice bath, discarding the media and washing monolayers twice with ice-cold PBS. Cells were then harvested in to 500 µl ice-cold PBS for 6-well plates or 800 µl ice-cold PBS for 6 cm plates and centrifuged at 500 g for 5 minutes at 4°C. A 200 µl pipette tip was used to remove all supernatant without disturbing the pellet and cells were lysed in 40 - 100 µl of RIPA^{+} (50 mM HEPES pH 7.4, 150 mM sodium chloride, 1% (v/v) Triton x100, 0.5% (v/v) sodium deoxycholate, 0.1% (w/v) SDS, 10 mM sodium fluoride, 5 mM EDTA, 10 mM sodium phosphate, 0.1 mM PMSF, 10 µg/ml benzamidine, 10 µg/ml soybean trypsin inhibitor, 2% (w/v) EDTA-free complete protease inhibitor cocktail) and vortexed to mix for no longer than 2 seconds. When required, lysates were stored at this point at -80^{0}C in 1.5 ml microcentrifuge tubes and thawed before analysis. Samples were rotated at 4°C for 30 minutes and centrifuged at 20,000g for 15 minutes at 4°C to remove insoluble cellular debris. Without disturbing the pellet, the supernatant was transferred in to a fresh microcentrifuge tube and the pellet discarded.

Determination of protein content

Protein content was then determined via a bicinchoninic acid (BCA) assay. 2 - 5 µl of the supernatant were added to the relevant wells on a 96-well plate and made up to a total volume of 10 µl with RIPA+ buffer (as previously described). A standard curve of protein concentrations (0 - 2 mg/ml) was prepared using appropriate volumes of 2 mg/ml BSA made up in RIPA+ buffer to a total volume of 10 µl. All assays were performed in duplicate.

49 parts BCA reagent (1% (w/v) 4,4-dicarboxy-2,2-biquinoline disodium salt, 2% (w/v) anhydrous sodium carbonate, 0.16% (w/v) sodium potassium tartrate, 0.4% (w/v) sodium hydroxide and 0.95% (w/v) anhydrous sodium bicarbonate) was mixed with 1 part 4% (w/v) copper (II) sulphate. 200 µl of this solution was added to each well and the colour change monitored by determining the absorbance at 560 nm Biorad iMARK microplate absorbance reader until the most concentrated standard dilution gave a reading of 700 - 800. The absorbance of each supernatant was determined at 560 nm and the protein content calculated using the equation of the best fit straight line as calculated by the A560 values of the standard dilutions.

SDS PAGE and transfer

Samples were equalised for protein content (10 - 50 µg) based on the results obtained from the BCA assay and volumes equalised by adding the required amount of RIPA+ buffer. SDS-loading buffer (50 mM Tris pH 6.8 at room temperature, 10% (v/v) glycerol, 12% (w/v) SDS, 100 mM dithiothreitol, 0.2% (w/v) bromophenol blue) was added to denature cellular proteins. Samples

were then heated at 70ºC for 30 seconds before being centrifuged for 30 seconds to recover any condensation.

8%, 10% or 12% (w/v) acrylamide resolving gels (Appendix 3) were prepared beforehand when possible and stored at 4°C. Samples were loaded on to the gel and separated via electrophoresis at 100-180 V in Tris-Glycine-SDS buffer (24.7 mM Tris, 0.19 M glycine).

Fractionated proteins were then transferred electrophoretically to a 0.2 µm diameter Protran nitrocellulose membrane for 45 minutes at 400 mA in transfer buffer (24.7mM Tris, 0.19 M glycine and 20% (v/v) methanol). When transferring proteins greater than 200 kDa, transfer was performed for 90 minutes at 400 mA in transfer buffer (as previously described).

Immunoblotting

To prevent non-specific antibody binding, membranes were incubated for 1 hour with 5% (w/v) non-fat milk powder made up in TBST (Tris-buffered saline (TBS), pH 7.6 at room temperature, containing 0.1% (v/v) Tween 20) (TBST-M) or 5% (w/v) BSA - TBST. Membranes were then incubated overnight with the appropriate primary antibody as described in Table 2.1 at 4ºC on a rotator. Following incubation, membranes were washed for 3 x 10 minutes in 30 ml TBST and incubated for one hour on a rotator at room temperature with the appropriate secondary horseradish peroxidase (HRP)-conjugated antibody as described in Table 2.1. Membranes were then washed in 30 ml TBST for 3 X 10 minutes before 1 minute incubation in Western Lightning® Plus, Enhanced Chemiluminescence Substrate or 1.5 minutes incubation in WESTAR Supernova HRP Detection Substrate and visualisation of antibody staining

Antibody	Species	Company	Catalogue Number	Diluent	Dilution
Flag M2	Mouse	Sigma/ Merck	F3165	5% TBST-M	1:1000
GAPDH	Mouse	Abcam	ab8245	5% TBST-M	1:10000 – 1:20000
GFP	Sheep	-	-	5% TBST-M	1:1000 - 1:2000
Nur77	Rabbit	SCBT	sc-990	5% TBST-M	1:200 – 1:500
P(Tyr705)-STAT3	Rabbit	CST	9131	5% BSA - TBST	1:200 -1:1000
SOCS3	Goat	SCBT	sc-7009	5% TBST-M	1:100 – 1:500
SOCS3	Rabbit	Abcam	ab16030	5% TBST-M	1:500 – 1:1000
STAT3	Rabbit	Abcam	ab68153	5% TBST-M	1:500 - 1:1000
Tubulin	Mouse	DSHB	12G10	5% TBST-M	1:1000 – 1:10000
VEGFR2	Goat	NB	AF357-SP	5% TBST-M	1:1000
VCAM1	Rabbit	CST	12367	5% TBST-M	1:1000

Table 2.1: Description of antibodies used in immunoblotting

CST; Cell Signalling Technology, DSHB; Developmental Studies Hybridoma Bank, GAPDH; glyceraldehyde 3-phosphate dehydrogenase, NB; Novus Biologicals, SCBT; Santa Cruz Biotechnology, SOCS; suppressor of cytokine signalling, STAT; signal transducer and activator of transcription, TBST-M; 5% (w/v) non-fat milk powder in tris-buffered saline containing 0.1% (v/v) Tween 20. AM1; vascular cell adhesion molecule 1, VEGFR2; vascular endothelial growth factor receptor 2.

using a Biorad ChemiDoc MP Imaging System. Immunoblots were quantified via densitometry performed using LI-COR Image Studio Lite Ver 5.2. The protein band of interest was then normalised to the loading control to correct for any loading errors and results were expressed as a % change from the vehicle control unless described otherwise.

2.2.3.2 VEGF enzyme-linked immunosorbent assay (ELISA)

HPAECs were maintained in 6-well plates until 80% confluency was reached, and then incubated in EGM-2 media containing no VEGF 2 hours prior to treatment to reduce background VEGF expression. Treatments were administered in 1 ml EGM-2 media containing no VEGF, a smaller volume was used to reduce dilution of VEGF protein. The experiment was attenuated via removal and storage of the media at -80ºC. Analysis of VEGF protein in the media was performed using a Human VEGF-A Platinum ELISA according to the manufacturer's instructions. Microwell strips were washed twice with 400 µl wash buffer per well for 10 seconds with care being taken to thoroughly aspirate media between washes. Excess buffer was removed by gently tapping the microwell strips on absorbent paper towels. A human VEGF-A standard dilution was then prepared and 100 µl of each dilution was pipetted into the relevant wells. 50 µl or 100 µl of sample diluent was added to sample well or blank wells respectively prior to 50 µl of sample being added to appropriate sample wells. All samples and standards were performed in duplicate. The wells were then covered with an adhesive film and incubated at room temperature for 2 hours on a shaker (400 rpm). Biotin-conjugate was prepared via the addition of 60 - 120 µl Biotin-conjugate solution to 5.94 - 11.88 ml 1X Assay Buffer depending on the number of microwell strips being used.

Microwell strips were then washed 6 X as previously described. 100 µl of Biotin-Conjugate was then added to each well before covering the wells with an adhesive cover and incubating for 1 hour as previously described. During incubation, Streptavidin-HRP was prepared via the addition of 60 - 120 µl Streptavidin-HRP solution to 5.94 - 11.88 ml 1X assay buffer depending on the number of microwell strips being used. Post-incubation, microwell strips were washed 6 X as previously described and 100 µl of Streptavidin-HRP was added to each well before covering the wells with an adhesive cover and incubating for 1 hour before washing the microwell strips 6 X as previously described. 100 µl of TNB Substrate Solution was then pipetted into all wells and the microwell strips incubated at room temperature for 30 minutes or until the highest standard developed a dark blue colour, with care being taken to not expose the microwell strips to intense light. The reaction was then quenched by adding 100 µl Stop Solution into each well. Absorbance of each well at 450 nm was then measured immediately using a NanoDrop ND-1000 Spectrophotometer.

2.2.4 Analysis of RNA

2.2.4.1 Plasmid DNA preparation and quantification

The DNA plasmid (Table 2.2) were purchased as lyophilised plasmid and re-suspended in sterile water according to manufacturer's instructions before storage at -20ºC. Plasmids were amplified by transforming XL1-Blue *E.coli* via heat shock treatment. This involved adding 500 ng of DNA to 50 µl of thawed competent cells and incubating on ice for 30 minutes, then incubating at 42ºC for 90 seconds in a water bath, immediately followed by incubation on ice for 2 minutes. 500 µl of Luria Bertani (LB) media (1% (w/v) bactotyptone, 0.5%

cDNA	Vector	Tag	A^R	Unique restriction sites	Supplier	NCBI reference Sequence:
VEGFA-T3	pCMV3-untagged	None	Amp	Kpn1 Xba1	SB	NM_001171625.1

Table 2.2: Description of DNA plasmids

A^R; antibiotic resistance: Amp; ampicillin, NECB; National Center for Biotechnology Information, SB; sino-biological, VEGF-T3; vascular endothelial growth factor transcript 3.

(w/v) yeast extract, 1% (w/v) NaCl) was then added to the cells and the suspension incubated in a 37ºC shaker for 45 minutes. Cells were then centrifuged at 1000 g for 5 minutes after which the volume of media was reduced to the appropriate amount (1 ml/glycerol stock plus 100 µl/LB-agar plate). The cells were then re-suspended. To make glycerol stocks, 400 µl of autoclaved sterile 50% (v/v) glycerol was mixed with 1 ml of the resulting LB media and stored at -80ºC. 100 µl of the remaining LB media was spread under aseptic conditions onto LB-agar plates supplemented with ampicillin (50 µg/ml) and incubated overnight at 37ºC. If necessary, plates were then stored at 4ºC until required, though no longer than 6 weeks. A starter culture was prepared by picking of a single colony from the agar plate and inoculating 5 ml in LB media with relevant selection antibiotic (Ampicillin (50 µg/ml)) in a 37ºC shaker overnight. For a culture from glycerol stocks, 5 ml of LB media supplemented with the relevant antibiotic was inoculated with a stab of glycerol stock and incubated overnight in a 37ºC shaker.

Plasmid DNA was then extracted using the Promega Wizard *Plus* Miniprep DNA Purification System following the manufacturer's instructions. The overnight culture was centrifuged for 5 minutes at 10,000g and the resulting pellet was thoroughly resuspended in 250 µl Cell Resuspension Solution. 250 µl of Cell Lysis Solution was then added to the suspension which was inverted 4 X to mix. 10 µl of Alkaline Protease Solution was added and mixed as previously described. To cease the reaction, 350 µl of Neutralizing Solution was added to each sample and mixed as previously described. The solution was then centrifuged at maximum speed for 10 minutes at room temperature which resulted in the production of a clear lysate. This was decanted into a

spin column which had previously been inserted in to a collection tube, which was centrifuged at maximum speed for 1 minute at room temperature. Wash Solution was then prepared by the addition of 35 ml 95% ethanol to the Column Wash Solution. 750 µl of Wash Solution was added to the spin tube prior to centrifugation at maximum speed for 1 minute at room temperature. This was then repeated with 250 µl of Wash Solution. The spin tube, still inserted in a collection tube, was then centrifuged at maximum speed for 2 minute at room temperature. The spin column was then transferred to a sterile 1.5 ml centrifuge tube and centrifuged at maximum speed for 1 minute at room temperature to remove any excess Wash Solution prior to being transferred in to a fresh sterile 1.5 ml centrifuge tube. 100 µl of nuclease-free water was added to spin column which was centrifuged at maximum speed for 1 minute at room temperature. The concentration of the resulting DNA was measured via UV absorbance at 260nm/280nm (A260/280) on a Thermo Scientific™ NanoDrop Lite Spectrophotometer. A260/280 values greater than 1.8 were considered suitable for analysis. Plasmid DNA was stored at -80ºC.

2.2.4.2 Restriction enzyme digestion

Restriction enzyme digestion was performed according to the Promega Assembly of Restriction Enzymes Digestions protocol. All stages were performed on ice. 1 µg DNA was added to 2 µl of the appropriate 10X reaction buffer and 0.2 µl of acetylated BSA (10 µg/ul). The volume was made up to a total of 19.5 µl with sterile, deionized H_2O which was mixed *via* pipetting. 0.5 µl of restriction enzyme (10 u/µl) was then added before mixing gently with a pipette and centrifuged at 10,000g for 5 seconds before incubation at 37°C for

4 hours. Promega Blue/Orange 6x Loading Dye was then added to a final concentration of 1x and agarose gel analysis was performed.

2.2.4.3 RNA purifcation

HPAECs were seeded and maintained in 6 cm dishes until 80% confluent. Post-treatment RNA was isolated using a Qiagen RNeasy micro kit according to the manufacturer's instructions. Medium was removed from the HPAECs which were then lysed directly into 600 µl Buffer RLT. The lysate suspension was transferred into a microcentrifuge tube and mixed using a 1000 µl pipette tip until no cell clumps were visible. The lysate was then passed 10 times through a 20-gauge needle (0.9 mm diameter) using a RNase-free syringe. 500 - 600 µl (equal amount to the volume of lysate) 70% ethanol was then added to the lysate and mixed using a 1000 µl pipette tip. The lysate was then transferred to a RNeasy spin column placed in a 2 ml collection tube at a maximum of 700 µl at a time and centrifuged at 10,000g for 15 seconds at room temperature. The flow-through was discarded after each centrifugation. 700 µl Buffer RW1 was then added to the spin column prior to centrifugation at 10,000g for 15 seconds at room temperature. The flow through was discarded and 350 µl Buffer WB1 was added to the spin column before centrifugation at 12,000g for 15 seconds at room temperature. To reduce the risk of DNA contamination a PureLink™ DNase Set was utilised. The spin column was then transferred to a fresh collection tube prior to the addition of 80 µl DNase mix (8 µl DNase Buffer, 10 µl DNase, 62 µl RNase-free water) and incubated at room temperature for 15 minutes. RNA purification was then continued using the Qiagen RNeasy micro kit. 350 µl Buffer RW1 was then added to the spin column which was centrifuged at 12,000 g for 15 seconds at

room temperature prior to being transferred to a fresh collection tube. 500 µl Buffer RPE containing ethanol (made up as described in the manufacturer's instructions) was added to the spin column. The spin column was centrifuged at 10,000g for 15 seconds at room temperature before a final wash with 500 µl Buffer RPE and centrifugation at 10,000g for 2 minutes at room temperature. The spin column was then transferred into a fresh collection tube and centrifuged at top speed for 1 minute prior to transferring the spin column into a new collection tube. 40 µl RNase-free water was then added to the spin column which was centrifuged for at 10,000g for 1 minute at room temperature. The concentration of RNA was determined via UV absorbance at 260 nm (A260). The purity of RNA was calculated as a ratio of A260:A280, with a ratio of 2.0 indicating RNA purity. RNA was then made up to a concentration of 2 µg/10µl in RNase-free water and stored at -80ºC.

Purified RNA was reverse transcribed using an Applied Biosystems high-capacity cDNA reverse transcription kit according to the manufacturer's instructions. 10 µl 2x reverse transcriptase mastermix (2 µl 10x RT buffer, 0.8 µl 25x 100 Mm dNTP mix, 2 µl 10x RT random primer, 1 µl Multiscribe reverse transcriptase, 1 µl RNAse inhibitor, 3.2 µl nuclease-free water) was added to 10 µl of 2 µg/10 µl RNA sample. Reverse treanscription was then performed in a Techne Progene thermal cycler at 25ºC for 10 minutes, 37ºC for 2 hours and then 85ºC for 5 minutes to produce cDNA which was then made up to a concentration of 10 ng/ml in RNase-free water and stored at -80ºC. When measuring SOCS3 mRNA this was repeated with all samples in the absence of Multiscribe reverse transcriptase to ensure no contaminating genomic DNA was present. When measuring VEGF mRNA the IL-6/sIL-6Rα sample was

always repeated in the absence of Multiscribe reverse transcriptase to ensure no contaminating genomic DNA was present.

2.2.4.4 Polymerase chain reaction

1 µl of cDNA (10 ng/µl) was added to a PCR mix consisting of 5 µl Pfu buffer, 1 µl dNTP mix (10 mM), 1 µl sense primer (25 pmol/µl) (Table 2.3), 1 µl antisense primer (25 pmol/µl) (Table 2.3), 0.42 µl Pfu thermostable DNA polymerase and 40.58 µl nuclease-free water to make a total volume of 50 µl. PCR was then performed in a Techne Progene thermal cycler. VEGF primer sequences were taken from Medford et al. (2009) and checked using Clustal Omega multiple sequence alignment program. Initial denaturation was at 94ºC for 2 minutes, followed by 35 cycles of denaturation at 94ºC for 1 minutes, annealing at 43ºC for 0.5 minutes and extension at 72ºC for 3 minutes, followed by a final extension at 72ºC for 5 minutes. The resulting PCR mix was stored at 4ºC for short term use or -20ºC for long term storage before analysis by agarose gel electrophoresis.

2.2.4.5 Agarose gel electrophoresis

Agarose gels were prepared at either 1% (w/v), 1.5% (w/v) or 2% (w/v) agarose concentrations (Appendix 4) in 1X TAE buffer (40 mM Tris, 20 mM acetate, 1 mM EDTA, pH 8.6 at room temperature). SYBR safe was incorporated in to the agarose gel at a final concentration of 1X as per manufacturer's instructions to enable visualisation of nucleic acids under UV illumination. 2 µl Promega Blue/Orange 6x Loading Dye was added to 10 µl PCR product which was mixed via pipetting and loaded onto the gel. Samples were then fractionated by electrophoresis at 100 V in 1 X TAE buffer. DNA

Gene	Primer sequence
Human VEGF-A	**Sense:**5'-GAGATGAGCTTCCTACAGCAC-3' **Antisense:**5'-TCACCGCCTCGGCTTGTCACAT-3'

Table 2.3: Polymerase chain reaction primer sequences

Vascular endothelial growth factor A (VEGF-A)

fractionation was visualised under UV light and captured using a Biorad ChemiDoc MP Imaging System.

2.2.4.6 Real-time quantitative PCR

1 µl of cDNA (10 ng/µl) was added to 10 µl of Taqman Universal Master MixII, no uracil-N-glycosylase (UNG), 1 µl of the relevant probe and 8 µl of RNase free H_2O to make a total volume of 20 µl which was then added to wells on a 96-well plate. The 96-well plate was then sealed with optical adhesive film and centrifuged for 30 seconds. Real-time quantitative (q)PCR was then carried out using Stepone software according to the manufacturer's instructions. The cycle conditions for real-time qPCR were 95°C for 15 minutes, followed by 40 cycles of 95°C for 15 seconds, and 60°C for 1 minute. All assays were performed in duplicate. RNase-free water was used as a negative control. Average CT values were calculated for each sample and normalised to glyceraldehyde 3-phosphate dehydrogenase (GAPDH) which was used as a loading control. The amount of RNA was then calculated as a % of the maximum SOCS3 mRNA level.

2.2.5 Analysis of cell permeability

2.2.5.1 FITC-dextran *in vitro* vascular permeability assay

Collagen-coated transwell inserts were seeded with HPAECs at a density of $1x10^6$ cells/well and placed inside a receiver well containing EGM-2. The cells were then incubated overnight in the cell culture incubator. The same plates were then seeded with a further $1x10^6$ cells and incubated for a further 48 hours to ensure monolayer confluency. EGM-2 media containing relevant treatments were then applied to the receiver wells and the cells left to incubate

for the appropriate time before removing treatment media from the wells. 75 µl of 250 mg/ml high molecular weight FITC-dextran diluted in EGM-2 medium was added to each transwell insert. 250 µl EGM-2 medium alone was added to the receiver well. Cells were incubated for 45 minute in the cell culture incubator before the incubation was terminated by removing the inserts from the receiver well. Whilst being careful to protect the receiver medium from light to prevent photobleaching, the receiver medium was thoroughly mixed and 100 µl transferred to a 96-well opaque plate for fluorescence measurement at 485 nm excitation/535 nm emission wavelengths on a GloMax® GM3000 Luminescence Detection Plate Reader. All measurements were taken in duplicate with the mean value used for statistical analysis.

2.2.5.2 Fluorescent imaging of VE-cadherin

HPAECs were seeded on to 4-well Nunc™ Lab-Tek™ chambers at $1x10^5$ cells and incubated for 2 - 3 days in the cell culture incubator to reach 100% confluency. Post-treatment HPAECs were fixed via incubating in absolute methanol at -20ºC for 10 minutes immediately after completion of treatments. Cells were then washed with 500 µl ice- cold 0.1% v/v triton/PBS for 5 minutes prior to 2 5 minute washes in 500 µl PBS at room temperature. Cells were then blocked via incubation for 1 hour at room temperature in 1% (w/v) BSA, 2.96 M glycine in PBST (PBS + 0.1% (v/v) Tween 20) before overnight incubation in 500 µl/well 2 µg/ml anti-VE Cadherin antibody in 1% (w/v) BSA in PBST at 4ºC. Cells were then washed with 500 µl PBS room temperature 3 X 5 minutes per wash before incubation in 4 µg/ml Alexa Fluor 568-conjugated goat anti-rabbit IgG (H+L) cross-adsorbed secondary antibody, for 1 hour in the dark at room temperature. The secondary antibody was then removed, and the cells

washed with PBS at room temperature 3 X 5 minutes per wash prior to 20 minutes incubation with 500 µl 1 µM Hoechst 33342 in PBS at room temperature. Cells were then washed for 3 X 5 minutes in 500 µl ice-cold PBS before either being immediately imaged or stored in the dark at 4ºC in 500 µl PBS for no longer than 24 hours prior to imaging using a Nikon ECLIPSE TE2000-E confocal microscope. Images were taken at 400x magnification with a large pinhole, a pixel dwell of 20 millisecond and an average of 4 using EZ-C1 3.90 software. 3 images were taken for each treatment, 1 from the left, centre and right of each chamber. For representative figures, a 5 cm x 5 cm section of the image was cropped from the centre of the image using EZ-C1 3.90 freeviewer software.

2.2.6 Analysis of cell membrane stability

AS-M.5 WT and SOCS3 KO cells were seeded at a density of $6x10^4$ – $1x10^5$ cells and incubated overnight prior to treatment with either EGM-2 medium or hypotonic EGM-2 medium (1 part EGM-2 medium:9 parts sterile H_2O) containing SYTOX™ Green Nucleic Acid Stain (167 nM) and Wheat Germ Agglutinin (WGA), Alexa Fluor™ 594 Conjugate (1 µg/ml) for the appropriate before 2 X 5 minute washes in Hank's balanced salt solution (HBSS). EGM-2 medium was then added to the cells prior to immediate imaging on a Nikon ECLIPSE TE2000-E confocal microscope. Images were taken at 200x magnification with a medium pinhole, 8.64 millisecond pixel dwell and average of 2. Images were then exported in tif format for red and blue channels only to measure WGA fluorescence, and green channels only to measure SYTOX fluorescence, and analysed using ImageJ software. Average background density was calculated from three raw integrated density measurements. The

total raw integrated density was then measured and used to calculate the corrected total cell fluorescence (CTCF) via the following equation.

CTCF = integrated density – (area of selected cell X mean fluorescence of background readings)

The CTCF was calculated for all 3 images of each chamber and an average CTCF calculated. For each treatment, the CTCF value for SYTOX was then normalised against the CTCF value for WGA to correct for different cell density.

2.2.7 Statistical Analysis

All results were analysed by one-way analysis of variance followed by Bonferroni post-hoc test. Statistical analysis was performed using Graphpad Prism 5 software. Error bars on graphs represent standard error of the mean.

3. Prostanoids induce SOCS3 protein expression in endothelial cells.

3.1 Introduction

PGI_2 was first identified in the pulmonary arterioles where it inhibited platelet aggregation (Moncada et al. 1976). It was later determined that PGI_2 was also able to induce vasodilation (Dusting et al. 1978), therefore making it a prime drug target in vascular disorders. Reduced PGI_2 is characteristic of PAH (Section 1.3.4.1) and consequentially, prostanoid drugs which act by re-establishing PGI_2 signalling are currently used in the treatment of PAH (Del Pozo et al. 2017) (Section 1.6.1).

Although treatment options for PAH are limited, the prostanoid epoprostenol has shown some success in improving survival rates (Sitbon et al. 2002) and other prostanoids, such as BPS and treprostinil, have shown to be beneficial in improving exercise capacity and QOL (Simonneau et al. 2002; Barst et al. 2003).

With the exception of elevating cAMP to stimulate PKA-induced vasodilation, the mechanisms by which prostanoid-activated pathways improve patient survival rates have not been fully determined. As previously mentioned (Section 1.5), cAMP also induces SOCS3, an inhibitor of IL-6 induced JAK-STAT signalling (Sands et al. 2006; Yarwood et al. 2008), and there is growing evidence to support that IL-6 is a key factor in PAH development (Section 1.4.2).

To induce vasodilation, prostanoid drugs stimulate IP on SMCs, however the effects of prostanoids on ECs is yet to be fully investigated. Thus, to establish

if VECs respond to prostanoids and express SOCS3 protein, HPAECs were treated with BPS, treprostinil and the selexipag metabolite, ACT-333679. HPAECs were chosen as an ideal cell line as *in vivo* they are heavily involved in the vascular remodelling characteristic of PAH and, as HPAECs border the arterial lumen, they are ideally located as a potential drug target. SOCS3 protein was measured to establish if prostanoids are capable of inducing SOCS3 expression in these cell types, as SOCS3 is a key negative regulator of IL-6 signalling activity (Section 1.4.3) (reviewed by Babon et al. 2014).

3.2 Results

3.2.1 Beraprost-mediated induction of SOCS3

BPS is currently used for the treatment of PAH and has been discussed in Section 1.6.1. To investigate the effect of BPS on SOCS3 protein expression, HPAECs were treated with 10 μM BPS alongside 6 μM MG-132 at 0.5 hours, 1, 2, 4 and 8 hours. Due to the high turnover of SOCS3 protein via proteasomal degradation (Siewert et al. 1999; Haan et al. 2003), treatment with the proteasome inhibitor MG-132 (6 μM) was used to inhibit the degradation of SOCS3 when measuring SOCS3 protein expression (Haan et al. 2003; Wiejak et al. 2013). As Fsk, which directly binds and activates AC isoforms (Seamon et al. 1981), has previously been shown to induce SOCS3 (Woolson et al. 2009; Wiejak et al. 2013; Piao et al. 2014; Wiejak et al. 2019), Fsk (50 μM) in combination with MG-132 (6 μM) was used as a positive control for SOCS3 induction. MG-132 (6 μM) alone was used as a negative control. Cells were then harvested and lysed as previously described (Section 2.2.3.1) before protein content was determined. Immunoblotting was carried out and the

membranes were probed for SOCS3. STAT3 used as a loading control for protein content. Nur77, which is the product of a gene upregulated by cAMP via a PKA/cAMP responsive element binding protein (CREB)-dependent mechanism independent of EPAC1 (Fass et al. 2003; Hamid et al. 2008; Martin et al. 2008; Martin et al. 2009), was used as a positive control to ensure cAMP-mobilising drugs were active for experiments investigating cAMP-mediated changes in protein expression.

Fsk alongside MG-143 produced a significant accumulation of SOCS3 and Nur77 after 4 hours of treatment. A time-dependent transient increase of SOCS3 protein expression occurred post-BPS treatment which was significant after 2 hours and 4 hours of treatment (Figure 3.1), whilst Nur77 protein expression was significantly increased after 2 hours only. Although increased at 1 and 8 hours after BPS treatment, expression of SOCS3 was not significant at these time points. As 2 hours of BPS treatment significantly increased SOCS3 protein expression, cells were treated for 2 hours with BPS for all future experiments unless stated otherwise.

3.2.2 Treprostinil-mediated induction of SOCS3

Treprostinil is currently approved worldwide for the treatment of PAH and has been discussed in Section 1.6.1. To investigate the effect of treprostinil on SOCS3 protein expression, HPAECs were treated with 10 μM treprostinil for 1 hour, 2 and 4 hours alongside MG-132 (6 μM). 4 hours treatment with Fsk (50 μM) alongside MG-132 (6 μM) was used as a positive control. 4 hours treatment with MG-132 (6 μM) alone was used as a negative control.

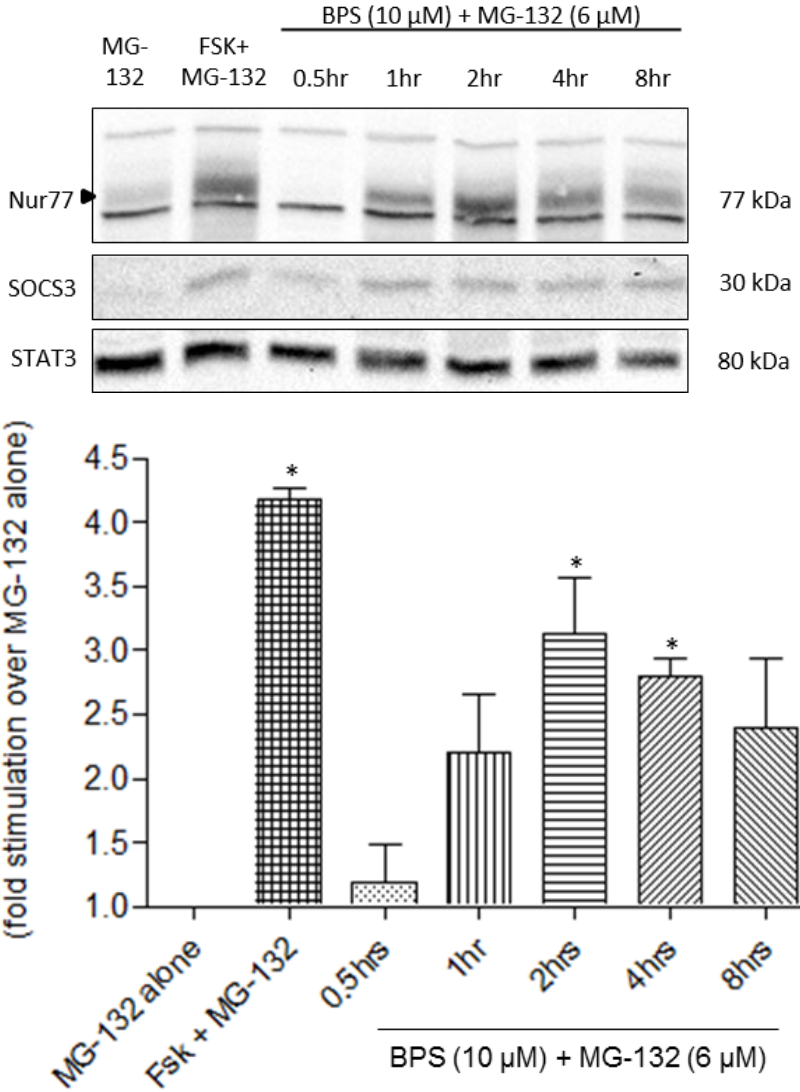
BPS (10 µM) + MG-132 (6 µM)
MG-132
FSK+ MG-132
0.5hr
1hr
2hr
4hr
8hr
Nur77
77 kDa
SOCS3
30 kDa
STAT3
80 kDa
SOCS3 protein expression (fold stimulation over MG-132 alone)
4.5
4.0
3.5
3.0
2.5
2.0
1.5
1.0
*
*
*
MG-132 alone
Fsk + MG-132
0.5hrs
1hr
2hrs
4hrs
8hrs
BPS (10 µM) + MG-132 (6 µM)
Nur77 protein expression (fold stimulation over MG-132 alone)
7
6
5
4
3
2
1
**
**
MG-132 alone
Fsk + MG-132
0.5hrs
1hr
2hrs
4hrs
8hrs
BPS (10 µM) + MG-132 (6 µM)

Figure 3.1: Beraprost-mediated time-dependent induction of SOCS3

HPAECS were treated with beraprost sodium salt (BPS) (10 μM) for 0.5 hours, 1, 2, 4 and 8 hours in the presence of MG-132 (6 μM). 4 hour treatment with forskolin (Fsk) (50 μM) and MG-132 (6 μM) was used as a positive control. 4 hour treatment with MG-132 (6 μM) only was used as a negative control. Whole cell lysates were equalised for protein content and resolved via SDS-PAGE for immunoblotting with the indicated antibodies. Levels of SOCS3 and Nur77 were normalised and measured as a fold difference compared to treatment with MG-132 alone. * indicates $p<0.05$ versus MG-132 treatment only, ** indicates $p<0.01$. Quantification for *n=4* experiments is shown.

Fsk significantly induced SOCS3 and Nur77 protein expression after 4 hours of treatment. Significant induction of SOCS3 was achieved after 1 hour, 2 and 4 hours of treatment with treprostinil, with maximum induction occurring 2 hours post-treatment (Figure 3.2). Significant induction of Nur77 protein was detectable after 2 and 4 hours of treatment. As a result, cells were treated with treprostinil for 2 hours in all future experiments unless indicated otherwise.

3.2.3 Selexipag-mediated induction of SOCS3

Selexipag, discussed in Section 1.6.1, if the first oral synthetic selective IP agonist developed (reviewed by Duggan et al. 2017). Selexipag is a pro-drug and is metabolised in vivo to ACT-333679 by carboxylesterase 1. As SOCS3 induction experiments were performed on HPAECs *in vitro*, cells were treated with the active metabolite ACT-333679 instead of selexipag in all experiements. HPAECs were treated with 1 μM ACT-333679 for 1 hour, 2 and 4 hours alongside MG-132 (6 μM). 4 hours of treatment with Fsk (50 μM) alongside MG-132 (6 μM) was used as a positive control. 4 hours of treatment with MG-132 (6 μM) alone was used as a negative control. Cells were harvested and lysed (Section 2.2.3.1) before protein content was determined and immunoblotting was carried out to assess SOCS3 and Nur77 induction, with STAT3 used as a loading control.

Fsk significantly induced SOCS3 and Nur77 protein expression after 4 hours of treatment. Significant induction of SOCS3 was achieved only after 4 hours of ACT-333679 stimulation (Figure 3.3) while Nur77 was significantly induced after 2 and 4 hours of treatment (Figure 3.3). Based on these resuls, cells were treated with ACT-333679 for 4 hours in all future experiments unless indicated otherwise.

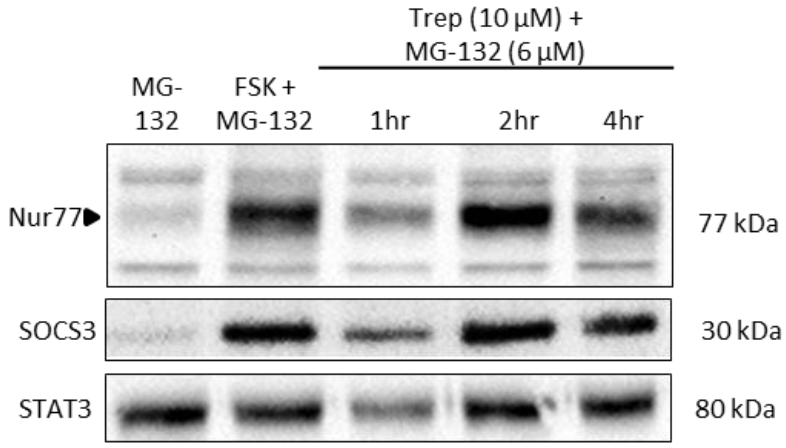
Trep (10 µM) +
MG-132 (6 µM)
MG-
132
FSK +
MG-132
1hr
2hr
4hr
Nur77
77 kDa
SOCS3
30 kDa
STAT3
80 kDa

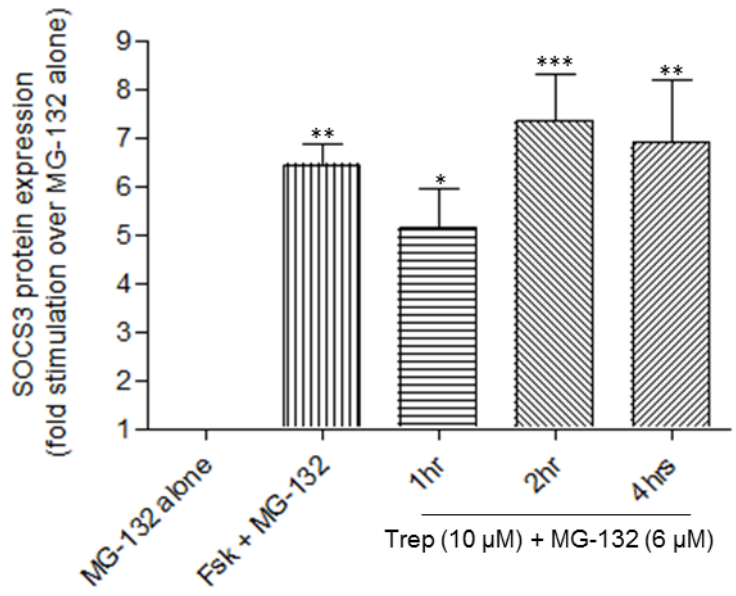
SOCS3 protein expression
(fold stimulation over MG-132 alone)
MG-132 alone
Fsk + MG-132
1hr
2hr
4hrs
Trep (10 µM) + MG-132 (6 µM)

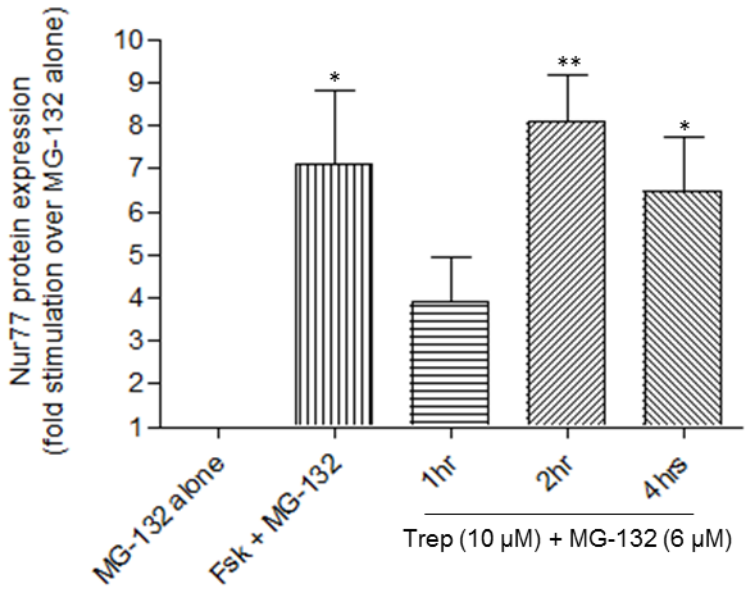
Nur77 protein expression
(fold stimulation over MG-132 alone)
MG-132 alone
Fsk + MG-132
1hr
2hr
4hrs
Trep (10 µM) + MG-132 (6 µM)

Figure 3.2: Treprostinil-mediated induction of SOCS3

HPAECS were treated with treprostinil (Trep) (10 μM) for 1 hour, 2 and 4 hours in the presence of MG-132 (6 μM). 4 hour forskolin (Fsk) (50 μM) and MG-132 (6 μM) treatment was used as a positive control. MG-132 (6 μM) alone was used as a negative control. Whole cell lysates were then equalised for protein content and resolved via SDS-PAGE for immunoblotting with the indicated antibodies. Levels of SOCS3 and Nur77 were measured as a fold difference compared to treatment with MG-132 alone. * indicates $p<0.05$ versus treatment with MG-132 alone, ** indicates $p<0.01$, *** indicates $p<0.001$. Quantification for *n=4* experiments is shown.

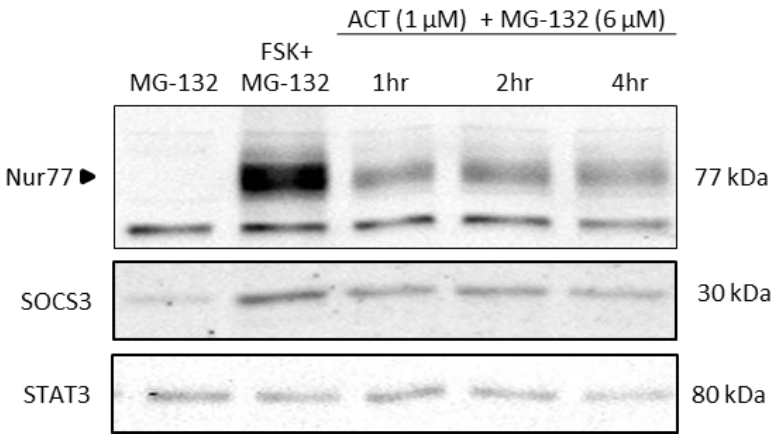
ACT (1 μM) + MG-132 (6 μM)
MG-132
FSK+ MG-132
1hr
2hr
4hr
Nur77
77 kDa
SOCS3
30 kDa
STAT3
80 kDa

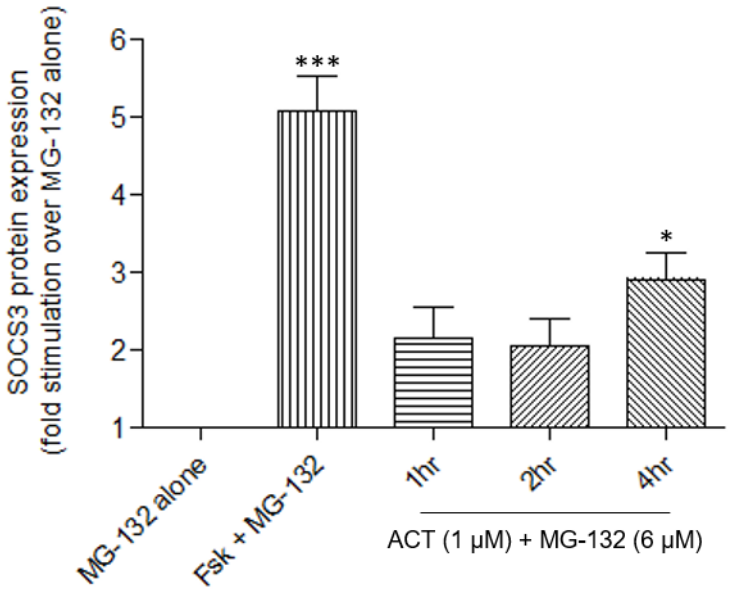
SOCS3 protein expression
(fold stimulation over MG-132 alone)
***
*
MG-132 alone
Fsk + MG-132
1hr
2hr
4hr
ACT (1 μM) + MG-132 (6 μM)

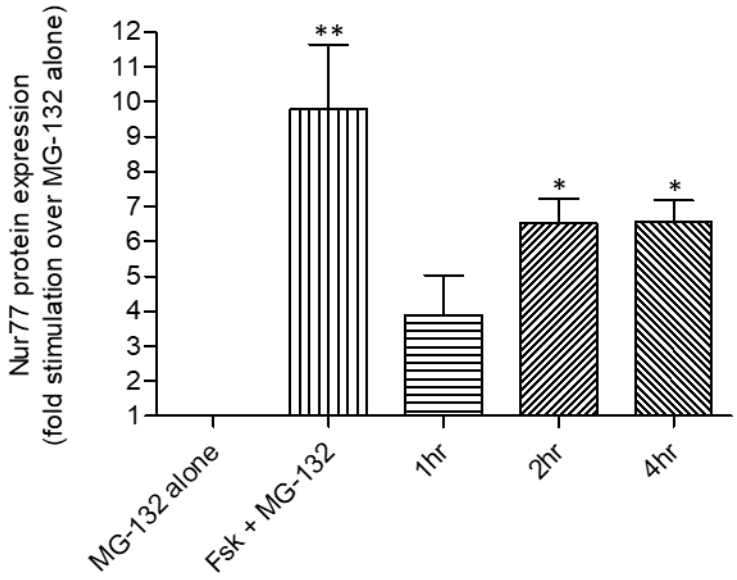
Nur77 protein expression
(fold stimulation over MG-132 alone)
**
*
*
MG-132 alone
Fsk + MG-132
1hr
2hr
4hr

Figure 3.3: ACT-333679-mediated time-dependent induction of SOCS3

HPAECS were treated with ACT-333679 (1 μM) for 1 hour, 2 and 4 hours in the presence of MG-132(6 μM). 4 hour forskolin (Fsk) (50 μM) and MG-132 (6 μM) treatment was used as a positive control. 4 hour MG-132 (6 μM) alone was used as a negative control. Whole cell lysates were then equalised for protein content and resolved via SDS-PAGE for immunoblotting with the indicated antibodies. Levels of SOCS3 and Nur77 were measured as a fold difference compared to treatment with MG-132 alone. * indicates $p<0.05$ versus treatment with MG-132 alone, ** indicates $p<0.01$. Quantification for *n=4* experiments is shown.

3.2.4 Prostanoid induction of SOCS3 in human pulmonary microvascular endothelial cells.

Vascular remodelling in PAH typically occurs in the small pulmonary arterioles and veins located in the lungs (reviewed by Tuder 2017). Thus HPMECs, which line the capillaries and venules within the lungs, are another key cell type involved in the vascular remodelling characteristic of PAH. To establish if HPMECs respond to prostanoids in the same manner as HPAECs, prostanoid induction of SOCS3 was measured in HPMECs.

HPMECs were treated with BPS, treprostinil and ACT-333679 for the optimum time points as identified in time course experiments in HPAECs (Sections 3.2.1 – 3.2.3). 4 hours of treatment with Fsk (50 μM) alongside MG-132 (6 μM) was used as a positive control. 4 hours of treatment with MG-132 (6 μM) alone was used as a negative control.

Fsk significantly induced SOCS3 and Nur77 protein expression after 4 hours of treatment. Similar to the response seen in HPAECs, BPS, treprostinil and ACT-333679 significantly induced SOCS3 in HPMECs (Figure 3.4). Likewise, BPS and treprostinil significantly induced Nur77 expression after 2 hours of treatment in HPMECs. 4 hours treatment with ACT-33679 did not result in significant accumulation of Nur77 (Figure 3.4).

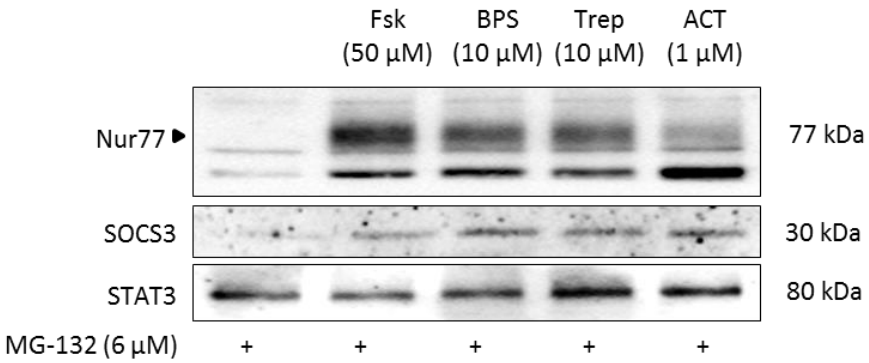
Fsk
(50 µM)
BPS
(10 µM)
Trep
(10 µM)
ACT
(1 µM)
Nur77
77 kDa
SOCS3
30 kDa
STAT3
80 kDa
MG-132 (6 µM)
+
+
+
+
+

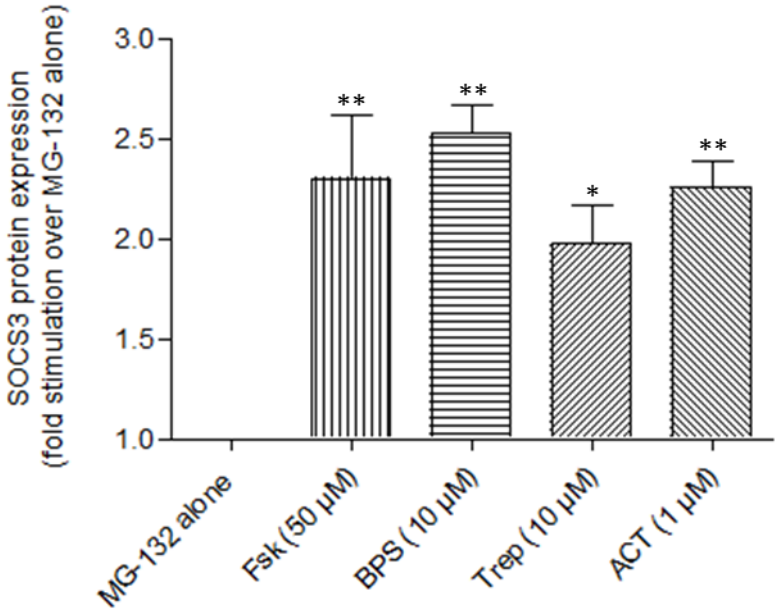
SOCS3 protein expression
(fold stimulation over MG-132 alone)
3.0
2.5
2.0
1.5
1.0
**
**
*
**
MG-132 alone
Fsk (50 µM)
BPS (10 µM)
Trep (10 µM)
ACT (1 µM)

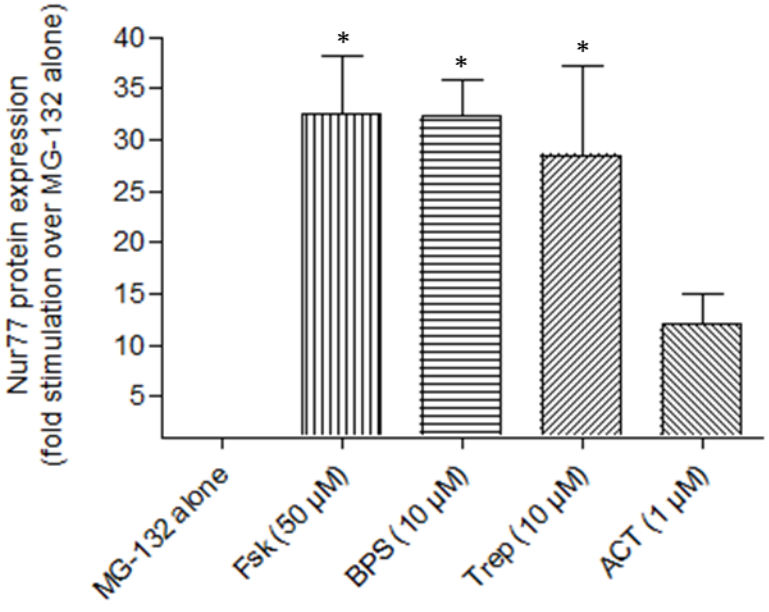
Nur77 protein expression
(fold stimulation over MG-132 alone)
40
35
30
25
20
15
10
5
*
*
*
MG-132 alone
Fsk (50 µM)
BPS (10 µM)
Trep (10 µM)
ACT (1 µM)

Figure 3.4: Prostanoid-mediated induction of SOCS3 in human pulmonary microvascular endothelial cells

HPMECS were treated with beraprost sodium salt (BPS) (10 μM) or treprostinil (Trep) (10 μM) for 2 hours, or the selexipag metabolite ACT-333679 (ACT) (1 μM) for 4 hours in the presence of MG-132 (6 μM). 4 hour treatment with forskolin (Fsk) (50 μM) alongside MG-132 (6 μM) was used as a positive control. MG-132 (6 μM) alone was used as a negative control. Whole cell lysates were equalised for protein content and seperated via SDS-PAGE for immunoblotting with the indicated antibodies. Levels of SOCS3 and Nur77 were measured as a fold difference compared to treatment with MG-132 alone. * indicates $p<0.05$ versus treatment with MG-132 alone, ** indicates $p<0.01$, **** indicates $p<0.0001$. Quantification for *n=4* are shown.

3.2.5 Prostanoid-mediated induction of SOCS3 mRNA.

To determine if the effects of prostanoids on SOCS3 protein expression were due an increase of SOCS3 mRNA, RT-qPCR was performed as previously described (Section 2.2.4.6) on RNA purified from BPS-treated HPAECs. HPAECs were treated with 10 μM BPS at 0 hours, 0.5, 1, 2 and 4 hours. 1 hour Fsk treatment was used as a positive control with vehicle as a negative control. Glyceraldehyde 3-phosphate dehydrogenase (GAPDH) was used to normalise the results. The C_T value of each treatment was then and expressed as a fold difference of the vehicle control.

BPS triggered a rapid and significant increase in SOCS3 mRNA, detectable at the earliest time point (30 minutes) and sustained for 60 minutes. However the increase was transient as mRNA levels returned to basal levels after 2 hours and for at least 4 hours (Figure 3.5A).

For previous experiments in which SOCS3 protein expression has been measured (Section 3.2.1 – 3.2.4), cells were treated with the proteasome inhibitor MG-132 in order to maximise detection of SOCS3. To ensure the effect of MG132 was not due to any unanticipated effect on SOCS3 gene expression, cells were treated with BPS (10 μM) or Fsk (50 μM) for 1 hour in the presence and absence of MG-132 prior to harvesting cells. A vehicle treatment was used as a negative control. This has been shown as a bar graph for easier comparison between treatments with and without MG-132. The presence of MG-132 had no significant effect on SOCS3 mRNA levels either on its own or in combination with BPS or Fsk (Figure 3.5B). Thus, the effect of MG-132 on potentiation of prostanoid-mediated SOCS3 induction was

A

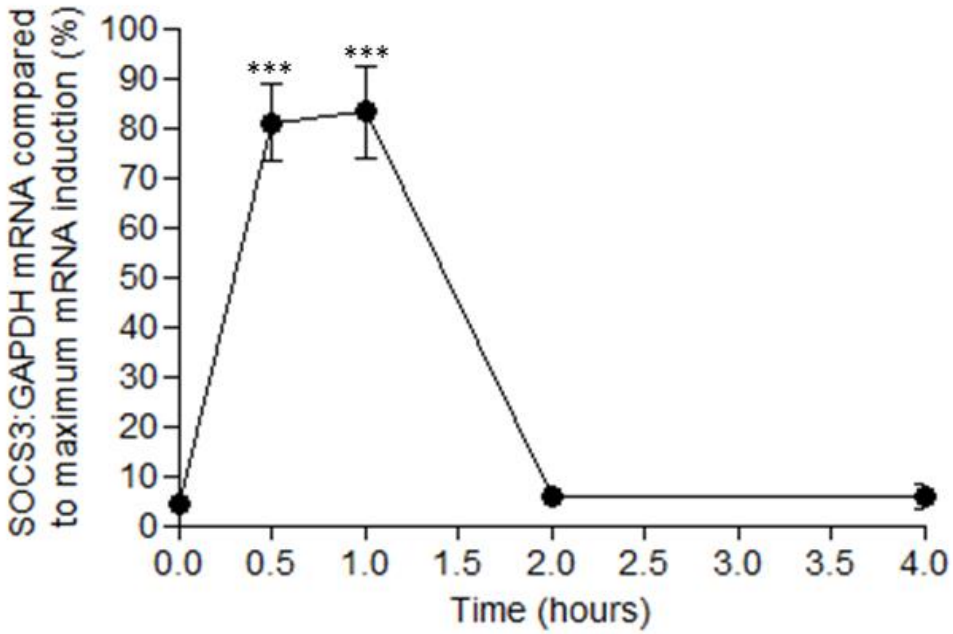
SOCS3:GAPDH mRNA compared to maximum mRNA induction (%)
100
90
80
70
60
50
40
30
20
10
0
***
***
0.0
0.5
1.0
1.5
2.0
2.5
3.0
3.5
4.0
Time (hours)

B

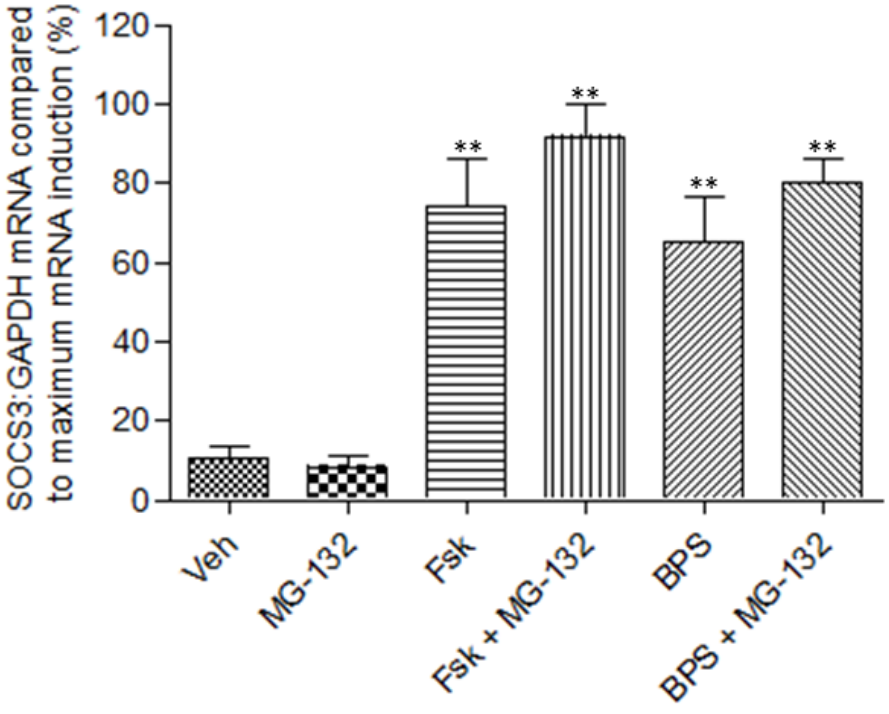
SOCS3:GAPDH mRNA compared to maximum mRNA induction (%)
120
100
80
60
40
20
0
**
**
**
**
Veh
MG-132
Fsk
Fsk + MG-132
BPS
BPS + MG-132

Figure 3.5: Prostanoid-mediated induction of SOCS3 gene expression

A) HPAECs were treated with beraprost sodium (BPS) (10 μM) for 0 hours, 0.5, 1, 2 and 4 hours. RNA was then purified for reverse transcription and analysis by real time – qPCR. GAPDH values were used to normalise the results. The C_T value of each treatment was calculated and expressed as a fold difference compared to the vehicle control. *** indicates P<0.001 versus treatment with BPS for 0 hours. Quantification for *n=4* is shown. B) HPAECS were treated with MG-132 (6 μM) alone for 1 hour and for 1 hour with either BPS (10 μM) or forskolin (Fsk) (50 μM) in the presence and absence of MG-132 (6 μM). A vehicle (Veh) treatment was used as a negative control. RNA was then purified for reverse transcription and analysis by real time – qPCR. The level of SOCS3 mRNA was normalised to GAPDH concentrations and expressed as a percentage of the maximum SOCS3 mRNA expression level. ** indicates p<0.01 versus SOCS3 mRNA levels post-vehicle treatment.

independent of any effect on SOCS3 mRNA levels and consistent with stabilisation of SOCS3 protein.

3.2.6 Identifying the signalling pathway in prostanoid induction of SOCS3

As experiments have shown prostanoids to increase SOCS3 protein expression in relevant cell types, it is important to identify the key receptors and proteins involved.

BPS is an IP agonist, whereas treprostinil has been shown to demonstrate affinity for IP and EP_2 (Whittle et al, 2012), and selexipag is a highly selective, potent IP agonist (Kuwano et al., 2007). To investigate if treprostinil acts via EP_2 in prostanoid induction of SOCS3, HPAECs were treated with prostanoids in the presence and absence of the EP_2 selective antagonist PF-04418948 (10 μM) (Forselles et al., 2011). Cells were treated with PF-04418948 30 minutes prior to treatment with either BPS, treprostinil of ACT-333679. Fsk (50 μM) treatment in the presence and absence of PF-04418948 (10 μM) was also performed. As Fsk is cell permeable and acts directly on AC, treatment with Fsk should not be affected by PF-04418948. Thus, it was used to ensure treatment with PF-04418948 had no effect on signalling downstream from AC. For easy comparison between protein expression induced by the drug in the presence and absence of PF-04418948, the results have been shown as expression by drug alone, set at 1, with the drug alongside PF-04418948 expressed as fold difference to this.

In none of the treatments did PF-04418948 inhibit prostanoid induction of SOCS3 or Nur77 when compared to treatment with the agonist alone (Figure 3.6), suggesting all the prostanoids are able to activate receptors other than

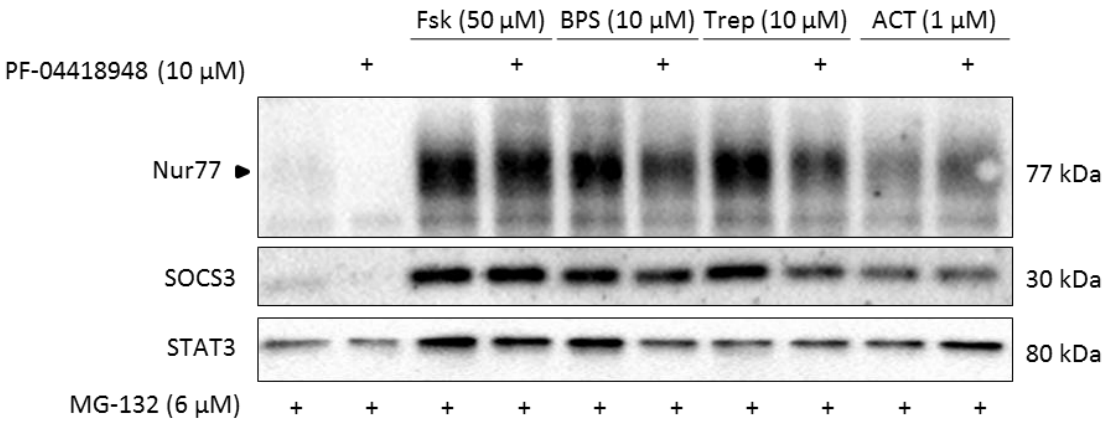
Fsk (50 µM)
BPS (10 µM)
Trep (10 µM)
ACT (1 µM)
PF-04418948 (10 µM)
Nur77
77 kDa
SOCS3
30 kDa
STAT3
80 kDa
MG-132 (6 µM)

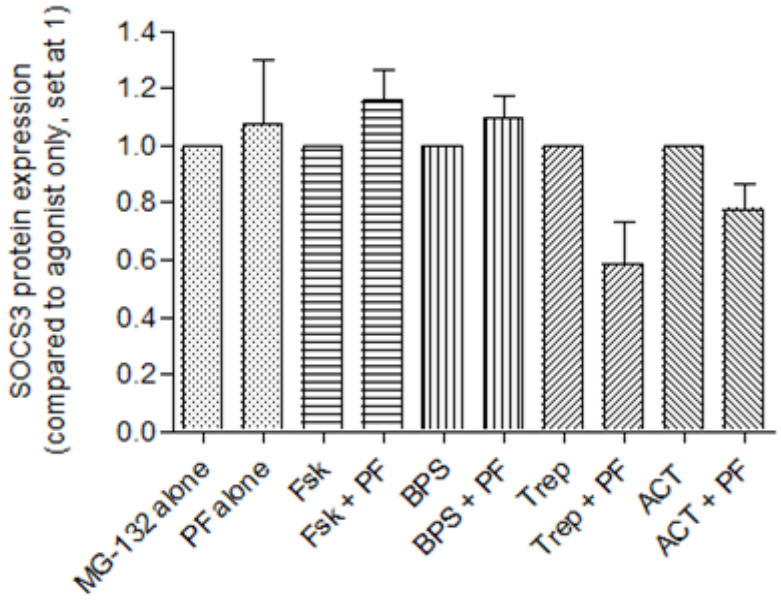
SOCS3 protein expression
(compared to agonist only, set at 1)
1.4
1.2
1.0
0.8
0.6
0.4
0.2
0.0
MG-132 alone
PF alone
Fsk
Fsk + PF
BPS
BPS + PF
Trep
Trep + PF
ACT
ACT + PF

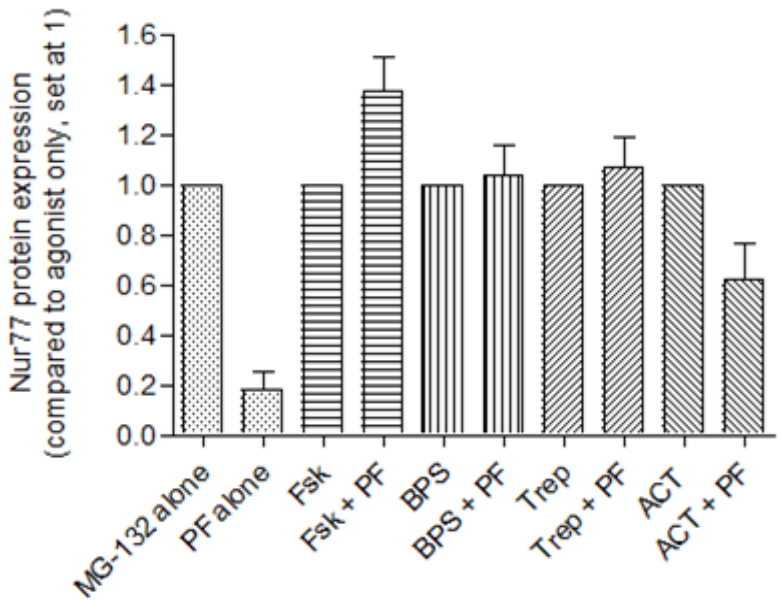
Nur77 protein expression
(compared to agonist only, set at 1)
1.6
1.4
1.2
1.0
0.8
0.6
0.4
0.2
0.0
MG-132 alone
PF alone
Fsk
Fsk + PF
BPS
BPS + PF
Trep
Trep + PF
ACT
ACT + PF

Figure 3.6: The EP-2-selective antagonist PF-04418948 has no effect on prostanoid induction of SOCS3

HPAECs were treated with beraprost sodium salt (BPS) (10 μM) for 2 hours, Treprostinil (Trep) (10 μM) for 2 hours, or ACT-333679 (ACT) (1 μM) for 4 hours in the presence or absence of the EP-2 receptor antagonist PF-04418948 (PF) (10 μM). 4 hour treatment with forskolin (Fsk) (50μM) in the presence and absence of PF was used to ensure there was no downstream effect of PF. All treatments were given alongside MG-132 (6 μM). Treatment with MG-132 (6 μM) or PF (10 μM) alone for 4 hours were used as negative controls. Cells were treated with PF-04418948 30 minutes prior to prostanoid treatment. Whole cell lysates were then equalised for protein content and resolved via SDS-PAGE for immunoblotting with the indicated antibodies. Levels of SOCS3 and Nur77 after PF-04418948 (10 μM) treatment were measured as a fold difference compared to treatment with the relevant agonist only (set at 1). Quantification for *n=5* experiments is shown.

EP_2 sufficiently to elevate cAMP and induce SOCS3 gene expression. As treprostinil shows greater affinity to EP_2 than the other drugs measured, we would expect to see some reduction in treprostinil-mediated induction of SOCS3 in the presence of PF-04418948 and although it does appear less, statistical analysis showed this not to be significant.

A large body of research has suggested that cAMP-mediated induction of SOCS3 occurs via a PKA-independent, EPAC1-dependent mechanism (Gasperini et al. 2002; Sands et al. 2006; Borland et al. 2009; Woolson et al. 2009; Wiejak et al. 2019). However, whether prostanoid induction of SOCS3 in HPAECs is via EPAC1 has not been investigated. To address this, SOCS3 protein expression was measured after treatment with either EPAC or PKA activators alone or in combination.

HPAECs were treated with the EPAC activator 8-CPT-2Me-cAMP sodium salt (8-CPT) (200 μM) or with PKA activator 6-Bnz-cAMP sodium salt (6-Bnz) (100 μM) for 4 hours in the presence of MG-132 (6 μM). The combined stimulatory effects of treatment with 8-CPT (200 μM) and 6-Bnz (100 μM) alongside MG-132 (6 μM) was also investigated (Figure 3.7A). Cells were treated with Fsk (10 μM) alone or in the presence of the PKA inhibitor myrPKI14-22 amide (PKI) (1 μM) to determine the role of PKA in Fsk induction of SOCS3 in HPAECs. PKI was administered 30 minutes prior to Fsk treatment. Treatment with MG-132 (6 μM) alone and PKI (1 μM) alone were used as negative controls.

Neither the EPAC activator (8-CPT) or PKA activator (6-Bnz) alone or in combination significantly induced SOCS3 under conditions in which significant induction by Fsk was detectable (Figure 3.7A). Consistent with previous

A

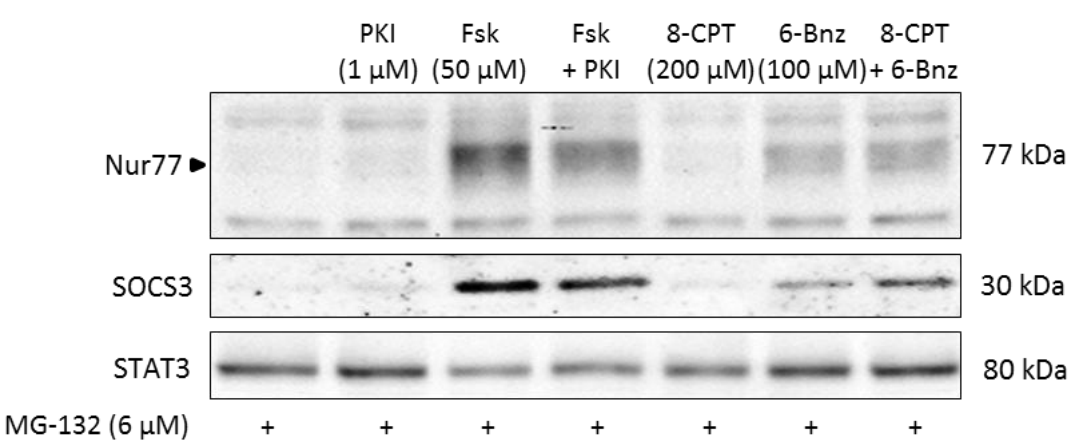

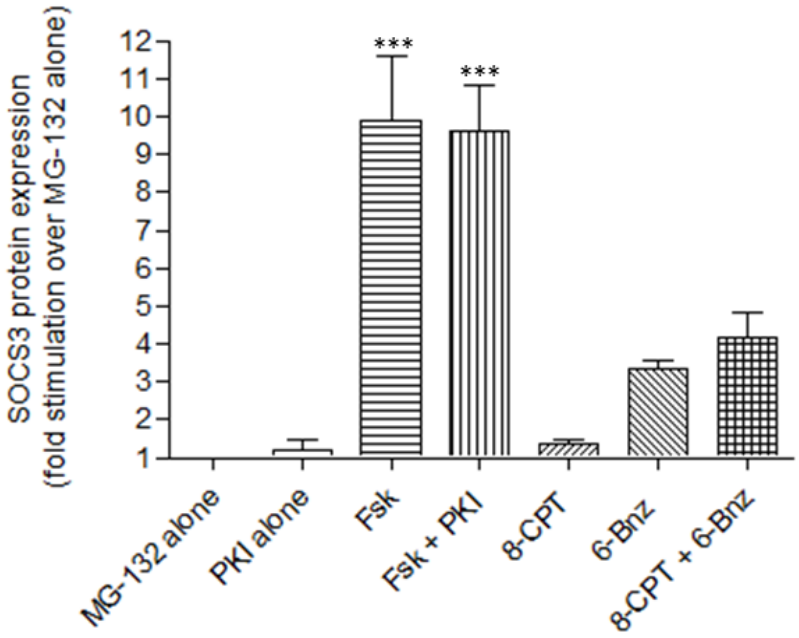

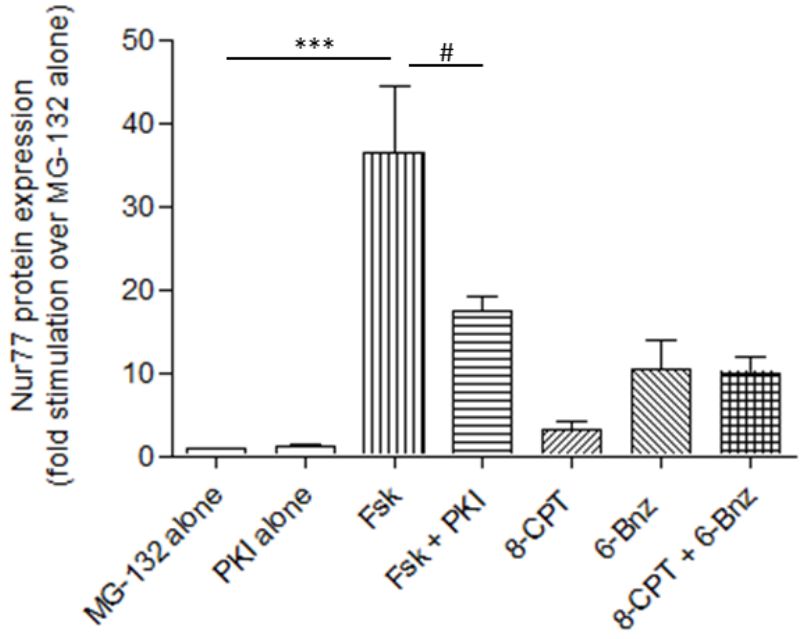

Figure continued on next page.

B

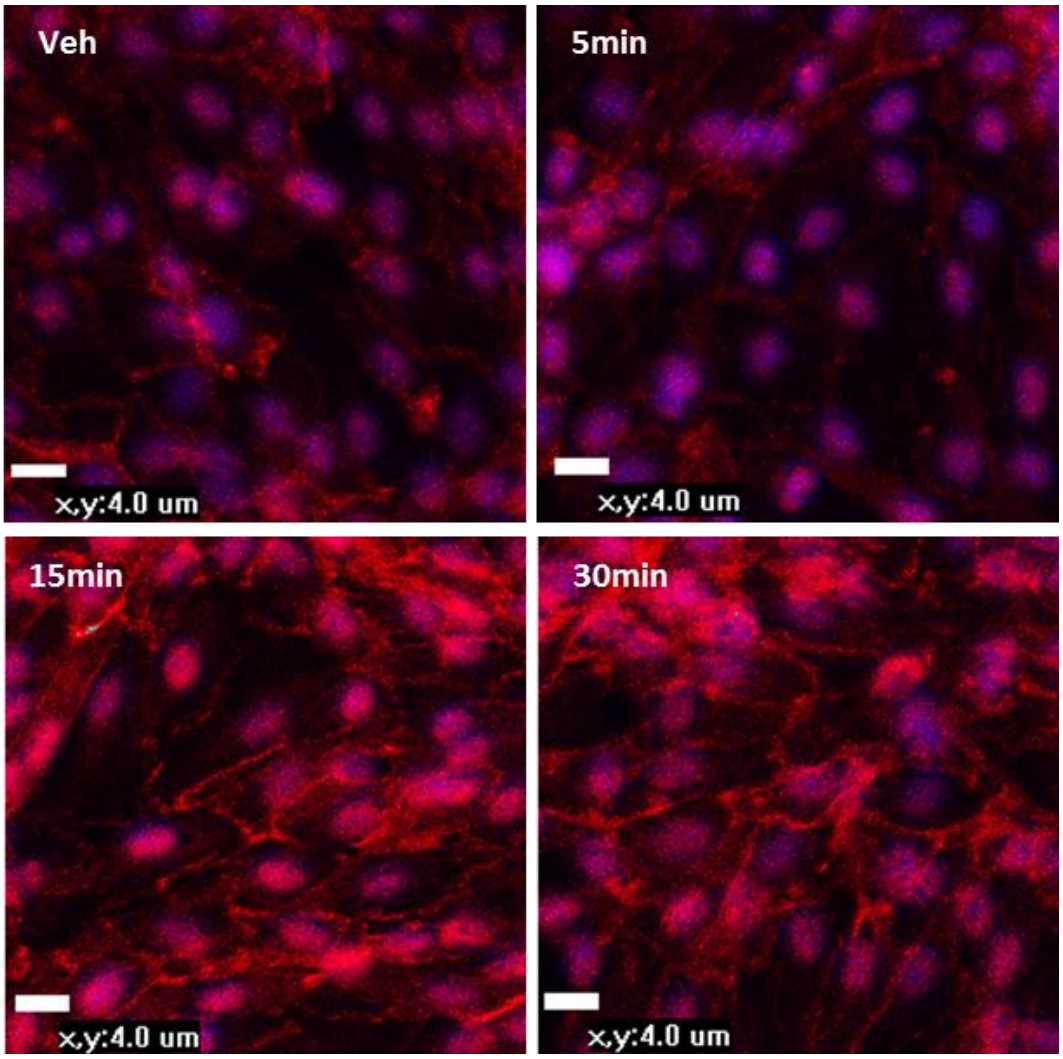

Figure 3.7: Induction of SOCS3 by forskolin in HPAECs does not require EPAC or PKA

A) HPAECS were treated for 4 hours with 8-CPT-2Me-cAMP (8-CPT) (200 μM), 6-Bnz-cAMP sodium salt (6-Bnz) (100 μM), or both in the presence of MG-132 (6 μM). 4 hour treatment with forskolin (Fsk) (50 μM) with MG-132 (6 μM) was used as a positive control. Treatment with Fsk in the presence of MG-132 (6 μM) and myristoylated PKI 14-22 amide (PKI) (1 μM) was used to measure the effect of PKA. PKI was administered 30 minutes prior to Fsk treatment. MG-132 (6 μM) only and PKI (1 μM) only treatments were used as negative controls. Whole cell lysates were then equalised for protein content and resolved via SDS-PAGE for immunoblotting with Nur77 and SOCS3. Immunoblotting with STAT3 was used for a loading control. The concentration of SOCS3 and Nur77 was measured as a fold difference compared to MG-132 only treatment. Quantification for *n=4* has been shown. * indicates $p<0.05$ versus treatment with MG-132 alone, ** indicates $p<0.01$, *** indicates $p<0.001$, # indicates $p<0.05$ versus treatment with Fsk. B) HPAECs were treated with 8-CPT (200 μM) for 5 minutes, 15 and 30 minutes prior to fixing in methanol as previously described. A 30 minute vehicle treatment was used as a positive control. Fixed cells were stained with VE-cadherin (red) and nuclear stain Hoescht 33342 (blue) prior to confocal imaging. These data are representative of *n=2* experiments which produced similar results.

findings (Sands et al. 2006; Yarwood et al. 2008; Wiejak et al. 2019), pharmacological inhibition of PKA had no effect on Fsk-mediated induction of SOCS3, but significantly reduced induction of PKA/CREB target gene product Nur77, thereby demonstrating that PKI effectively inhibited PKA under our experimental conditions but that this had no impact on SOCS3 expression. Together these data suggest that prostanoid induction of SOCS3 cannot be recapitulated by activation of EPAC and PKA.

EPAC is known to increases VE-cadherin localisation to cell junctions (Fukuhara et al. 2005; Kooistra et al. 2005), thus to ensure the EPAC activator was active, the effect of 8-CPT (200μM) on localising VE-cadherin expression to cell junctions was assessed by confocal imaging. Cell junction expression of VE-cadherin was increased after 15 and 30 minute treatments with 8-CPT suggesting that it is active under these conditions (Figure 3.7B).

3.3 Discussion

Treatment with both BPS and treprostinil resulted in time-dependent induction of SOCS3 in HPAECS that was significant after 2 hours (Figures 3.1 and 3.2). ACT-333679, the pro-drug of a recently developed synthetic analog, also increased SOCS3 expression after 4 hours of treatment (Figure 3.3). Results were similar in HPMECs, ECs isolated from different microvessles involved in the vascular remodelling characteristic of PAH, in which both prostanoids and ACT-333679 induced SOCS3 after the same treatment time (Figure 3.4). In HPAECs, data derived from RT-qPCR demonstrated that this is due to a robust but transient prostanoid-mediated increase in SOCS3 mRNA (Figure 3.5).

Previous studies have shown cAMP mobilising drugs, in this case a PGE_2 agonist, to increase SOCS3 transcription in THP-1 cells (Cheon et al. 2006). Thus, it is probable BPS is working in the same manner as opposed to altering SOCS3 RNA degradation or turnover. To confirm this, actinomycin D, a transcriptional inhibitor, could be incorporated into future experiments as described by Cheon et al. (2006). Additionally, a reporter gene assay in which HPAECs are transfected with constructs in which the expression of luciferase is under control of the human SOCS3 promoter would allow measurement of SOCS3 gene transcription via luciferase activity. This method has previously been used in HUVECs to determine a role for the AP1 transcription factor in forskolin/rolipram and 8-pCPT, but not 6-Bnz, mediated increase in SOCS3 promoter activity (Wiejak et al. 2014).

As prostanoids stimulate the production of cAMP via activation of AC (Boskey et al. 1996) this is most likely due to cAMP-mediated induction of SOCS3. In the case of BPS and treprostinil, these experiments supported this hypothesis, as protein expression of Nur77, a highly responsive PKA activated gene and a measure of cAMP activity (Hamid et al. 2008), was also increased post-treatment (Figures 3.1 and 3.2). With regards to ACT-333679, although still significantly increased compared to the negative control, Nur77 protein expression was comparably less than the level of induction observed with either BPS or treprostinil. In contrast to the other prostanoid drugs, ACT-333679 did not significantly induce Nur77 protein expression in HPMECs compared to basal levels.

This could be due to prostanoids activating a range of different prostaglandin, and other, receptors, whereas ACT-333679 is highly selective for IP (Kuwano

et al., 2007). Treprostinil in particular appears to show a high affinity to EP_2 (3.6 nM compared to 1172 nM for ilaprost) (Whittle et al. 2012) and recent research in HPASMCs has shown that the anti-proliferative effects of treprostinil, but not ACT-333679, are due to activation of EP_2 (Patel et al. 2018) as opposed to IP which is the primary receptor for beraprost and ACT. In addition, treprostinil has been shown to exerts its anti-proliferative effects in PASMCs isolated from MCT-rat models and in human lung fibroblasts via PPAR, although reports disagree on whether this via PPARβ or PPARγ (Ali et al. 2006; Lai et al. 2009). This may suggest a tissue specific PPAR response to treprostinil.

To determine if treprostinil is acting via EP_2 receptors, we used an EP_2 antagonist (PF-04418948) to assess its role in prostanoid-mediated induction of SOCS3 in HPAECs. Results suggest EP_2 is not required for SOCS3 induction by either BPS, treprostinil or ACT-333679 (Figure 3.6). However, no positive control was included to ensure the EP_2 antagonist was active, thus further experimentation is required to ensure the EP_2 selective antagonist is active in the conditions used. For instance, determining the effect of PF-04418948 on (R)-Butaprost-mediated induction of Nur77 under the same conditions (PF-04418948 (10 μM) treatment 30 minute prior to treatment with (R)-Butaprost in HPAECs). (R)-Butaprost (Abcam; Cat. No. Ab144476), is a selective EP_2 antagonist. If PF-04418948 is found to be active under these conditions, a dose-concentration course and time course of PF-04418948 inhibition of (R)-Butaprost-induced Nur77 expression could be utilised to determine the optimal conditions for PF-04418948 antagonism in HPAECs prior to repeating the experiment. Additionally, the use of an IP-selective

antagonist such as Ro 1138452 hydrochloride (Bley et al., 2006) would provide further information regarding the role of the IP in BPS, treprostinil, and ACT-333679-mediated SOCS3 and Nur77 induction.

As well as prostanoids acting on different receptor subtypes, there may also be cell-specific differences in the receptors expressed. RT-PCR could be performed to identify the different prostaglandin receptor subtypes expressed in HPAECs and HPMECs, and to investigate the balance of prostaglandin receptors versus non- prostaglandin receptors activated by prostanoids such as PPARs.

Combined, these experiments would build a picture of the different receptor subtypes being activated in a cell-specific manner. Identifying the primary prostanoid receptors responsible for the induction of SOCS3 would not only provide a new mechanism of action for existing prostanoid use in PAH treatment but potentially provide new therapeutic targets for the future development of drugs aimed at reducing the pulmonary vascular inflammation involved in disease progression. Establishing the predominant signalling pathway utilised by prostanoids is important for this aim.

As previously mentioned, it is well established that prostanoids modulate cAMP activity depending on the prostanoid receptor subtype they activate (Boskey et al. 1996; Tsuboi et al. 2002). Research suggests cAMP induction of SOCS3 has been shown to occur via EPAC1 in COS1 cells (Borland et al. 2009), HUVECs (Yarwood et al. 2008), and human aortic endothelial cells (Babon et al. 2008). Additionally, in HUVECs, the EPAC agonist I942 was shown to suppress IL-6/sIL-6Rα induced JAK/STAT signalling and

consequential expression of inflammatory genes such as ICAM1 and VCAM1 (Wiejak et al. 2019), potentially via SOCS3 induction . However our results did not support this hypothesis. Instead they showed that EPAC activation via treatment with 8-CPT, a selective EPAC1 activator, alone had no effect on SOCS3 protein expression (Figure 3.7). 8-CPT did however increase VE-cadherin staining at cell junctions, consistent with published findings (Fukuhara et al. 2005; Kooistra et al. 2005), proving that the drug was active at the concentration used. An alternative method to measure the role of EPAC1 in prostanoid induction of SOCS3 would be to utilise EPAC1 agonists and antagonists.

The EPAC1 agonist, N-(2,4-dimethylbenzenesulfonyl)-2-(naphthalen-2-yloxy)acetamide (I942) (MolPort; Cat. No. 868145-09-9), has been shown to induce SOCS3 in HUVECs which was attenuated via treatment with the EPAC inhibitor ESI-09 (Tocris; Cat. No. 4773) (Wiejak et al. 2019). EPAC1 siRNA was also utilised in this experiment and blocked I942-mediated induction of SOCS3 (Wiejak et al. 2019). However, this has not been investigated in HPAECs.

Interestingly, PKA activators appear to trigger a small increase in SOCS3 expression but this did not reach significance (Figure 3.7). In addition, a PKA inhibitor had no effect on Fsk induction of SOCS3 but did significantly reduce Fsk induction of Nur77. This supports existing data that PKA is not involved in cAMP-mediated induction of SOCS3 (Woolson et al. 2009; Wiejak et al. 2019). Interestingly, in human breast cancer cells the PKA inhibitor H89 was found to inhibit PGE_2-mediated upregulation of SOCS3 mRNA (Barclay et al. 2007), and in HUVECs H89 was found to partially inhibit Fsk/rolipram-mediated

induction of SOCS3 (Wiejak et al. 2019), suggesting that PKA and EPAC may both be required for optimal SOCS3 induction. Contradictory to this, treatment with PKA and EPAC activiators together did not significantly increase SOCS3 induction in HPAECs (Figure 3.7).

Further optimisation of 8-CPT and 6-Bnz treatment via dose-concentration and time courses are required to ensure the appropriate concentration and treatment times are being used for maximum SOCS3 accumulation. Additionally, whether cAMP is crucial for prostanoid and selexipag induction of SOCS3 in HPAECs needs to be established in case there is an alternative signalling mechanism occurring which is yet to be identified. CRISPR/Cas9 technology has been used to produce AC deficient HEK293 cells that demonstrated a significant reduction in the Fsk-stimulated cAMP response (Soto-Velasquez et al. 2018). Utilising this model in VECs would be ideal to measure a role for cAMP in prostanoid-mediated stimulation of SOCS3 expression in the context of this research.

As discussed, it has been suggested that treprostinil can mediate its anti-proliferative effects via PPAR (Ali et al. 2006; Lai et al. 2009). Numerous PPARγ antagonists are available (Tocris, Cat. #1326, Cat. # 2022 and Cat. # 2301) that could be administed to HPAECs prior to measuring treprostinil-induced SOCS3 expression to determine the impact of PPARs. Lung-specific PPARβ-deficient mice have previously been utilised to determine an anti-proliferative role for treprostinil mediated via PPARs (Ali et al. 2006). Similar models could be utilised to determine the treprostinil/PPARs relationship in VECs.

To conclude, these experiments confirm that the BPS, treprostinil, and ACT-333679, the biologically active metabolite of pro-drug selexipag, do induce SOCS3 protein expression as a result of increased SOCS3 gene transcription. However, further work is required to establish the key proteins and receptors involved.

4. Prostanoids attenuate IL-6 *trans*-signalling

4.1 Introduction

As prostanoids induce the expression of SOCS3 protein in HPAECs and HPMECs (Chapter 3), and SOCS3 negatively regulates IL-6 *trans*-signalling (Schmitz et al. 2000) (Section 1.4.3), it could be hypothesised that prostanoids are able to limit IL-6 *trans*-signalling and pro-inflammatory effects. With the exception of a minority of cells, IL-6 binds to cleaved sIL-6Rα extracellularly prior to binding to membrane bound gp-130 to initiate IL-6 *trans*-signalling via JAK/STAT activation (Section 1.4.1). Consequently, IL-6 induced tyrosine 705 phosphorylation of STAT3 can be used as a measure of IL-6 signalling activity. IL-6 signalling initiates the transcription of numerous pro-angiogenic and pro-survival factors such as adhesion molecules and VEGF which are associated with PAH progression (Section 1.4.1). Thus, prostanoid inhibition of IL-6 *trans*-signalling may contribute to the therapeutic properties of prostanoids and exploring this relationship may identify potential targets for future drug development.

4.2 Results

4.2.1 Lentiviral expression of SOCS3 inhibits IL-6/sIL-6Rα induced tyrosine 705 phosphorylation of STAT3 in HPAECs

To initially determine if SOCS3 inhibits IL-6 *trans*-signalling activity in HPAECs, lentiviral SOCS3 gene delivery was utilised to determine the effect of increasing SOCS3 expression. SOCS3 has a half-life of 40 – 120 minutes depending on the cell type (Siewert et al. 1999; Fletcher et al. 2010; Munro 2016b), and is barely detectable at basal concentrations even in the presence of a proteasome inhibitor (Figures 3.1 – 3.4, 3.6, 3.7). Treatment with a SOCS3 lentivirus results in constitutive SOCS3 activity that allows us to measure the effect of SOCS3 on IL-6/sIL-6Rα signalling activity without any additional stimulation. Tyrosine 705 phosphorylation of STAT3 was considered representative of IL-6 *trans*-signalling activity. To ensure the effects were not a consequence of treatment with lentivirus, HPAECs were treated in parallel with a GFP-expressing lentivirus. This also allowed confirmation of lentivirus transduction via fluorescence microscopy.

HPAECs at 70% confluency were treated with either Flag-SOCS3 lentivirus or GFP lentivirus at a concentration of $1x10^6$ TU/µl and $2x10^6$ TU/µl respectively for 5 days as previously described (Section 2.2.2.2). Transduction of cells by lentivirus was monitored via fluorescence microscopy as previously described (Section 2.2.2.2). Cells were then harvested and lysed for SDS-PAGE and immunoblotting to determine Flag-SOCS3 and GFP protein expression. STAT3 was used as a control to ensure equivalent loading.

Treatment with Flag-SOCS3 lentivirus alone was sufficient to cause SOCS3 protein expression, whilst GFP lentivirus alone was sufficient to cause GFP protein expression (Figure 4.1A). Fluorescence imaging indicated high transduction rates for the GFP lentivirus at the concentration used with all cells in the image taken also expressing GFP (Figure 4.1B), however the rates were not calculated.

Although the action of IL-6 alone was not measured in HPAECs, treatment with IL-6 alone in other cells such as leucocytes is not sufficient to elicit tyrosine 705 phosphorylation of JAK/STAT (Romano et al. 1997). Thus, when measuring the effects of IL-6 induced signalling in HPAECs, cells were treated with an IL-6/sIL-6R complex made up at least 30 minutes and no more than two weeks prior to treatment to represent *trans*-signalling conditions. To measure the effect of Flag-SOCS3 expression on IL-6/sIL-6Rα signalling, HPAECs were treated with either GFP or Flag-SOCS3 lentivirus as previously described prior to 30 minute treatment with IL-6/sIL-6Rα. Cells were harvested and lysed as previously described (Section 2.2.3.1) prior to SDS-PAGE and immunoblotting for Flag-SOCS3 and GFP.

In the absence of IL-6/sIL-6R treatment, there is no tyrosine 705 phosphorylation in either GFP- or Flag-SOCS3-expressing cells. IL-6 *trans*-signalling resulted in significant tyrosine 705 phosphorylation in GFP-expressing HPAECs, which was significantly reduced after treatment with Flag-SOCS3 lentivirus (Figure 4.1C). However, Flag-SOCS3 was not sufficient to reduce tyrosine 705 phosphorylation to basal (no IL-6/sIL-6Rα treatment) levels (Figure 4.1C). This supports our hypothesis that increasing SOCS3 in HPAECs will limit IL-6 *trans*-signalling.

A

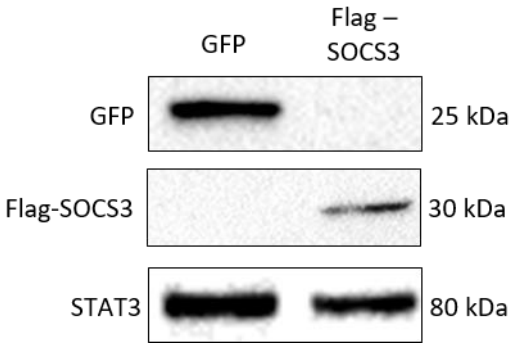
GFP
Flag – SOCS3
GFP
25 kDa
Flag-SOCS3
30 kDa
STAT3
80 kDa

B

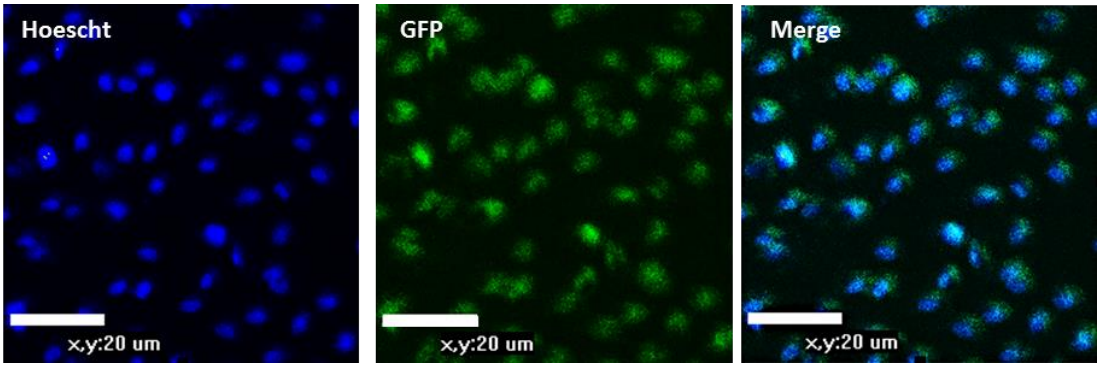
Hoescht
GFP
Merge
x,y:20 um
x,y:20 um
x,y:20 um

C

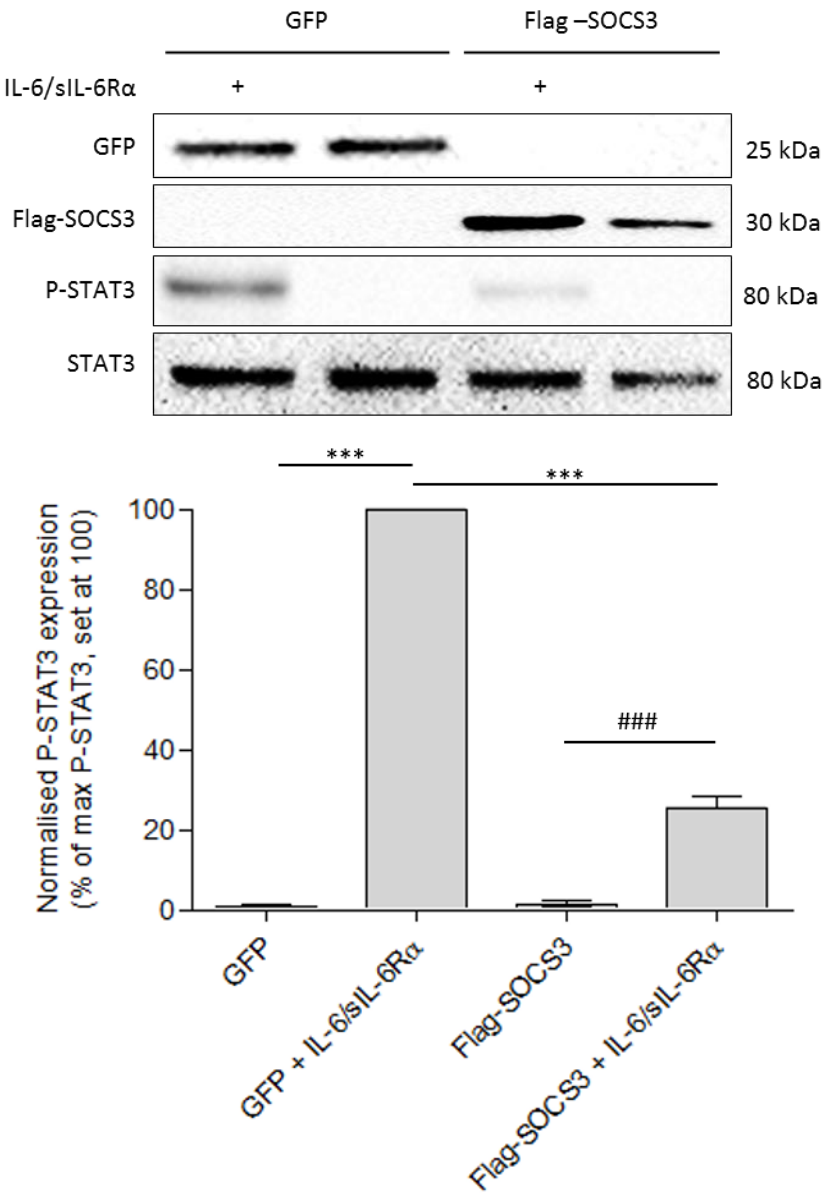
GFP
Flag –SOCS3
IL-6/sIL-6Rα
+
+
GFP
25 kDa
Flag-SOCS3
30 kDa
P-STAT3
80 kDa
STAT3
80 kDa
***
***
Normalised P-STAT3 expression (% of max P-STAT3, set at 100)
100
80
60
40
20
0
###
GFP
GFP + IL-6/sIL-6Rα
Flag-SOCS3
Flag-SOCS3 + IL-6/sIL-6Rα

Figure 4.1: Lentiviral expression of SOCS3 inhibits IL-6/sIL-6Rα induced tyrosine 705 phosphorylation of STAT3 in HPAECs

A) HPAECs were treated with either Flag-SOCS3 lentivirus or green fluorescent protein (GFP) lentivirus for 24 hours as described in Section 2.2.2.2. Cells were then incubated in fresh media for 2 – 5 days before harvesting. Whole cell lysates were equalised for protein content and fractionated via SDS-PAGE for immunoblotting with anti-GFP and Flag-antibodies. Total STAT3 was used as a protein loading control. B) Fluorescence images taken 5 days post-infection with GFP lentivirus (GFP-expressing cells = green). Cells were fixed with methanol for 10 minutes at -20°C and then incubated at room temperature with the nuclear stain Hoechst 33342 (blue) for 20 minutes prior to imaging. C) HPAECs were treated with either Flag-SOCS3 or GFP lentiviruses for 24 hours prior to incubation in fresh media for 2 – 5 days before harvesting. Cells were treated with IL-6 (5 ng/ml) and sIL-6Rα (25 ng/ml) (IL-6/sIL-6Rα) 30 minute prior to harvest. Whole cell lysates were then equalised for protein content and fractionated via SDS-PAGE for immunoblotting with antibodies against GFP, Flag M2 and Tyr705 P-STAT3. The concentration of P-STAT3 was compared to maximum P-STAT3 expression, set as 100. Immunoblotting with STAT3 was used for a loading control. *** indicates $p<0.0001$ compared to GFP + IL-6/sIL-6Rα. ### indicates $p<0.0001$ compared to Flag-SOCS3. Quantification for *n=3* experiments have been shown.

4.2.2 Prostanoid mediated inhibition of IL-6/sIL-6Rα induced tyrosine 705 phosphorylation of STAT3 in HPAECs

As lentiviral delivery of the SOCS3 gene significantly inhibited IL-6/sIL-6Rα induced phosphorylation of STAT3 at tyrosine 705 in HPAECs and prostanoids induced SOCS3 expression in HPAECs (Section 3.2.1 – 3.2.2), the effects of BPS and treprostinil on IL-6 *trans*-signalling activity were then measured.

HPAECs were serum starved for 2 hours before being treated for 4 hours with Fsk (50 μM), BPS (10 μM) or treprostinil (10 μM). Treatment with IL-6/sIL-6Rα occurred 30 minutes prior to cell lysis. Treatment with Fsk (50 μM), BPS (10 μM) and treprostinil (10 μM) in the absence of IL-6/sIL-6Rα were used as negative controls.

As ACT-333679, the pro-drug of selexipag, also induced SOCS3 (Section 3.2.3), the experiment was repeated with treatment of ACT-333679. Again, cells were serum starved for 2 hours before being treated for 4 hours with Fsk (50 μM) or ACT-333679 (1 μM) in the presence or absence of IL-6/sIL-6Rα which was administered 30 minutes prior to cell lysis. Consistent with previous findings (Sands et al. 2006; Wiejak et al. 2019), 4 hours of treatment with Fsk significantly inhibited IL-6/sIL-6Rα-mediated STAT3 phosphorylation at tyrosine 705 (Figure 4.2). Treatment with BPS (Figure 4.2A), treprostinil (Figure 4.2A) and ACT-333679 (Figure 4.2B) for 4 hours also significantly inhibited IL-6/sIL-6Rα-mediated phosphorylation of STAT3 treatment (Figure 4.2A/B).

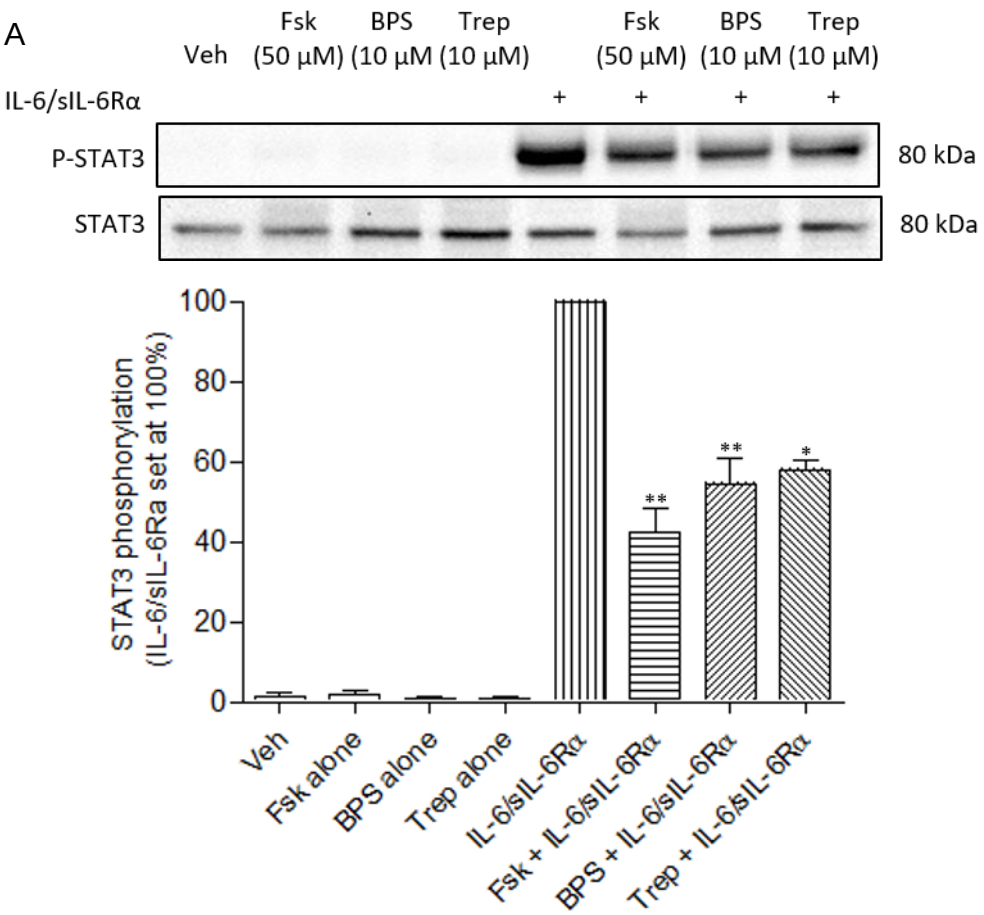
A
Veh
Fsk (50 µM)
BPS (10 µM)
Trep (10 µM)
Fsk (50 µM)
BPS (10 µM)
Trep (10 µM)
IL-6/sIL-6Rα
+ + + +
P-STAT3
80 kDa
STAT3
80 kDa
STAT3 phosphorylation (IL-6/sIL-6Ra set at 100%)
100
80
60
40
20
0
**
**
*
Veh
Fsk alone
BPS alone
Trep alone
IL-6/sIL-6Rα
Fsk + IL-6/sIL-6Rα
BPS + IL-6/sIL-6Rα
Trep + IL-6/sIL-6Rα

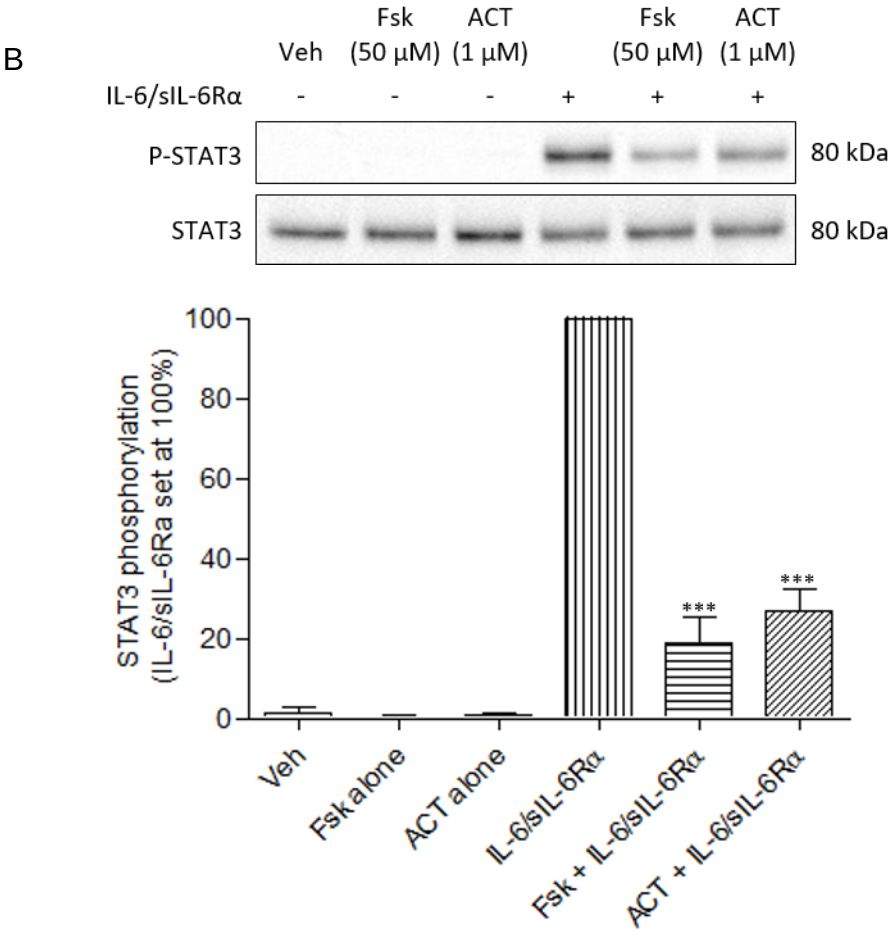
B
Veh
Fsk (50 µM)
ACT (1 µM)
Fsk (50 µM)
ACT (1 µM)
IL-6/sIL-6Rα
- - - + + +
P-STAT3
80 kDa
STAT3
80 kDa
STAT3 phosphorylation (IL-6/sIL-6Ra set at 100%)
100
80
60
40
20
0
***
***
Veh
Fsk alone
ACT alone
IL-6/sIL-6Rα
Fsk + IL-6/sIL-6Rα
ACT + IL-6/sIL-6Rα

Figure 4.2: Prostanoids inhibit IL-6/sIL-6Rα-induced tyrosine 705 phosphorylation of STAT3 in HPAECs

A) HPAECs were serum starved for 2 hours before treatment for 4 hours with beraprost sodium salt (BPS) (10 μM), treprostinil (Trep) (10 μM) or forskolin (Fsk) (50 μM) which was used as a positive control, with and without the presence of IL-6 (5 ng/ml) and sIL-6Rα (25 ng/ml) (IL-6/sIL-6Rα) for 30 minutes prior to harvest. Whole cell lysates were then equalised for protein content and fractionated via SDS-PAGE for immunoblotting with antibodies against Tyr705-phosphorylated STAT3 (P-STAT3) and total STAT3 which was used as a loading control. Levels of P-STAT3 were measured as a percentage of IL-6/sIL-6Rα treatment alone (set at 100%). * indicates $p<0.05$ compared to IL-6/sIL-6Rα treatment alone, ** indicates $p<0.01$. Quantification for *n=4* experiments is shown. B) HPAECs were serum starved for 2 hours before treatment for 4 hours with ACT-333679 (1 μM) or Fsk (50 μM) which was used as a positive control, with and without the presence of IL-6/sIL-6Rα. Cells were treated with IL-6/sIL-6Rα 30 minutes prior to harvest. Whole cell lysates were then equalised for protein content and fractionated via SDS-PAGE for immunoblotting with P-STAT3 and total STAT3 which was used as a loading control. Levels of P-STAT3 were measured as a percentage compared to IL-6/sIL-6Rα treatment alone (set at 100%). *** indicates $p<0.001$ versus IL-6/sIL-6Rα alone. Quantification for *n=4* experiments has been shown.

4.2.3 Prostanoid-mediated inhibition of IL-6 *trans*-signalling is dependent on SOCS3

In HPAECs, BPS, treprostinil and selexipag metabolite ACT-333679 increase SOCS3 expression (Section 3.2, Figures 3.1 - 3.3) and attenuate IL-6/sIL-6Rα induced phosphorylation of STAT3 (Figure 4.2), however whether SOCS3 induction and IL-6 inhibition are linked is unclear. Thus, it was important to determine if prostanoid-mediated limitation of IL-6 *trans*-signalling activity was dependent on SOCS3. To test this we utilised AS-M.5 cells, an established immortalised human endothelial cell model (Krump-Konvalinkova et al. 2003), and a SOCS3 KO AS-M.5 line generated in house using CRISPR/Cas9 technology (Williams et al. 2018).

Initially, WT and SOCS3 KO AS-M.5 cells were stimulated with BPS or treprostinil for 2 hours in the presence of proteasome inhibitor MG-132 to prevent SOCS3 degradation. MG-132 alone was used as a negative control and treatment with Fsk for four hours in the presence of MG-132 was used as a positive control. In WT AS-M.5 cells, Fsk treatment produced a significant induction of SOCS3 protein. 2 hours of stimulation with either BPS or treprostinil also significantly induced SOCS3 protein expression (Figure 4.3). However, treating AS-M.5 SOCS3 KO cells under the same conditions did not results in SOCS3 expression. In contrast, the cAMP-inducible gene product Nur77 was significantly induced by Fsk, BPS and treprostinil in WT and SOCS3 KO cells (Figure 4.3), demonstrating a positive response to the drugs thus confirming downregulation of SOCS3 is a result of SOC3 knockdown.

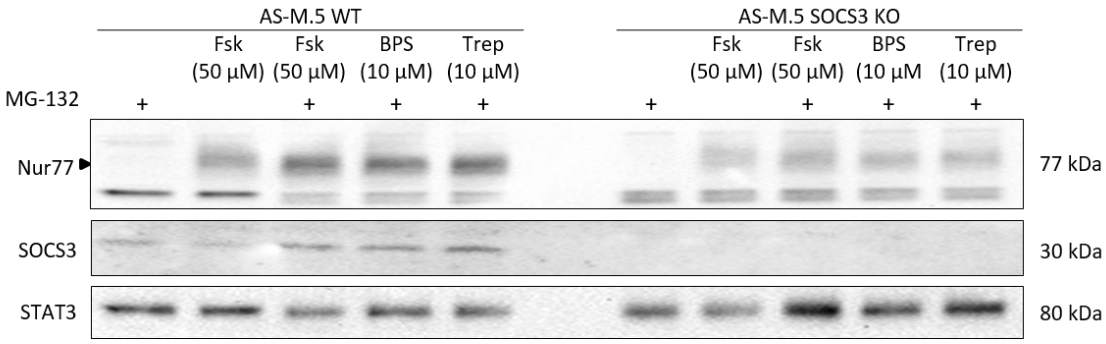
AS-M.5 WT
AS-M.5 SOCS3 KO
Fsk (50 µM)
Fsk (50 µM)
BPS (10 µM)
Trep (10 µM)
Fsk (50 µM)
Fsk (50 µM)
BPS (10 µM)
Trep (10 µM)
MG-132
+
+
+
+
+
+
+
+
Nur77
77 kDa
SOCS3
30 kDa
STAT3
80 kDa

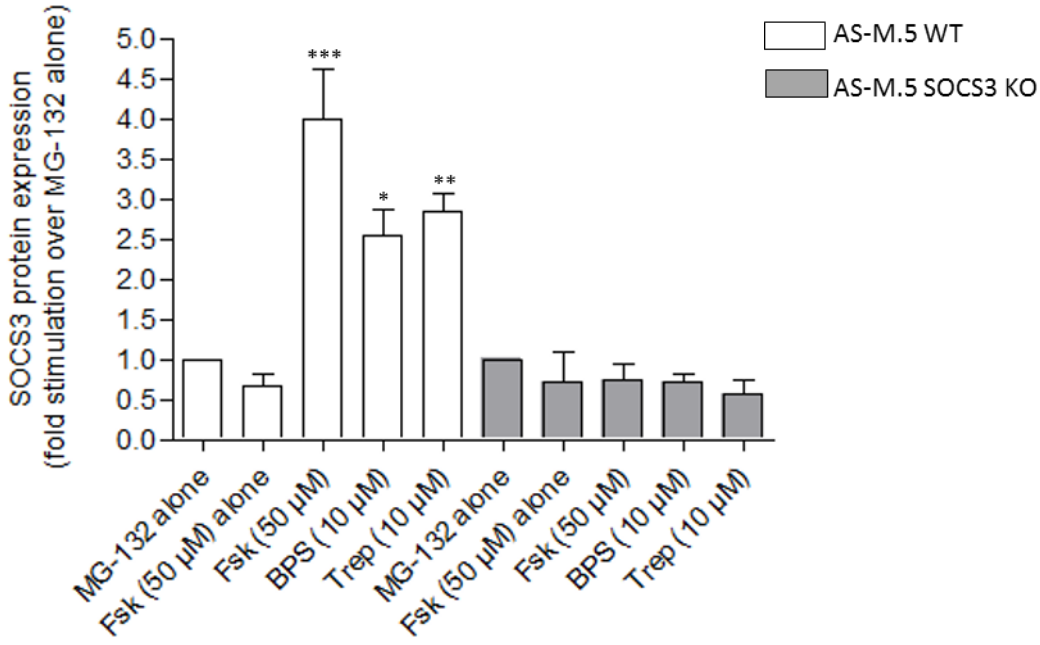
AS-M.5 WT
AS-M.5 SOCS3 KO
SOCS3 protein expression
(fold stimulation over MG-132 alone)
5.0
4.5
4.0
3.5
3.0
2.5
2.0
1.5
1.0
0.5
0.0
***
*
**
MG-132 alone
Fsk (50 µM) alone
Fsk (50 µM)
BPS (10 µM)
Trep (10 µM)
MG-132 alone
Fsk (50 µM) alone
Fsk (50 µM)
BPS (10 µM)
Trep (10 µM)

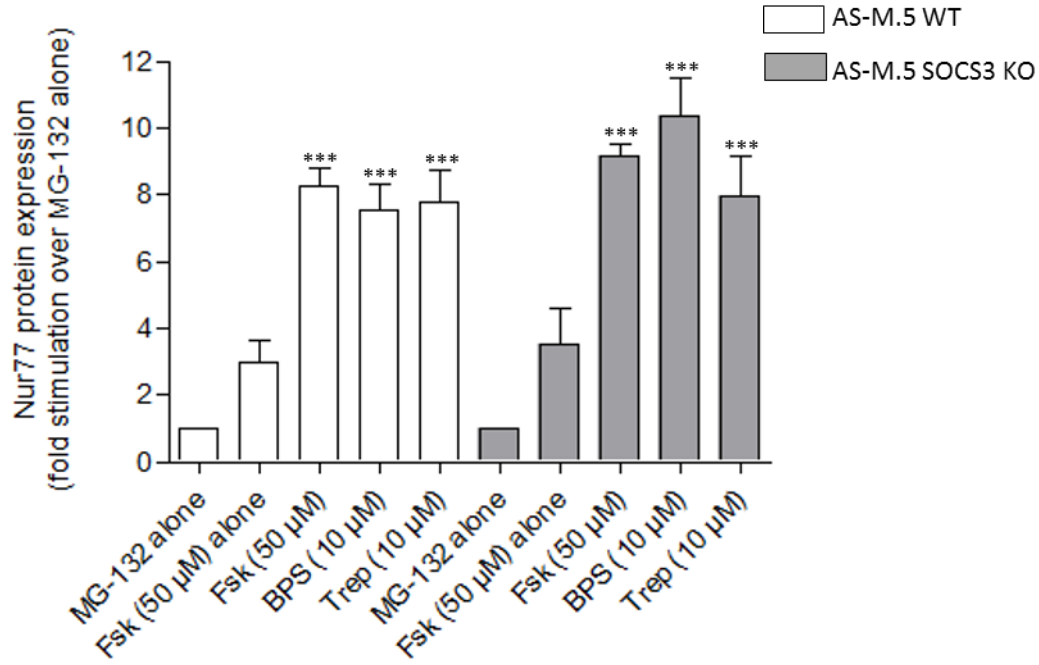
AS-M.5 WT
AS-M.5 SOCS3 KO
Nur77 protein expression
(fold stimulation over MG-132 alone)
12
10
8
6
4
2
0
***
***
***
***
***
***
MG-132 alone
Fsk (50 µM) alone
Fsk (50 µM)
BPS (10 µM)
Trep (10 µM)
MG-132 alone
Fsk (50 µM) alone
Fsk (50 µM)
BPS (10 µM)
Trep (10 µM)

Figure 4.3: Prostanoid mediated induction of SOCS3 in AS-M.5 WT and AS-M.5 SOCS3 KO cells

Cells were treated with beraprost (BPS) (10 μM) or treprostinil (Trep) (10 μM) for two hours in the presence of MG-132 (6 μM). Fsk (50 μM) + MG-132 (6 μM) was used a positive control for SOCS3 induction. Treatment with MG-132 (6 μM) alone was used as a negative control. Whole cell lysates were then equalised for protein content and fractionated via SDS-PAGE for immunoblotting with antibodies against Nur77, SOCS3 and STAT3 (protein loading control). Levels of SOCS3 and Nur77 were measured as a fold difference compared to treatment with MG-132 only, set at 1. * indicates $P<0.05$ compared to treatment with MG-132 alone, ** indicates $p<0.001$, *** indicates $p<0.0001$. Quantification for *n=5* experiments has been shown.

As SOCS3 KO AS-M.5 cells were shown to not express SOCS3 (Figure 4.3), these cells were used to assess any role for SOCS3 in prostanoid inhibition of IL-6 mediated tyrosine 705 phosphorylation of STAT3. Cells were serum starved for two hours before being treated for 4 hours with Fsk (50 μM), or 2 hours with BPS (10 μM) or treprostinil (10 μM) in the presence or absence of IL-6/sIL-6Rα which was administered 30 minutes prior to harvesting the cells. This experiment was performed in AS-M.5 WT and AS-M.5 SOCS3 KO cells in parallel.

Fsk significantly reduced the phosphorylation of STAT3 caused by treatment with IL-6/sIL-Rα in WT but not SOCS3 KO AS-M.5 cells (Figure 4.4). BPS and treprostinil also significantly reduced IL-6/sIL-Rα-mediated tyrosine 705 STAT3 phosphorylation in AS-M.5 WT but not SOCS3 KO AS-M.5 cells. This demonstrates prostanoid inhibition of IL-6 *trans*-signalling was in part due to the inhibitory effects of SOCS3. In addition, unlike WT AS-M.5 cells, SOCS3 KO AS-M.5 cells displayed a pronounced basal phosphorylation of STAT3 that could be seen in the absence of IL-6/sIL-6Rα stimulation and which, in the case of Fsk showed no significance difference compared to IL-6/sIL-Rα-mediated tyrosine 705 STAT3 phosphorylation (Figure 4.4). Although still pronounced, there was a significant difference between tyrosine 705 STAT3 phosphorylation in the vehicle, BPS and treprostinil treatment and maximum phosphorylation of STAT3 resulting from treatment with IL-6/sIL-Rα (Figure 4.4).

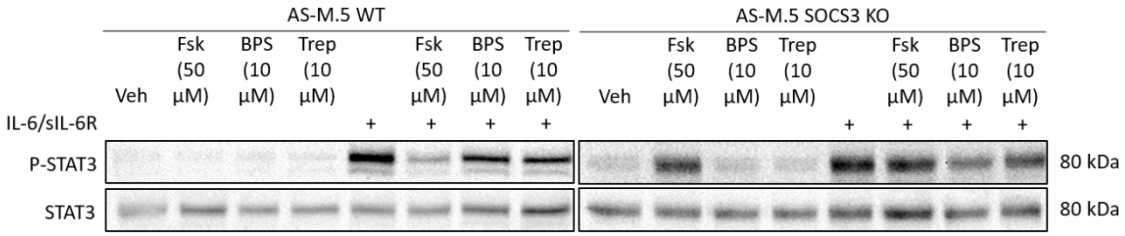
AS-M.5 WT
AS-M.5 SOCS3 KO
Veh
Fsk (50 µM)
BPS (10 µM)
Trep (10 µM)
IL-6/sIL-6R
P-STAT3
STAT3
80 kDa
80 kDa

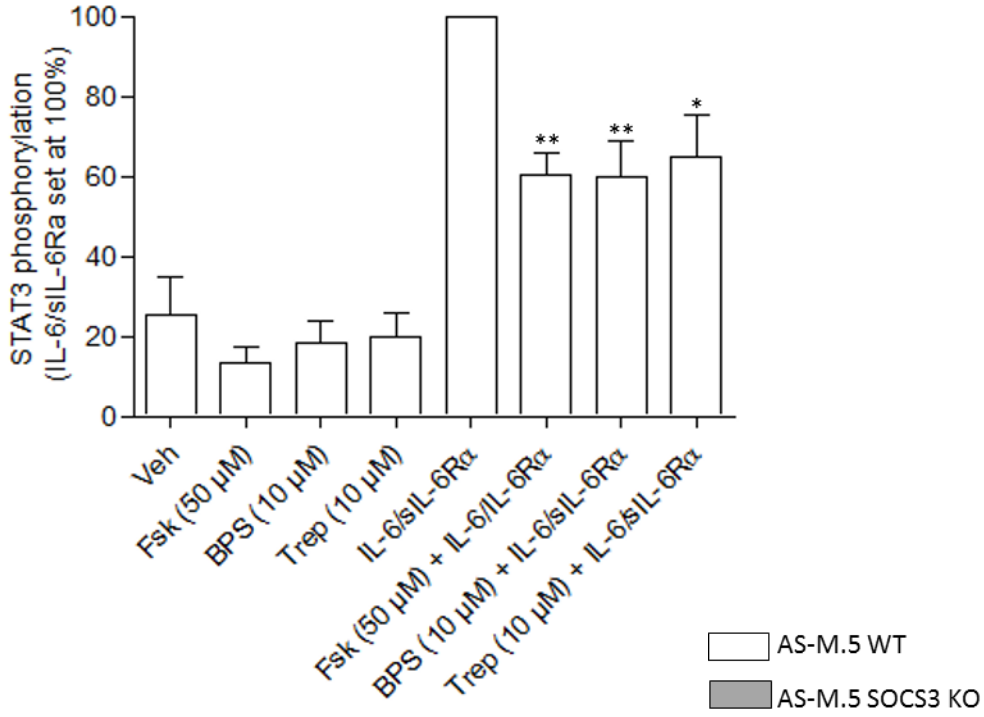
STAT3 phosphorylation (IL-6/sIL-6Ra set at 100%)
Veh
Fsk (50 µM)
BPS (10 µM)
Trep (10 µM)
IL-6/sIL-6Rα
Fsk (50 µM) + IL-6/IL-6Rα
BPS (10 µM) + IL-6/sIL-6Rα
Trep (10 µM) + IL-6/sIL-6Rα
AS-M.5 WT
AS-M.5 SOCS3 KO

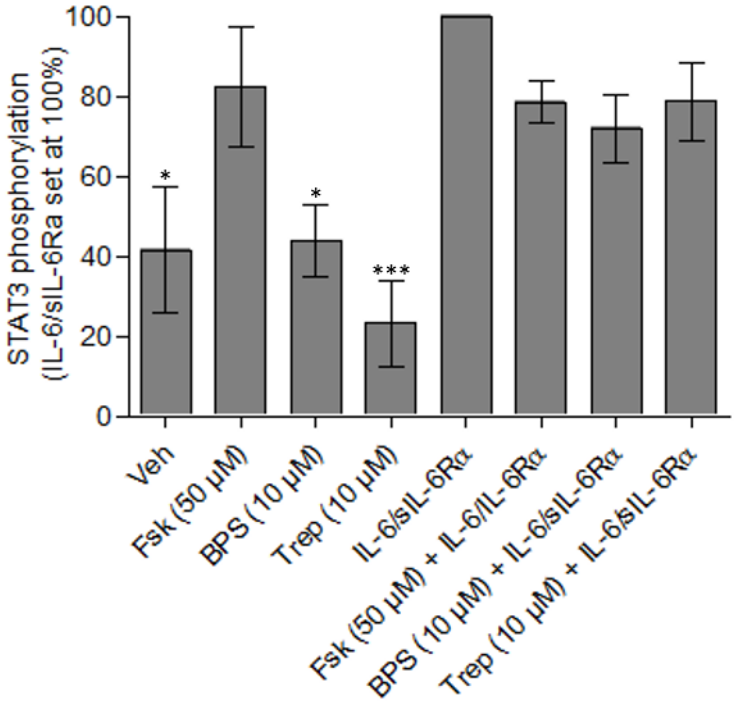
STAT3 phosphorylation (IL-6/sIL-6Ra set at 100%)
Veh
Fsk (50 µM)
BPS (10 µM)
Trep (10 µM)
IL-6/sIL-6Rα
Fsk (50 µM) + IL-6/IL-6Rα
BPS (10 µM) + IL-6/sIL-6Rα
Trep (10 µM) + IL-6/sIL-6Rα

Figure 4.4: Prostanoid mediated inhibition of phosphorylation of total-STAT3 at tyrosine 795 in AS-M.5 WT cells and AS-M.5 SOCS3 KO cells

Cells were serum starved for 2 hours before 2 hours of treatment with beraprost sodium salt (BPS) (10 μM), treprostinil (Trep) (10 μM) or forskolin (Fsk) (50 μM), which was used as a positive control, in the presence and absence of IL-6 (5 ng/ml) and sIL-6Rα (25 ng/ml) (IL-6/sIL-6Rα) which was applied 30 minutes prior to harvest. Whole cell lysates were then equalised for protein content and fractionated via SDS-PAGE for immunoblotting with phospho-STAT3 and total STAT3. Immunoblotting with Nur77 was performed to show elevation of cAMP. The concentration of P-STAT3 was measured as a difference compared to IL-6/sIL-6Rα treatment only, set at 100%. * indicates $p<0.05$ compared to treatment with IL-6/sIL-6Rα alone, ** indicates $p<0.01$, *** indicates $P<0.001$. Quantification for *n=4* experiments has been shown.

4.2.4 Gene silencing of SOCS3 in HPAECs

In AS-M.5 cells, BPS and treprostinil significantly limit IL-6/sIL-6Rα mediated STAT3 phosphorylation at tyrosine 705; however this was not the case in SOCS3 KO AS-M.5 cells (Figure 4.4). This suggests BPS and treprostinil-mediated inhibition of IL-6 *trans*-signalling in AS-M.5 cells is due in part to the induction of SOCS3. Although these cell types are representative of endothelial cells, it was necessary to test this in HPAECs as they are involved in the pathogenesis and vascular remodelling characteristic of PAH (Masri et al. 2007; reviewed by Ranchoux et al. 2018).

To achieve this, Flexitube GeneSolution siRNA, purchased from Qiagen and prepared by colleagues from the University of Glasgow, was utilised to silence SOCS3 gene expression in HPAECs as previously described (Section 2.2.2.3). Flexitube GeneSolution siRNA was chosen as it includes siRNA for 4 genes, in this case 4 different SOCS3 variants (SOCS3-1, -4, -6, and SOCS3-7). Control siRNA and HiPerFect only treatments were used as negative controls. HPAECs were treated for 4 hours with Fsk (50 μM) in the presence of MG-132 (6 μM). Treatment with MG-132 (6 μM) alone was used as a negative control while Fsk (50 μM) and MG-132 (6 μM) in the absence of siRNA was used a positive control for SOCS3 induction. Cells were harvested and lysed as previously described before protein content was determined and immunoblotting for SOCS3 performed.

SOCS3 protein expression was undetectable after MG-132 only treatment, while 4 hours treatment with Fsk and MG-132 triggered a significant accumulation of SOCS3 protein (Figure 4.5A). This was not affected by treatment with negative control siRNA or HiPerFect. 48 hours of incubation

with 100 nM of SOCS3 siRNAs 1, 4, 6, and 7 was not sufficient to attenuate Fsk-induced SOCS3 induction compared to SOCS3 expression post-treatment with negative control siRNA (Figure 4.5A).

To ensure the siRNA was active, fresh Flexitube GeneSolution SOCS3 siRNA was purchased and prepared prior to repeating the experiment. As treatment with MG-132 alone had not resulted in SOCS3 protein expression in any condition previously (Figure 4.5A), just one MG-132 only negative control treatment was performed. Again, SOCS3 accumulation induced by Fsk in the presence of MG-132 was not attenuated by 48 hours of incubation with SOCS3 siRNA 1, 4, 6, and 7 compared with negative control siRNA and HiPerFect treated HPAECs (Figure 4.5B).

An attempt to optimise the formation of transfection complexes and overall cell transfection was performed by increasing the volume of HiPerFect as recommended by the supplier. The experiment was repeated exactly as previously described (Section 2.2.2.3) but with 12 µl HiPerFect and 78 µl Opti-MEM media. However, SOCS3 protein expression was the same as seen in previous experiments with a significant induction by Fsk which was not limited by 48 hours of incubation with SOCS3 siRNA 1, 4, 6, and 7 compared to treatment with negative control siRNA and HiPerFect (Figure 4.5C).

As siRNA transfection was not successful in silencing SOCS3 gene induction under the conditions used, lentivirus-mediated shRNA delivery was utilised as an alternative strategy. Lentiviruses containing pLV[shRNA]-mCherry:T2A:Puro- U6>hSOCS3 (SOCS3) and pLV[shRNA]-mCherry:T2A:Puro-U6>Scramble (control) shRNA, supplied by VectorBuilder,

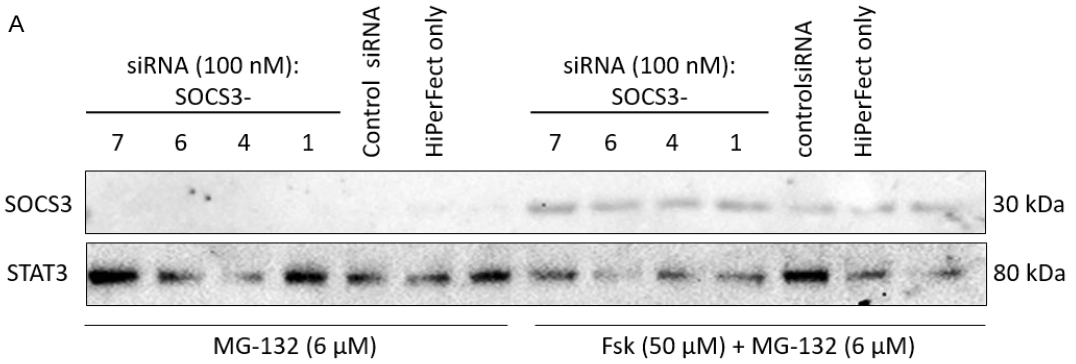
A
siRNA (100 nM): SOCS3-
7
6
4
1
Control siRNA
HiPerFect only
siRNA (100 nM): SOCS3-
7
6
4
1
controlsiRNA
HiPerFect only
SOCS3
STAT3
30 kDa
80 kDa
MG-132 (6 µM)
Fsk (50 µM) + MG-132 (6 µM)

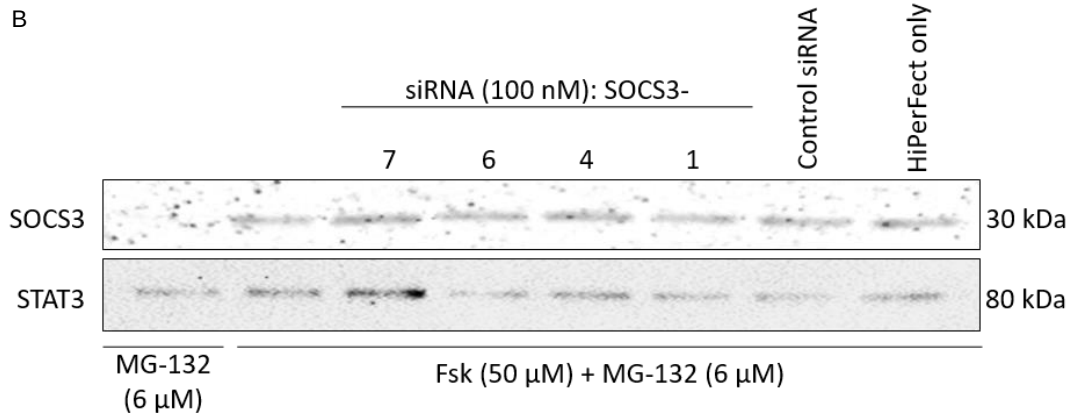
B
siRNA (100 nM): SOCS3-
7
6
4
1
Control siRNA
HiPerFect only
SOCS3
STAT3
30 kDa
80 kDa
MG-132 (6 µM)
Fsk (50 µM) + MG-132 (6 µM)

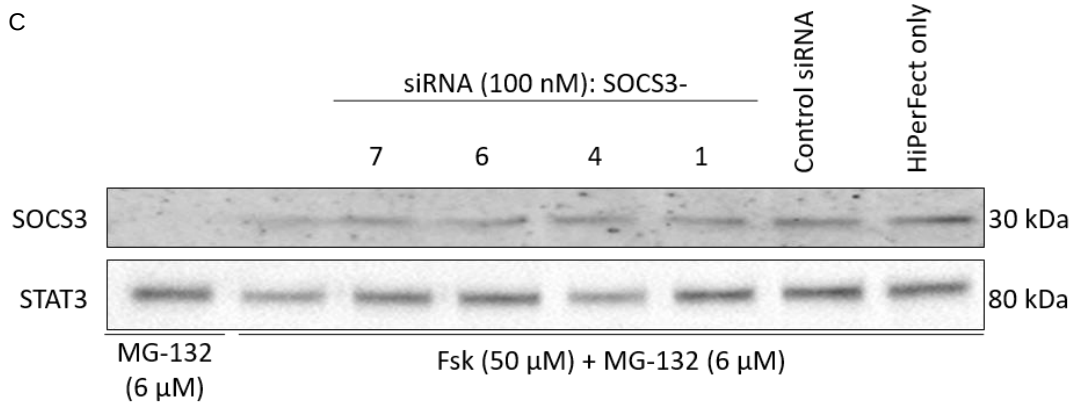
C
siRNA (100 nM): SOCS3-
7
6
4
1
Control siRNA
HiPerFect only
SOCS3
STAT3
30 kDa
80 kDa
MG-132 (6 µM)
Fsk (50 µM) + MG-132 (6 µM)

Figure 4.5: SOCS3 siRNA is not sufficient to silence SOCS3 gene expression in HPAECs

A) HPAECs were maintained in 6 cm dishes until reaching 70% confluency. SOCS3-1, 4, 6 and 7 siRNA (100 nM) were prepared individually in 3 µl HiPerFect and 87 µl Opti-MEM media and incubated at room temperature for 10 minutes prior to mixing with 900 µl Optim-MEM. HPAECs were incubated in the siRNA-containing media for 48 hours prior to 4 hours treatment with forskolin (Fsk) (50 µM) in the presence of MG-132 (6 µM) or with MG-132 alone. Treatment with Fsk (50 µM) + MG-132 (6 µM) in the absence of siRNA was used as a positive control for SOCS3 induction. Treatment with control siRNA (100 nM) and HiPerFect only were used as siRNA negative controls. Whole cell lysates were then equalised for protein content and fractionated via SDS-PAGE for immunoblotting with SOCS3 and STAT3 antibodies. Experiment completed to *n=1*. B) Experiment completed as above but just one treatment with MG-132 (6 µM) alone was used as a negative control. Experiment completed to *n=1*. C) HPAECs were maintained in 6cm dishes until reaching 70% confluency. SOCS3 siRNA-1, 4, 6 and SOCS3 siRNA-7 (100 nM) were prepared individually in 12 µl HiPerFect and 78 µl Opti-MEM media and incubated at room temperature for 10 minutes prior to mixing with 900 µl Optim-MEM. The experiment was completed as previously described. Experiment completed to *n=1.*

were prepared and lentiviral concentration determined as previously described (Section 2.2). shRNA-containing media was prepared at concentrations ranging from $9.37x10^4$ TU/µl to $1.872x10^6$ TU/µl and applied to cells overnight. Cells were then maintained in fresh EGM-2 media for 5 days prior to 4 hours treatment with Fsk (50 µM) in the presence of MG-132 (6 µM). Treatment with MG-132 (6 µM) alone and Fsk (50 µM) in the presence of MG-132 (6 µM) in the absence of lentiviral treatment were used as negative and positive controls of SOCS3 induction respectively. Treatment with Fsk (50 µM) and MG-132 (6 µM) in the absence of shRNA but presence of polybrene (8 µg/ml) was also performed to ensure any effects on SOCS3 expression were not a result of polybrene treatment. Cells were harvested and lysed as previously described prior to SDS-PAGE and immunoblotting for SOCS3 (Section 2.2.3.1). Immunoblotting with STAT3 was used as a loading control.

SOCS3 protein was expressed 4 hours after treatment with Fsk and MG-132 in the absence of lentiviral treatment and in the polybrene only control, but not after treatment with MG-132 only (Figure 4.6A). None of the lentivirus concentrations were successful in reducing SOCS3 protein expression compared to SOCS3 expression in the polybrene only treatment (Figure 4.6A).

As numerous resources advised lower cell densities can enhance shRNA infection (Qiagen 2014; Aznan et al. 2018; ThermoFisherSCIENTIFIC 2019), an attempt to optimise SOCS3 gene silencing by lentiviral delivery of SOCS3 shRNA was performed by treating HPAECs at 40% confluency as opposed to 70% confluency. Cells were incubated for 6 days post-infection but otherwise

experimental details remained the same as described above. SOCS3 protein was expressed in all conditions (Figure 4.6B) including the negative control treatment (MG-132 only) so it is difficult to draw conclusions from this particular experiment.

To determine if HPAECs were being successfully infected with the virus, the experiment was repeated as previously described with lentiviral treatment administered when the cells reached 70% confluency. Lentivirus-treated cells were then maintained in puromycin (2 µg/ml)-containing EGM-2 post-treatment. In this experiment, cells were incubated for 10 days post-lentiviral treatment. This was because cells which had not been infected by the lentivirus necrosed after treatment with puromycin-containing EGM-2, thus a longer incubation period was required for the puromycin-resistant cells to reach confluency adequate for cell harvest. For one treatment, cells which had not been treated with lentivirus were also treated with puromycin (2 µg/ml)-containing EGM-2 containing media to ensure the antibiotic sufficiently killed non-transfected kills. After 24 hours of incubation, the majority of cells had died and detached from the flask, thus the cell count was not high enough to continue incubating these cells.

SOCS3 was not expressed 4 hours post-treatment with MG-132 alone but was expressed after treatment with Fsk and MG-132 in the absence of shRNA and the presence of polybrene only (Figure 4.6C). Although the shRNA-treated cells had demonstrated antibiotic resistance as a result of transfection, treatment with shRNA was not sufficient to reduce Fsk-mediated SOCS3 induction.

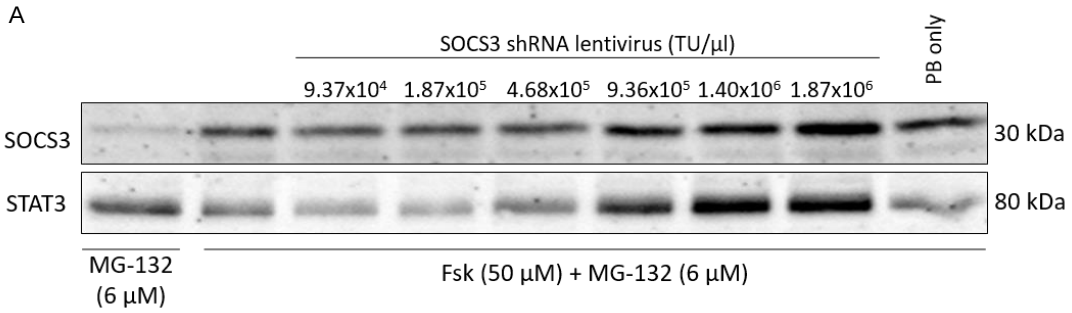
A
SOCS3 shRNA lentivirus (TU/μl)
9.37x10⁴ 1.87x10⁵ 4.68x10⁵ 9.36x10⁵ 1.40x10⁶ 1.87x10⁶
PB only
SOCS3
STAT3
30 kDa
80 kDa
MG-132 (6 μM)
Fsk (50 μM) + MG-132 (6 μM)

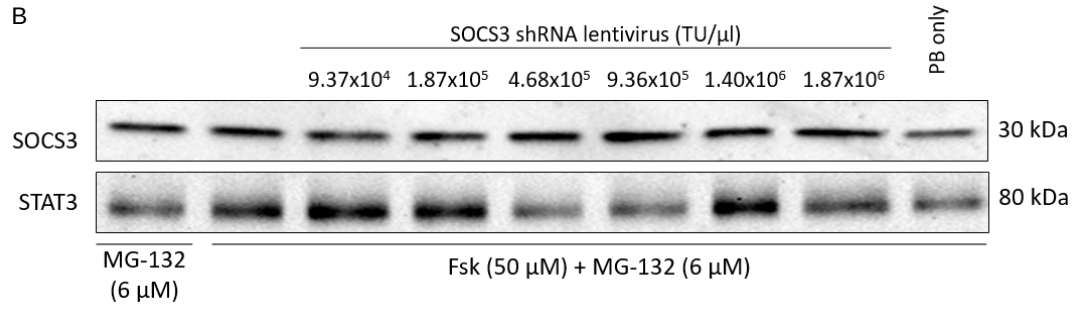
B
SOCS3 shRNA lentivirus (TU/μl)
9.37x10⁴ 1.87x10⁵ 4.68x10⁵ 9.36x10⁵ 1.40x10⁶ 1.87x10⁶
PB only
SOCS3
STAT3
30 kDa
80 kDa
MG-132 (6 μM)
Fsk (50 μM) + MG-132 (6 μM)

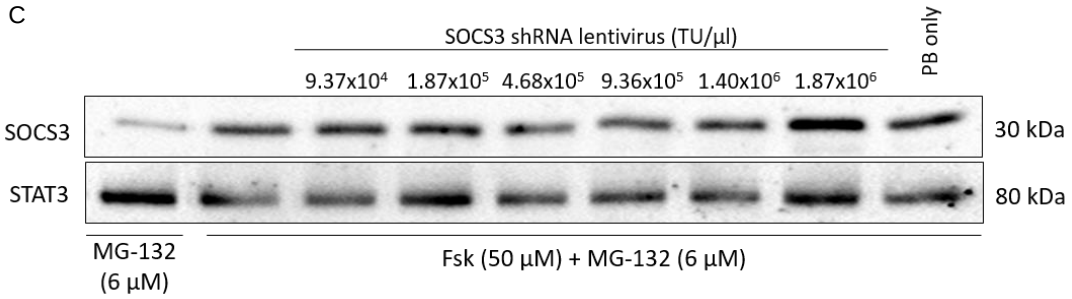
C
SOCS3 shRNA lentivirus (TU/μl)
9.37x10⁴ 1.87x10⁵ 4.68x10⁵ 9.36x10⁵ 1.40x10⁶ 1.87x10⁶
PB only
SOCS3
STAT3
30 kDa
80 kDa
MG-132 (6 μM)
Fsk (50 μM) + MG-132 (6 μM)

Figure 4.6: Lentiviral delivery of SOCS3 shRNA is not sufficient to silence SOCS3 gene expression

A) HPAECs were seeded in 6 cm dishes and grown to 70% confluency prior to overnight treatment with SOCS3 shRNA lentivirus at $9.37x10^4$ TU/µl, $1.87x10^5$, $4.68x10^5$, $9.36x10^5$, $1.40x10^6$ and $1.87x10^6$ TU/µl. SOCS3 shRNA lentivirus was prepared in polybrene (PB) (8 µg/ml) containing DMEM. Cells were then maintained in endothelial cell growth medium (ECGM) for 4 days prior to 4 hours of treatment with Fsk (50 µM) in the presence of MG-132 (6 µM). Treatment with Fsk (50 µM) in the presence of MG-132 (6 µM) for 4 hours without lentiviral treatment was used as a positive control. Treatment with MG-132 (6 µM) alone without lentiviral treatment was used as a negative control. Incubation with PB (8 µg/ml) in the absence of lentiviral treatment was also performed. Cells were harvested and whole cell lysates were equalised for protein content and fractionated via SDS-PAGE for immunoblotting with SOCS3. Immunoblotting with STAT3 was used for a loading control. Experiment performed to *n=1*. B) The experiment was performed as described above apart from HPAECs were treated with SOCS3 shRNA at 40% confluency. Experiment performed to *n=1*. C) The experiment was performed as described above apart from the ECGM media was supplemented with puromycin (2 µg/ml) and cells were incubated for 10 days post-shRNA treatment as opposed to 4 days. Experiment performed to *n=1*.

To further establish if the shRNA lentivirus was successfully infecting HPAECs, cells were imaged for mCherry expression. Cells were seeded in Nunc™ Lab-Tek™ Chambered Coverglass at a density of $2x10^4$ cells per chamber and left to incubate overnight. The lentivirus was then prepared at the same concentrations used for the previous experiments ($9.37x10^4$ TU/µl, $1.87x10^5$, $4.68x10^5$, $9.36x10^5$, $1.404x10^6$ and $1.872x10^6$ TU/µl) and applied to cells as previously described. As a negative control, HPAECs were maintained in fresh EGM-2 in the absence of lentiviral treatment. Cells were incubated for 5 days and then prepared for imaging of mCherry as previously described (Section 2.2.2.4)

There was no mCherry expressed in the absence of lentiviral treatment. SOCS3 shRNA lentiviral treatment at $9.37x10^4$ TU/µl, 1.87x105, $4.68x10^5$, and $1.872x10^6$ TU/µl also produced no mCherry expression (Figure 4.7A). Lentivirus concentrations of $9.36x10^5$ TU/µl and $1.404x10^6$ TU/µl did result in mCherry expression (Figure 4.7A) suggesting these concentrations are suitable for successful transfection of HPAECs. The average percentage of infected cells was calculated as described (Section 2.2.2.4) to generate infection efficiency data. A shRNA concentration of $1.404x10^6$ TU/µl resulted in 98.6% infection efficiency, compared to 72.6% for $9.36x10^5$ TU/µl of lentivirus (Figure 4.7B).

4.3 Discussion

Treatment with a SOCS3-containing lentivirus is sufficient to cause SOCS3 expression with no further stimulation (Figure 4.1a), and to inhibit IL-6/sIL-

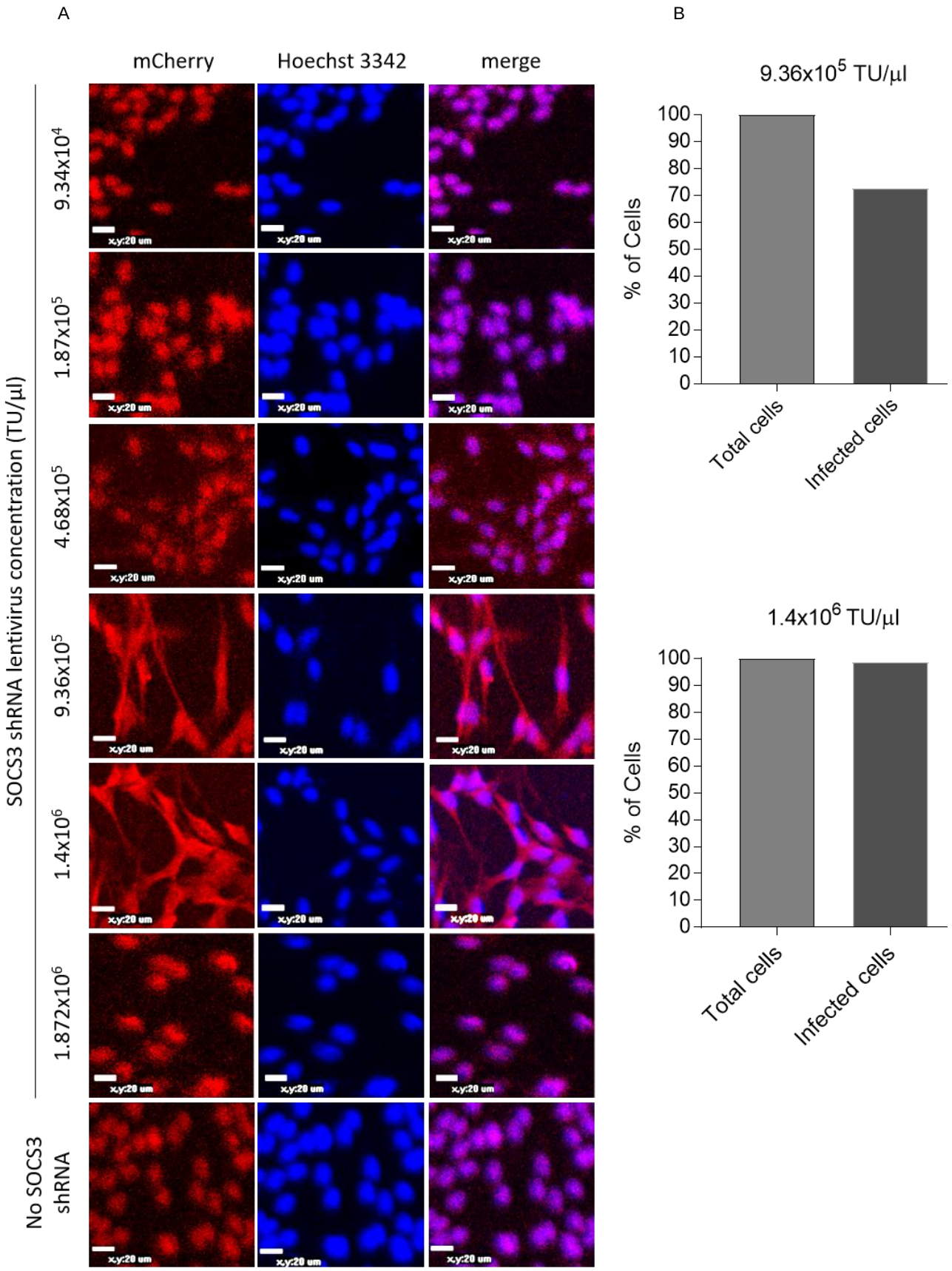
A
mCherry
Hoechst 3342
merge
SOCS3 shRNA lentivirus concentration (TU/µl)
9.34x10^4
1.87x10^5
4.68x10^5
9.36x10^5
1.4x10^6
1.872x10^6
No SOCS3 shRNA
x,y:20 um
B
9.36x10^5 TU/µl
% of Cells
100
90
80
70
60
50
40
30
20
10
0
Total cells
Infected cells
1.4x10^6 TU/µl
% of Cells
100
90
80
70
60
50
40
30
20
10
0
Total cells
Infected cells

Figure 4.7: Lentiviral delivery of SOCS3 shRNA in HPAECs results in mCherry expression at $9.36x10^5$ and $1.40x10^6$ TU/µl

A) HPAECs were seeded in Nunc™ Lab-Tek™ Chambered Coverglass at a density of $2x10^4$ cells per chamber and left to incubate overnight prior to treatment with SOCS3 shRNA lentivirus at $9.37x10^4$ TU/µl, $1.87x10^5$, $4.68x10^5$, $9.36x10^5$, $1.40x10^6$ and $1.87x10^6$ TU/µl. Lentiviral media was replaced with fresh endothelial cell growth media after 24 hours and incubated for 5 days prior to fixing in methanol. Cells incubated in the absence of lentivirus were used as a negative control. Cells were counterstained with Hoechst 33342 (1 µM) (blue) prior to imaging for mCherry expression (red). Experiment completed to *n=1*. B) Infection counts for cells treated with lentivirus concentrations of $9.36x10^5$ TU/µl and $1.404x10^6$ TU/µl.

6Rα mediated tyrosine 705 phosphorylation of STAT3 (Figure 4.1b). This supports other research that has shown SOCS3 to limit IL-6 *trans*-signalling activity (reviewed by Babon et al. 2014) and is relevant to the hypothesis because IL-6 is a key inflammatory mediator in the progression of PAH (Section 1.4.2) (Savale et al. 2009; Steiner et al. 2009; Maston et al. 2018; Tamura et al. 2018). Prostanoids are currently used in the treatment of PAH (O'Connell et al. 2016) and, in the case of BPS, treprostinil and the selexipag metabolite ACT-333679, also induce SOCS3 protein expression in cells involved in the pathogenesis of PAH (Chapter 3, Figures 3.1 and 3.4). Thus, this may indicate a novel therapeutic mechanism which has yet to be explored.

To address this, the ability of BPS or treprostinil to limit IL-6/sIL-6Rα mediated tyrosine 705 phosphorylation of SOCS3 in HPAECs was measured and shown to be significant in HPAECs and WT AS-M.5 cells (Figures 4.2, 4.3 and 4.4). However, neither BPS nor treprostinil significantly limited IL-6 *trans*-signalling activity in AS-M.5 SOCS3 KO cells (Figure 4.3). As Nur77 was significantly induced by all treatments in both cell types (Figure 4.2), knockdown of SOCS3 must be a result of SOCS3 gene knockout and not an indirect effect of SOCS3 KO on cAMP signalling. Consequently, impaired inhibition of IL-6-mediated phosphorylation of STAT3 by BPS and treprostinil in AS-M.5 SOCS3 KO cells must also be due to SOCS3 gene knockout and not an indirect effect of SOCS3 KO on cAMP signalling.

Although not significant, there is a slight decrease in tyrosine 705 STAT3 phosphorylation post-treatment with forskolin, BPS and treprostinil in AS-M.5 SOCS3 KO cells. This reduction may be due to the effects of other inhibitory pathways. For instance, JAK/STAT signalling is also inhibited by PTPs such

as SHP2. SHP2 contains an SH2 domain (Hof et al. 1998) like that seen in SOCS3, thus it is able to bind to the phosphorylated tyrosine 759 residue of gp130 (Section 1.4.1). In the absence of SOCS3, and therefore with less competition for binding, it is reasonable to believe SHP2, which is ubiquitously expressed, will bind to tyrosine 759 to mediate JAK/STAT signalling. Research has shown PTP to regulate endothelial barrier function in human lung microvascular ECs and interact with VE-cadherin (Sui et al. 2005). Dysfunctional endothelial barrier function is associated with both IL-6 *trans*-signalling activity (Alsaffar et al. 2018) and PAH (reviewed by Ranchoux et al. 2018). In HPAECs, PTP mRNA has been shown to be expressed (Sui et al. 2005), but the effects of PTP in limiting IL-6 activity in these cells has not been investigated. However, the effect of PTPs on IL-6/sIL-6Rα activity has been determined in other cell types. For instance, in T-cells, IL-6/sIL-6Rα-induced STAT3 phosphorylation was suppressed by overexpression of T-cell-PTP (Yamamoto et al. 2002), and in HUVECS, PTP-MEG2 knockdown resulted in increased IL-6 signalling and activity, as measured by VEGF signalling (Hao et al. 2012).

Research has indicated crosstalk between cAMP and PTPs. In Jurkat T-cells, cAMP-mediated PKA regulates ERK1,2 signalling via phosphorylation of haematopoietic (He)PTP at serine 23 (Saxena et al. 1999). Additionally, in macrophages, cAMP-mediated PKA activates SHP2 to trigger apoptosis and protects against Bordetella adenylate cyclase toxin (Cerny et al. 2015; Ahmad et al. 2016). Interactions between cAMP and PTPs in vascular cells are not well understood, but this may be a potential route of cAMP-mediated inhibition of IL-6 activity. PTP inhibitors, such as the SHP2/SHP1 potent inhibitor NSC

87877 (Tocris; Cat. No. 2613), could be utilised in future experiments to determine the extent of PTP inhibition of IL-6-mediated phosphorylation of STAT3.

Another unexpected finding was that phosphorylation of STAT3 occurred in the absence of stimulation by IL-6/sIL-6Rα in AS-M.5 SOCS3 KO cells (Figure 4.4). Endo et al. (1997) suggested there was constitutive inhibition of JAK by SOCS proteins and the presence of constitutively expressed SOCS3 has been found in other experiments performed by the Palmer lab (currently unpublished), which supports potential constitutive SOCS3 inhibition of JAK/STAT signalling.

Current SOCS3 antibodies available are not sensitive enough to detect low levels of expression. Towards the end of this project, a more sensitive chemiluminescent substrate (WESTAR SUPERNOVA horseradish peroxidase (HRP) detection, Cyanogen; Cat. No. XLS3) was utilised. This may explain why the SOCS3 band in MG-132 only treatments is more pronounced in later experiments (Figure 4.6) compared to immunoblots in earlier experiments (Chapter 3), although the use of WESTAR SUPERNOVA HRP detection substrate also resulted in the speckled dots apparent on some figures. To ensure sensitivity and linearity of protein detection by the WESTAR SUPERNOVA HRP, detection of protein samples over a range of concentrations (0 ng/µl, 10, 20, 30, 40 ng/µl) was measured by utilising protein samples from previously lysed cells treated with Fsk. SDS-PAGE and immunoblotting for STAT3, SOCS3 and Nur77 was then completed which showed the WESTAR SUPERNOVA HRP detection substrate detected small

changes in protein content, including SOCS3, over a range of concentrations in a linear manner (Figure 4.8).

Utilising other sensitive methods of protein detection may give some clarification on the presence of constitutive SOCS3 protein. SOCS3 ELISA kits (MyBioSource, Inc.; Cat. No. MBS703435) are now commercially available and claim to detect very low protein levels. Alternatively, the use of immunofluorescence antibodies in immunocytochemistry or flow cytometric analysis of HPAECs may help determine if constitutive SOCS3 protein is present in ECs.

To further explore a role for SOCS3 in prostanoid treatment of PAH, techniques were utilised to silence SOCS3 expression in HPAECs. Neither shRNA nor siRNA were successful in reducing Fsk-induced SOCS3 protein expression (Figure2 4.4 and 4.6). The effect of shRNA and siRNA on SOCS3 RNA levels were not determined but should be considered in the future as qPCR will enable greater sensitivity than western blotting alone. One potential reason for unsuccessful silencing of SOCS3 protein is that the experiments were not optimised for successful transfection of the RNA into the cells. For siRNA, an increased amount of HiPerFect was used to try and improve siRNA transfection. However, a range of HiPerFect concentrations alongside altering variables such as cell confluency and treatment time was not tested due to time limits.

With regards to shRNA experiments, the confluency of the cells at the time of lentiviral treatment was reduced to enable greater transduction efficiency. However, this was not sufficient to enable silencing of SOCS3 expression.

A

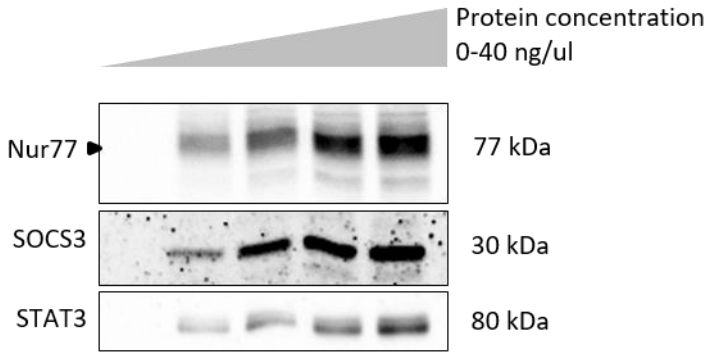
Protein concentration
0-40 ng/ul
Nur77
77 kDa
SOCS3
30 kDa
STAT3
80 kDa

B

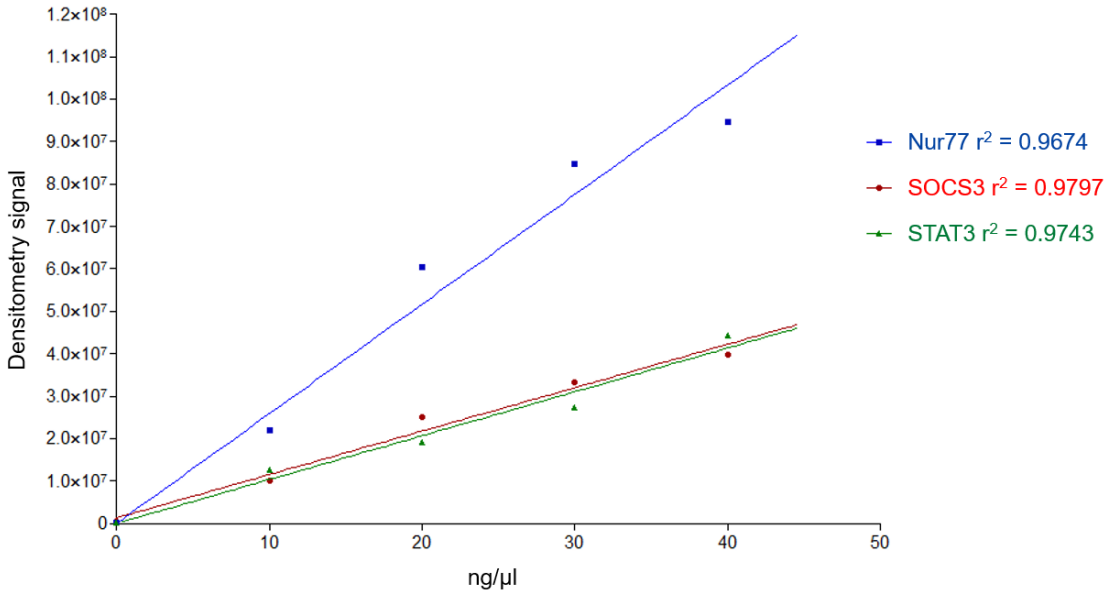
Densitometry signal
1.2×10⁸
1.1×10⁸
1.0×10⁸
9.0×10⁷
8.0×10⁷
7.0×10⁷
6.0×10⁷
5.0×10⁷
4.0×10⁷
3.0×10⁷
2.0×10⁷
1.0×10⁷
0
0
10
20
30
40
50
ng/µl
Nur77 r² = 0.9674
SOCS3 r² = 0.9797
STAT3 r² = 0.9743

Figure 4.8 Sensitivity and linearity of WESTAR SUPERNOVA HRP detection substrate

A) Increasing concentrations of protein from cells previously treated with forskolin (Fsk) (10 µM) and lysed were separated via SDS-PAGE for immunoblot analysis with SOCS3, Nur77 and STAT3 as previously described (Section 2.2.3.2). B) Densitometry values for SOCS3, Nur77 and STAT3 acquired using LICOR Image Studio Lite software were plotted on a graph against protein concentration to measure linearity of protein detection. Experiment completed to *n=1*.

Further measures to determine if cells were being successfully infected by the lentivirus such as treatment with puromycin-containing media (Figure 4.6C) suggested HPAECs were demonstrating puromycin-resistance as a result of lentivirus infection but not SOCS3 knockdown. Similarly, fluorescent images of cells taken 5 days post-treatment with shRNA lentivirus demonstrate mCherry expression (Figure 4.7). These results suggest HPAECs are being successfully infected by the lentivirus, but that the lentivirus is not sufficient to silence SOCS3 gene expression. Alternatively, the process of lentiviral infection may be initiating an immune response, thus increasing SOCS3 production to a greater extent than it is silencing it.

As attempts to silence SOCS3 gene expression via siRNA and shRNA in HPAECs were unsuccessful, alternative methods to measure the role of SOCS3 in prostanoid mediated inhibition of IL-6 *trans*-signalling should be utilised in the future. HPAEC SOCS3 KO cells could potentially be developed using CRISPR (Gilbert et al. 2013) or transcription activator-like effector nucleases (TALEN) technology (Sun and Zhao 2013). However, genome engineering techniques such as these may also not be successful in HPAECs due to them being primary cells and having a limited passage capacity.

Mutagenesis of HPAECs may provide a different approach. SU/Hx animal models with a gp130YF knock in mutation at tyrosine 759, essentially preventing the attenuation of JAK-mediated gp130 phosphorylation which would normally result from SOCS3 or SHP2 binding to gp130, have been utilised previously to measure the impact of STAT3 hyper-activation (Atsumi et al. 2002; Tsuji et al. 2009). In animal models, mice carrying this mutation

experienced greater RVSP after hypoxia compared to healthy mice (unpublished data provided by Professor Tim Palmer, University of Hull). Creating the same mutation in HPAECs or utilising lung ECs isolated from WT and gp130YF knock in mice would provide an alternative method to attenuate SOCS3 inhibition of JAK/STAT signalling.

Alternatively, lentiviral delivery of mutated SOCS3 *in vitro* that results in loss of function to either the SH2 or KIR domain of SOCS3 have previously been shown to enhance JAK/STAT signalling. KIR single point mutations (L22D and F25A) have previously been found to attenuate the ability of SOCS3 to inhibit cytokine signalling as measured by breast tumour kinase-mediated STAT3 phosphorylation (Gao et al. 2012). In HEK 293 cells transiently transfected with SOCS F136L, a F136L mutation within the SH2 domain of SOCS3 causing loss-of-function, resulted in increased erythropoietin/JAK2 mediated cell growth (Suessmuth et al. 2009). Whether HPAECs could withstand such mutations and their effect on SOCS3 inhibition of IL-6/sIL-6Rα induced JAK/STAT signalling are yet to be investigated.

To conclude, prostanoids significantly limit IL-6/sIL-6Rα signalling activity in HPAECs and WT but not in SOCS3 KO AS-M.5 cells, suggesting the effects of prostanoids may be mediated by SOCS3. However, further work to knockdown SOCS3 expression in HPAECs is required before we can conclusively demonstrate this in ECs relevant to PAH.

Although immunoblotting has shown the reduction in IL-6/sIL-6Rα-induced tyrosine 705 phosphorylation of STAT3 by prostanoids in HPAECs to be significant, it is unclear as to whether this would be sufficient to have

therapeutic affects in PAH. Thus, the impact of BPS, treprostinil and ACT-333679 on IL-6/sIL-6Rα-mediated gene transcription and cell barrier function was determined.

5. Prostanoids limit functional effects of IL-6 *trans*-signalling

5.1 Introduction

As previously discussed, IL-6 *trans*-signalling is associated with the proliferation, migration and survival of ECs, as well as impacting EC permeability enabling inflammatory and pro-growth factors to access the underlying PASMCs (Section 1.4.2). Affected ECs and SMCs contribute to the vascular remodelling and characteristic plexiform lesions associated with PAH.

To be therapeutically beneficial, drugs would need to prevent or potentially reverse these IL-6-mediated effects. BPS, treprostinil and ACT-333679 limited IL-6 *trans*-signalling in HPAECs, which are involved in PAH vascular remodelling, measured via tyrosine 705 phosphorylation of STAT3 (Figure 4.2). The following experiments aim to determine if prostanoid inhibition of IL-6 *trans*-signalling activity is sufficient to reduce functional effects of IL-6/sIL-6Rα in HPAECs.

5.2 Results

5.2.1 Prostanoids limit IL-6/sIL-6Rα-induced cell permeability

IL-6/sIL-6Rα, but not IL-6 alone, compromised EC barrier function in ovarian ECs according to the redistribution of actin filaments (Wei et al. 2013), and IL-

$6^{-/-}$ KO mice were protected from mechanical ventilation and hydrochloric acid - induced alveolar-capillary permeability (Gurkan et al. 2011). Endothelial permeability enables the movement of inflammatory factors and GF through the EC monolayer where they can stimulate SMCs resulting in a pro-inflammatory, proliferative phenotype that contributes to the development of PAH (Section 1.3.1). As increased cell permeability contributes to PAH progression, the effect of prostanoids on IL-6/sIL-6Rα induced cell permeability in confluent HPAECs was measured via a FITC-dextran cell permeability assay (Anderl et al. 2012).

Transwell collagen coated inserts were seeded with $1x10^6$ cells. This was repeated after 24 hours to ensure confluency of the cell monolayer. Cells were treated 72 hours after the initial seeding for 2 hours with BPS (10 μM). Fsk (50 μM) treatment for 4 hours was used as a positive control of IL-6/sIL-6Rα inhibition (Figure 4.2). 4 hours of vehicle treatment was used as a negative control. Cells were then treated with IL-6/sIL-6Rα for 24 hours prior to the assay being performed as previously described (Section 2.2.5.1).

In the absence of IL-6/sIL-6Rα, Fsk and BPS had no significant effect on cell permeability compared to the vehicle (Figure 5.1). In contrast, IL-6/sIL-6Rα treatment significantly increased cell permeability, which was attenuated by treatment with either BPS or Fsk (Figure 5.1). Treating with high concentrations of IL-6 (100 ng/ml) to mimic overexpression of IL-6 reduced VE-cadherin expression local to cellular junctions (Kayakabe et al. 2012), and treating IL-6/sIL-6Rα signalling in HUVECs resulted in increased cell permeability and reduced VE-cadherin expression at cellular junctions (Lo et al. 2011). As a result, it was next investigated whether IL-6/sIL-6Rα altered

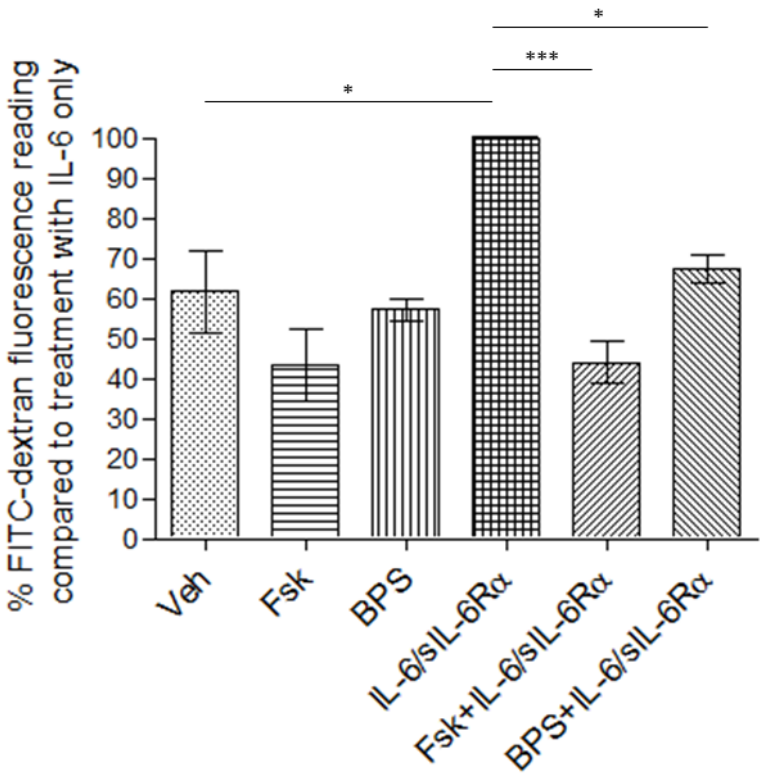

Figure 5.1: Prostanoids limit IL-6/sIL-6Rα induced HPAEC permeability

Confluent HPAECs were treated for 2 hours with beraprost sodium salt (BPS) (10 μM), or for 4 hours with forskolin (Fsk) (50 μM), which was used as a positive control, in the presence and absence of IL-6 (5 ng/ml) and sIL-6Rα (25 ng/ml) (IL-6/sIL-6Rα) which was added 24 hours prior to treatment with FITC-dextran as described in the Materials and Methods. Cells were incubated with FITC-dextran for 45 minutes before fluorescence readings were taken from the receiver media. Results were calculated as the percentage difference of fluorescence compared to treatment with IL-6/sIL-6Rα alone. * indicates $P<0.05$, which was considered significant. *** indicates <0.0001. Quantification for *n=4* experiments has been shown.

VE-cadherin in confluent monolayers of HPAECs as an alternative measure of IL-6/sIL-6Rα-induced cell permeability.

HPAECs were seeded on to 4-well Nunc™ Lab-Tek™ chambers as described in Section 2.2.5.2. Cells were then treated with or without Fsk (50 µM) for 4 hours prior to treatment with or without IL-6/sIL-6Rα. Cells were then prepared, and images taken as previously described (Section 2.2.5.2). Prominent VE-cadherin staining was evident at cellular junctions in the vehicle treatment (Figure 5.2A). Post-treatment with IL-6/sIL-6Rα there was a loss of localised VE-cadherin which was partially rescued by treatment with Fsk (Figure 5.2A). Interestingly, Fsk alone disrupted VE-cadherin localisation.

Numerous attempts to complete this experiment were made, however only the one example shown in Figure 5.2A was of good enough quality to interpret. Details of the fixation, staining and imaging protocols used for the different attempts are described in the below schematic (Figure 5.2B). A representative image of vehicle treated cells has been used for all optimisation conditions for comparison. The initial experiment showed no VE-cadherin localisation at cellular junctions in any treatment. As VE-cadherin expression at cellular junctions increases with increased monolayer confluency (Ferreri et al. 2008), this may be result from a lack of cell confluency so increased the initial cell density. Also, as fixation via methanol permeates the cell membrane (Jamur and Oliver 2010), the 0.1% v/v triton/PBS wash was removed. The final change was magnification used, with images taken at 400x magnification as opposed to 800x (Figure 5.2B, opt. 1). However, as the staining of these cells appeared to be non-specific with high background staining, the 0.1% v/v triton/PBS wash

A

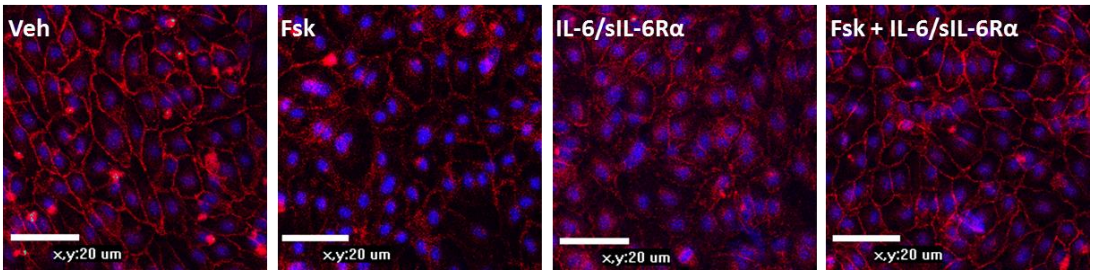

B

Exp. 1	• Seeding density: 80,000 incubated overnight. • Antibody concentrations: VE-cadherin (1 µg/ml), Alexa Fluor 568-conjugated goat anti-rabbit IgG (H+L) (2 µg/ml), Hoeshct 33342 (1 µM). • Wash volumes/times: wash after fixation - 200 µl 0.1% v/v triton/PBS for 5 min, 200 µl PBS 2x 5 minutes. Washes after fixation - 200 µl PBS 3x 5 minutes. • Magnification: 800x, medium pinhole, pixel dwell 20ms, average 4. • Results: No cell junction localisation – potentially too low cell density.	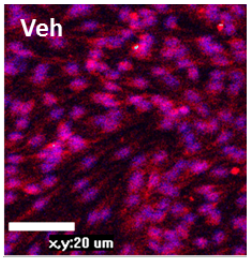
Opt. 1	• Seeding density: 100,000 - incubated overnight. • Antibody concentrations: VE-cadherin (1 µg/ml), Alexa Fluor 568-conjugated goat anti-rabbit IgG (H+L) (1 µg/ml), Hoeshct 3332 (0.5 µM). • Wash volumes/times: 200 µl PBS, 3x 5 minutes. • Magnification: 400x, medium pinhole, pixel dwell 20ms, average 4. • Results: Image very blurred, no cell junction VE-cadherin localisation.	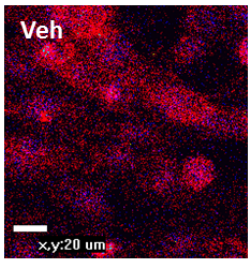
Opt. 2	• Seeding density: 100,000 - incubated overnight. • Antibody concentrations: see above. • Wash volumes/times: wash after fixation - 500 µl 0.1% v/v triton/PBS for 5 min, 500 µl PBS 2x 5 minutes. Washes after fixation - 500 µl PBS 3x 5 minutes. • Magnification: 800x, large pinhole, pixel dwell 20ms, average 4 • Results: Images used for Figure 5.2A.	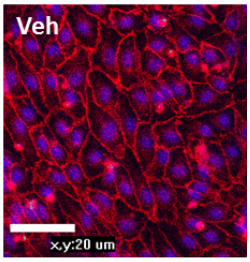
Opt. 3	• Seeding density: 80,000 – incubated for 48 hours. • Antibody concentrations: see above. • Wash volumes/times: wash after fixation - 500 µl 0.1% v/v triton/PBS for 5 min, 500 µl PBS 2x 5 minutes. Washes after fixation - 500 µl PBS 3x 5 minutes. • Magnification: 400x, medium pinhole, pixel dwell 20ms, average 4. • Results: No VE-cadherin cell junction localisation. Image not as clear as previous attempt (Opt.2).	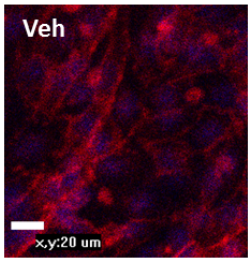
Opt. 4	Seeding density: 200,000 – incubated overnight. Antibody concentrations: see above. Wash volumes/times: wash after fixation – 1ml 0.1% v/v triton/PBS for 5 min, 1ml PBS 2x 5 minutes. Washes after fixation – 1ml PBS 3x 5 minutes. Magnification: 400x, medium pinhole, pixel dwell 20ms, average 4. Results: Image not as clear as previous attempt (Opt.2).	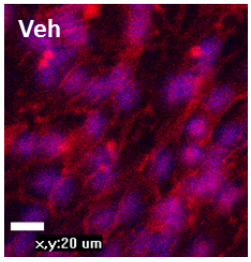

Figure 5.2: VE-cadherin staining of HPAECs post-treatment with IL-6/sIL-6Rα and forskolin

A) Cells were treated for 4 hours with Forskolin (Fsk) (50 μM) in the presence and absence of IL-6 (5 ng/ml) and sIL-6Rα (25 ng/ml) (IL-6/sIL-6Rα) which was applied 24 hours prior to fixing cells. A vehicle (Veh) control was also performed. Cells were prepared for imaging as described (Section 2.2.5.2) and then visualised at 800x magnification using a Nikon ECLIPSE TE2000-E confocal microscope. Images were retained using EZ-C1 3.90 software. B) Cell seeding, staining and imaging details of all experiments completed to optimise imaging of VE-cadherin in HPAECSs. Exp; experiment, Opt; optimisation.

was reincorporated in future experiments to increase cell permeability (Jamur and Oliver 2010). To reduce background staining, the concentration of Alexa Fluor 568-conjugated goat anti-rabbit IgG (H+L) and Hoescht 33342 was reduced to 1 µg/ml and 0.5 µM respectively. In addition, a larger volume of PBS (0.5 ml) was used for washing steps to ensure efficient washing of cells between incubation with antibodies and Hoechst 33342. In addition, magnification was increased back up to 800x (Figure 5.2B, opt. 2). This resulted in good quality images that clearly demonstrated VE-cadherin expression at cellular junctions. 2 further repeats (Figure 5.2B, opt. 3 and opt. 4) of the method used in optimisation 2 were completed but images were taken at 400x magnification. For optimisation 4 conditions, wash volumes were further increased to 1 ml. Neither opt. 3 nor opt. 4 resulted in better quality images than those seen in opt. 2.

As BPS, treprostinil and ACT-333679 limited IL-6/sIL-6Rα-induced STAT3 tyrosine 705 phosphorylation to a similar degree as Fsk (Figure 4.2), further experiments were performed to determine if BPS could also prevent IL-6 *trans*-signalling-mediated loss of localised VE-cadherin. HPAECs were prepared as described above prior to pre-treatment with or without BPS (10 µM) for 3 hours in the presence or absence of IL-6/sIL-6Rα treatment for a further 24 hours. Treatment with Fsk (50 µM) with or without IL-6/sIL-6Rα was also included. Treatment with LPS (1 µg/ml) was included as a positive control stimulus to induce loss of VE-cadherin from the cell surface (Flemming et al. 2015; Zheng et al. 2018). A vehicle control was also completed. Cells were prepared for fluorescence microscopy as previously described (Section 2.2.5.2). Confocal images were taken in which VE-cadherin localisation appears similar in post-

vehicle, LPS only and IL-6/sIL-6Rα only treatments but increased with treatment of Fsk in the presence of IL-6/sIL-6Rα (Figure 5.3). In contrast to the previous experiment (Figure 5.2A), treatment with Fsk alone increased VE-cadherin localisation to the cellular junctions, as did treatment with BPS alone (Figure 5.3). Although attempts were taken to optimise imaging of VE-cadherin expression (Figure 5.2B), the images displayed in the figure were the best quality acquired. Unfortunately, due to images being too blurry to identify individual cells and VE-cadherin expression around the whole of the cells, imageJ analysis or manual cell counting was not possible thus statistical analysis has not been performed and only visual interpretation of the figures shown has been described.

5.2.3 The effects of prostanoids on IL-6 stimulated gene and protein expression

As discussed, IL-6 induces genes that promote PAH pathogenesis (Section 1.4.1), including those for cell adhesion molecules. A recent study in HUVECs found IL-6 induced both ICAM1 and VCAM1 after 48 hours of stimulation (Wiejak et al. 2019). This is interesting as increased serum soluble-ICAM1 levels correlate with increased mPAP, systolic PAP and diastolic pulmonary arterial pressure (Sungprem et al. 2009) and has been suggested as a possible biomarker for PAH (Pendergrass et al. 2010; Oguz et al. 2014), and upregulation of plasma VCAM1 levels is associated with vascular diseases including PAH (Pendergrass et al. 2010; Agassandian et al. 2015). Therefore, IL-6/sIL-6Rα induction of adhesion molecules may be one mechanism in which IL-6 *trans*-signalling contributes to PAH progression.

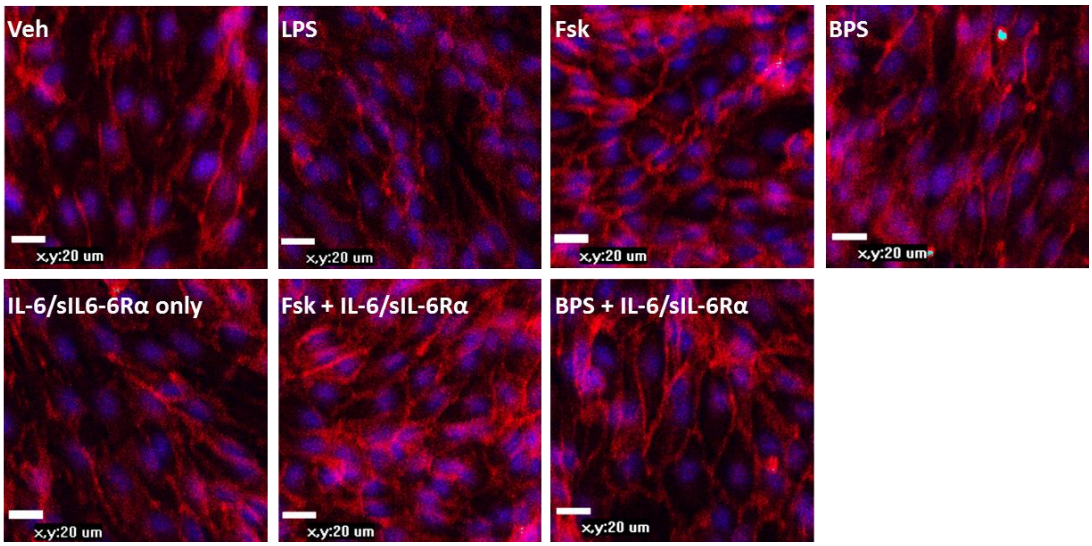

Figure 5.3 VE-cadherin staining of HPAECs post-treatment with IL-6/sIL-6Rα and beraprost sodium salt

HPAECs were treated for 2 hours with beraprost sodium salt (BPS) (10 μM) in the presence and absence of IL-6 (5 ng/ml) and sIL-6Rα (25 ng/ml) (IL-6/sIL-6Rα) which was applied for 24 hours. 4 hours of treatment with forskolin (Fsk) (50 μM) was used as a positive control, treatment with lipopolysaccharide (LPS) (1 μg/ml) for 24 hours was used as a negative control. Cells were prepared for imaging as described (Section 2.2.5.2) and then visualised at 400x magnification using a Nikon ECLIPSE TE2000-E confocal microscope. Images were retained using EZ-C1 3.90 software. Experiment was completed to *n=5*. Representative images have been shown.

To test this, HPAECs were treated with or without IL-6/sIL-6Rα for up to 24 hours. Cells were then harvested and lysed prior to analysis by SDS-PAGE and immunoblotting for VCAM1 and STAT3. The 16-hour IL-6/sIL-6Rα treatment was harvested at a different time to the other treatments, thus a separate 16-hour control was performed. VCAM1 expression is not increased after 16 hours treatment with IL-6/sIL-6Rα in comparison to the 16-hour vehicle control (Figure 5.4A). All other treatments were harvested at the same time as the 24-hour vehicle control. LPS was used as a positive control of VCAM1 expression (Lin et al. 2007; Sawa et al. 2008), but was not sufficient to induce VCAM1 after 24 hours treatment in HPAECs in comparison to the 24-hour vehicle control (Figure 5.4A). Similarly, none of the IL-6/sIL-6Rα treatments influenced VCAM1 expression compared to the vehicle control (Figure 5.4A). This could be indicative of high basal VCAM1 expression in HPAECs, making it difficult to detect further VCAM1 induction.

As IL-6/sIL-6Rα induction of VCAM1 was not successful, IL-6/sIL-6Rα induction of ICAM1 was considered. Although treatment with LPS did result in more pronounced ICAM1 expression after 24 hour, IL-6/sIL-6Rα induction of ICAM1 in human saphenous vein (HSV)ECs also showed high basal levels of ICAM1 protein which were not affected by treatment with IL-6/sIL-6Rα (Figure 5.4B) (unpublished data provided by Dr J.J.L.Williams, University of Glasgow).

As it was crucial to identify an IL-6/sIL-6Rα-induced gene in HPAECs, VEGFR2 induction was investigated. IL-6 is also known to promote angiogenesis via upregulation of VEGF (Cohen et al. 1996; Wei et al. 2003b; Huang et al. 2004) and VEGFR2 (Waldner et al. 2010). VEGF is the key VEGF

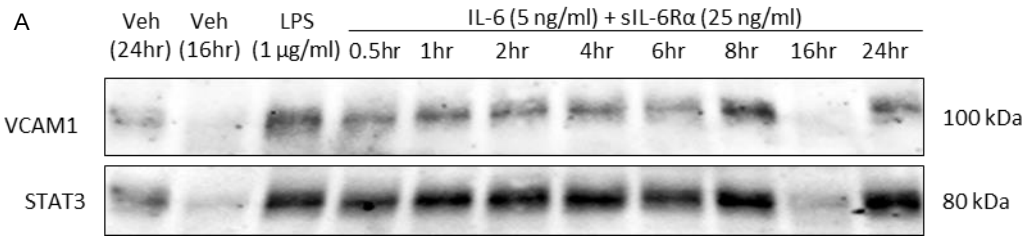
A
Veh (24hr)
Veh (16hr)
LPS (1 μg/ml)
IL-6 (5 ng/ml) + sIL-6Rα (25 ng/ml)
0.5hr
1hr
2hr
4hr
6hr
8hr
16hr
24hr
VCAM1
100 kDa
STAT3
80 kDa

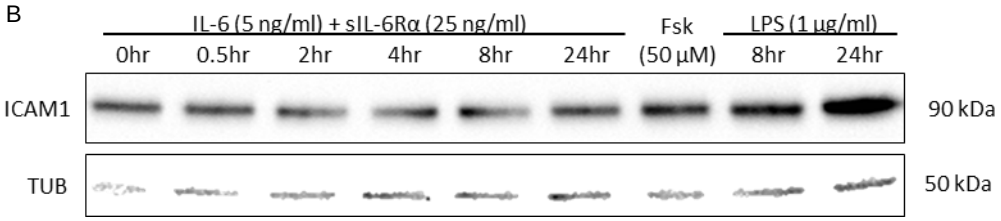
B
IL-6 (5 ng/ml) + sIL-6Rα (25 ng/ml)
Fsk (50 μM)
LPS (1 μg/ml)
0hr
0.5hr
2hr
4hr
8hr
24hr
8hr
24hr
ICAM1
90 kDa
TUB
50 kDa

Figure 5.4: IL-6/sIL-6Rα has no effect on ICAM1 or VCAM1 protein expression in HSVECs and HPAECs respectively

A) HPAECS were treated with IL-6 (5 ng/ml) + sIL-6Rα (25 ng/ml) for 0.5 hours, 1, 2, 4, 8, and 24 hours. A vehicle (Veh) control was performed as a negative control and cells were treated with lipopolysaccharide (LPS) (1 µg/ml) for 24 hours as a positive control. A 16-hour treatment with IL-6 (5 ng/ml) + sIL-6Rα (25 ng/ml) was performed in parallel alongside a 16-hour Veh control. Whole cell lysates were then equalised for protein content and fractionated via SDS-PAGE for immunoblotting with VCAM1. Immunoblotting with STAT3 was used for a loading control. Experiment performed to *n=1*. B) HSVECS were treated with IL-6/sIL-6Rα for 0 hours, 0.5, 2, 4, 8 and 24 hours. 4 hour treatment with forskolin (Fsk) (50 µM) was used as a negative control. Treatment with LPS (1 µg/ml) for 8 hours and 24 hours was used as a positive control. Whole cell lysates were then equalised for protein content and fractionated via SDS-PAGE for immunoblotting with ICAM1. Immunoblotting with tubulin (TUB) was used for a loading control. Experiment performed to *n=1*. This data was provided by Dr J.J.L Williams, University of Glasgow.

receptor in VECs (Millauer et al. 1993; Quinn et al. 1993; Shalaby et al. 1995) and VEGFR mRNA and protein is elevated in ECs of plexiform lesions isolated from PAH patients (Tuder et al. 2001).

As it is crucial for VEGF signalling, which is also increased in PAH and associated with EC dysregulation and vascular remodelling (Section 1.3.2) (Partovian et al. 1998; Papaioannou et al. 2009), it is likely a key factor in PAH development. Thus, as an alternative to adhesion molecules, IL-6/sIL-6α stimulation of VEGFR2 protein expression was determined in HPAECs.

HPAECs were treated with or without IL-6/sIL-6Rα for up to 24 hours. LPS has previously been shown to upregulate VEGF/VEGFR2 signalling in Th1 and Th17 cells (Kim et al. 2010), and as LPS has previously been used as a pro-inflammatory control in these experiments, 24 hours of treatment with LPS was used as a positive control. Cells were harvested and lysed as previously described before protein content was determined. Immunoblotting was carried out and the membranes were probed for VEGFR2 and STAT3. VEGFR2 protein was present in unstimulated HPAECs and its levels were not increased at any time point post-IL-6/sIL-6Rα treatment (Figure 5.5A).

As high basal levels of VEGFR2 were potentially hiding any IL-6/sIL-6Rα-mediated induction of VEGFR2 protein expression, efforts were made to reduce basal protein expression in order to maximise detection of any IL-6/sIL-6Rα-mediated induction. Initially, HPAECs were incubated in EGM-2 or M199 at a range of serum concentrations for up to 24 hours prior to harvesting for lysis and analysis by SDS-PAGE and immunoblotting for VEGFR2 and STAT3 as previously described. However, basal VEGFR2 levels were not reduced in

any condition tested when compared to incubation in normal EGM-2 (Figure 5.5B).

As serum levels did not impact basal VEGFR2 protein expression, but cAMP-modulating agents have been shown to reduce IL-6 mediated inflammatory protein expression, the effect of BPS on basal VEGFR2 was measured. Samples from a previous experiment in which HPAECs were treated with or without BPS (10 µM) for up to 8 hours were utilised (Section 3.1). As this experiment had initially been completed to determine BPS-mediated SOCS3 induction, cells had also been treated with MG-132. Thus, MG-132 alone was used as a negative control. 4 hours of treatment with Fsk in the presence of MG-132 was used a positive control. Like previous experiments, basal VEGFR2 protein was detectable in lysates in the negative control treatment (MG-132 only). As BPS induction of VEGFR2 protein expression was only measured for *n=1* experiments it cannot be used to draw conclusions. However, treatment with BPS appeared to trigger a transient increase in VEGFR2 expression after 0.5 hours, 1 and 2 hours of treatment returning to basal levels 4 hours post-BPS treatment (Figure 5.5C) which is supported by published research.

BPS has previously been shown to stimulate transcription of the VEGF gene after 2 hours and VEGF mRNA is still elevated 24 hours post-treatment with BPS in C2/2 cells, a progenitor cell of the peripheral airway epithelium, and rat aortic SMC (Atsuta et al. 2009). As 2 hours was the earliest time treatment measured, whether gene induction occurs earlier than this is unknown. As VEGF and VEGFR2 protein expression is initially induced in a parallel manner (Cooper et al. 1999), it is likely BPS promotes VEGFR2 expression in a similar

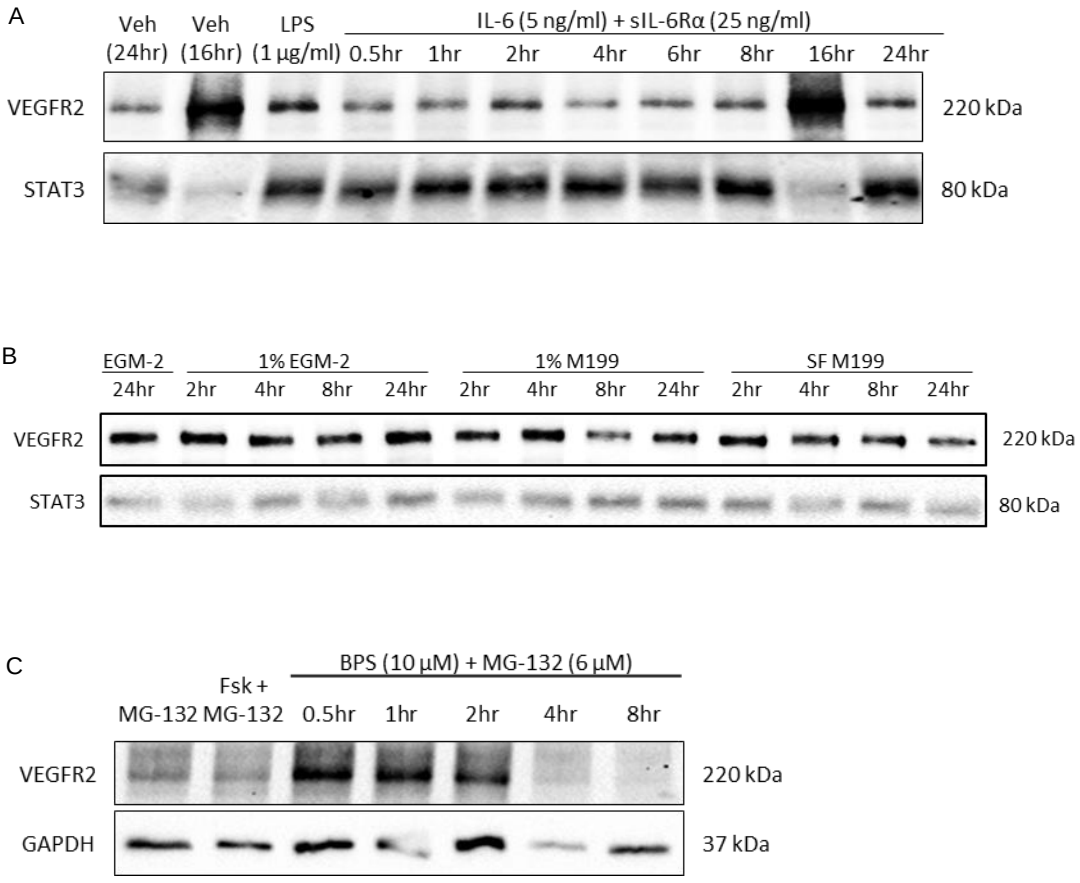
A
Veh (24hr)
Veh (16hr)
LPS (1 μg/ml)
IL-6 (5 ng/ml) + sIL-6Rα (25 ng/ml)
0.5hr
1hr
2hr
4hr
6hr
8hr
16hr
24hr
VEGFR2
220 kDa
STAT3
80 kDa
B
EGM-2
1% EGM-2
1% M199
SF M199
24hr
2hr
4hr
8hr
24hr
2hr
4hr
8hr
24hr
2hr
4hr
8hr
24hr
VEGFR2
220 kDa
STAT3
80 kDa
C
BPS (10 μM) + MG-132 (6 μM)
MG-132
Fsk + MG-132
0.5hr
1hr
2hr
4hr
8hr
VEGFR2
220 kDa
GAPDH
37 kDa

Figure 5.5: IL-6/sIL-6Rα has no effect on VEGFR2 protein expression

A) HPAECS were treated with IL-6 (5 ng/ml) + sIL-6Rα (25 ng/ml) for 0.5 hours, 1, 2, 4, 8, and 24 hours. A vehicle (Veh) control was performed as a negative control and cells were treated with lipopolysaccharide (LPS) (1 µg/ml) for 24 hours as a positive inflammatory control. A 16-hour treatment with IL-6 (5 ng/ml) + sIL-6Rα (25 ng/ml) was performed in parallel alongside a 16 hour vehicle (Veh) control. Whole cell lysates were then equalised for protein content and fractionated via SDS-PAGE for immunoblotting with VEGFR2. Immunoblotting with STAT3 was used for a loading control. Experiment performed to *n=1*. B) HPAECs were incubated in either 1% FBS EGM-2, 1% FBS M199 or serum free (SF) M199 for 2 hours, 4, 8, or 24 hours. 24 hours incubation in fresh 2% FBS EGM-2 was used as a control. Whole cell lysates were then equalised for protein content and fractionated via SDS-PAGE for immunoblotting with VEGFR2. Immunoblotting with STAT3 was used for a loading control. Experiment performed to *n=1*. C) HPAECS were treated with beraprost sodium salt (BPS) (10 µM) for 0.5 hours, 1, 2, 4 and 8 hours in the presence of MG-132 (6 µM). 4 hour treatment with forskolin (Fsk) (50 µM) with MG-132 (6µM) was used as a positive control. MG-132 (6 µM) only was used as a negative control. Whole cell lysates were then equalised for protein content and fractionated via SDS-PAGE for immunoblotting with VEGFR2. Immunoblotting with GAPDH was used for a loading control. Experiment performed to *n=1*.

timeframe to VEGF which would be consistent with the increase in VEGFR2 expression seen 0.5 hours, 1 and 2 hours post-treatment with BPS (Figure 5.5C).

As IL-6/sIL-6Rα did not stimulate protein expression of ICAM1, VCAM1 or VEGFR2, we investigated the effect of IL-6/sIL-6Rα on RNA levels of the STAT3-regulated gene VEGF (Niu et al. 2002; Wei et al. 2003a; Chen et al. 2008). VEGF is increased in the lung tissue of chronic hypoxia and MCT induced lung injury in animal models (Burke et al., 2009, Cho et al., 2009). Additionally, VEGF levels correlate with increased systolic pressure in the pulmonary artery (Papaioannou et al., 2009).

A human VEGFA transcript variant 3 (VEGFA-T3) DNA plasmid (Figure 5.6A) that included a 630 bp VEGFA sequence (Chapter 2, Table 4), and an ampicillin resistant gene, supplied by Sino Biological was expanded in transformed XL1-Blue *E.coli* and prepared (Section 2.2.4.1). Restriction enzyme digests (Section 2.2.4.2) were performed to verify the plasmid. The restrictions enzymes Xba1 and Kpn1 were utilised as these cleaved the plasmid at unique sites that in combination were predicted to generate two DNA products of approximately 0.75 kbp and 5.5 kbp. Cleavage with either Xba1 and Kpn1 individually was predicted to result in a DNA product of 6.2 kbp consistent with the predicted size of VEGFA-T3 cDNA. These were confirmed in digests using three of the resulting cDNA preparations and monitored via 1.5% (w/v) agarose gel electrophoresis. The resulting DNA bands were consistent with the estimated results. When Xba1 and Kpn1 are used in combination there is band visible between 3 and 10 kbps, and a smaller band at 0.75 kbp (Figure 5.6B). When only one restriction enzyme is utilised there

is a visible band between 3 and 10 kbps which is indicative of a DNA product slightly larger than that seen when Xba1 and Kpn1 are used in combination (Figure 5.6B). A lower agarose gel % may have enabled more accurate identification of kbp size for the larger DNA products, however higher agarose concentrations were used to allow for separation of smaller DNA products at the 500 bp region. DNA products are consistent between all three of the colonies isolated (Figure 5.6B).

As restriction enzyme and agarose gel analysis demonstrated successful expansion and preparation of the VEGFA-T3 plasmid DNA, it was subsequently used to optimise PCR conditions required for amplification and detection of endogenous VEGF mRNA in RT-PCRs from HPAECs. PCR was performed as described (Section 2.2.4.4) using plasmid cDNA from each of the three colonies. Reactions were analysed via 2% (w/v) agarose gel electrophoresis. The main PCR product for all colonies was a single band at approximately the 300 bp (Figure 5.6C). Interestingly, this is more consistent with VEGFA exon 2 (367 bp) or exon 7 (313 bp) than the total transcript size (Zhang et al. 2016a). Nevertheless, this was used as a positive control for RT-PCR analysis of VEGFA expression when measuring IL-6/sIL-6Rα-mediated induction of VEGF RNA in HPAECs.

HPAECs were treated with IL-6/sIL-6Rα for up to 48 hours before RNA was purified and reverse transcribed as previously described (Section 2.2.4.4). As cells treated with IL-6/sIL-6Rα for 16 hours were harvested prior to the other treatments, a separate 16 hour vehicle control was also performed. Reaction products were analysed via agarose gel electrophoresis (Section 2.2.4.5) (Figure 5.7A). VEGFA-T3 plasmid DNA was used as a positive control while a

A

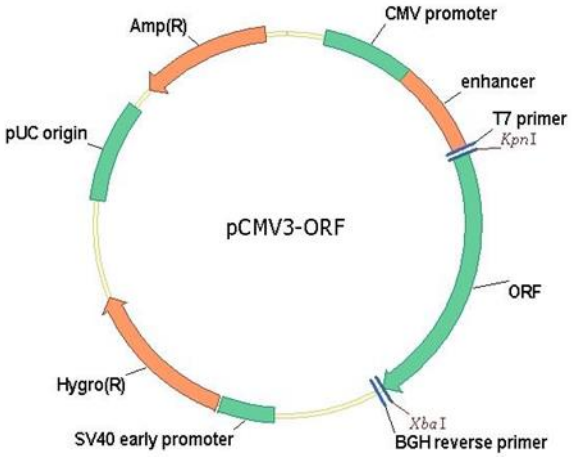
Amp(R)
CMV promoter
enhancer
T7 primer
KpnI
pUC origin
pCMV3-ORF
ORF
Hygro(R)
XbaI
SV40 early promoter
BGH reverse primer

B

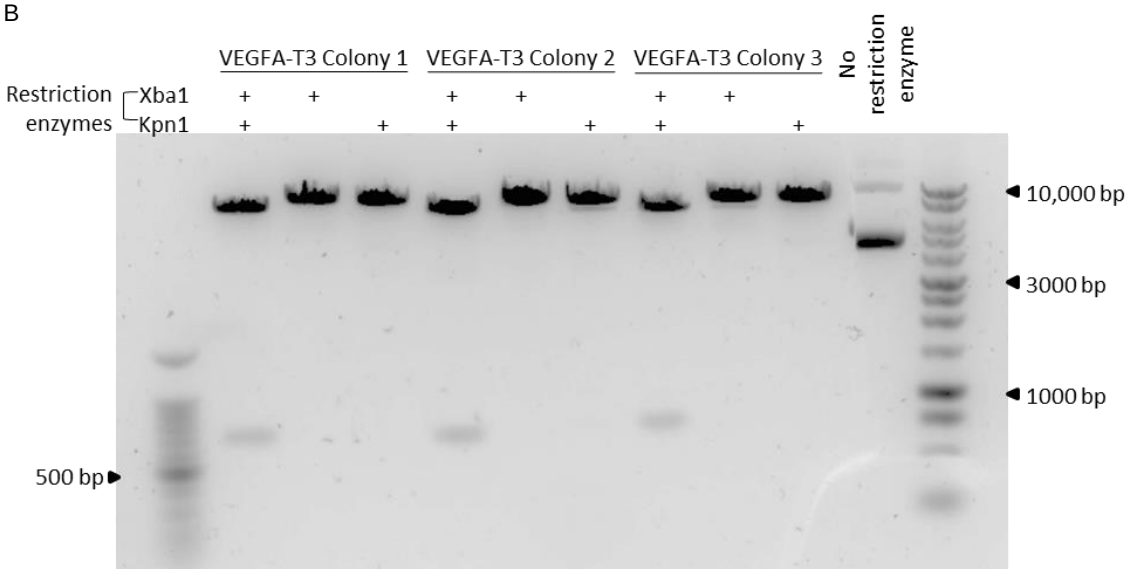
VEGFA-T3 Colony 1
VEGFA-T3 Colony 2
VEGFA-T3 Colony 3
No restriction enzyme
Restriction enzymes
Xba1
Kpn1
10,000 bp
3000 bp
1000 bp
500 bp

C

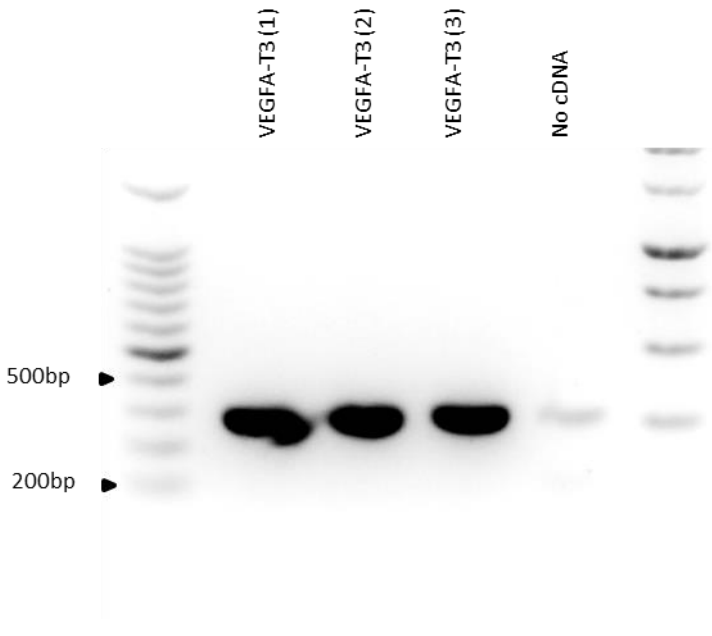
VEGFA-T3 (1)
VEGFA-T3 (2)
VEGFA-T3 (3)
No cDNA
500bp
200bp

Figure 5.6: Human VEGFA-transcript variant 3

A) VEGFA-T3 plasmid map, provided by supplier. B) VEGFA-T3 plasmid DNA was extracted from three VEGFA-T3 colonies using the Promega Wizard Plus Miniprep DNA Purification System according to manufacturer's instructions. A restriction enzyme digest was then performed with Xba1 and Kpn1 restriction enzymes on DNA isolated from each colony prior to 1.5% agarose gel analysis. DNA fractionation was monitored under UV light and captured using a Biorad ChemiDoc MP Imaging System. C) VEGF-T3 plasmid DNA was analysed via 2% agarose gel electrophoresis. DNA migration was monitored under UV light and captured using a Biorad ChemiDoc MP imaging system.

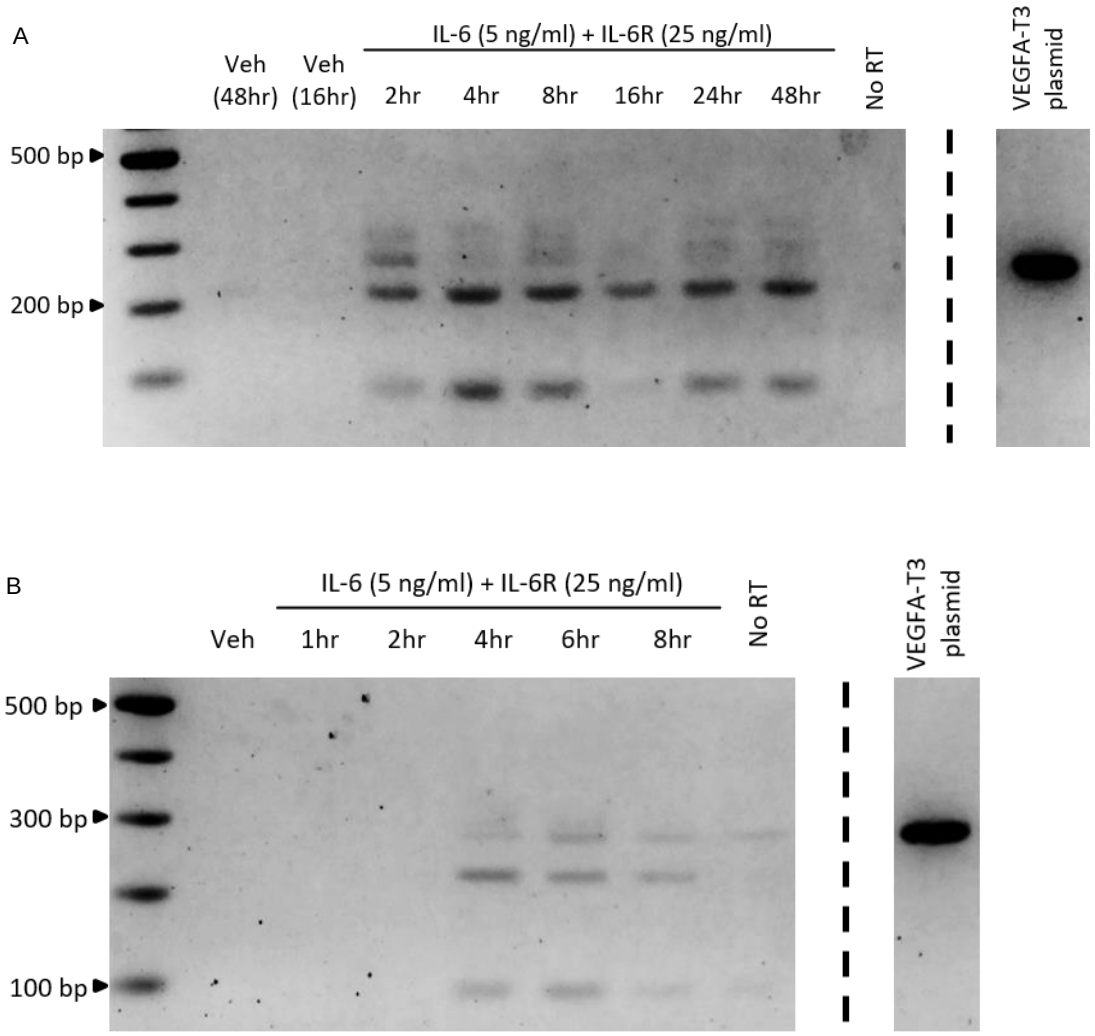
A
IL-6 (5 ng/ml) + IL-6R (25 ng/ml)
Veh (48hr)
Veh (16hr)
2hr
4hr
8hr
16hr
24hr
48hr
No RT
VEGFA-T3 plasmid
500 bp
200 bp
B
IL-6 (5 ng/ml) + IL-6R (25 ng/ml)
Veh
1hr
2hr
4hr
6hr
8hr
No RT
VEGFA-T3 plasmid
500 bp
300 bp
100 bp

Figure 5.7: IL-6/sIL-6Rα induces VEGF gene expression

A) HPAECS were treated with IL-6 (5 ng/ml) + sIL-6Rα (25 ng/ml) for 2 hours, 4, 8, 16, 24, and 48 hours. A vehicle (Veh) control was performed as a negative control. RNA was then purified from cell lysates and reverse transcribed to form cDNA (10 ng/ml). A no reverse transcriptase (RT) was performed at this point. Resulting cDNA was amplified via a PCR and separated via 2% agarose gel electrophoresis as described (Sections 2.2.4.4 – 2.2.4.5). VEGF-T3 plasmid cDNA was used as a positive control. DNA fractionation was monitored under UV light and captured using a Biorad ChemiDoc MP imaging system. B) HPAECS were treated with IL-6 (5 ng/ml) + sIL-6Rα (25 ng/ml) for 1 hour, 2, 4, 6 and 8 hours. A Veh control was performed as a negative control. RNA was then purified from cell lysates and reverse transcribed to form cDNA (10 ng/ml). A no RT was performed at this point. Resulting cDNA was amplified via a PCR and separated via 2% agarose gel electrophoresis as described (Sections 2.2.4.4 – 2.2.4.5). VEGF-T3 plasmid cDNA was used as a positive control. DNA migration was monitored under UV light and captured using a Biorad ChemiDoc MP imaging system.

negative control sample, incubated without reverse transcriptase, was also included to assess contamination with genomic DNA. VEGFA RNA was present 2 hours post-IL-6/sIL6Rα treatment and this was sustained for at least the last time point examined (48 hours). One band is visible between 300 and 400 bps which is consistent with the VEGF-T3 plasmid and VEGFA isoform 2. A slightly smaller DNA product consistent with VEGFA isoform 7 is also visible. Bands representative of two smaller DNA products are also visible consistent with VEGF isoforms described by Harper and Bates (2008).

As the initial time-point was too late to identify the earliest treatment time required to induce VEGF RNA expression, the experiment was repeated over a shorter time frame. HPAECs were treated with IL-6/sIL-6Rα for up to 8 hours prior to undergoing RNA purification, reverse transcription and PCR in the same manner as previously described (Sections 2.2.4.4 and Sections 2.2.4.5). Agarose gel analysis showed VEGF RNA to be present 4 hours post-IL-6/sIL6Rα treatment and this was sustained after 8 hours (Figure 5.7B). Along with the longer time course, this suggests VEGF RNA is induced in HPAECs within 4 hours of treatment with IL-6/sIL-6Rα.

As the PCR results suggested IL-6 induced VEGF gene expression, a VEGF-A ELISA was performed as previously described (Section 2.2.3.2) to determine if this resulted in any detectable change in IL-6 mediated VEGF protein expression and, if so, was this limited by prostanoid treatment. Initially, a VEGF-A ELISA was performed with increasing concentrations of VEGF-A standard (supplied by manufacturer) to produce a standard curve of VEGF-A

concentration versus absorbance (Figure 5.8A). HPAECs were then treated with BPS (10 μM) for 2 hours prior to 24 hours treatment with IL-6/sIL-6Rα. Treatment with BPS alone and IL-6/sIL-6Rα alone was also measured and a vehicle control was performed. The VEGF protein content of the treated medium was then determined by ELISA performed according to the manufacturer's instructions (Section 2.2.3.2). Levels of detectable VEGF-A protein were at the lower limit of the sensitivity of the assay as determined by the low absorbance (and thus low concentration) of detectable VEGF-A in all conditions; however, the data is included for information (Figure 5.8B).

5.3 Discussion

As previously mentioned, BPS, treprostinil and ACT-333679 significantly inhibited IL-6 *trans*-signalling activity in HPAECs (Figure 4.2). However, for this to have therapeutic benefit, it must be sufficient to limit the functional effects of IL-6 *trans*-signalling that contribute to PAH progression.

The prostanoid BPS significantly protected HPAECs from the increased cell permeability resulting from treatment with IL-6/sIL-6Rα (Figure 5.1). As an increase in cell permeability is associated with EC dysfunction which has been associated with PAH progression and suggested as a potential therapeutic target (reviewed by Ranchoux et al. 2018), this suggests BPS may be beneficial for this particular effect of IL-6/sIL-6Rα. To provide more conclusive appear to increase VE-cadherin localisation at cellular junctions when compared to treatment with IL-6/sIL-6Rα alone. Interestingly, research published after these experiments were completed supported that IL-6 causes

A

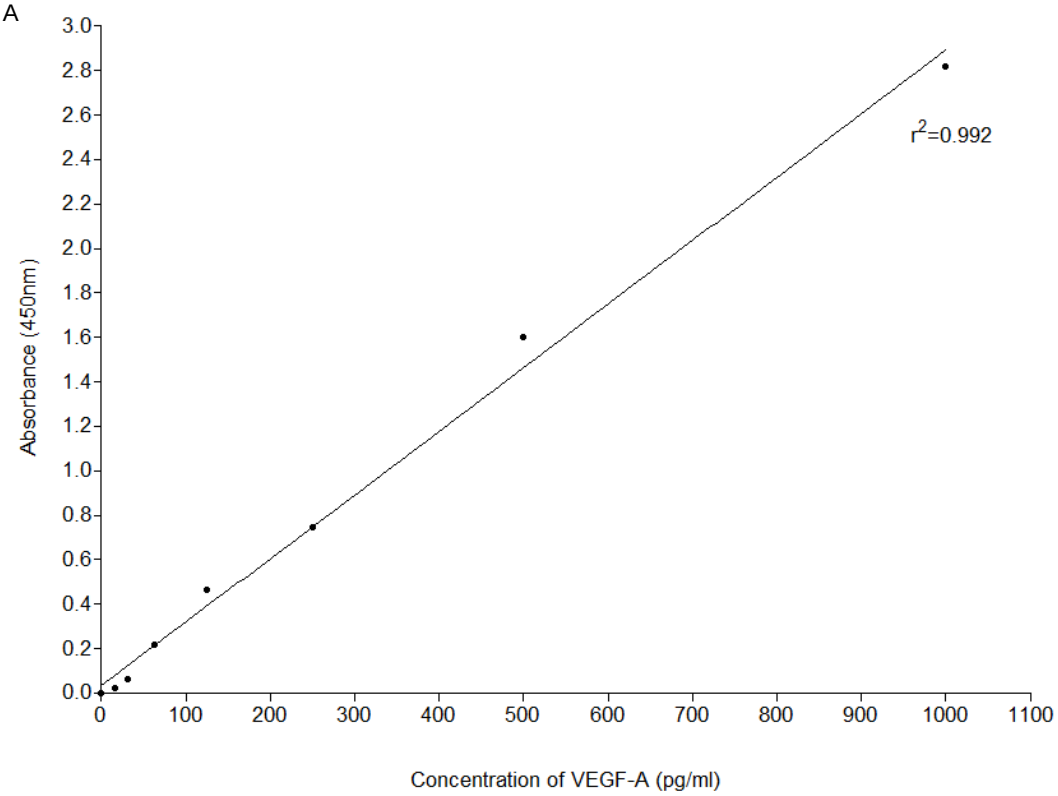

B

Treatment	Average absorbance reading	VEGF-A concentration (pg/ml)
Veh	0.080	0.084
BPS (10 µM)	0.052	0.026
IL-6/sIL-6Rα	0.053	0.026
BPS (10 µM) + IL-6/sIL-6Rα	0.068	0.034

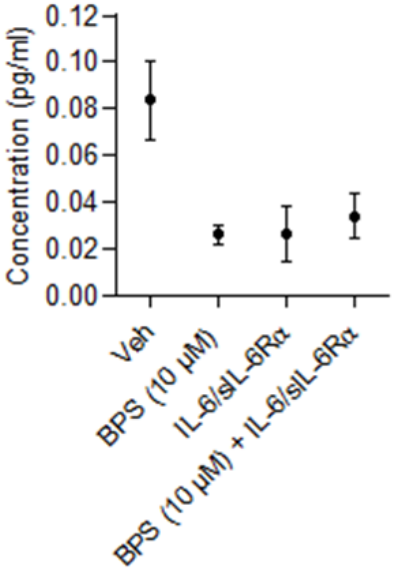

Figure 5.8: VEGF-A protein is undetectable via ELISA

A) VEGF-A standard curve produced by preparing VEGF-A standard dilutions and analysing via an enzyme-linked immunosorbent assay (ELISA) as described in the manufacturer's instructions. The absorbance of known VEGF-A concentrations were measured immediately upon completion of the ELISA using a Thermo Scientific™ NanoDrop 1000 Spectrophotometer and plotted on a graph using GraphPad Prism software. B) HPAECs were treated with BPS (10 μM) for 2 hours prior to 24 hour treatment with IL-6 (5 ng/ml) + sIL-6Rα (25 ng/ml) (IL-6/sIL-6Rα). The experiment was attenuated via removal and storage of the media. A vehicle control and treatment with IL-6/sIL-6Rα alone was also performed. The concentration of VEGF protein in the sample media was then determined via an ELISA performed according to the manufacturer's protocol. The absorbance of each sample was measured using a Thermo Scientific™ NanoDrop 1000 Spectrophotometer and compared to the VEGF-A standard curve to determine VEGF-A protein concentration. Experiment performed to $n=3$.

a loss of VE-cadherin local to cellular junctions but reports this is a direct consequence of IL-6/sIL-6Rα signalling, not a result of increased permeability (Alsaffar et al. 2018). Thus, VE-cadherin may not be an accurate measure of IL-6/sIL-6Rα induced cell permeability.

IL-6 *trans*-signalling has many other functional affects that would contribute to the vascular remodelling characteristic of PAH and should be measured in HPAECs. For instance, IL-6/sIL-6Rα has been shown to stimulate cell migration, cell proliferation, and angiogenesis (Yao et al. 2006; Liu et al. 2017), IL-6/sIL-6Rα induced migration of HPAECs could easily be measured via established cell migration assays such as scratch wound assays (reviewed by Justus et al. 2014). Similarly, IL-6/sIL-6Rα induced HPAEC proliferation could be measured via BrdU incorporation assays (Gallagher et al. 2007). Treating cells with IL-6/sIL-6Rα in the presence and absence of a prostanoid drug, as performed in Figure 5.1, would determine the effect of IL-6 alone, and the ability of prostanoids to limit this effect.

To study the effect of IL-6/sIL-6Rα on angiogenesis endothelial tube formation assays (Ponce 2009; DeCicco-Skinner et al. 2014) could be utilised. However, to gain a more realistic perspective a co-culture system would be better. Many co-culture systems that utilise fibroblasts to form a matrix which supports endothelial cell tube formation have been developed (Richards and Mellor 2016). Ideally, the incorporation of HPASMCs into such systems would allow for a more representative environment of that local to PAH pathology.

The key genes induced by IL-6/sIL-6Rα that mediate pro-inflammatory effects have already been identified and include adhesion molecules (Kuppner et al.

1990; Kvale et al. 1992). IL-6 induction of ICAM-1 and VCAM-1 protein induction was measured in HPAECs and in all cases levels of protein in untreated cells were the same as in treated cells (Figure 5.4), suggesting high basal levels of these proteins. It could be that the process of maintaining and passaging these cells is sufficient to induce an inflammatory response. IL-6/sIL-6Rα has been shown to induce ICAM1 and VCAM1 after 48 hours of treatment, and VCAM1 (Wiejak et al. 2019), which is a longer time period than used for these experiments in HPAECs. Thus, a longer time course may be beneficial. Also, in both experiments there appeared to be high basal levels of ICAM1 and VCAM1. In the future, serum-starving cells prior to stimulating with IL-6/sIL-6Rα may reduce basal expression of adhesion molecules, although this did not have an effect on VEGFR2 expression in the same cell type (Figure 5.5B). Alternatively, measuring mRNA levels via PCR or promoter activity via luciferase reporter assays may indicate if IL-6/sIL-6Rα induces VCAM1/ICAM1 gene transcription. High basal-levels of adhesion molecules may also be specific to ECs, thus measuring IL-6/sIL-6Rα-induction of ICAM1 and VCAM1 in other cells involved in PAH pathology, such as PASMCs, may also be valuable.

Research has shown that in gastric carcinoma and human cervical cancer C33A cells IL-6 induces angiogenesis by upregulating VEGF (Wei et al. 2003b; Huang et al. 2004). Similarly to adhesion molecules, VEGFR2 protein was found to be expressed in HPAECs in the absence of IL-6/sIL-6Rα stimulation and this was not altered with treatment of IL-6/sIL-6Rα. Treatment with BPS, however, stimulated VEGFR2 expression. This has been found previously with VEGF in rat aortic SMCs where BPS increased VEGF mRNA through a

PKA/CREB-dependent mechanism (Atsuta et al. 2009). In HPAECs, IL-6/sIL-6Rα appeared to stimulate VEGF-A transcription 2 - 48 hours post-treatment (Figure 5.7) but VEGF protein expression, measured by an ELISA, did not increase in line with this (Figure 5.7). Measuring the impact of BPS or other prostanoids on the IL-6-mediated increase in VEGF mRNA may offer an alternative to measuring the effect on protein levels. However, as BPS has also been shown to induce VEGF, treatment alongside a PKI may be required. Alternatively, the EPAC1 agonist I942 which has been shown to induce SOCS3 and limit IL-6 induction of adhesion molecules (Wiejak et al. 2019) could be utilised to determine the impact of SOCS3 without having to control for PKA activation.

Measuring the impact of prostanoids on the aforementioned effects of IL-6 would result in a greater understanding on the potential therapeutic mechanism of prostanoids, as well as potentially highlighting new therapeutic targets within the IL-6 *trans*-signalling pathway.

6 Potential role of SOCS3 in cell membrane integrity.

6.1 Introduction

The primary aims of this PhD research have revolved around the anti-inflammatory role of SOCS3; however potential other roles of SOCS3 may have a therapeutic benefit in PAH. SOCS3 has been shown to interact with cavin-1 via the proline (P), glutamic acid (E), serine (S), and threonine (T) (PEST) motif of the SH2 domain of SOCS3 and multiple regions of cavin-1

(Williams et al. 2018). As discussed (Section 1.3.3.2), cavin-1 interacts with CAV1 to stabilise caveolae at the plasma membrane (Liu et al. 2008), and caveolae have been shown to have a mechanoprotective function in endothelial cells, including preventing membrane rupture in response to increased cardiac output (Cheng et al. 2015).

Cavin-1 and SOCS3 appear to interact in a mutually beneficial mechanism where SOCS3 enhances cavin-1 stability and thus caveolae stability, but cavin-1 is also required for cAMP-mediated SOCS3 inhibition of IL-6 signalling and SOCS3 localisation to the plasma membrane (Williams et al. 2018). Evidence for this has been found in human myoblasts expressing *CAV3* mutations. *CAV3* codes for Cavin-3, a muscle cell-specific cavin homologue. Loss of cavin-3 resulted in a loss of caveolae at the plasma membrane and caused hyperactivation of IL-6 signalling determined via confocal microscopy of immunofluorescent pSTAT3 and pSTAT3 nuclear translocation which was rescued via transduction with Cavin-3-GFP (Dewulf et al. 2019), although whether this involved SOCS3 was not investigated.

As caveolae have numerous functions including mechanoprotection (Sinha et al. 2011) and plasma membrane signalling (Sowa et al. 2001), caveolae dysfunction is associated with numerous diseases including muscular dystrophies (Hayashi et al. 2009), cancer (Moon et al. 2014), and cardiovascular disease including PAH. Several heterozygous mutations in *CAV1*, including 474delA, 473delC, F160X, and 479_480delTT, have been identified in PAH patients (Austin et al. 2012; Garg et al. 2015). In addition, fibroblasts from PAH patients were found to have reduced co-localisation of cavin-1 with caveolin-1 and decreased stability of the caveolin-1 complexes

necessary for caveolae formation (Han et al. 2016). Thus, SOCS3 regulation of cavin-1 stability and maintenance of cellular caveolae may provide an alternative mechanism by which SOCS3 mediates its potential therapeutic benefits in PAH.

6.2 Results

6.2.1 Membrane stability in AS-M.5 WT cells compared to AS-M.5 SOCS3 KO cells

AS-M.5 WT and AS-M.5 SOCS3 KO cells were utilised to investigate the role of SOCS3 in cell membrane stability. AS-M.5 WT and AS-M.5 SOCS3 KO cells were seeded in Nunc™ Lab-Tek™ chambers at $4x10^4$ – $6\ x10^4$ cells/chamber and $8x10^4$– $1x10^5$ cells/chamber respectively to achieve a high cell density and incubated for 48 hours until confluent. AS-M SOCS3 KO cells were seeded at a higher seeding density as they demonstrated lower levels of attachment to the cell culture flask and a slower growth rate.

Initial experiments to determine the optimum staining protocol were completed. Cells were treated with hypotonic EGM-2 medium (1 part EGM-2 medium:9 parts sterile H_2O) for 10 minutes. The use of hypotonic solutions to induce cellular swelling, causing the plasma membrane to stretch is an established model of plasma membrane mechanical stress (Pietuch et al. 2013; Yamamoto and Ando 2015; Tachikawa et al. 2017). Cells incubated in fresh EGM-2 medium for 10 minutes were used as a vehicle control. Post-treatment, cells were fixed via a 10 minute incubation in ice-cold methanol at -20°C prior to 3 x 5 minute washes with PBS at room temperature. Cells were then treated

with SYTOX (167 nM) for 10 minutes at room temperature before staining with 1 µM Hoechst 33342 in PBS at room temperature prior to being visualised via fluorescence microscopy. As SYTOX is non-cell permeable, it will only stain the nucleic acid of ruptured cells. If SOCS3 is necessary for cell membrane stability, AS-M.5 SOCS3 KO cells should be more vulnerable to membrane rupture as a result of incubation in hypotonic media and will show greater SYTOX staining.

Cells prepared in the manner described showed SYTOX staining of all the vehicle control cells and after 10 minutes of hypotonic treatment in both cell types (Figure 6.1A), suggesting either methanol fixation of the cells was damaging the cell membrane, or potentially that Hoechst 33342 was transporting residue SYTOX into the cell. The experiment was repeated with the following changes; cells were fixed in 4% formaldehyde via incubation at room temperature for 10 minutes and cells were stained with WGA (1 µg/ml) via incubation at room temperature for 20 minutes as an alternative to Hoechst 33342. Again, both cell types demonstrated SYTOX staining in all cells in the vehicle control sample and those that had been treated with hypotonic media (Figure 6.1B). Thus, in future experiments cells were stained during the treatment process and imaged immediately to avoid fixing the cells. Preliminary experiments also identified the risk of fluorescence bleed-through from the green SYTOX stain when imaging the red WGA stain when scanning the images with both lasers at the same time. This is evident from the nuclei staining seen in the WGA images as WGA should not stain nucleic acid, and the colour of the merged image. To prevent this in further experiments, images were taken using the individual lasers and merged post-imaging.

A

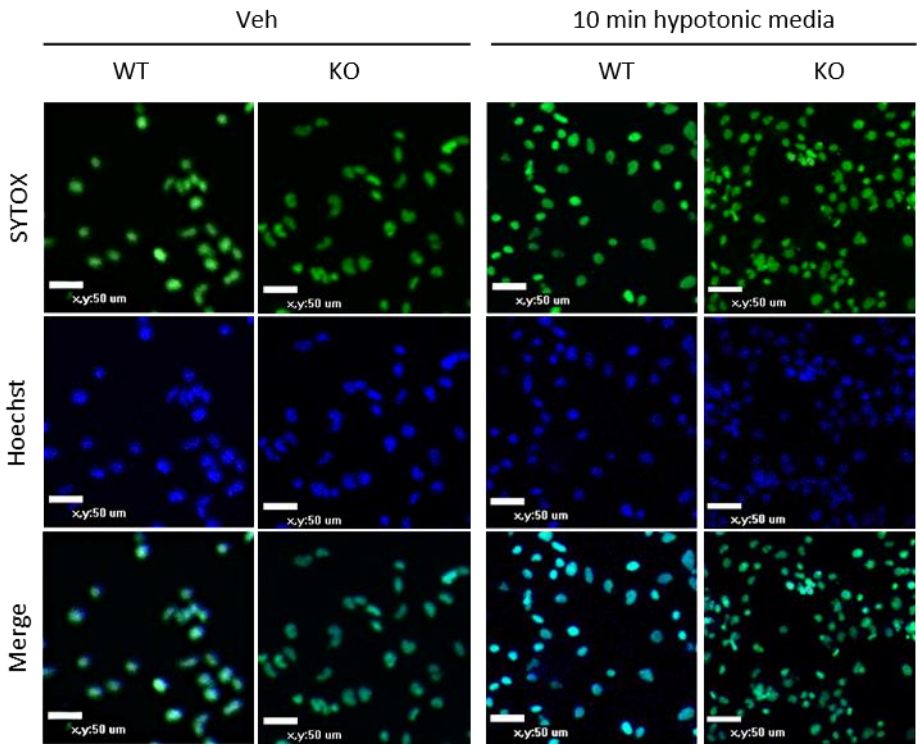
Veh
10 min hypotonic media
WT
KO
WT
KO
SYTOX
Hoechst
Merge
x,y:50 um

B

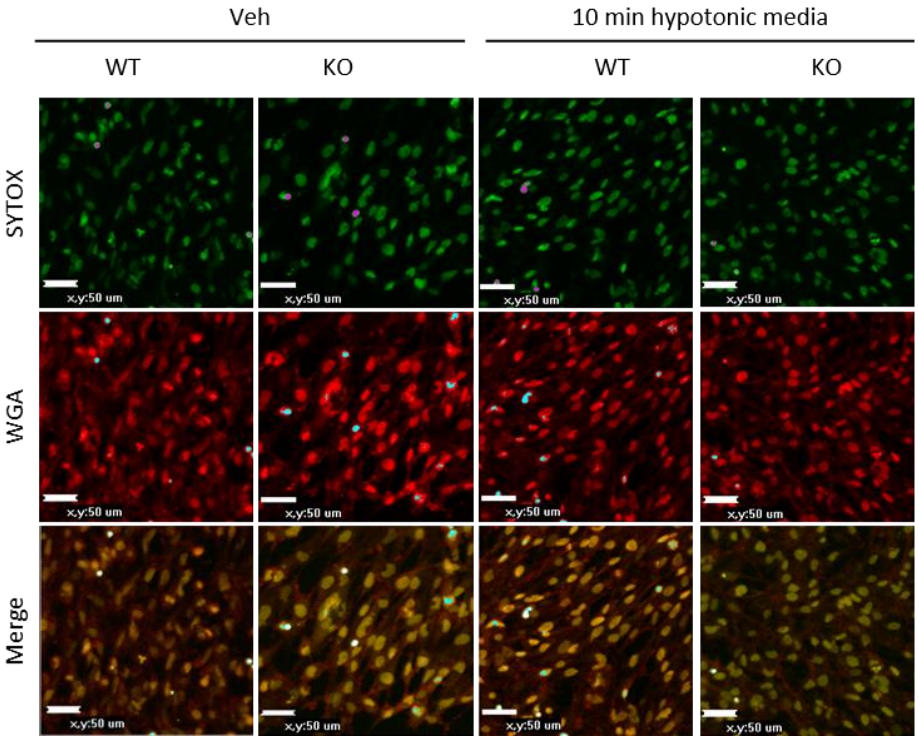
Veh
10 min hypotonic media
WT
KO
WT
KO
SYTOX
WGA
Merge
x,y:50 um

Figure 6.1: Representative images of AS-M.5 WT vs AS-M.5 SOCS3 KO from preliminary hypotonic experiments

A) AS-M.5 WT and AS-M.5 SOCS3 KO Cells were incubated in hypotonic EGM-2 medium (1 part EGM-2 medium:9 parts sterile H2O) for 10 minutes prior to immediate fixing in methanol. Cells incubated in fresh EGM-2 medium for 10 minutes were used as a vehicle (Veh) control. Cells were then stained with SYTOX™ Green Nucleic Acid Stain (SYTOX) (167 nM) and Hoechst 33342 (1 µM) prior to imaging with a Nikon ECLIPSE TE2000-E confocal microscope. B) AS-M.5 WT and AS-M.5 SOCS3 KO cells were incubated in hypotonic EGM-2 medium (1 part EGM-2 medium:9 parts sterile H2O) for 10 minutes prior to immediate fixing in 4% paraformaldehyde. Cells incubated in fresh EGM-2 medium for 10 minutes were used as a Veh control. Cells were then stained with SYTOX (167 nM) and WGA (1 µg/ml) prior to imaging with a Nikon ECLIPSE TE2000-E confocal microscope.

These changes were incorporated into the final protocol (Section 2.2.6) which was used for the experiments described below.

AS-M.5 WT and AS-M.5 SOCS3 KO cells were seeded in Labtek chambers at $4x10^4$ – $6x10^4$ cells and $8x10^4$ – $1x10^5$ cells respectively. Cells were then treated with hypotonic EGM-2 medium (1 part EGM-2 medium:9 parts sterile H_2O) containing SYTOX (167 nM) and WGA (1 µg/ml) for 2 minutes, 4 and 10 minutes prior to 2 X 5 minute washes with HBSS. Cells were then immediately imaged via fluorescence microscopy. The amount of SYTOX DNA staining was measured as previously described (Section 2.6) and compared to minimum SYTOX expression. Cells incubated in fresh EGM-2 medium containing SYTOX and WGA for 10 minutes were used as a vehicle control and were prepared in parallel to the cells treated with hypotonic media.

SYTOX expression was the same for both cell types in the vehicle control (Figure 6.2). The staining seen in these conditions were caused by factors other than hypotonic media such as toxicity of the stains, thus, this level of staining should not be attributed to cell membrane vulnerability in any conditions. SYTOX expression in AS-M.5 WT was consistent with that seen in the vehicle treatment for the 2 minute, 4 minute and 10 minute treatment times (Figure 6.2). In the AS-M.5 SOCS3 KO cells, SYTOX expression after 2 minutes and 4 minutes incubation in hypotonic media are comparable to that seen in the vehicle control but there appears to be greater SYTOX staining after 10 minutes treatment with hypotonic media compared to the other treatment times (Figure 6.2). Statistical analysis did not show this to be significant, most likely due to the relatively large standard error of the mean (SEM) values for AS-M.5 SOCS3 KO results. This may be because 10 minutes

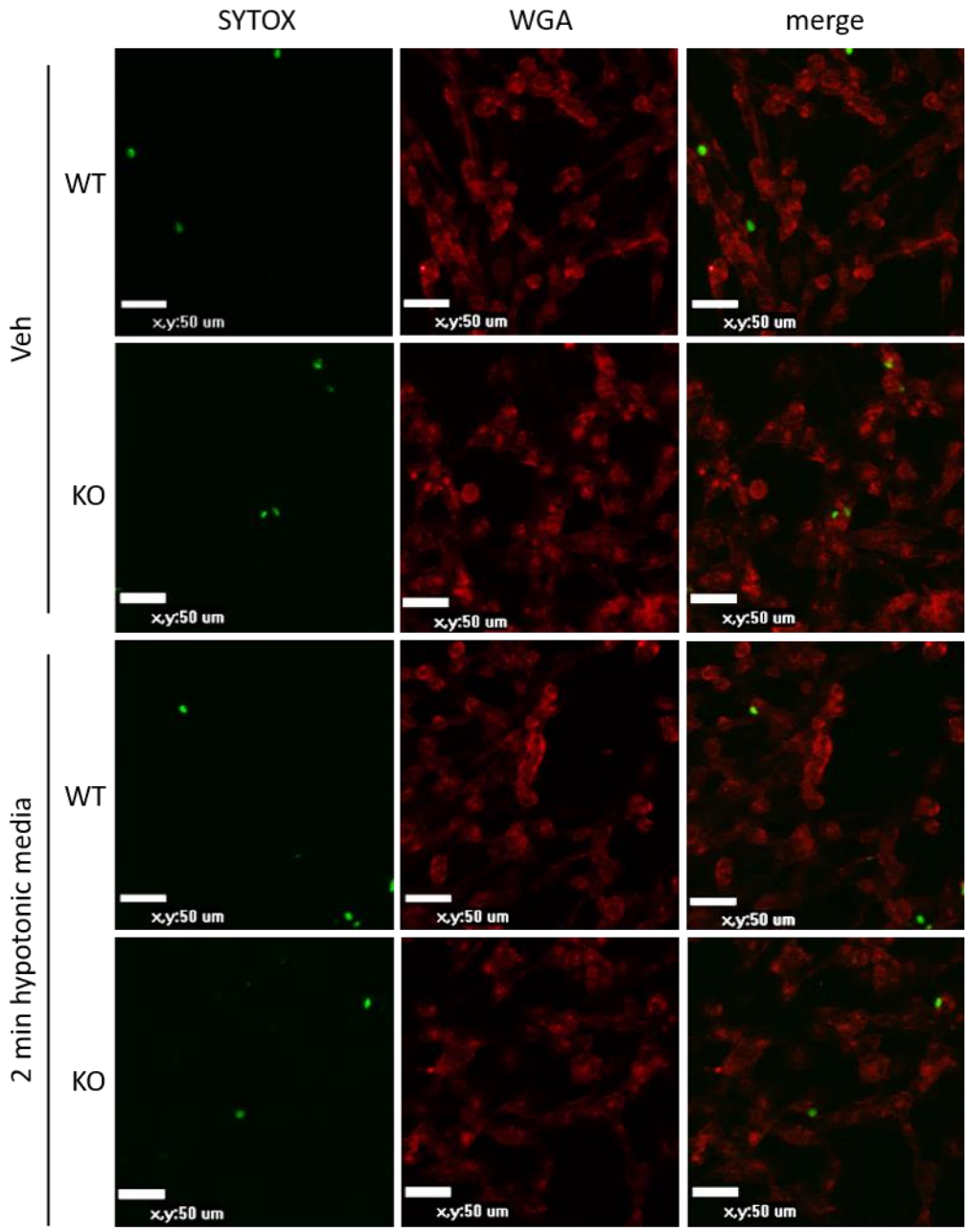

Figure continued on next page.

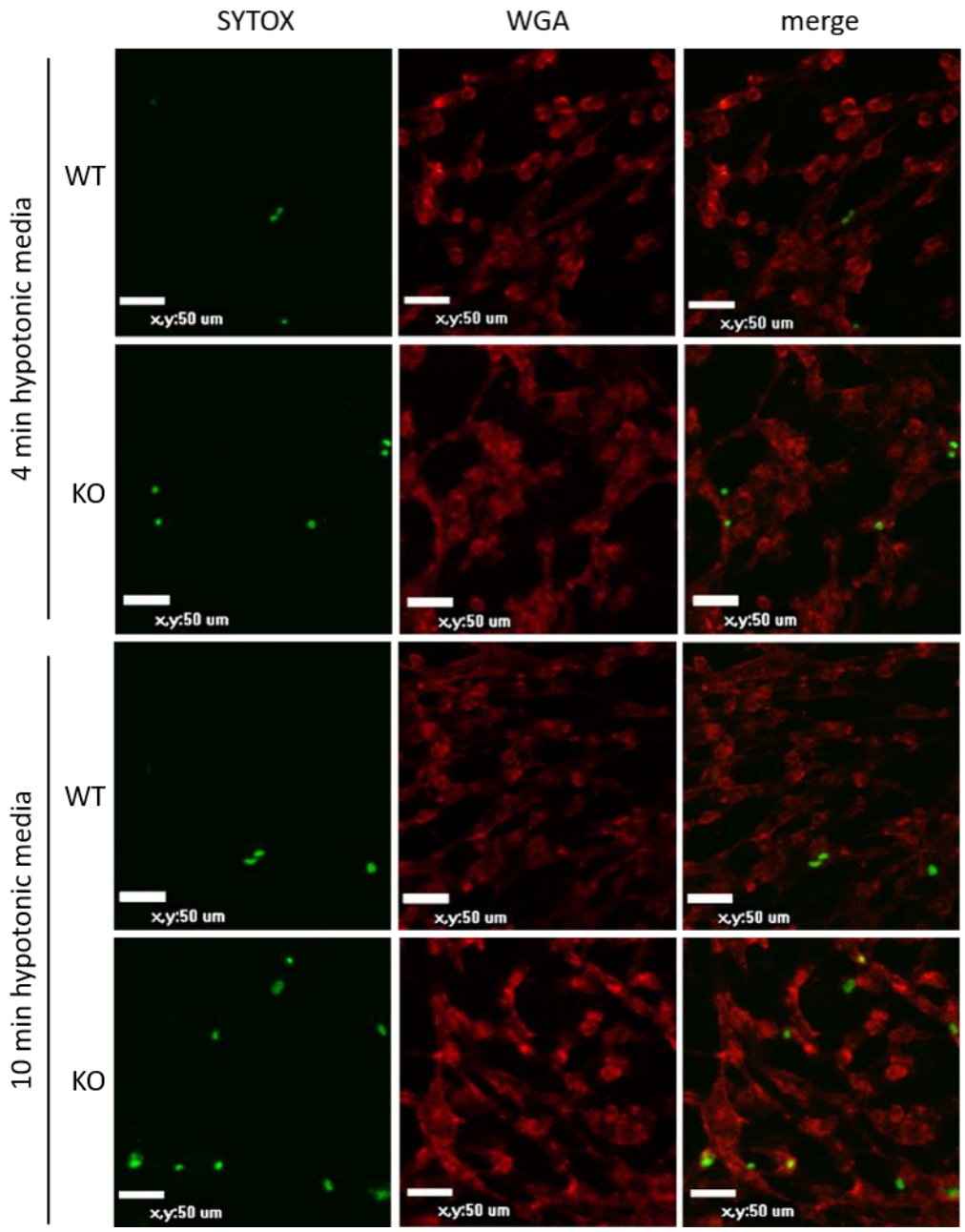

Figure continued on next page.

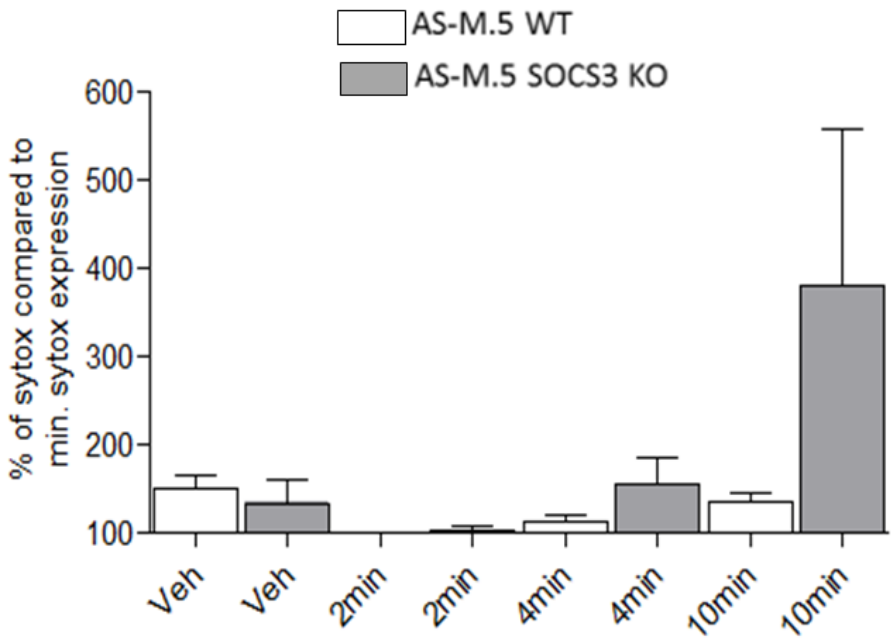

Figure 6.2: SYTOX DNA staining in AS-M.5 WT vs AS-M.5 SOCS3 KO post-short hypotonic treatments

AS-M.5 WT and AS-M.5 SOCS3 KO cells were incubated in hypotonic EGM-2 medium (1 part EGM-2 medium:9 parts sterile H2O) containing SYTOX™ Green Nucleic Acid Stain (SYTOX) (167 nM) and Wheat Germ Agglutinin, Alexa Fluor™ 594 Conjugate (WGA) (1 µg/ml) for 2 minutes, 4 or 10 minutes. Cells incubated in fresh EGM-2 medium containing SYTOX and WGA for 10 minutes were used as a vehicle (Veh) control. Cells were then washed twice for 5 minute washes in HBSS, incubated in fresh EGM-2 medium and imaged immediately using a Nikon ECLIPSE TE2000-E confocal microscope. Analysis of the images was completed using ImageJ software. Quantification for n=5 experiments has been shown.

is approaching the maximum time SOCS3 KO cells can withstand treatment with hypotonic media but has not exceeded that time, thus there is variability in the number of ruptured cells.

To test this, the experiment was repeated as described previously but cells were treated in hypotonic media for longer times of 15 and 30 minutes. Cells incubated in fresh EGM-2 medium containing SYTOX and WGA for 30 minutes were used as a vehicle control. Similar to the shorter time course, SYTOX expression was the same for both cell types in the vehicle control (Figure 6.3) and this level of staining should not be attributed to cell membrane vulnerability in any condition. AS-M.5 WT cells demonstrated similar levels of SYTOX staining after 15 and 30 minutes of treatment time. SYTOX staining in AS-M.5 SOCS3 KO cells appeared to increase between each time point (Figure 6.3), however statistical analysis did not show this to be significant.

6.3 Discussion

For both the short and long hypotonic treatment time course, AS-M.5 WT cells show similar levels of SYTOX treatment for all conditions whereas AS-M.5 SOCS3 KO cells appear to show increased SYTOX expression but statistical analysis shows this is not significant. In the short time course (Figure 6.2), large SEM values for SYTOX staining in AS-M.5 SOCS3 KO cells results suggested the experiment could be better optimised. An attempt to do this by increasing the treatment time also resulted in relatively large SEM values at the 15 minute and 30 minute treatment time points for both cell types. This could demonstrate a vulnerability to hypotonic media in all cells types at thes

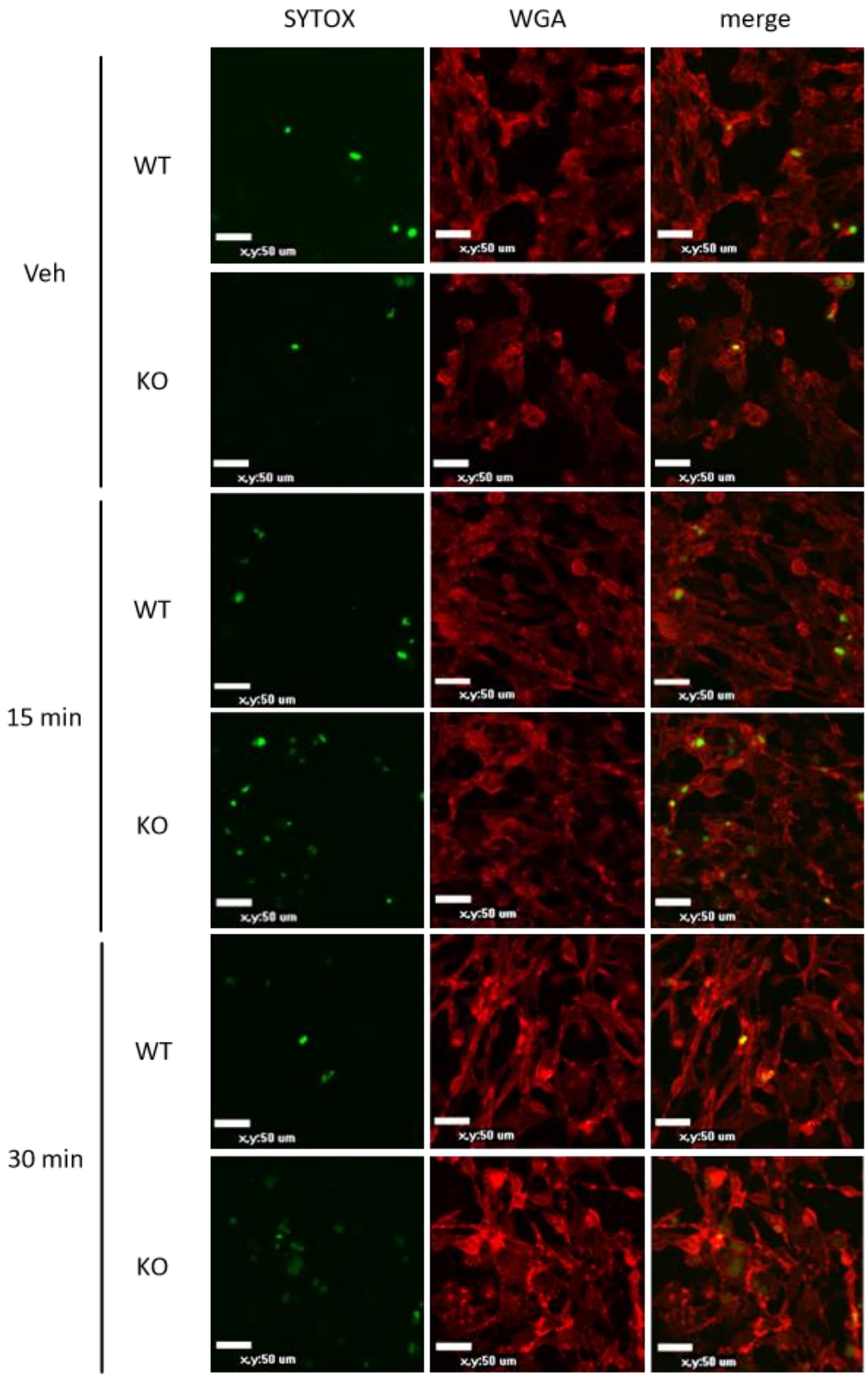

Figure continued on next page.

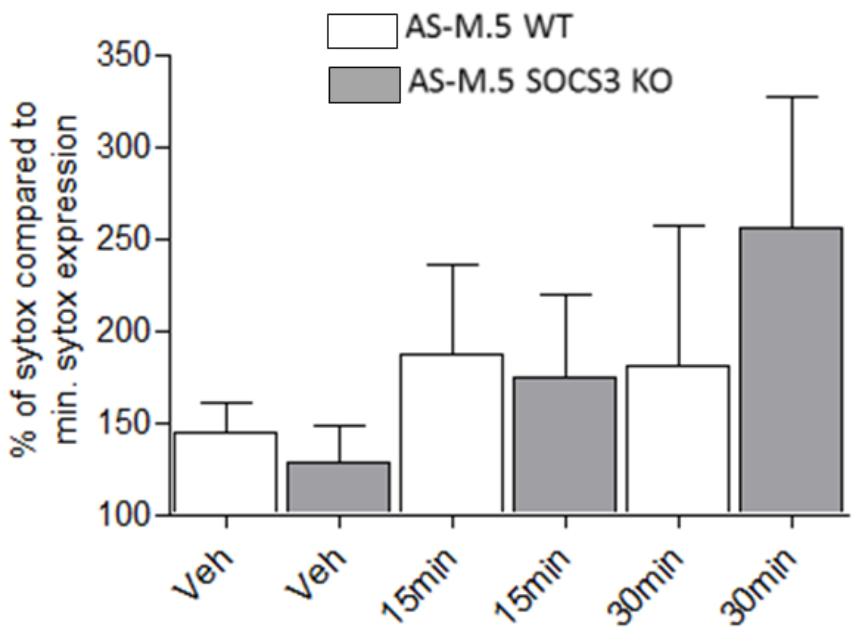

Figure 6.3: SYTOX DNA staining in AS-M.5 WT vs AS-M.5 SOCS3 KO post-hypotonic treatment

AS-M.5 WT and AS-M.5 SOCS3 KO Cells were incubated in hypotonic EGM-2 medium (1 part EGM-2 medium:9 parts sterile H2O) containing SYTOX™ Green Nucleic Acid Stain (SYTOX) (167 nM) and Wheat Germ Agglutinin, Alexa Fluor™ 594 Conjugate (WGA) (1 µg/ml) for 15 or 30 minutes. Cells incubated in fresh EGM-2 medium containing SYTOX and WGA for 30 minutes were used as a vehicle (Veh) control. Cells were then washed twice for 5 minute washes in HBSS, incubated in fresh EGM-2 medium and imaged immediately using a Nikon ECLIPSE TE2000-E confocal microscope. Analysis of the images was completed using ImageJ software. Quantification for n=5 experiments has been shown.

time points, or potential other factors may have a greater influence during longer treatment times than during a short exposure to hypotonic media. The effect of increasing passage number and increased cell seeding density were correlated against % SYTOX expression compared to the vehicle treatment after 30 minutes of treatment for *n=5* experiments. AS-M.5 WT cells demonstrate a low negative correlation between SYTOX staining and increased passage number (r^2 value = -0.3372) and a low positive correlation between SYTOX staining and seeding density (r^2 = 0.3528) (Figure 6.4). On the other hand, AS-M.5 SOCS3 KO cells appear to be much more affected by these parameters with a strong positive correlation between SYTOX staining and increased passage number (r^2 value = 0.8352) and a negative correlation between SYTOX staining and seeding density (r^2 = - 0.0.6218) (Figure 6.4) suggesting they are less vulnerable to membrane damage at lower passages and higher confluency. However, as we are looking at % changes of SYTOX compared to the vehicle control, correlation analysis does not identify if the effect of passage number and seeding density occurs in the hypotonic-media treated cells, the vehicle controls or both. It also shouldn't be used as conclusive evidence of an effect but could be considered for future experiments.

Another noteworthy comparison between the AS-M.5 WT and SOCS3 KO cells are the morphological changes that occur post-hypotonic treatment that can be seen in WGA stained cells. For the short time course, the appearance of the AS-M.5 WT cells remains the same in all conditions however AS-M.5 SOCS3 KO cells appear larger after 10 minutes treatment when compared to AS-M.5 SOCS3 KO in the other treatment times (Figure 6.2). This would

A

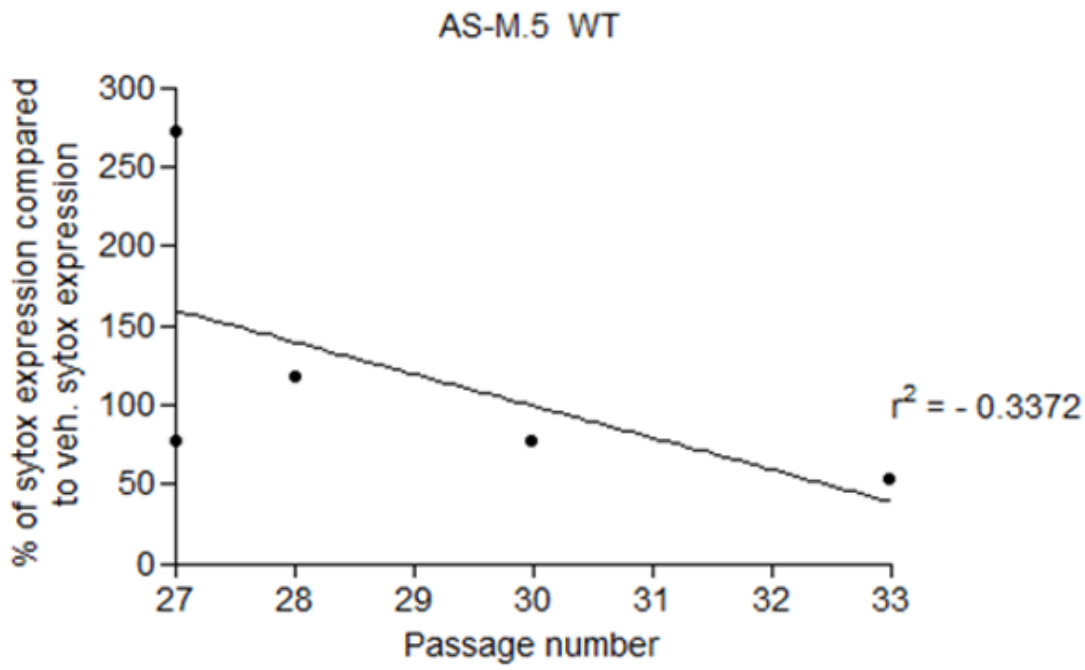

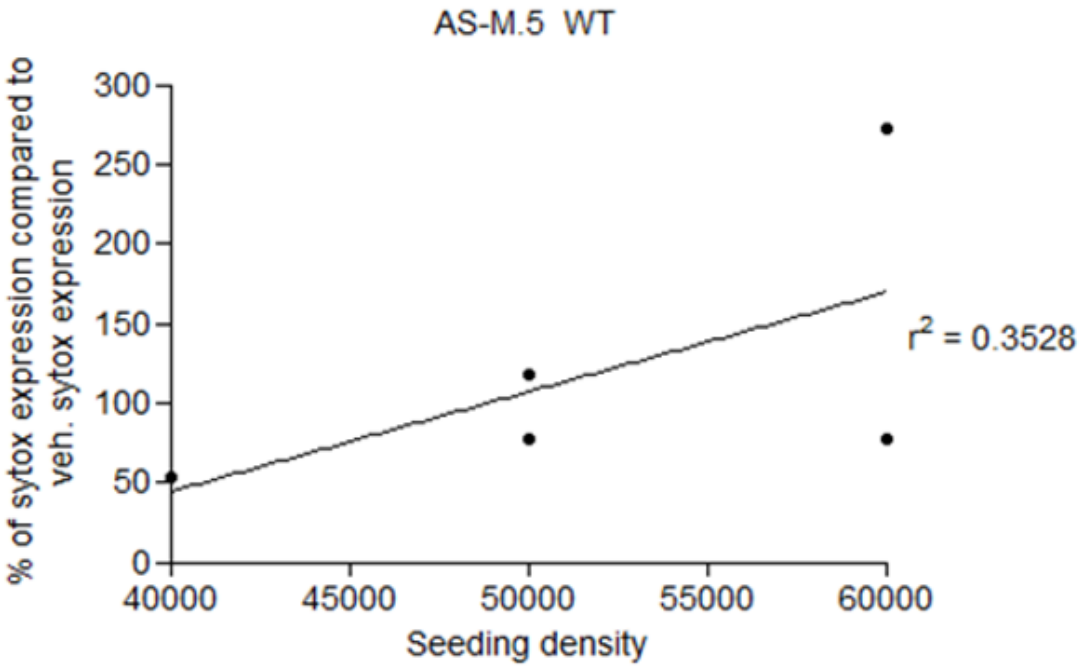

Figure continued on next page.

B

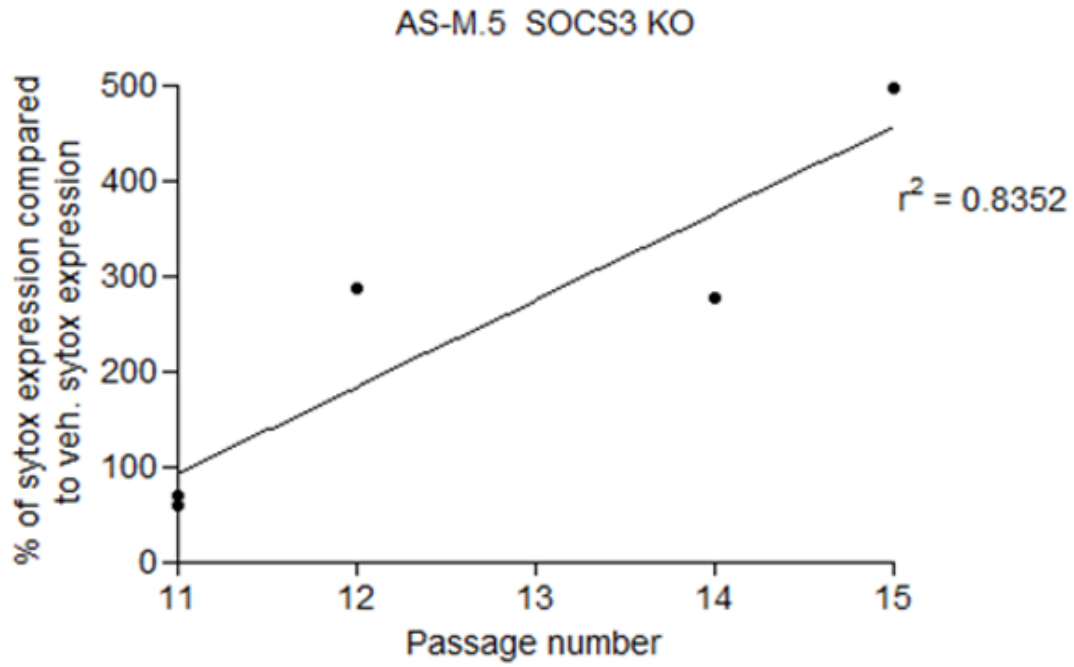
AS-M.5 SOCS3 KO
% of sytox expression compared to veh. sytox expression
500
400
300
200
100
0
11
12
13
14
15
Passage number
r^2 = 0.8352

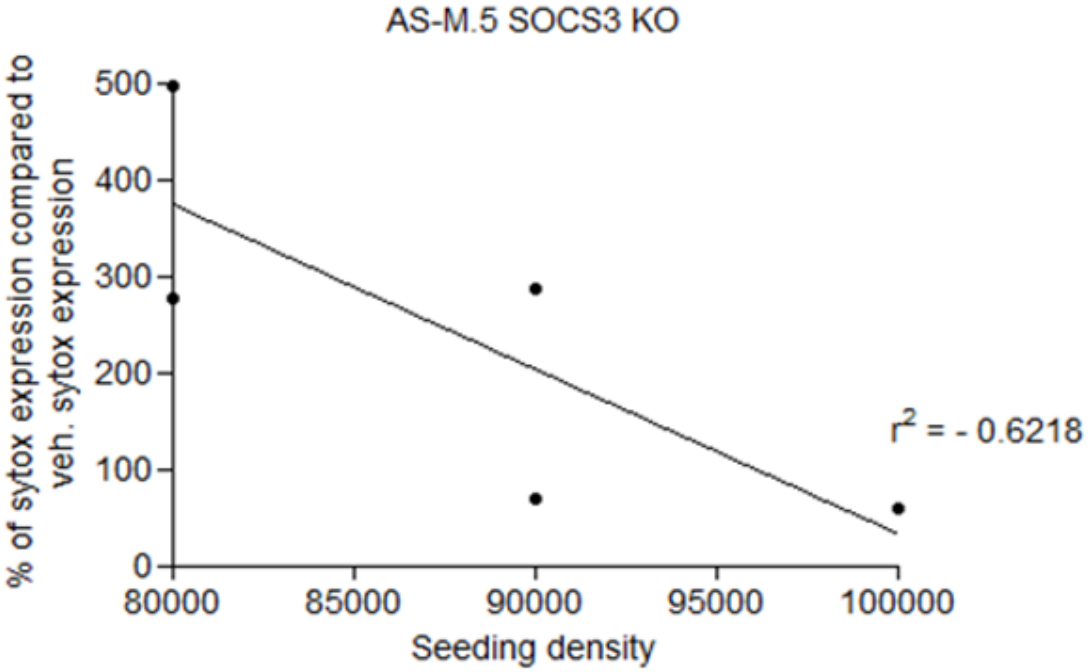
AS-M.5 SOCS3 KO
% of sytox expression compared to veh. sytox expression
500
400
300
200
100
0
80000
85000
90000
95000
100000
Seeding density
r^2 = - 0.6218

Figure 6.4: Correlation analysis for SYTOX expression compared to passage number and seeding density in AS-M.5 WT and AS-M.5 SOCS3 KO cells

A) Correlation analysis for SYTOX expression after 30 minutes of treatment with hypotonic media for *n=5* experiments compared to passage number and seeding density of AS-M.5 WT cells. B) Correlation analysis for SYTOX expression after 30 minutes of treatment with hypotonic media for *n=5* experiments compared to passage number and seeding density of AS-M.5 SOCS3 KO cells.

support the theory that AS-M.5 SOCS3 KO cells have a reduced plasma membrane stability as they are more vulnerable to hypotonic media passing through the membrane and thus become more turgid prior to rupturing. For the longer time course, an increase in size is more apparent in both cell types after 15 minutes of treatment with hypotonic media compared to the vehicle control cells. After 30 minutes of treatment, both cell types appear larger but the AS-M.5 SOCS3 KO cells also display a more bulbous appearance (Figure 6.3), which again suggests their membranes are less able to protect from the osmotic influx of hypotonic media. Morphological changes in the cells has not been analysed but should be considered in future experiments.

Cells that are more prone to rupture may also be more likely to detach from the culture chamber, especially post-rupture. Thus, SYTOX-stained cells may be lost during the washing process and thus not included in the final SYTOX counts. This would skew the total cell:SYTOX ratio in favour of the more robust cells. To investigate any potential effect total viable cell counts could be taken prior to hypotonic treatment and immediately after. Minimising the number of cells lost as a result of the counting process would be crucial to ensure a reduction in cell number is a result of hypotonic treatment and not a result of the counting process.

As AS-M.5 WT cells do demonstrate a faster growth rate and tend to form a more confluent monolayer than their SOCS3 KO counterparts, a co-culture system could potentially be utilised to remove any differences caused as a result of cell confluency. Individual cell types could be labelled using cell tracker dyes such as CellTracker™ Red CMTPX Dye (Invitrogen, Cat. # C34552) (Yeow et al. 2017) prior to seeding Nunc™ Lab-Tek™ chambers with

an equal amount of both cells and performing the experiment as previously described. As AS-M.5 WT and AS-M.5 SOCS3 KO cells could then be easily distinguished in the resulting fluorescent images, it will be possible to measure SYTOX uptake in the individual cell types in the same chamber under identical conditions.

In vitro techniques to mechanically stretch cells have previously been used to measure the role of caveolae plasma membrane integrity, with FITC movement into the cell cytoplasm being used as a measure of cell membrane damage (Cheng et al. 2015; Yeow et al. 2017). This type of experiment could be replicated in AS-M.5 WT and AS-M.5 SOCS3 KO to measure if SOCS3 KO cells were more vulnerable to membrane rupture as a result of mechanical stretching.

If the plasma membrane of AS-M.5 SOCS3 KO cells was found to be less stable than in the AS-M.5 WT cells the next step would be to determine if expressing SOCS3 in SOCS3 KO cells, potentially via lentiviral delivery of SOCS3 or by treatment with prostanoids, would be sufficient to rescue plasma membrane integrity in AS-M.5 SOCS3 KO cells.

These experiments have investigated the role of SOCS3 in mechanoprotection as this is intrinsically linked to plasma membrane integrity and there is a body of research highlighting the role of EC permeability in PAH (Zhou et al. 2016; Ranchoux et al. 2018; Zhou et al. 2018). Further work is required to fully establish the interaction of SOCS3 and cavin-1/CAV1 and determine if this role of SOCS3 would have any therapeutic potential for PAH. Caveolae has numerous other functions, for instance regulation of signalling molecules and

intracellular trafficking (reviewed by Kovtun et al. 2015), which if lost or dysregulated could potentially be detrimental in PAH. Thus, it is not just the role of SOCS3 in mechanoprotection that should be considered.

7. Final Discussion

Current treatment of PAH is aimed at relieving the symptoms of PAH, not targeting the cause (Section 1.6). As a result, there is no cure for PAH and no recent improvements regarding survival rates. In addition, treatment is associated with many side effects such as flushing, nausea, and headaches (Lau et al. 2017), as well the complications of complex administration procedures (Sitbon et al. 2002; Kumar et al. 2016). Thus, there is a need for novel therapeutic options that target the pathological changes which occur in PAH prior to and following the onset of the disease, whilst also improving a patient's QOL and survival rates.

Although prostacyclins were discovered in 1976 (Moncada et al. 1976), and the first prostanoid clinically approved for PAH treatment was epoprostenol in the US in 1995 for its vasodilatory effects, relatively little consideration has been given to other potential effects of prostanoids which could be exploited. This is surprising considering the prostanoid epoprostenol is the only drug to have shown a capacity to improve survival rates (Sitbon et al. 2002). Thus, this research has addressed this gap in the literature and highlighted a novel alternative mechanism activated by prostanoids that could provide therapeutic benefits to the patient by reducing the inflammatory component of PAH. However, it would appear the system is much more complex that the original

hypothesis suggested (Section 1.7), with potential other interactions between prostanoids and IL-6 signalling involved, as highlighted in Figure 7.1.

7.1 Inducing SOCS3 for the treatment of PAH and other diseases

The prostanoids BPS and treprostinil, and ACT-333679, the active metabolite of the IP agonist selexipag, induced SOCS3 in HPAECs and HPMECs *in vitro* (Chapter 3). These cell types were investigated as they are affected by the vascular remodelling and inflammation typical of PAH. Although the exact signalling pathway is yet to be established, attempts to define the pathway with EPAC and PKA agonists were unsuccessful (Figure 3.7), this does provide a potential mechanism activated by prostanoids which has not been explored with regards to PAH. Prostanoids were also shown to limit IL-6 *trans*-signalling potentially via SOCS3, although further experiments to determine a role for SOCS3 utilising siRNA and shRNA knock-down of SOCS3 were not successful (Figures 4.5 and 4.6). In conclusion, the hypothesis was correct in that prostanoids have the capacity to both induce SOCS3 and inhibit IL-6/sIL-6Rα signalling, however the exact mechanisms involved are yet to be confirmed (Figure 7.1).

None the less, as the function of SOCS3 is becoming better understood, its potential therapeutic benefit is being explored for a number of inflammatory diseases in which IL-6 signalling and STAT3 hyperactivation are key factors including multiple sclerosis, cancers, rheumatoid arthritis, and diabetes (Mahony et al. 2016; Durham et al. 2019). Elevated IL-6 signalling activity has also been associated with PAH (Hashimoto-Kataoka et al. 2015; Jasiewicz et

al. 2015; Matura et al. 2015; Fang et al. 2017; Maston et al. 2018; Tamura et al. 2018), however attempts to minimise the effects of IL-6 with SOCS3-based therapies have yet to be investigated. There are challenges involved in SOCS3-based therapies, namely its short-half life and a body of research that shows SOCS3 may be detrimental in a number of illnesses.

7.1.1 Increasing the stability of SOCS3

SOCS3 has a half-life of 40 - 120 minutes depending on the cell type (Siewert et al. 1999; Fletcher et al. 2010). Numerous mechanisms for the regulation and degradation of SOCS3 have been identified. Key tyrosine residues (tyrosine^{204} and tyrosine^{221}) have been identified within the SOCS3 box region of SOCS3 which when phosphorylated make SOCS3 a target for proteasomal degradation (Haan et al. 2003). SOCS3 Y204F,Y221F phosphorylation-deficient COS-7 cells, prepared via transfection with a Y204F,Y221F SOCS3 plasmid, demonstrated a half-life of 4 - 8 hours compared to the 2 hour half-life of WT cells (Haan et al. 2003), although densitometry analysis was not performed in these experiments so it is difficult to establish if there is a significant change in SOCS3 expression. Also, the proteasome inhibitor MG-132 protects SOCS3 from degradation (Haan et al. 2003; Liu et al. 2003) suggesting the role of proteasomal degradation is substantial.

SOCS3 also contains a PEST domain, a common amino acid sequence found in proteins with a short half-life, within its SH2 domain which acts a proteolytic target (Rogers et al. 1986; Yasukawa et al. 2003). Deletion of the PEST domain in HEK 293T cells increases the stability of SOCS3 (Babon et al. 2006). The author's claim this increases stability to a greater extent than

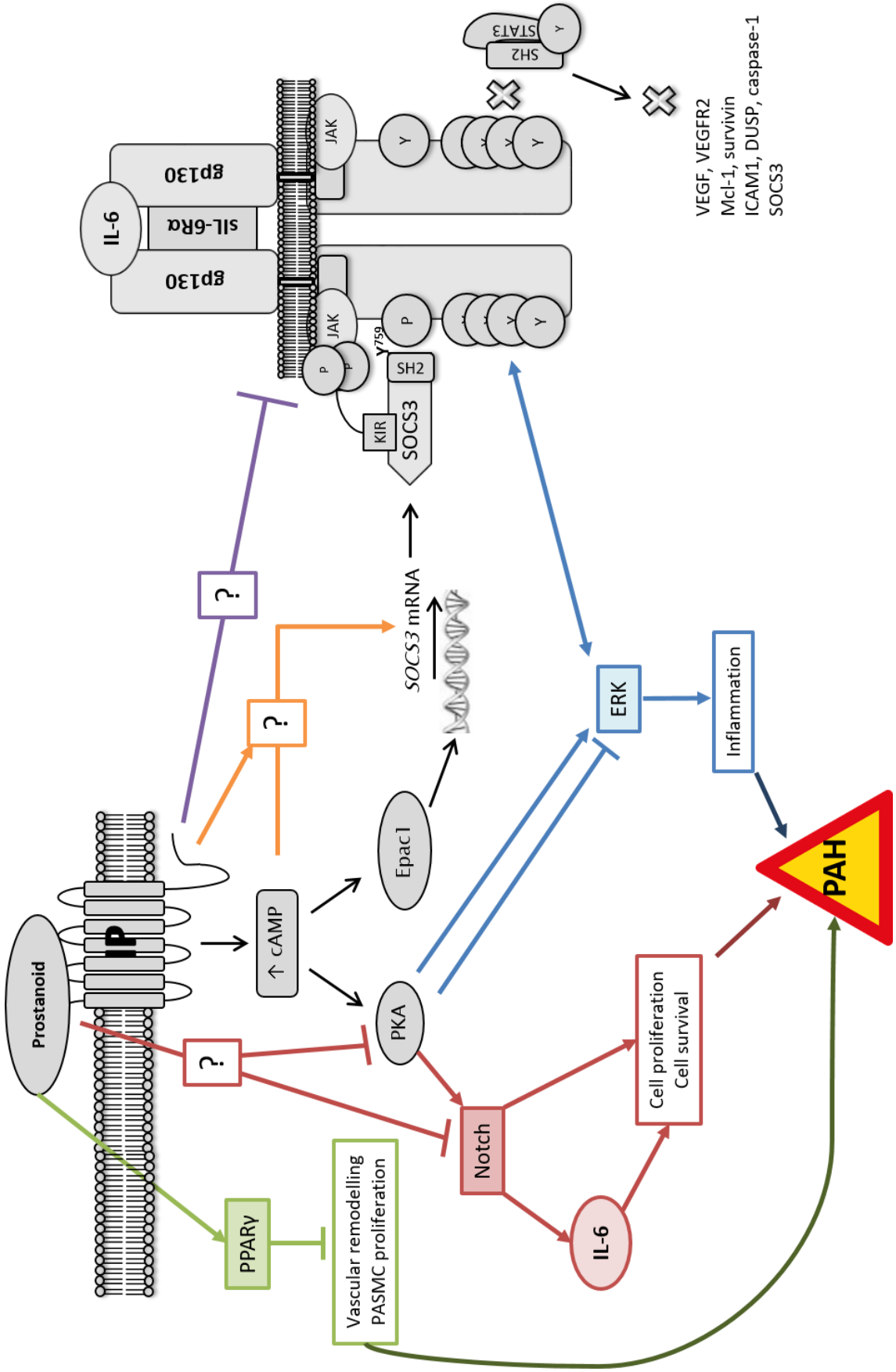
Prostanoid
IP
↑ cAMP
Epac1
PKA
?
?
?
SOCS3 mRNA
ERK
Inflammation
PAH
Notch
IL-6
Cell proliferation
Cell survival
PPARγ
Vascular remodelling
PASMC proliferation
IL-6
sIL-6Rα
gp130
gp130
JAK
JAK
Y
P
Y759
SH2
KIR
SOCS3
SH2
STAT3
VEGF, VEGFR2
Mcl-1, survivin
ICAM1, DUSP, caspase-1
SOCS3

Figure 7.1: Ongoing hypothesis highlighting prostanoid-mediated signalling pathways that may PAH pathogenesis.

The original hypothesis (grey) (Figure 1.9) plus addition signalling pathways to be considered in the context of prostanoid-inhibition of IL-6 *trans*-signalling activity and PAH. Prostanoids limited IL-6 activity in part due to SOCS3 but there is also a potential SOCS3-independent mechanism (purple). Prostanoids induced SOCS3 but this appeared to be via a currently unknown PKA/EPAC-independent mechanism (orange). Mobilisation of cAMP activates PKA which also interacts with Notch and ERK (red and blue respectively). Prostanoid activation of PPARγ (green). cAMP; cyclic adenosine monophosphate, EPAC1; exchange protein directly activated by cAMP 1, ERK; extracellular signal–regulated kinase, gp130; glycoprotein-130, ICAM1; intracellular adhesion molecule 1, IL-6; interleukin 6, IP; prostaglandin I_2 receptor, JAK; janus kinase, KIR; kinase inhibitory region, PKA; protein kinase A (cAMP dependent protein kinase), PPAR; peroxisome proliferator-activated receptor, SOCS3; suppressor of cytokine signalling 3, sIL-6Rα; soluble IL-6 receptor α, STAT3; signal transducer and activator of transcription 3, VEGF; vascular endothelial growth factor, VEGFR; vascular endothelial growth factor receptor.

deleting the SOCS box, without affecting the structure or ability of SOCS3 to inhibit STAT activity. Regulation of SOCS3 via ubiquitination of the N-terminal region of SOCS3 has also been evidenced. An N-terminal truncated form of SOCS3, created by alternative translation initiation as a result of endoplasmic reticulum stress, was found to be more stable than WT (Sasaki et al. 2003). A lysine residue at position 6 (Lys6) which was lost in the truncated SOCS3 was identified as a key ubiquitination site (Sasaki et al. 2003). Additional key lysine residues in SOCS3 have since been identified that recruit E3 ubiquitin ligases resulting in the rapid ubiquitination of SOCS3 and also of gp130 and JAK2 (Kershaw et al. 2014; Munro 2016a). A SOCS3 mutant in which lysine was mutated to arginine at positions 6, 23, 28, 40, 85, 91, 122, 173 (lys-less SOCS3) was shown to have increased stability compared to WT SOCS3 whilst still maintaining proper function as measured by SOCS3 ability to inhibit erythropoietin-induced STAT3 tyrosine 705 phosphorylation and to interact with E3 ligase components (Munro 2016a).

Thus, ubiquitination is another key factor in SOCS3 stability, providing an additional mechanism to exploit to improve the short half-life of SOCS3. The relevant E3 ligase for SOCS3 has yet to identified, however doing so would provide a potential target to improve SOCS3 stability. Small molecule inhibitors have been used to inhibit E3 ligases previously. For instance, thalidomide, used to treat multiple myeloma (Singhal et al. 1999; Mercurio et al. 2017) binds and inhibits the E3 ligase cereblon (Ito et al. 2010; Liu et al. 2015). Also, drugs targeting mouse double minute 2 homolog (the E3 ligase responsible for p53 degradation) are in early phase clinical trials for cancers, e.g. AMG232 (Sun et al. 2014).

Thus, there are numerous mechanisms that could be targeted to increase the stability of SOCS3. However, some research suggests increasing SOCS3 expression may also have detrimental effects.

7.1.2 SOCS3 in disease

Another challenge associated with increasing SOCS3 for therapeutic purposes is SOCS3 expression seems to have conflicting roles in the progression of some diseases. For instance, in atherosclerosis SOCS3 induced by IL-10 initiates EC apoptosis, thus preventing EC dysfunction (Yin et al. 2013). However, in the same disease, overexpression of SOCS3 in T-cells appears to contribute to vascular inflammation and the development of atherosclerotic plaques (Taleb et al. 2009).

Similarly, there is evidence to support both protective and causative roles for SOCS3 in diabetes. SOCS3 is overexpressed in the skeletal muscle of obese humans and as SOCS3 inhibits insulin signal transduction in the liver (Sachithanandan et al. 2010) and in adipose tissue (Emanuelli et al. 2001; Shi et al. 2004; Ueki et al. 2004), this provided rationale to examine the potential impact of SOCS3 on insulin in skeletal muscle. Skeletal muscle-specific SOCS3 knockout (SOCS3 MKO) in mice resulted in normal muscle development, body mass, and energy homeostasis but when fed a high fat diet, SOCS3 MKO mice were protected from insulin resistance compared to WT mice, even though both mice types experienced a similar increase in weight gain (Jorgensen et al. 2013). This was due to increased skeletal muscle insulin receptor substrate 1 expression and enhanced Akt phosphorylation post-insulin treatment in the SOCS MKO compared to the WT mice (Jorgensen et al. 2013), although how SOCS3 attenuated this was not specified. SOCS3

MKO mice also demonstrated a higher glucose tolerance than their WT counterparts. No difference in activity levels, food intake or oxygen utilisation were found, but SOCS MKO mice exhibited a higher respiratory exchange ratio which the authors attributed to greater carbohydrate oxidation as a result of increased insulin sensitivity and metabolic flexibility (Jorgensen et al. 2013). On the other hand, the anti-inflammatory effects of SOCS3 appear to reduce the dysfunction caused by diabetes in animal models. SOCS1 and SOCS3 expression was increased in the renal cortex of streptozotocin (STZ)-induced diabetic rats and in human immortalised proximal tubule epithelial cells from normal adult human kidney and glomerular mesangial cells under hyperglycemic conditions (Ortiz-Munoz et al. 2010). SOCS3 adenovirus injection into STZ diabetic rats resulted in reduced inflammation, measured by ICAM, RANTES and MCP-1 protein expression, and reduced fibrosis, measured via TGF-β and collagen IV expression, compared to WT and control-adenovirus groups (Ortiz-Munoz et al. 2010).

In other diseases such as cancer and obesity, SOCS3 has been shown to either directly or indirectly enable disease progression. Although IL-6 signalling is considered key for the growth and metastasis of many cancers (reviewed by Kumari et al. 2016), and limiting IL-6 signalling is a key mechanismfor approved cancer drugs and those currently being developed (Angevin et al. 2014; Dijkgraaf et al. 2015), SOCS3 has also been shown to promote cancer development. In prostate cancer, downregulating SOCS3 causes prostate cancer cell death via the activation of apoptotic pathways, suggesting SOCS3 protects prostate cancer cells (Puhr et al. 2009), and in cutaneous T-cell

lymphoma, SOCS3 protected cells from growth inhibition caused by IFN-γ treatment (Brender et al. 2005).

Leptin, a key regulator of energy homeostasis, acts via JAK/STAT signalling and is therefore negatively regulated by SOCS3. As a result, downregulating SOCS3 via a heterozygous SOCS3 KO mutation has been shown to protect against diet-induced obesity in mice (Howard et al. 2004). Neural cell-specific SOCS3 KO mice also demonstrated enhanced leptin-induced hypothalamic STAT3 tyrosine 705 phosphorylation, lower food intake and overall reduced diet–induced obesity (Mori et al. 2004). As a result, dysregulated energy homeostasis and obesity should be considered as potential side effects of any SOCS3-based therapeutic.

Collectively, this suggests a complex role for SOCS3 in disease where its inhibition of JAK/STAT signalling results in enabling disease progression in some cases, but inhibiting it in others. Therefore, the specificity and selectivity of any SOCS3-based therapeutics developed for PAH or any other disease should be carefully considered to avoid potential outcomes such as obesity and increased vulnerability to cancer and atherosclerosis.

In addition, the impact of novel SOCS3 interactions has not been considered. For instance, a link between SOCS3 and Cavin-1 stability and function has recently been identified (Williams et al. 2018), however the potential impact of this in endothelial permeability and if it could protect against the development of PAH has yet to be established. Attempts to identify a role for SOCS3 in endothelial cell membrane stability were unsuccessful (Chapter 6). Further optimisation and experiments are required to conclusively measure the impact

of SOCS3 on EC membrane stability. However, this does support there are roles of SOCS3 yet to be characterised and fully understood.

Our research demonstrates a novel mechanism in which BPS, treprostinil and ACT-333679 induce SOCS3 expression in HPAECs, HPMECs and the established EC model, AS-M.5 cells (Krump-Konvalinkova et al. 2003) (Chapter 3), as well as limit IL-6 signalling as measured via tyrosine 705 STAT3 phosphorylation in HPAECs and AS-M.5 cells, and cell permeability studies in HPAECs (Chapter 4). Experiments in AS-M.5 SOCS3 KO cells suggests prostanoid inhibition of IL-6 signalling is due in part to the induction of SOCS3 (Figure 4.4). Although further experiments are required to fully clarify this, these results do support that increasing SOCS3 expression, for instance via prostanoid treatment, is sufficient to reduce IL-6 *trans*-signalling activity. This may prove to be therapeutically beneficial in diseases such as PAH where the pro-inflammatory effects of IL-6 are a key component of disease progression (Section 1.4.2).

Like SOCS3, prostanoids can also impact numerous other signalling pathways and these should be considered prior to any changes made in prostanoid treatment of PAH, or other diseases.

7.2 The wider impact of prostanoid treatment

The primary aim of prostanoid treatment for PAH is the activation of the GPCR IP resulting in the stimulation of cAMP-mediated PKA activity to induce vasodilation via PKA regulation of K^+ channels (Haynes et al. 1992; reviewed by Clapp and Gurung 2015). However, activation of cAMP has a much broader

function than just vasodilation. This thesis has considered a potential anti-inflammatory role of cAMP via the induction of SOCS3 which binds to gp130 and inhibits further activation of IL-6/sIL-6Rα signalling. However, cAMP also interacts with the IL-6 signalling pathway via the Ras/Raf/ERK axis, a downstream mediator of IL-6.

7.2.1 cAMP activation and ERK 1/2

Initial research identified cAMP-mediated induction of PKA to limit Ras/Raf/ERK signalling. In oocyte extracts prepared from *Xenopus laevis*, incubation with PKA inhibited MAPK activity whereas PKI treatment alone was sufficient to enhance MAPK signalling (VanRenterghem et al. 1994). This was shown to be via PKA phosphorylation of the Raf1 serine 249 residue(Dhillon et al. 2002), which is required for Raf1 activity (King et al. 1998). Finally, cAMP-mediated signalling independent of EPAC1 has also been shown to regulate IL-6 activity via inhibition of Ras/Raf/ERK signalling pathway (Woolson et al. 2009).

However, other research shows cAMP to activate ERK1/2. Fsk was shown to increase ERK activation in mice cortical neurones which was mediated via Fsk-induction of PKA (Ambrosini et al. 2000), although the effects of PKA inhibition were not investigated. In human melanocytes, Fsk-mediated cAMP activated ERK1/2 signalling via Ras mediated activation of B-raf in a PKA- and EPAC-independent manner (Busca et al. 2000). Interestingly, ras was not shown to be involved in cAMP activation of ERK in NIH/3T3 fibroblasts suggesting this is a melanocyte-specific mechanism (Busca et al. 2000), supporting that cAMP regulation of ERK1/2 activity is cell-specific.

This suggests a complex system in which cAMP can either limit or stimulate ERK1/2 signalling, depending on the cell type and Raf proteins involved, to regulate cell behaviour (reviewed by Dumaz and Marais 2005) (Figure 7.1). This ought to be further explored in vascular cells as it may provide an alternative signalling mechanism in which prostanoid activation of cAMP limits IL-6 signalling. In addition to modulating ERK activity, cAMP-mediated PKA acts on numerous other signalling pathways which may be important in PAH, including NOTCH.

7.2.2 PKA activation and Notch

cAMP and PKA have been shown to enhance Notch signalling in monocytes and C6 glioma cells (Angulo-Rojo et al. 2013; Larabee et al. 2013). Notch1 is increased in the lungs of PAH patients, HPAECs maintained in hypoxic conditions, and in SU/Hx rat models of PAH compared to WT rats (Dabral et al. 2016). In HPAECs, Notch1 was found to increase cell proliferation and inhibit apoptosis via downregulation of p21 and upregulation of Bcl-2 and Survivin respectively, whilst siRNA-mediated knockdown of Notch1 protected cells from hypoxia-induced proliferation (Dabral et al. 2016). In SU/Hx rats, treating with AMG2008827, a Notch inhibitor that prevents proteolytic cleavage of Notch into the active Notch intracellular domain (NICD) by selectively targeting γ-secretase, reduced RVSP and RH hypertrophy (Dabral et al. 2016). In addition, two Notch3 missense mutations (c.2519 G>A p.G840E, c.2698 A>C p.T900P) which are associated with increased cell proliferation and viability have been identified in child PAH patients (Chida et al. 2014). Collectively, this suggests Notch enables PAH progression.

Notch also enhances IL-6 induced JAK/STAT signalling. In breast cancer cells, increased Notch was associated with increased IL-6 mRNA and protein expression, as well as increased JAK/STAT activation measured by tyrosine 705 STAT3 phosphorylation and levels of the JAK/STAT target gene Bcl-xL (Jin et al. 2013). Notch, increased by either NICD transfection or increasing cell density, was also found to upregulate IL-6 gene transcription in NIH/3T3 cells resulting in IL-6-mediated cell apoptosis via cleavage of caspase 3 (Matsuno et al. 2018). The authors suggested that Notch/IL-6 hyperactivity may contribute to apoptotic resistance via the development of dysfunction apoptosis-resistant cells (Matsuno et al. 2018). Apoptotic resistance in EC and SMCs is characteristic of PAH (Masri et al. 2007; Courboulin et al. 2011).

Activation of EP_3 in HUVECs prmoteded Notch-induced angiogenesis and tube formation via the down-regulation of PKA (Chen et al. 2017) but in ECs isolated from the retinas of mice or in HUVECs, PKA did not appear to mediate Notch activity at all (Nedvetsky et al. 2016). This suggests a complex, cell-specific cAMP/PKA/Notch axis exists which should be considered further due to the potentially detrimental effect that mobilising cAMP may have as a result of enhanced PKA/Notch and Notch/IL-6 signalling (Figure 7.1). Treatment with Notch inhibitors is being considered for the treatment of cancer but so far clinical trials have had mixed success (Pant et al. 2016; Wu et al. 2017) (Clinical trial identifier; NCT01122901), should be considered to limit IL-6-mediated inflammation and angiogenesis.

Interestingly, prostanoids are not specific to IP and the activation of cAMP, and therefore cAMP effector proteins such as PKA and EPAC, but also activate PPARs (Bishop-Bailey and Hla 1999).

7.2.3 Prostanoid activation of PPARγ receptors

Anti-proliferative effects of treprostinil on human IPAH PASMCs were observed in IP knockout cells, and were unaffected by IP antagonists, but were inhibited by GW9662, a PPARγ antagonist, in human IPAH PASMCs (Falcetti et al. 2010). In addition, SMC specific knockdown of PPARγ in mice resulted in spontaneous muscularisation of the distal pulmonary arteries causing increased RVSP and RV hypertrophy (Hansmann et al. 2008). This provides evidence of an alternative prostanoid target that may also mediate the therapeutic effects of prostanoids in PAH. Reinforcing this is research showing activation of PPARγ in rats protected them from MCT-induced PASMC proliferation and pulmonary vascular remodelling (Zhang et al. 2014), and from RV dysfunction (Xu et al. 2017).

Controversially, PPARγ receptors are upregulated in the SMC layer of small pulmonary arteries from child IPAH patients compared to those from control child small pulmonary arteries (Falcetti et al. 2010), though this may be a protective response. Thus, activation of PPARγ appears to protect against the vascular changes characteristic of PAH (Figure 7.1). Interestingly, PPARβ/δ activation had opposing effects, causing VEGF-mediated EC proliferation and endothelial tube formation (Piqueras et al. 2007). Although prostanoids are not known to activate this receptor type in VECs, if the role of PPARγ is to be exploited for PAH in the future, the specificity of the agonists used will need to be considered.

To summarise, the wider impact of prostanoids in the context of PAH is mostly unknown. This research has aimed to increase our knowledge of prostanoid inhibition of IL-6/sIL-6Rα via cAMP-mediated SOCS3, but researching

prostanoid stimulation of ERK, Notch and PPARγ signalling in VECs may be worthwhile to better understand how to improve the therapeutic efficacy of prostanoids. Similarly, identifying the most efficient means of reducing IL-6 signalling in PAH will result in more effective treatment.

7.3 Limiting IL-6 signalling activity in PAH

Research supports that IL-6 is a key factor is the development of PAH (Jasiewicz et al. 2015; Huang et al. 2016; Fang et al. 2017; Maston et al. 2018; Tamura et al. 2018) (Section 1.4.2), yet IL-6 signalling is still not targeted in the treatment of PAH. Drugs that target IL-6 have been approved for autoimmune diseases such as rheumatoid arthritis (Woodrick and Ruderman 2010; Hashizume et al. 2015), and demonstrate effectiveness in clinical remission and increased QOL, with infections and hypersensitivity reactions noted as the most frequent adverse effects (Oton et al. 2018). As previously mentioned (Section 1.6.2.2), there has been one promisingcase of PAH where tocilizumab was administered in addition conventional PAH therapy (Arita et al. 2010). This supports the potential of larger re-purposing studies to test the efficacy of tociluzimab and other anti-IL-6 therapies such as siltuximab in the treatment of PAH. Similarly, JAK inhibitors such as tofacitinib and baracitinib, which are used in the treatment of inflammatory diseases including rheumatoid arthritis and ulcerative colitis (Gaudino et al. 2017; Bonovas et al. 2018; Wragg et al. 2018), should be considered as potential treatments of PAH alongside current therapy.

It is also of note that treatment with prostanoids and non-prostanoid IP antagonists such as selexipag is currently advised when patients are in WHO functional class III and worse (Galie et al. 2015). At this more developed stage, the impact of reducing IL-6 signalling will be limited, and it may be too late to attenuate further disease progression. Chapter 5 showed that prostanoids protect HPAECs from IL-6 induced cell permeability (Figure 5.1), and other groups have shown activation of cAMP and cAMP effector proteins such as EPAC to limit the expression of IL-6 induced inflammatory gene expression in HUVECs (Wiejak et al. 2019). In addition, animal models show silencing of IL-6 or gp130 protects against PAH progression by reducing inflammatory cell infiltration and vascular remodelling (Savale et al. 2009; Huang et al. 2016), although these studies are limited as IL-6 knockdown occurs prior to PAH development so they do not measure the impact of limiting IL-6 post-PAH diagnosis. However, due to IL-6 being an established contributor to the pathological changes characteristic of PAH and the evidence which supports prostanoids ability to reduce IL-6 signalling, we propose reducing the WHO functional class at which prostanoids are currently prescribed in the aim of preventing further disease progression resulting from IL-6 signalling activity.

8. Future work

With regards to further research, these experiments have investigated the effect of prostanoids on healthy vascular cells only. Therefore, the response of PAH tissue to prostanoids and IL-6/sIL-6Rα stimulation/inhibition should also be investigated, especially as differences in receptor levels have been identified between control and PAH cells (Falcetti et al. 2010; Patel et al. 2018).

In addition, research has shown only some inflammatory cells and hepatocytes to express mbIL-6Rα (Hirata et al. 1989; Rojkind et al. 1995; Wang and Fuller 1995). As a result these experiments the response of HPAECs to IL-6/sIL-6Rα, but not the response to IL-6 alone. Interestingly, PASMCs isolated from PAH patients and animal models of PAH demonstrate an increased expression of mbIL-6Rα (Tamura et al. 2018), suggesting both IL-6 classic signalling and IL-6 *trans*-signalling may be occurring in PAH. As the HPAECs used in these experiments are not isolated from PAH patients, an assumption has been made that they will only respond to IL-6 *trans*-signalling. However, to confirm this, the response to IL-6 only in the cell types utilised in these experiments should be measured. Additionally, RT-PCR could be utilised to compare the ratio of mbIL-6Rα vs sIL-6Rα, as well as the ratio of different prostaglandin receptors and PPARs, in control HPAECs and PAH-HPAECs. This would provide a better informed judgement regarding the best therapeutic signalling pathways to target, and whether the focus should be on targeting IL-6 classic- or *trans*-signalling, or investigating the balance between them both.

Once therapeutic targets have been identified, for instance increasing SOCS3, animal models of PAH could be utilised to test any therapeutic benefit. Tamura et al. (2018) demonstrated success utilising a curative model in which MCT-rat models of PAH were treated with the IL-6/sIL-6Rα antagonist ERBF one-week post-MCT injection. Treatment with ERBF in this manner resulted in reduced mPAP, PVR, RV hypertrophy and cardiac output compared to the control group at comparable levels to beginning treatment with ERBF at the same time as injecting with MCT (Tamura et al. 2018). Similarly, in Su/Hx models of PAH, starting treatment with ERBF five weeks post-SU5416

injection significantly reduced STAT3 activation, decreased MCL-1 protein expression and increased apoptosis, measured via TUNEL staining, compared to control mice to a similar extent as initiating treatment alongside SU5416 treatment and hypoxia exposure (Tamura et al. 2018). This provides a model for measuring the curative effect of prostanoids on key factors, such as IL-6 activity, in animal models of PAH. As Chapter 4 showed prostanoid inhibition of IL-6 signalling to be due in part to SOCS3 (Figure 4.4), it would be interesting to determine the curative impact of SOCS3 overexpression in animal models of PAH. Adeno-associated virus treatment to introduce SOCS3, or a cre/lox system to mutate key ubiquitination sites of SOCS3 resulting in increased SOCS3 stability, could be administered to the animal post-initiation of PAH, or in animals with lung-specific overexpression of IL-6 as these have previously been shown to develop plexiform lesions comparable to those characteristic of PAH (Steiner et al. 2009).

The exact mechanism of prostanoid-mediated induction of SOCS3 in HPAECs is still to be determined. Thus, further experiments to determine the role of EPAC, PKC and ERK, as these have previously been shown crucial for cAMP-mediated induction of SOCS3 in HUVECs and COS-7 cells (Yarwood et al. 2008; Borland et al. 2009), would be explored. Additionally, SOCS3-independent regulation of IL-6 signalling activity would be explored, for instance the potential role of a prostanoid/PPARγ signalling axis and a prostanoid/PKA/notch signalling axis.

Other roles of SOCS3 within VECs would also be explored in the context of PAH, and other vascular disease. The SOCS3/cavin interaction (Williams et al. 2018) is one such role that could potentially be exploited to increase the

ability of VECs to withstand higher levels of stress. Utilising AS-M.5 SOCS3 KO to investigate a potential role for SOCS3 in membrane stability (Chapter 6) is a starting point for this line of research. Further optimisation of the technique used has been discussion in Section 6.3, however other models of cellular stress, such as modelling blood flow, could be utilised. Cavin1 proteins are also required for other caveolae functions such as transcytosis, signal transduction and lipid homeostasis (reviewed by Cheng and Nichols 2016), all of which are necessary for proper EC function. Thus, as SOCS3 stabilises cavin-1, the effect of SOCS3 on caveolae functions other than mechanoprotection should be explored.

To summarise, future experiments would focus on defining the key elements involved in prostanoid induction of SOCS3, as well as the wider implications of prostanoid treatment such as PPARγ activation and potential PKA/IL-6 interactions (Figure 1.7). In addition, the receptor profiles of VECs involved in PAH need to be confirmed to identify which signalling pathways will be best to target. Other effects of SOCS3 expression, for instance on caveolae function, should also be investigated. Combined, these experiments will highlight potential drug targets which could be further explored using the curative model of PAH in animal models previously described.

8.1 Future perspectives

PAH is currently a debilitating disease with no cure, thus novel treatments are required that target the pathological changes responsible for the disease. This research has started to address that gap in the literature and identified a novel

mechanism for the beneficial effects of prostanoid treatment for PAH in which IL-6/sIL-6Rα signalling activity is inhibited. As research has shown IL-6 induced inflammation and vascular remodelling enables PAH progression (Section 1.4.2), a study to determine the effect of treating with prostanoids at an earlier functional class, potentially alongside clinically approved IL-6 inhibitors, may prove to have an immediate impact. However, research should continue to improve the specificity, selectivity and safety of prostacyclin-based therapies to improve patient QOL. For instance, the introduction of new drug delivery systems that allow for sustained release of PGI_2, or relevant analogues, that specifically target the damaged pulmonary vasculature (Ishihara et al. 2015; Segura-Ibarra et al. 2018) are encouraging and could lead to a novel method of prostanoid drug delivery which minimises the adverse effects and reduced QOL associated with current prostanoid treatments. Clinically approved PPARγ agonists such as thiazolidinediones, currently used in the treatment of type 2 diabetes (Vijay et al. 2009; Gupta et al. 2012), could also be repurposed as a PAH therapy as there is evidence to support enhancing PPARγ signalling would be beneficial (Section 7.2).

Based on current research that proposes increasing SOCS3 expression or stability as a novel method of combatting disease (reviewed by Mahony et al. 2016; reviewed by Durham et al. 2019) and the results of these experiments, i.e. a role for SOCS3 in prostanoid-mediated inhibition of IL-6 signalling and function, SOCS3-based therapies will be beneficial to diseases with a large inflammatory component, such as PAH. Thus, expanding this research will be of interest to other groups aiming to stabilise SOCS3 (Section 7.1) to identify and develop more effective treatments for a range of diseases. Although, as

there is a potential risk when increasing SOCS3 expression (Section 7.1.2), the specificity of SOCS3-based therapies will need to be carefully considered.

To summarise, this research has identified a novel mechanism of prostanoid inhibition of IL-6 *trans*-signalling. These findings, in addition to future research identifying the most promising drug targets and developing new drug delivery systems, will form a bulk of research that enables the establishment of novel PAH therapies that address the limitations of current available PAH treatment. By targeting the underlying pathological causes of the disease, novel treatment will improve the prognosis and QOL for PAH patients.

9. References

Agassandian, M., Tedrow, J. R., Sembrat, J., Kass, D. J., Zhang, Y., Goncharova, E. A., Kaminski, N., Mallampalli, R. K. and Vuga, L. J. (2015) VCAM-1 is a TGF-beta1 inducible gene upregulated in idiopathic pulmonary fibrosis. *Cell Signal* 27 (12), 2467-73.

Ahmad, J. N., Cerny, O., Linhartova, I., Masin, J., Osicka, R. and Sebo, P. (2016) cAMP signalling of Bordetella adenylate cyclase toxin through the SHP-1 phosphatase activates the BimEL-Bax pro-apoptotic cascade in phagocytes. *Cell Microbiol* 18 (3), 384-98.

Ahmmed, G. U. and Malik, A. B. (2005) Functional role of TRPC channels in the regulation of endothelial permeability. *Pflugers Arch* 451 (1), 131-42.

Akdis, M., Aab, A., Altunbulakli, C., Azkur, K., Costa, R. A., Crameri, R., Duan, S., Eiwegger, T., Eljaszewicz, A., Ferstl, R., Frei, R., Garbani, M., Globinska, A., Hess, L., Huitema, C., Kubo, T., Komlosi, Z., Konieczna, P., Kovacs, N., Kucuksezer, U. C., Meyer, N., Morita, H., Olzhausen, J., O'Mahony, L., Pezer, M., Prati, M., Rebane, A., Rhyner, C., Rinaldi, A., Sokolowska, M., Stanic, B., Sugita, K., Treis, A., van de Veen, W., Wanke, K., Wawrzyniak, M., Wawrzyniak, P., Wirz, O. F., Zakzuk, J. S. and Akdis, C. A. (2016) Interleukins (from IL-1 to IL-38), interferons, transforming growth factor beta, and TNF-alpha: Receptors, functions, and roles in diseases. *J Allergy Clin Immunol* 138 (4), 984-1010.

Alastalo, T. P., Li, M., Perez Vde, J., Pham, D., Sawada, H., Wang, J. K., Koskenvuo, M., Wang, L., Freeman, B. A., Chang, H. Y. and Rabinovitch, M. (2011) Disruption of PPARgamma/beta-catenin-mediated regulation of apelin impairs BMP-induced mouse and human pulmonary arterial EC survival. *J Clin Invest* 121 (9), 3735-46.

Ali, F. Y., Egan, K., FitzGerald, G. A., Desvergne, B., Wahli, W., Bishop-Bailey, D., Warner, T. D. and Mitchell, J. A. (2006) Role of prostacyclin versus peroxisome proliferator-activated receptor beta receptors in prostacyclin sensing by lung fibroblasts. *Am J Respir Cell Mol Biol* 34 (2), 242-6.

Alsaffar, H., Martino, N., Garrett, J. P. and Adam, A. P. (2018) Interleukin-6 promotes a sustained loss of endothelial barrier function via Janus kinase-mediated STAT3 phosphorylation and de novo protein synthesis. *Am J Physiol Cell Physiol* 314 (5), C589-C602.

Ambrosini, A., Tininini, S., Barassi, A., Racagni, G., Sturani, E. and Zippel, R. (2000) cAMP cascade leads to Ras activation in cortical neurons. *Brain Res Mol Brain Res* 75 (1), 54-60.

Anderl, J., Ma, J. and Armstrong, L. (2012) *Improved Assays for Quantification of In Vitro Vascular Permeability.* Nature Methods: *http://www.merckmillipore.com/GB/en/product/In-Vitro-Vascular-Permeability-Assay-24-well,MM_NF-ECM644?bd=1#anchor_Description*

Andreassen, A. K., Wergeland, R., Simonsen, S., Geiran, O., Guevara, C. and Ueland, T. (2006) N-terminal pro-B-type natriuretic peptide as an indicator of disease severity in a heterogeneous group of patients with chronic precapillary pulmonary hypertension. *Am J Cardiol* 98 (4), 525-9.

Angevin, E., Tabernero, J., Elez, E., Cohen, S. J., Bahleda, R., van Laethem, J. L., Ottensmeier, C., Lopez-Martin, J. A., Clive, S., Joly, F., Ray-Coquard, I., Dirix, L.,

Machiels, J. P., Steven, N., Reddy, M., Hall, B., Puchalski, T. A., Bandekar, R., van de Velde, H., Tromp, B., Vermeulen, J. and Kurzrock, R. (2014) A phase I/II, multiple-dose, dose-escalation study of siltuximab, an anti-interleukin-6 monoclonal antibody, in patients with advanced solid tumors. *Clin Cancer Res* 20 (8), 2192-204.

Angulo-Rojo, C., Manning-Cela, R., Aguirre, A., Ortega, A. and Lopez-Bayghen, E. (2013) Involvement of the Notch pathway in terminal astrocytic differentiation: role of PKA. *ASN Neuro* 5 (5), e00130.

Anonymous (2017) *Abbreviations.* December 11 2017. Journal of Biological Chemistry. http://www.jbc.org/site/misc/abbrev.xhtml

Arita, Y., Sakata, Y., Sudo, T., Maeda, T., Matsuoka, K., Tamai, K., Higuchi, K., Shioyama, W., Nakaoka, Y., Kanakura, Y. and Yamauchi-Takihara, K. (2010) The efficacy of tocilizumab in a patient with pulmonary arterial hypertension associated with Castleman's disease. *Heart Vessels* 25 (5), 444-7.

Arnold, P., Boll, I., Rothaug, M., Schumacher, N., Schmidt, F., Wichert, R., Schneppenheim, J., Lokau, J., Pickhinke, U., Koudelka, T., Tholey, A., Rabe, B., Scheller, J., Lucius, R., Garbers, C., Rose-John, S. and Becker-Pauly, C. (2017) Meprin Metalloproteases Generate Biologically Active Soluble Interleukin-6 Receptor to Induce Trans-Signaling. *Sci Rep* 7, 44053.

Aronoff, D. M., Canetti, C. and Peters-Golden, M. (2004) Prostaglandin E2 inhibits alveolar macrophage phagocytosis through an E-prostanoid 2 receptor-mediated increase in intracellular cyclic AMP. *J Immunol* 173 (1), 559-65.

Asada, Y., Kisanuki, A., Hatakeyama, K., Takahama, S., Koyama, T., Kurozumi, S. and Sumiyoshi, A. (1994) Inhibitory effects of prostacyclin analogue, TFC-132, on aortic neointimal thickening in vivo and smooth muscle cell proliferation in vitro. *Prostaglandins Leukot Essent Fatty Acids* 51 (4), 245-8.

Atkinson, C., Stewart, S., Upton, P. D., Machado, R., Thomson, J. R., Trembath, R. C. and Morrell, N. W. (2002) Primary pulmonary hypertension is associated with reduced pulmonary vascular expression of type II bone morphogenetic protein receptor. *Circulation* 105 (14), 1672-8.

Atsumi, T., Ishihara, K., Kamimura, D., Ikushima, H., Ohtani, T., Hirota, S., Kobayashi, H., Park, S. J., Saeki, Y., Kitamura, Y. and Hirano, T. (2002) A point mutation of Tyr-759 in interleukin 6 family cytokine receptor subunit gp130 causes autoimmune arthritis. *J Exp Med* 196 (7), 979-90.

Atsuta, H., Uchiyama, T., Kanai, H., Iso, T., Tanaka, T., Suga, T., Maeno, T., Arai, M., Nagai, R. and Kurabayashi, M. (2009) Effects of a stable prostacyclin analogue beraprost sodium on VEGF and PAI-1 gene expression in vascular smooth muscle cells. *Int J Cardiol* 132 (3), 411-8.

Austin, E. D., Loyd, J. E. and Phillips, J. A., III (1993) Heritable Pulmonary Arterial Hypertension. In Pagon, R. A., Adam, M. P., Ardinger, H. H., Wallace, S. E., Amemiya, A., Bean, L. J. H., Bird, T. D., Fong, C. T., Mefford, H. C., Smith, R. J. H., and Stephens, K. (editors) *GeneReviews(R).* Seattle (WA):

Austin, E. D., Ma, L., LeDuc, C., Berman Rosenzweig, E., Borczuk, A., Phillips, J. A., 3rd, Palomero, T., Sumazin, P., Kim, H. R., Talati, M. H., West, J., Loyd, J. E. and Chung, W. K. (2012) Whole exome sequencing to identify a novel gene (caveolin-1) associated with human pulmonary arterial hypertension. *Circ Cardiovasc Genet* 5 (3), 336-43.

Awad, K. S., Elinoff, J. M., Wang, S., Gairhe, S., Ferreyra, G. A., Cai, R., Sun, J., Solomon, M. A. and Danner, R. L. (2016) Raf/ERK drives the proliferative and invasive phenotype of BMPR2-silenced pulmonary artery endothelial cells. *Am J Physiol Lung Cell Mol Physiol* 310 (2), L187-201.

Aznan, A. N., Abdul Karim, N., Wan Ngah, W. Z. and Jubri, Z. (2018) Critical factors for lentivirus-mediated PRDX4 gene transfer in the HepG2 cell line. *Oncol Lett* 16 (1), 73-82.

Babon, J. J., Kershaw, N. J., Murphy, J. M., Varghese, L. N., Laktyushin, A., Young, S. N., Lucet, I. S., Norton, R. S. and Nicola, N. A. (2012) Suppression of cytokine signaling by SOCS3: characterization of the mode of inhibition and the basis of its specificity. *Immunity* 36 (2), 239-50.

Babon, J. J., McManus, E. J., Yao, S., DeSouza, D. P., Mielke, L. A., Sprigg, N. S., Willson, T. A., Hilton, D. J., Nicola, N. A., Baca, M., Nicholson, S. E. and Norton, R. S. (2006) The structure of SOCS3 reveals the basis of the extended SH2 domain function and identifies an unstructured insertion that regulates stability. *Mol Cell* 22 (2), 205-16.

Babon, J. J., Sabo, J. K., Soetopo, A., Yao, S., Bailey, M. F., Zhang, J. G., Nicola, N. A. and Norton, R. S. (2008) The SOCS box domain of SOCS3: structure and interaction with the elonginBC-cullin5 ubiquitin ligase. *J Mol Biol* 381 (4), 928-40.

Babon, J. J., Varghese, L. N. and Nicola, N. A. (2014) Inhibition of IL-6 family cytokines by SOCS3. *Semin Immunol* 26 (1), 13-9.

Badesch, D. B., Champion, H. C., Sanchez, M. A., Hoeper, M. M., Loyd, J. E., Manes, A., McGoon, M., Naeije, R., Olschewski, H., Oudiz, R. J. and Torbicki, A. (2009) Diagnosis and assessment of pulmonary arterial hypertension. *J Am Coll Cardiol* 54 (1 Suppl), S55-66.

Badlam, J. B. and Bull, T. M. (2017) Steps forward in the treatment of pulmonary arterial hypertension: latest developments and clinical opportunities. *Ther Adv Chronic Dis* 8 (2-3), 47-64.

Bai, Y., Li, Z. X., Wang, H. L., Lian, G. C. and Wang, Y. (2017) The protective effects of PCPA against monocrotaline-induced pulmonary arterial hypertension are mediated through the downregulation of NFAT-1 and NF-kappaB. *Int J Mol Med* 40 (1), 155-163.

Balasubramaniam, V., Le Cras, T. D., Ivy, D. D., Grover, T. R., Kinsella, J. P. and Abman, S. H. (2003) Role of platelet-derived growth factor in vascular remodeling during pulmonary hypertension in the ovine fetus. *Am J Physiol Lung Cell Mol Physiol* 284 (5), L826-33.

Baran, P., Nitz, R., Grotzinger, J., Scheller, J. and Garbers, C. (2013) Minimal interleukin 6 (IL-6) receptor stalk composition for IL-6 receptor shedding and IL-6 classic signaling. *J Biol Chem* 288 (21), 14756-68.

Barclay, J. L., Anderson, S. T., Waters, M. J. and Curlewis, J. D. (2007) Characterization of the SOCS3 promoter response to prostaglandin E2 in T47D cells. *Mol Endocrinol* 21 (10), 2516-28.

Barst, R. J., McGoon, M., McLaughlin, V., Tapson, V., Rich, S., Rubin, L., Wasserman, K., Oudiz, R., Shapiro, S., Robbins, I. M., Channick, R., Badesch, D., Rayburn, B. K., Flinchbaugh, R., Sigman, J., Arneson, C., Jeffs, R. and Beraprost Study, G.

(2003) Beraprost therapy for pulmonary arterial hypertension. *J Am Coll Cardiol* 41 (12), 2119-25.

Bauer, P. M., Yu, J., Chen, Y., Hickey, R., Bernatchez, P. N., Looft-Wilson, R., Huang, Y., Giordano, F., Stan, R. V. and Sessa, W. C. (2005) Endothelial-specific expression of caveolin-1 impairs microvascular permeability and angiogenesis. *Proc Natl Acad Sci U S A* 102 (1), 204-9.

Bazan, J. F. (1990) Structural design and molecular evolution of a cytokine receptor superfamily. *Proc Natl Acad Sci U S A* 87 (18), 6934-8.

Ben Ami, E. and Demetri, G. D. (2016) A safety evaluation of imatinib mesylate in the treatment of gastrointestinal stromal tumor. *Expert Opin Drug Saf* 15 (4), 571-8.

Benza, R. L., Miller, D. P., Foreman, A. J., Frost, A. E., Badesch, D. B., Benton, W. W. and McGoon, M. D. (2015) Prognostic implications of serial risk score assessments in patients with pulmonary arterial hypertension: a Registry to Evaluate Early and Long-Term Pulmonary Arterial Hypertension Disease Management (REVEAL) analysis. *J Heart Lung Transplant* 34 (3), 356-61.

Benza, R. L., Miller, D. P., Gomberg-Maitland, M., Frantz, R. P., Foreman, A. J., Coffey, C. S., Frost, A., Barst, R. J., Badesch, D. B., Elliott, C. G., Liou, T. G. and McGoon, M. D. (2010) Predicting survival in pulmonary arterial hypertension: insights from the Registry to Evaluate Early and Long-Term Pulmonary Arterial Hypertension Disease Management (REVEAL). *Circulation* 122 (2), 164-72.

Berridge, M. J. (1993) Inositol trisphosphate and calcium signalling. *Nature* 361 (6410), 315-25.

Bertero, T., Cottrill, K. A., Lu, Y., Haeger, C. M., Dieffenbach, P., Annis, S., Hale, A., Bhat, B., Kaimal, V., Zhang, Y. Y., Graham, B. B., Kumar, R., Saggar, R., Saggar, R., Wallace, W. D., Ross, D. J., Black, S. M., Fratz, S., Fineman, J. R., Vargas, S. O., Haley, K. J., Waxman, A. B., Chau, B. N., Fredenburgh, L. E. and Chan, S. Y. (2015) Matrix Remodeling Promotes Pulmonary Hypertension through Feedback Mechanoactivation of the YAP/TAZ-miR-130/301 Circuit. *Cell Rep* 13 (5), 1016-32.

Biscetti, F., Gaetani, E., Flex, A., Straface, G., Pecorini, G., Angelini, F., Stigliano, E., Aprahamian, T., Smith, R. C., Castellot, J. J. and Pola, R. (2009) Peroxisome proliferator-activated receptor alpha is crucial for iloprost-induced in vivo angiogenesis and vascular endothelial growth factor upregulation. *J Vasc Res* 46 (2), 103-8.

Bishop-Bailey, D. and Hla, T. (1999) Endothelial cell apoptosis induced by the peroxisome proliferator-activated receptor (PPAR) ligand 15-deoxy-Delta12, 14-prostaglandin J2. *J Biol Chem* 274 (24), 17042-8.

Bonovas, S., Lytras, T., Nikolopoulos, G., Peyrin-Biroulet, L. and Danese, S. (2018) Systematic review with network meta-analysis: comparative assessment of tofacitinib and biological therapies for moderate-to-severe ulcerative colitis. *Aliment Pharmacol Ther* 47 (4), 454-465.

Borland, G., Bird, R. J., Palmer, T. M. and Yarwood, S. J. (2009) Activation of protein kinase Calpha by EPAC1 is required for the ERK- and CCAAT/enhancer-binding protein beta-dependent induction of the SOCS-3 gene by cyclic AMP in COS1 cells. *J Biol Chem* 284 (26), 17391-403.

Boskey, A. L., Stiner, D., Doty, S. B. and Binderman, I. (1996) The Effect of Misoprostol and Prostanoids On cAMP Production and Calcification in a Differentiating Chick Limb-Bud Culture System. *Am J Ther* 3 (3), 179-188.

Bossone, E., D'Andrea, A., D'Alto, M., Citro, R., Argiento, P., Ferrara, F., Cittadini, A., Rubenfire, M. and Naeije, R. (2013) Echocardiography in pulmonary arterial hypertension: from diagnosis to prognosis. *J Am Soc Echocardiogr* 26 (1), 1-14.

Bottini, P. B., Carr, A. A., Prisant, L. M., Flickinger, F. W., Allison, J. D. and Gottdiener, J. S. (1995) Magnetic resonance imaging compared to echocardiography to assess left ventricular mass in the hypertensive patient. *Am J Hypertens* 8 (3), 221-8.

Bourgeois, A., Lambert, C., Habbout, K., Ranchoux, B., Paquet-Marceau, S., Trinh, I., Breuils-Bonnet, S., Paradis, R., Nadeau, V., Paulin, R., Provencher, S., Bonnet, S. and Boucherat, O. (2018) FOXM1 promotes pulmonary artery smooth muscle cell expansion in pulmonary arterial hypertension. *J Mol Med (Berl)* 96 (2), 223-235.

Braunstein, J., Brutsaert, S., Olson, R. and Schindler, C. (2003) STATs dimerize in the absence of phosphorylation. *J Biol Chem* 278 (36), 34133-40.

Bravo, J. and Heath, J. K. (2000) Receptor recognition by gp130 cytokines. *EMBO J* 19 (11), 2399-411.

Brender, C., Lovato, P., Sommer, V. H., Woetmann, A., Mathiesen, A. M., Geisler, C., Wasik, M. and Odum, N. (2005) Constitutive SOCS-3 expression protects T-cell lymphoma against growth inhibition by IFNalpha. *Leukemia* 19 (2), 209-13.

Bressollette, E., Dupuis, J., Bonan, R., Doucet, S., Cernacek, P. and Tardif, J. C. (2001) Intravascular ultrasound assessment of pulmonary vascular disease in patients with pulmonary hypertension. *Chest* 120 (3), 809-15.

Brock, M., Trenkmann, M., Gay, R. E., Michel, B. A., Gay, S., Fischler, M., Ulrich, S., Speich, R. and Huber, L. C. (2009) Interleukin-6 modulates the expression of the bone morphogenic protein receptor type II through a novel STAT3-microRNA cluster 17/92 pathway. *Circ Res* 104 (10), 1184-91.

Brooks, A. J., Dai, W., O'Mara, M. L., Abankwa, D., Chhabra, Y., Pelekanos, R. A., Gardon, O., Tunny, K. A., Blucher, K. M., Morton, C. J., Parker, M. W., Sierecki, E., Gambin, Y., Gomez, G. A., Alexandrov, K., Wilson, I. A., Doxastakis, M., Mark, A. E. and Waters, M. J. (2014) Mechanism of activation of protein kinase JAK2 by the growth hormone receptor. *Science* 344 (6185), 1249783.

Burke, D. L., Frid, M. G., Kunrath, C. L., Karoor, V., Anwar, A., Wagner, B. D., Strassheim, D. and Stenmark, K. R. (2009) Sustained hypoxia promotes the development of a pulmonary artery-specific chronic inflammatory microenvironment. *Am J Physiol Lung Cell Mol Physiol* 297 (2), L238-50.

Burmeister, B. T., Wang, L., Gold, M. G., Skidgel, R. A., O'Bryan, J. P. and Carnegie, G. K. (2015) Protein Kinase A (PKA) Phosphorylation of Shp2 Protein Inhibits Its Phosphatase Activity and Modulates Ligand Specificity. *J Biol Chem* 290 (19), 12058-67.

Burton, V. J., Ciuclan, L. I., Holmes, A. M., Rodman, D. M., Walker, C. and Budd, D. C. (2011) Bone morphogenetic protein receptor II regulates pulmonary artery endothelial cell barrier function. *Blood* 117 (1), 333-41.

Busca, R., Abbe, P., Mantoux, F., Aberdam, E., Peyssonnaux, C., Eychene, A., Ortonne, J. P. and Ballotti, R. (2000) Ras mediates the cAMP-dependent activation of extracellular signal-regulated kinases (ERKs) in melanocytes. *EMBO J* 19 (12), 2900-10.

Cai, Z., Li, J., Zhuang, Q., Zhang, X., Yuan, A., Shen, L., Kang, K., Qu, B., Tang, Y., Pu, J., Gou, D. and Shen, J. (2018) MiR-125a-5p ameliorates monocrotaline-induced pulmonary arterial hypertension by targeting the TGF-beta1 and IL-6/STAT3 signaling pathways. *Exp Mol Med* 50 (4), 45.

Carpenter, R. L. and Lo, H. W. (2014) STAT3 Target Genes Relevant to Human Cancers. *Cancers (Basel)* 6 (2), 897-925.

Carvajal, J. A., Germain, A. M., Huidobro-Toro, J. P. and Weiner, C. P. (2000) Molecular mechanism of cGMP-mediated smooth muscle relaxation. *J Cell Physiol* 184 (3), 409-20.

Casserly, B. and Klinger, J. R. (2009) Brain natriuretic peptide in pulmonary arterial hypertension: biomarker and potential therapeutic agent. *Drug Des Devel Ther* 3, 269-87.

Cerny, O., Kamanova, J., Masin, J., Bibova, I., Skopova, K. and Sebo, P. (2015) Bordetella pertussis Adenylate Cyclase Toxin Blocks Induction of Bactericidal Nitric Oxide in Macrophages through cAMP-Dependent Activation of the SHP-1 Phosphatase. *J Immunol* 194 (10), 4901-13.

Chakinala, M. M., Coyne, D. W., Benza, R. L., Frost, A. E., McGoon, M. D., Hartline, B. K., Frantz, R. P., Selej, M., Zhao, C., Mink, D. R. and Farber, H. W. (2018) Impact of declining renal function on outcomes in pulmonary arterial hypertension: A REVEAL registry analysis. *J Heart Lung Transplant* 37 (6), 696-705.

Chan, K., Ioannidis, S., Coghlan, J. G., Hall, M. and Schreiber, B. E. (2018) Pulmonary Arterial Hypertension With Abnormal V/Q Single-Photon Emission Computed Tomography. *JACC Cardiovasc Imaging* 11 (10), 1487-1493.

Chaouat, A., Coulet, F., Favre, C., Simonneau, G., Weitzenblum, E., Soubrier, F. and Humbert, M. (2004) Endoglin germline mutation in a patient with hereditary haemorrhagic telangiectasia and dexfenfluramine associated pulmonary arterial hypertension. *Thorax* 59 (5), 446-8.

Chen, D., Tang, J., Wan, Q., Zhang, J., Wang, K., Shen, Y. and Yu, Y. (2017) E-Prostanoid 3 Receptor Mediates Sprouting Angiogenesis Through Suppression of the Protein Kinase A/β-Catenin/Notch Pathway. *Arteriosclerosis, Thrombosis, and Vascular Biology* 37 (5), 856-866.

Chen, L., Daum, G., Chitaley, K., Coats, S. A., Bowen-Pope, D. F., Eigenthaler, M., Thumati, N. R., Walter, U. and Clowes, A. W. (2004) Vasodilator-stimulated phosphoprotein regulates proliferation and growth inhibition by nitric oxide in vascular smooth muscle cells. *Arterioscler Thromb Vasc Biol* 24 (8), 1403-8.

Chen, S. H., Murphy, D. A., Lassoued, W., Thurston, G., Feldman, M. D. and Lee, W. M. (2008) Activated STAT3 is a mediator and biomarker of VEGF endothelial activation. *Cancer Biol Ther* 7 (12), 1994-2003.

Chen, Y., Bhushan, A. and Vale, W. (1997) Smad8 mediates the signaling of the ALK-2 [corrected] receptor serine kinase. *Proc Natl Acad Sci U S A* 94 (24), 12938-43.

Cheng, J. P., Mendoza-Topaz, C., Howard, G., Chadwick, J., Shvets, E., Cowburn, A. S., Dunmore, B. J., Crosby, A., Morrell, N. W. and Nichols, B. J. (2015) Caveolae

protect endothelial cells from membrane rupture during increased cardiac output. *J Cell Biol* 211 (1), 53-61.

Cheng, J. P. X. and Nichols, B. J. (2016) Caveolae: One Function or Many? *Trends Cell Biol* 26 (3), 177-189.

Cheng, J. W. (2008) Ambrisentan for the management of pulmonary arterial hypertension. *Clin Ther* 30 (5), 825-33.

Cheon, H., Rho, Y. H., Choi, S. J., Lee, Y. H., Song, G. G., Sohn, J., Won, N. H. and Ji, J. D. (2006) Prostaglandin E2 augments IL-10 signaling and function. *J Immunol* 177 (2), 1092-100.

Chester, A. H. and Yacoub, M. H. (2014) The role of endothelin-1 in pulmonary arterial hypertension. *Glob Cardiol Sci Pract* 2014 (2), 62-78.

Chida, A., Shintani, M., Matsushita, Y., Sato, H., Eitoku, T., Nakayama, T., Furutani, Y., Hayama, E., Kawamura, Y., Inai, K., Ohtsuki, S., Saji, T., Nonoyama, S. and Nakanishi, T. (2014) Mutations of NOTCH3 in childhood pulmonary arterial hypertension. *Mol Genet Genomic Med* 2 (3), 229-39.

Chowdhury, H. M., Sharmin, N., Yuzbasioglu Baran, M., Long, L., Morrell, N. W., Trembath, R. C. and Nasim, M. T. (2019) BMPRII deficiency impairs apoptosis via the BMPRII-ALK1-BclX-mediated pathway in pulmonary arterial hypertension. *Hum Mol Genet* 28 (13), 2161-2173.

Christman, B. W., McPherson, C. D., Newman, J. H., King, G. A., Bernard, G. R., Groves, B. M. and Loyd, J. E. (1992) An imbalance between the excretion of thromboxane and prostacyclin metabolites in pulmonary hypertension. *N Engl J Med* 327 (2), 70-5.

Clackson, T. and Wells, J. A. (1995) A hot spot of binding energy in a hormone-receptor interface. *Science* 267 (5196), 383-6.

Clapp, L. H., Finney, P., Turcato, S., Tran, S., Rubin, L. J. and Tinker, A. (2002) Differential effects of stable prostacyclin analogs on smooth muscle proliferation and cyclic AMP generation in human pulmonary artery. *Am J Respir Cell Mol Biol* 26 (2), 194-201.

Clapp, L. H. and Gurung, R. (2015) The mechanistic basis of prostacyclin and its stable analogues in pulmonary arterial hypertension: Role of membrane versus nuclear receptors. *Prostaglandins Other Lipid Mediat* 120, 56-71.

Cogan, J. D., Pauciulo, M. W., Batchman, A. P., Prince, M. A., Robbins, I. M., Hedges, L. K., Stanton, K. C., Wheeler, L. A., Phillips, J. A., 3rd, Loyd, J. E. and Nichols, W. C. (2006) High frequency of BMPR2 exonic deletions/duplications in familial pulmonary arterial hypertension. *Am J Respir Crit Care Med* 174 (5), 590-8.

Cohen-Kaminsky, S., Hautefort, A., Price, L., Humbert, M. and Perros, F. (2014) Inflammation in pulmonary hypertension: what we know and what we could logically and safely target first. *Drug Discov Today* 19 (8), 1251-6.

Cohen, T., Nahari, D., Cerem, L. W., Neufeld, G. and Levi, B. Z. (1996) Interleukin 6 induces the expression of vascular endothelial growth factor. *J Biol Chem* 271 (2), 736-41.

Cook, S. J. and McCormick, F. (1993) Inhibition by cAMP of Ras-dependent activation of Raf. *Science* 262 (5136), 1069-72.

Cool, C. D., Stewart, J. S., Werahera, P., Miller, G. J., Williams, R. L., Voelkel, N. F. and Tuder, R. M. (1999) Three-dimensional reconstruction of pulmonary arteries

in plexiform pulmonary hypertension using cell-specific markers. Evidence for a dynamic and heterogeneous process of pulmonary endothelial cell growth. *Am J Pathol* 155 (2), 411-9.

Cooper, M. E., Vranes, D., Youssef, S., Stacker, S. A., Cox, A. J., Rizkalla, B., Casley, D. J., Bach, L. A., Kelly, D. J. and Gilbert, R. E. (1999) Increased renal expression of vascular endothelial growth factor (VEGF) and its receptor VEGFR-2 in experimental diabetes. *Diabetes* 48 (11), 2229-39.

Courboulin, A., Tremblay, V. L., Barrier, M., Meloche, J., Jacob, M. H., Chapolard, M., Bisserier, M., Paulin, R., Lambert, C., Provencher, S. and Bonnet, S. (2011) Kruppel-like factor 5 contributes to pulmonary artery smooth muscle proliferation and resistance to apoptosis in human pulmonary arterial hypertension. *Respir Res* 12, 128.

Croker, B. A., Krebs, D. L., Zhang, J. G., Wormald, S., Willson, T. A., Stanley, E. G., Robb, L., Greenhalgh, C. J., Forster, I., Clausen, B. E., Nicola, N. A., Metcalf, D., Hilton, D. J., Roberts, A. W. and Alexander, W. S. (2003) SOCS3 negatively regulates IL-6 signaling in vivo. *Nat Immunol* 4 (6), 540-5.

Crowe, T., Jayasekera, G. and Peacock, A. J. (2018) Non-invasive imaging of global and regional cardiac function in pulmonary hypertension. *Pulm Circ* 8 (1), 2045893217742000.

Cruz, J. A., Bauer, E. M., Rodriguez, A. I., Gangopadhyay, A., Zeineh, N. S., Wang, Y., Shiva, S., Champion, H. C. and Bauer, P. M. (2012) Chronic hypoxia induces right heart failure in caveolin-1-/- mice. *Am J Physiol Heart Circ Physiol* 302 (12), H2518-27.

D'Alonzo, G. E., Barst, R. J., Ayres, S. M., Bergofsky, E. H., Brundage, B. H., Detre, K. M., Fishman, A. P., Goldring, R. M., Groves, B. M., Kernis, J. T. and et al. (1991) Survival in patients with primary pulmonary hypertension. Results from a national prospective registry. *Ann Intern Med* 115 (5), 343-9.

Dabral, S., Tian, X., Kojonazarov, B., Savai, R., Ghofrani, H. A., Weissmann, N., Florio, M., Sun, J., Jonigk, D., Maegel, L., Grimminger, F., Seeger, W., Savai Pullamsetti, S. and Schermuly, R. T. (2016) Notch1 signalling regulates endothelial proliferation and apoptosis in pulmonary arterial hypertension. *Eur Respir J* 48 (4), 1137-1149.

Dahal, B. K., Cornitescu, T., Tretyn, A., Pullamsetti, S. S., Kosanovic, D., Dumitrascu, R., Ghofrani, H. A., Weissmann, N., Voswinckel, R., Banat, G. A., Seeger, W., Grimminger, F. and Schermuly, R. T. (2010) Role of epidermal growth factor inhibition in experimental pulmonary hypertension. *Am J Respir Crit Care Med* 181 (2), 158-67.

Dao, K. K., Teigen, K., Kopperud, R., Hodneland, E., Schwede, F., Christensen, A. E., Martinez, A. and Doskeland, S. O. (2006) Epac1 and cAMP-dependent protein kinase holoenzyme have similar cAMP affinity, but their cAMP domains have distinct structural features and cyclic nucleotide recognition. *J Biol Chem* 281 (30), 21500-11.

David, L., Mallet, C., Mazerbourg, S., Feige, J. J. and Bailly, S. (2007) Identification of BMP9 and BMP10 as functional activators of the orphan activin receptor-like kinase 1 (ALK1) in endothelial cells. *Blood* 109 (5), 1953-61.

de Rooij, J., Zwartkruis, F. J., Verheijen, M. H., Cool, R. H., Nijman, S. M., Wittinghofer, A. and Bos, J. L. (1998) Epac is a Rap1 guanine-nucleotide-exchange factor directly activated by cyclic AMP. *Nature* 396 (6710), 474-7.

DeCicco-Skinner, K. L., Henry, G. H., Cataisson, C., Tabib, T., Gwilliam, J. C., Watson, N. J., Bullwinkle, E. M., Falkenburg, L., O'Neill, R. C., Morin, A. and Wiest, J. S. (2014) Endothelial cell tube formation assay for the in vitro study of angiogenesis. *J Vis Exp* (91), e51312.

Del Pozo, R., Hernandez Gonzalez, I. and Escribano-Subias, P. (2017) The prostacyclin pathway in pulmonary arterial hypertension: a clinical review. *Expert Rev Respir Med* 11 (6), 491-503.

Demir, R. and Kucukoglu, M. S. (2015) Six-minute walk test in pulmonary arterial hypertension. *Anatol J Cardiol* 15 (3), 249-54.

Deng, Z., Morse, J. H., Slager, S. L., Cuervo, N., Moore, K. J., Venetos, G., Kalachikov, S., Cayanis, E., Fischer, S. G., Barst, R. J., Hodge, S. E. and Knowles, J. A. (2000) Familial primary pulmonary hypertension (gene PPH1) is caused by mutations in the bone morphogenetic protein receptor-II gene. *Am J Hum Genet* 67 (3), 737-44.

Dewachter, L., Adnot, S., Fadel, E., Humbert, M., Maitre, B., Barlier-Mur, A. M., Simonneau, G., Hamon, M., Naeije, R. and Eddahibi, S. (2006) Angiopoietin/Tie2 pathway influences smooth muscle hyperplasia in idiopathic pulmonary hypertension. *Am J Respir Crit Care Med* 174 (9), 1025-33.

Dewulf, M., Koster, D. V., Sinha, B., Viaris de Lesegno, C., Chambon, V., Bigot, A., Bensalah, M., Negroni, E., Tardif, N., Podkalicka, J., Johannes, L., Nassoy, P., Butler-Browne, G., Lamaze, C. and Blouin, C. M. (2019) Dystrophy-associated caveolin-3 mutations reveal that caveolae couple IL6/STAT3 signaling with mechanosensing in human muscle cells. *Nat Commun* 10 (1), 1974.

Dhillon, A. S., Pollock, C., Steen, H., Shaw, P. E., Mischak, H. and Kolch, W. (2002) Cyclic AMP-dependent kinase regulates Raf-1 kinase mainly by phosphorylation of serine 259. *Mol Cell Biol* 22 (10), 3237-46.

Diamant, M., Rieneck, K., Mechti, N., Zhang, X. G., Svenson, M., Bendtzen, K. and Klein, B. (1997) Cloning and expression of an alternatively spliced mRNA encoding a soluble form of the human interleukin-6 signal transducer gp130. *FEBS Lett* 412 (2), 379-84.

Dijkgraaf, E. M., Santegoets, S. J., Reyners, A. K., Goedemans, R., Wouters, M. C., Kenter, G. G., van Erkel, A. R., van Poelgeest, M. I., Nijman, H. W., van der Hoeven, J. J., Welters, M. J., van der Burg, S. H. and Kroep, J. R. (2015) A phase I trial combining carboplatin/doxorubicin with tocilizumab, an anti-IL-6R monoclonal antibody, and interferon-alpha2b in patients with recurrent epithelial ovarian cancer. *Ann Oncol* 26 (10), 2141-9.

Dorfmuller, P., Zarka, V., Durand-Gasselin, I., Monti, G., Balabanian, K., Garcia, G., Capron, F., Coulomb-Lhermine, A., Marfaing-Koka, A., Simonneau, G., Emilie, D. and Humbert, M. (2002) Chemokine RANTES in severe pulmonary arterial hypertension. *Am J Respir Crit Care Med* 165 (4), 534-9.

Duggan, S. T., Keam, S. J. and Burness, C. B. (2017) Selexipag: A Review in Pulmonary Arterial Hypertension. *Am J Cardiovasc Drugs* 17 (1), 73-80.

Dumaz, N. and Marais, R. (2005) Integrating signals between cAMP and the RAS/RAF/MEK/ERK signalling pathways. Based on the anniversary prize of the Gesellschaft fur Biochemie und Molekularbiologie Lecture delivered on 5 July 2003 at the Special FEBS Meeting in Brussels. *FEBS J* 272 (14), 3491-504.

Durham, G. A., Williams, J. J. L., Nasim, M. T. and Palmer, T. M. (2019) Targeting SOCS Proteins to Control JAK-STAT Signalling in Disease. *Trends Pharmacol Sci* 40 (5), 298-308.

Dusting, G. J., Chapple, D. J., Hughes, R., Moncada, S. and Vane, J. R. (1978) Prostacyclin (PGI2) induces coronary vasodilatation in anaesthetised dogs. *Cardiovasc Res* 12 (12), 720-30.

Eddahibi, S., Guignabert, C., Barlier-Mur, A. M., Dewachter, L., Fadel, E., Dartevelle, P., Humbert, M., Simonneau, G., Hanoun, N., Saurini, F., Hamon, M. and Adnot, S. (2006) Cross talk between endothelial and smooth muscle cells in pulmonary hypertension: critical role for serotonin-induced smooth muscle hyperplasia. *Circulation* 113 (15), 1857-64.

Emanuelli, B., Peraldi, P., Filloux, C., Chavey, C., Freidinger, K., Hilton, D. J., Hotamisligil, G. S. and Van Obberghen, E. (2001) SOCS-3 inhibits insulin signaling and is up-regulated in response to tumor necrosis factor-alpha in the adipose tissue of obese mice. *J Biol Chem* 276 (51), 47944-9.

Enderby, C. Y. and Burger, C. (2015) Medical treatment update on pulmonary arterial hypertension. *Ther Adv Chronic Dis* 6 (5), 264-72.

Endo, T. A., Masuhara, M., Yokouchi, M., Suzuki, R., Sakamoto, H., Mitsui, K., Matsumoto, A., Tanimura, S., Ohtsubo, M., Misawa, H., Miyazaki, T., Leonor, N., Taniguchi, T., Fujita, T., Kanakura, Y., Komiya, S. and Yoshimura, A. (1997) A new protein containing an SH2 domain that inhibits JAK kinases. *Nature* 387 (6636), 921-4.

Fagan, K. A., Fouty, B. W., Tyler, R. C., Morris, K. G., Jr., Hepler, L. K., Sato, K., LeCras, T. D., Abman, S. H., Weinberger, H. D., Huang, P. L., McMurtry, I. F. and Rodman, D. M. (1999) The pulmonary circulation of homozygous or heterozygous eNOS-null mice is hyperresponsive to mild hypoxia. *J Clin Invest* 103 (2), 291-9.

Falcetti, E., Hall, S. M., Phillips, P. G., Patel, J., Morrell, N. W., Haworth, S. G. and Clapp, L. H. (2010) Smooth muscle proliferation and role of the prostacyclin (IP) receptor in idiopathic pulmonary arterial hypertension. *Am J Respir Crit Care Med* 182 (9), 1161-70.

Fang, M., Huang, Y., Zhang, Y., Ning, Z., Zhu, L. and Li, X. (2017) Interleukin-6 -572C/G polymorphism is associated with serum interleukin-6 levels and risk of idiopathic pulmonary arterial hypertension. *J Am Soc Hypertens* 11 (3), 171-177.

Farber, H. W., Miller, D. P., Poms, A. D., Badesch, D. B., Frost, A. E., Muros-Le Rouzic, E., Romero, A. J., Benton, W. W., Elliott, C. G., McGoon, M. D. and Benza, R. L. (2015) Five-Year outcomes of patients enrolled in the REVEAL Registry. *Chest* 148 (4), 1043-54.

Fass, D. M., Butler, J. E. and Goodman, R. H. (2003) Deacetylase activity is required for cAMP activation of a subset of CREB target genes. *J Biol Chem* 278 (44), 43014-9.

Feron, O., Belhassen, L., Kobzik, L., Smith, T. W., Kelly, R. A. and Michel, T. (1996) Endothelial nitric oxide synthase targeting to caveolae. Specific interactions with caveolin isoforms in cardiac myocytes and endothelial cells. *J Biol Chem* 271 (37), 22810-4.

Ferreri, D. M., Minnear, F. L., Yin, T., Kowalczyk, A. P. and Vincent, P. A. (2008) N-cadherin levels in endothelial cells are regulated by monolayer maturity and p120 availability. *Cell Commun Adhes* 15 (4), 333-49.

Fisher, M. R., Forfia, P. R., Chamera, E., Housten-Harris, T., Champion, H. C., Girgis, R. E., Corretti, M. C. and Hassoun, P. M. (2009) Accuracy of Doppler echocardiography in the hemodynamic assessment of pulmonary hypertension. *Am J Respir Crit Care Med* 179 (7), 615-21.

Flemming, S., Burkard, N., Renschler, M., Vielmuth, F., Meir, M., Schick, M. A., Wunder, C., Germer, C. T., Spindler, V., Waschke, J. and Schlegel, N. (2015) Soluble VE-cadherin is involved in endothelial barrier breakdown in systemic inflammation and sepsis. *Cardiovasc Res* 107 (1), 32-44.

Fletcher, T. C., DiGiandomenico, A. and Hawiger, J. (2010) Extended anti-inflammatory action of a degradation-resistant mutant of cell-penetrating suppressor of cytokine signaling 3. *J Biol Chem* 285 (24), 18727-36.

Fong, T. A., Shawver, L. K., Sun, L., Tang, C., App, H., Powell, T. J., Kim, Y. H., Schreck, R., Wang, X., Risau, W., Ullrich, A., Hirth, K. P. and McMahon, G. (1999) SU5416 is a potent and selective inhibitor of the vascular endothelial growth factor receptor (Flk-1/KDR) that inhibits tyrosine kinase catalysis, tumor vascularization, and growth of multiple tumor types. *Cancer Res* 59 (1), 99-106.

Fox, E. R., Musani, S. K., Singh, P., Bidulescu, A., Nagarajarao, H. S., Samdarshi, T. E., Steffes, M. W., Wang, T. J., Taylor, H. A. and Vasan, R. S. (2013) Association of plasma B-type natriuretic peptide concentrations with longitudinal blood pressure tracking in African Americans: findings from the Jackson Heart Study. *Hypertension* 61 (1), 48-54.

Francis, M., Xu, N., Zhou, C. and Stevens, T. (2016) Transient Receptor Potential Channel 4 Encodes a Vascular Permeability Defect and High-Frequency Ca(2+) Transients in Severe Pulmonary Arterial Hypertension. *Am J Pathol* 186 (6), 1701-9.

Frost, A., Badesch, D., Gibbs, J. S. R., Gopalan, D., Khanna, D., Manes, A., Oudiz, R., Satoh, T., Torres, F. and Torbicki, A. (2019) Diagnosis of pulmonary hypertension. *Eur Respir J* 53 (1).

Fuentes, M. E., Durham, S. K., Swerdel, M. R., Lewin, A. C., Barton, D. S., Megill, J. R., Bravo, R. and Lira, S. A. (1995) Controlled recruitment of monocytes and macrophages to specific organs through transgenic expression of monocyte chemoattractant protein-1. *J Immunol* 155 (12), 5769-76.

Fukuhara, S., Sakurai, A., Sano, H., Yamagishi, A., Somekawa, S., Takakura, N., Saito, Y., Kangawa, K. and Mochizuki, N. (2005) Cyclic AMP potentiates vascular endothelial cadherin-mediated cell-cell contact to enhance endothelial barrier function through an Epac-Rap1 signaling pathway. *Mol Cell Biol* 25 (1), 136-46.

Gaine, S. and Simonneau, G. (2013) The need to move from 6-minute walk distance to outcome trials in pulmonary arterial hypertension. *Eur Respir Rev* 22 (130), 487-94.

Galie, N., Brundage, B. H., Ghofrani, H. A., Oudiz, R. J., Simonneau, G., Safdar, Z., Shapiro, S., White, R. J., Chan, M., Beardsworth, A., Frumkin, L., Barst, R. J., Pulmonary Arterial, H. and Response to Tadalafil Study, G. (2009a) Tadalafil therapy for pulmonary arterial hypertension. *Circulation* 119 (22), 2894-903.

Galie, N., Corris, P. A., Frost, A., Girgis, R. E., Granton, J., Jing, Z. C., Klepetko, W., McGoon, M. D., McLaughlin, V. V., Preston, I. R., Rubin, L. J., Sandoval, J., Seeger, W. and Keogh, A. (2013) Updated treatment algorithm of pulmonary arterial hypertension. *J Am Coll Cardiol* 62 (25 Suppl), D60-72.

Galie, N., Ghofrani, H. A., Torbicki, A., Barst, R. J., Rubin, L. J., Badesch, D., Fleming, T., Parpia, T., Burgess, G., Branzi, A., Grimminger, F., Kurzyna, M., Simonneau, G. and Sildenafil Use in Pulmonary Arterial Hypertension Study, G. (2005) Sildenafil citrate therapy for pulmonary arterial hypertension. *N Engl J Med* 353 (20), 2148-57.

Galie, N., Hoeper, M. M., Humbert, M., Torbicki, A., Vachiery, J. L., Barbera, J. A., Beghetti, M., Corris, P., Gaine, S., Gibbs, J. S., Gomez-Sanchez, M. A., Jondeau, G., Klepetko, W., Opitz, C., Peacock, A., Rubin, L., Zellweger, M., Simonneau, G. and Guidelines, E. S. C. C. f. P. (2009b) Guidelines for the diagnosis and treatment of pulmonary hypertension: the Task Force for the Diagnosis and Treatment of Pulmonary Hypertension of the European Society of Cardiology (ESC) and the European Respiratory Society (ERS), endorsed by the International Society of Heart and Lung Transplantation (ISHLT). *Eur Heart J* 30 (20), 2493-537.

Galie, N., Humbert, M., Vachiery, J. L., Gibbs, S., Lang, I., Torbicki, A., Simonneau, G., Peacock, A., Vonk Noordegraaf, A., Beghetti, M., Ghofrani, A., Gomez Sanchez, M. A., Hansmann, G., Klepetko, W., Lancellotti, P., Matucci, M., McDonagh, T., Pierard, L. A., Trindade, P. T., Zompatori, M. and Hoeper, M. (2015) 2015 ESC/ERS Guidelines for the diagnosis and treatment of pulmonary hypertension: The Joint Task Force for the Diagnosis and Treatment of Pulmonary Hypertension of the European Society of Cardiology (ESC) and the European Respiratory Society (ERS): Endorsed by: Association for European Paediatric and Congenital Cardiology (AEPC), International Society for Heart and Lung Transplantation (ISHLT). *Eur Respir J* 46 (4), 903-75.

Galie, N., Rubin, L., Hoeper, M., Jansa, P., Al-Hiti, H., Meyer, G., Chiossi, E., Kusic-Pajic, A. and Simonneau, G. (2008) Treatment of patients with mildly symptomatic pulmonary arterial hypertension with bosentan (EARLY study): a double-blind, randomised controlled trial. *Lancet* 371 (9630), 2093-100.

Gall, H., Felix, J. F., Schneck, F. K., Milger, K., Sommer, N., Voswinckel, R., Franco, O. H., Hofman, A., Schermuly, R. T., Weissmann, N., Grimminger, F., Seeger, W. and Ghofrani, H. A. (2017) The Giessen Pulmonary Hypertension Registry: Survival in pulmonary hypertension subgroups. *J Heart Lung Transplant* 36 (9), 957-967.

Gallagher, E., Enzler, T., Matsuzawa, A. and Karin, M. (2007) 5-bromo-2-deoxyuridine (BrdU) and 7-amino-actinomycin (7-AAD) staining for cell proliferation assay.

Gangopahyay, A., Oran, M., Bauer, E. M., Wertz, J. W., Comhair, S. A., Erzurum, S. C. and Bauer, P. M. (2011) Bone morphogenetic protein receptor II is a novel mediator of endothelial nitric-oxide synthase activation. *J Biol Chem* 286 (38), 33134-40.

Gao, Y., Cimica, V. and Reich, N. C. (2012) Suppressor of cytokine signaling 3 inhibits breast tumor kinase activation of STAT3. *J Biol Chem* 287 (25), 20904-12.

Garcia-Cardena, G., Fan, R., Stern, D. F., Liu, J. and Sessa, W. C. (1996) Endothelial nitric oxide synthase is regulated by tyrosine phosphorylation and interacts with caveolin-1. *J Biol Chem* 271 (44), 27237-40.

Garg, A., Kircher, M., Del Campo, M., Amato, R. S., Agarwal, A. K. and University of Washington Center for Mendelian, G. (2015) Whole exome sequencing identifies de novo heterozygous CAV1 mutations associated with a novel neonatal onset lipodystrophy syndrome. *Am J Med Genet A* 167A (8), 1796-806.

Gasperini, S., Crepaldi, L., Calzetti, F., Gatto, L., Berlato, C., Bazzoni, F., Yoshimura, A. and Cassatella, M. A. (2002) Interleukin-10 and cAMP-elevating agents cooperate to induce suppressor of cytokine signaling-3 via a protein kinase A-independent signal. *Eur Cytokine Netw* 13 (1), 47-53.

Gatfield, J., Mueller Grandjean, C., Sasse, T., Clozel, M. and Nayler, O. (2012) Slow receptor dissociation kinetics differentiate macitentan from other endothelin receptor antagonists in pulmonary arterial smooth muscle cells. *PLoS One* 7 (10), e47662.

Gaudino, M., Di Franco, A., Ohmes, L. B., Weltert, L., Lau, C., Gambardella, I., Salica, A., Munjal, M., Elsayed, M., Girardi, L. N., De Paulis, R. and Cornell International Consortium for Aortic, S. (2017) Biological solutions to aortic root replacement: valve-sparing versus bioprosthetic conduitdouble dagger. *Interact Cardiovasc Thorac Surg* 24 (6), 855-861.

Geraci, M. W., Gao, B., Shepherd, D. C., Moore, M. D., Westcott, J. Y., Fagan, K. A., Alger, L. A., Tuder, R. M. and Voelkel, N. F. (1999) Pulmonary prostacyclin synthase overexpression in transgenic mice protects against development of hypoxic pulmonary hypertension. *J Clin Invest* 103 (11), 1509-15.

Ghodsi, F. and Will, J. A. (1981) Changes in pulmonary structure and function induced by monocrotaline intoxication. *Am J Physiol* 240 (2), H149-55.

Ghofrani, H. A. and Grimminger, F. (2009) Soluble guanylate cyclase stimulation: an emerging option in pulmonary hypertension therapy. *Eur Respir Rev* 18 (111), 35-41.

Ghofrani, H. A., Seeger, W. and Grimminger, F. (2005) Imatinib for the treatment of pulmonary arterial hypertension. *N Engl J Med* 353 (13), 1412-3.

Giaid, A. and Saleh, D. (1995) Reduced expression of endothelial nitric oxide synthase in the lungs of patients with pulmonary hypertension. *N Engl J Med* 333 (4), 214-21.

Gilbert, L. A., Larson, M. H., Morsut, L., Liu, Z., Brar, G. A., Torres, S. E., Stern-Ginossar, N., Brandman, O., Whitehead, E. H., Doudna, J. A., Lim, W. A., Weissman, J. S. and Qi, L. S. (2013) CRISPR-mediated modular RNA-guided regulation of transcription in eukaryotes. *Cell* 154 (2), 442-51.

Gomez-Arroyo, J. G., Farkas, L., Alhussaini, A. A., Farkas, D., Kraskauskas, D., Voelkel, N. F. and Bogaard, H. J. (2012) The monocrotaline model of pulmonary

hypertension in perspective. *Am J Physiol Lung Cell Mol Physiol* 302 (4), L363-9.

Good, R. B., Gilbane, A. J., Trinder, S. L., Denton, C. P., Coghlan, G., Abraham, D. J. and Holmes, A. M. (2015) Endothelial to Mesenchymal Transition Contributes to Endothelial Dysfunction in Pulmonary Arterial Hypertension. *Am J Pathol* 185 (7), 1850-8.

Gore, B., Izikki, M., Mercier, O., Dewachter, L., Fadel, E., Humbert, M., Dartevelle, P., Simonneau, G., Naeije, R., Lebrin, F. and Eddahibi, S. (2014) Key role of the endothelial TGF-beta/ALK1/endoglin signaling pathway in humans and rodents pulmonary hypertension. *PLoS One* 9 (6), e100310.

Greig, S. L., Scott, L. J. and Plosker, G. L. (2014) Epoprostenol (Veletri(R), Caripul(R)): a review of its use in patients with pulmonary arterial hypertension. *Am J Cardiovasc Drugs* 14 (6), 463-70.

Grillari, J., Grillari-Voglauer, R. and Jansen-Durr, P. (2010) Post-translational modification of cellular proteins by ubiquitin and ubiquitin-like molecules: role in cellular senescence and aging. *Adv Exp Med Biol* 694, 172-96.

Gritsko, T., Williams, A., Turkson, J., Kaneko, S., Bowman, T., Huang, M., Nam, S., Eweis, I., Diaz, N., Sullivan, D., Yoder, S., Enkemann, S., Eschrich, S., Lee, J. H., Beam, C. A., Cheng, J., Minton, S., Muro-Cacho, C. A. and Jove, R. (2006) Persistent activation of stat3 signaling induces survivin gene expression and confers resistance to apoptosis in human breast cancer cells. *Clin Cancer Res* 12 (1), 11-9.

Grotendorst, G. R., Chang, T., Seppa, H. E., Kleinman, H. K. and Martin, G. R. (1982) Platelet-derived growth factor is a chemoattractant for vascular smooth muscle cells. *J Cell Physiol* 113 (2), 261-6.

Groth, A., Vrugt, B., Brock, M., Speich, R., Ulrich, S. and Huber, L. C. (2014) Inflammatory cytokines in pulmonary hypertension. *Respir Res* 15, 47.

Gryglewski, R. J. (2008) Prostacyclin among prostanoids. *Pharmacol Rep* 60 (1), 3-11.

Gupta, M., Teoh, H., Kajil, M., Tsigoulis, M., Quan, A., Braga, M. F. and Verma, S. (2012) The effects of rosiglitazone on inflammatory biomarkers and adipokines in diabetic, hypertensive patients. *Exp Clin Cardiol* 17 (4), 191-6.

Gurkan, O. U., He, C., Zielinski, R., Rabb, H., King, L. S., Dodd-o, J. M., D'Alessio, F. R., Aggarwal, N., Pearse, D. and Becker, P. M. (2011) Interleukin-6 mediates pulmonary vascular permeability in a two-hit model of ventilator-associated lung injury. *Exp Lung Res* 37 (10), 575-84.

Haan, C., Heinrich, P. C. and Behrmann, I. (2002) Structural requirements of the interleukin-6 signal transducer gp130 for its interaction with Janus kinase 1: the receptor is crucial for kinase activation. *Biochem J* 361 (Pt 1), 105-11.

Haan, C., Hermanns, H. M., Heinrich, P. C. and Behrmann, I. (2000) A single amino acid substitution (Trp(666)-->Ala) in the interbox1/2 region of the interleukin-6 signal transducer gp130 abrogates binding of JAK1, and dominantly impairs signal transduction. *Biochem J* 349 (Pt 1), 261-6.

Haan, S., Ferguson, P., Sommer, U., Hiremath, M., McVicar, D. W., Heinrich, P. C., Johnston, J. A. and Cacalano, N. A. (2003) Tyrosine phosphorylation disrupts elongin interaction and accelerates SOCS3 degradation. *J Biol Chem* 278 (34), 31972-9.

Hagen, M., Fagan, K., Steudel, W., Carr, M., Lane, K., Rodman, D. M. and West, J. (2007) Interaction of interleukin-6 and the BMP pathway in pulmonary smooth muscle. *Am J Physiol Lung Cell Mol Physiol* 292 (6), L1473-9.

Hamada, K., Shimizu, T., Matsui, T., Tsukita, S. and Hakoshima, T. (2000) Structural basis of the membrane-targeting and unmasking mechanisms of the radixin FERM domain. *EMBO J* 19 (17), 4449-62.

Hamid, T., Malik, M. T., Millar, R. P. and Kakar, S. S. (2008) Protein kinase A serves as a primary pathway in activation of Nur77 expression by gonadotropin-releasing hormone in the LbetaT2 mouse pituitary gonadotroph tumor cell line. *Int J Oncol* 33 (5), 1055-64.

Han, B., Copeland, C. A., Kawano, Y., Rosenzweig, E. B., Austin, E. D., Shahmirzadi, L., Tang, S., Raghunathan, K., Chung, W. K. and Kenworthy, A. K. (2016) Characterization of a caveolin-1 mutation associated with both pulmonary arterial hypertension and congenital generalized lipodystrophy. *Traffic* 17 (12), 1297-1312.

Hansmann, G., de Jesus Perez, V. A., Alastalo, T. P., Alvira, C. M., Guignabert, C., Bekker, J. M., Schellong, S., Urashima, T., Wang, L., Morrell, N. W. and Rabinovitch, M. (2008) An antiproliferative BMP-2/PPARgamma/apoE axis in human and murine SMCs and its role in pulmonary hypertension. *J Clin Invest* 118 (5), 1846-57.

Hao, Q., Samten, B., Ji, H. L., Zhao, Z. J. and Tang, H. (2012) Tyrosine phosphatase PTP-MEG2 negatively regulates vascular endothelial growth factor receptor signaling and function in endothelial cells. *Am J Physiol Cell Physiol* 303 (5), C548-53.

Harper, S. J. and Bates, D. O. (2008) VEGF-A splicing: the key to anti-angiogenic therapeutics? *Nat Rev Cancer* 8 (11), 880-7.

Harrison, R. E., Flanagan, J. A., Sankelo, M., Abdalla, S. A., Rowell, J., Machado, R. D., Elliott, C. G., Robbins, I. M., Olschewski, H., McLaughlin, V., Gruenig, E., Kermeen, F., Halme, M., Raisanen-Sokolowski, A., Laitinen, T., Morrell, N. W. and Trembath, R. C. (2003) Molecular and functional analysis identifies ALK-1 as the predominant cause of pulmonary hypertension related to hereditary haemorrhagic telangiectasia. *J Med Genet* 40 (12), 865-71.

Hashimoto-Kataoka, T., Hosen, N., Sonobe, T., Arita, Y., Yasui, T., Masaki, T., Minami, M., Inagaki, T., Miyagawa, S., Sawa, Y., Murakami, M., Kumanogoh, A., Yamauchi-Takihara, K., Okumura, M., Kishimoto, T., Komuro, I., Shirai, M., Sakata, Y. and Nakaoka, Y. (2015) Interleukin-6/interleukin-21 signaling axis is critical in the pathogenesis of pulmonary arterial hypertension. *Proc Natl Acad Sci U S A* 112 (20), E2677-86.

Hashizume, M., Tan, S. L., Takano, J., Ohsawa, K., Hasada, I., Hanasaki, A., Ito, I., Mihara, M. and Nishida, K. (2015) Tocilizumab, a humanized anti-IL-6R antibody, as an emerging therapeutic option for rheumatoid arthritis: molecular and cellular mechanistic insights. *Int Rev Immunol* 34 (3), 265-79.

Hayashi, Y. K., Matsuda, C., Ogawa, M., Goto, K., Tominaga, K., Mitsuhashi, S., Park, Y. E., Nonaka, I., Hino-Fukuyo, N., Haginoya, K., Sugano, H. and Nishino, I. (2009) Human PTRF mutations cause secondary deficiency of caveolins resulting in muscular dystrophy with generalized lipodystrophy. *J Clin Invest* 119 (9), 2623-33.

Hayer, A., Stoeber, M., Bissig, C. and Helenius, A. (2010) Biogenesis of caveolae: stepwise assembly of large caveolin and cavin complexes. *Traffic* 11 (3), 361-82.

Haynes, J., Jr., Robinson, J., Saunders, L., Taylor, A. E. and Strada, S. J. (1992) Role of cAMP-dependent protein kinase in cAMP-mediated vasodilation. *Am J Physiol* 262 (2 Pt 2), H511-6.

Hazan-Halevy, I., Harris, D., Liu, Z., Liu, J., Li, P., Chen, X., Shanker, S., Ferrajoli, A., Keating, M. J. and Estrov, Z. (2010) STAT3 is constitutively phosphorylated on serine 727 residues, binds DNA, and activates transcription in CLL cells. *Blood* 115 (14), 2852-63.

Hecker, M., Zaslona, Z., Kwapiszewska, G., Niess, G., Zakrzewicz, A., Hergenreider, E., Wilhelm, J., Marsh, L. M., Sedding, D., Klepetko, W., Lohmeyer, J., Dimmeler, S., Seeger, W., Weissmann, N., Schermuly, R. T., Kneidinger, N., Eickelberg, O. and Morty, R. E. (2010) Dysregulation of the IL-13 receptor system: a novel pathomechanism in pulmonary arterial hypertension. *Am J Respir Crit Care Med* 182 (6), 805-18.

Heinrich, P. C., Behrmann, I., Haan, S., Hermanns, H. M., Muller-Newen, G. and Schaper, F. (2003) Principles of interleukin (IL)-6-type cytokine signalling and its regulation. *Biochem J* 374 (Pt 1), 1-20.

Heinrich, P. C., Behrmann, I., Muller-Newen, G., Schaper, F. and Graeve, L. (1998) Interleukin-6-type cytokine signalling through the gp130/Jak/STAT pathway. *Biochem J* 334 (Pt 2), 297-314.

Heldin, C. H., Miyazono, K. and ten Dijke, P. (1997) TGF-beta signalling from cell membrane to nucleus through SMAD proteins. *Nature* 390 (6659), 465-71.

Heldin, C. H. and Moustakas, A. (2016) Signaling Receptors for TGF-beta Family Members. *Cold Spring Harb Perspect Biol* 8 (8).

Hemmann, U., Gerhartz, C., Heesel, B., Sasse, J., Kurapkat, G., Grotzinger, J., Wollmer, A., Zhong, Z., Darnell, J. E., Jr., Graeve, L., Heinrich, P. C. and Horn, F. (1996) Differential activation of acute phase response factor/Stat3 and Stat1 via the cytoplasmic domain of the interleukin 6 signal transducer gp130. II. Src homology SH2 domains define the specificity of stat factor activation. *J Biol Chem* 271 (22), 12999-3007.

Hernandez-Oropeza, J. L., Rodriguez-Reyna, T. S., Carrillo-Perez, D. L., Rodriguez-Andoney, J. J., Narvaez-David, R., Salado-Morales, Y., Rivero-Sigarroa, E., Dominguez-Cherit, G. and Pulido-Zamudio, T. (2018) Pulmonary Vasoreactivity and Phenotypes in Pulmonary Arterial Hypertension Associated to Connective Tissue Diseases. *Rev Invest Clin* 70 (2), 82-7.

Hirata, Y., Taga, T., Hibi, M., Nakano, N., Hirano, T. and Kishimoto, T. (1989) Characterization of IL-6 receptor expression by monoclonal and polyclonal antibodies. *J Immunol* 143 (9), 2900-6.

Hoeper, M. M., Barst, R. J., Bourge, R. C., Feldman, J., Frost, A. E., Galie, N., Gomez-Sanchez, M. A., Grimminger, F., Grunig, E., Hassoun, P. M., Morrell, N. W., Peacock, A. J., Satoh, T., Simonneau, G., Tapson, V. F., Torres, F., Lawrence, D., Quinn, D. A. and Ghofrani, H. A. (2013a) Imatinib mesylate as add-on therapy for pulmonary arterial hypertension: results of the randomized IMPRES study. *Circulation* 127 (10), 1128-38.

Hoeper, M. M., Bogaard, H. J., Condliffe, R., Frantz, R., Khanna, D., Kurzyna, M., Langleben, D., Manes, A., Satoh, T., Torres, F., Wilkins, M. R. and Badesch, D. B. (2013b) Definitions and diagnosis of pulmonary hypertension. *J Am Coll Cardiol* 62 (25 Suppl), D42-50.

Hoeper, M. M., Huscher, D., Ghofrani, H. A., Delcroix, M., Distler, O., Schweiger, C., Grunig, E., Staehler, G., Rosenkranz, S., Halank, M., Held, M., Grohe, C., Lange, T. J., Behr, J., Klose, H., Wilkens, H., Filusch, A., Germann, M., Ewert, R., Seyfarth, H. J., Olsson, K. M., Opitz, C. F., Gaine, S. P., Vizza, C. D., Vonk-Noordegraaf, A., Kaemmerer, H., Gibbs, J. S. and Pittrow, D. (2013c) Elderly patients diagnosed with idiopathic pulmonary arterial hypertension: results from the COMPERA registry. *Int J Cardiol* 168 (2), 871-80.

Hoeper, M. M., Kramer, T., Pan, Z., Eichstaedt, C. A., Spiesshoefer, J., Benjamin, N., Olsson, K. M., Meyer, K., Vizza, C. D., Vonk-Noordegraaf, A., Distler, O., Opitz, C., Gibbs, J. S. R., Delcroix, M., Ghofrani, H. A., Huscher, D., Pittrow, D., Rosenkranz, S. and Grunig, E. (2017) Mortality in pulmonary arterial hypertension: prediction by the 2015 European pulmonary hypertension guidelines risk stratification model. *Eur Respir J* 50 (2).

Hoeper, M. M. and Simon, R. G. J. (2014) The changing landscape of pulmonary arterial hypertension and implications for patient care. *Eur Respir Rev* 23 (134), 450-7.

Hof, P., Pluskey, S., Dhe-Paganon, S., Eck, M. J. and Shoelson, S. E. (1998) Crystal structure of the tyrosine phosphatase SHP-2. *Cell* 92 (4), 441-50.

Hoff, P. M., Wolff, R. A., Bogaard, K., Waldrum, S. and Abbruzzese, J. L. (2006) A Phase I study of escalating doses of the tyrosine kinase inhibitor semaxanib (SU5416) in combination with irinotecan in patients with advanced colorectal carcinoma. *Jpn J Clin Oncol* 36 (2), 100-3.

Holub, M. C., Szalai, C., Polgar, A., Toth, S. and Falus, A. (1999) Generation of 'truncated' interleukin-6 receptor (IL-6R) mRNA by alternative splicing; a possible source of soluble IL-6R. *Immunol Lett* 68 (1), 121-4.

Holz, G. G., Kang, G., Harbeck, M., Roe, M. W. and Chepurny, O. G. (2006) Cell physiology of cAMP sensor Epac. *J Physiol* 577 (Pt 1), 5-15.

Hoodless, P. A., Haerry, T., Abdollah, S., Stapleton, M., O'Connor, M. B., Attisano, L. and Wrana, J. L. (1996) MADR1, a MAD-related protein that functions in BMP2 signaling pathways. *Cell* 85 (4), 489-500.

Horbelt, D., Denkis, A. and Knaus, P. (2012) A portrait of Transforming Growth Factor beta superfamily signalling: Background matters. *Int J Biochem Cell Biol* 44 (3), 469-74.

Horsten, U., Schmitz-Van de Leur, H., Mullberg, J., Heinrich, P. C. and Rose-John, S. (1995) The membrane distal half of gp130 is responsible for the formation of a ternary complex with IL-6 and the IL-6 receptor. *FEBS Lett* 360 (1), 43-6.

Hoshikawa, Y., Voelkel, N. F., Gesell, T. L., Moore, M. D., Morris, K. G., Alger, L. A., Narumiya, S. and Geraci, M. W. (2001) Prostacyclin receptor-dependent modulation of pulmonary vascular remodeling. *Am J Respir Crit Care Med* 164 (2), 314-8.

Howard, J. K., Cave, B. J., Oksanen, L. J., Tzameli, I., Bjorbaek, C. and Flier, J. S. (2004) Enhanced leptin sensitivity and attenuation of diet-induced obesity in mice with haploinsufficiency of Socs3. *Nat Med* 10 (7), 734-8.

Huang, S. P., Wu, M. S., Shun, C. T., Wang, H. P., Lin, M. T., Kuo, M. L. and Lin, J. T. (2004) Interleukin-6 increases vascular endothelial growth factor and angiogenesis in gastric carcinoma. *J Biomed Sci* 11 (4), 517-27.

Huang, W. C., Hsu, C. H., Sung, S. H., Ho, W. J., Chu, C. Y., Chang, C. P., Chiu, Y. W., Wu, C. H., Chang, W. T., Lin, L., Lin, S. L., Cheng, C. C., Wu, Y. J., Wu, S. H., Hsieh, T. Y., Hsu, H. H., Fu, M., Dai, Z. K., Kuo, P. H., Hwang, J. J., Cheng, S. M. and committee, T. p. h. (2019) 2018 TSOC guideline focused update on diagnosis and treatment of pulmonary arterial hypertension. *J Formos Med Assoc*.

Huang, Z., Liu, Z., Luo, Q., Zhao, Z., Zhao, Q., Zheng, Y., Xi, Q. and Tang, Y. (2016) Glycoprotein 130 Inhibitor Ameliorates Monocrotaline-Induced Pulmonary Hypertension in Rats. *Can J Cardiol*.

Humbert, M., Monti, G., Brenot, F., Sitbon, O., Portier, A., Grangeot-Keros, L., Duroux, P., Galanaud, P., Simonneau, G. and Emilie, D. (1995) Increased interleukin-1 and interleukin-6 serum concentrations in severe primary pulmonary hypertension. *Am J Respir Crit Care Med* 151 (5), 1628-31.

Humbert, M., Monti, G., Fartoukh, M., Magnan, A., Brenot, F., Rain, B., Capron, F., Galanaud, P., Duroux, P., Simonneau, G. and Emilie, D. (1998) Platelet-derived growth factor expression in primary pulmonary hypertension: comparison of HIV seropositive and HIV seronegative patients. *Eur Respir J* 11 (3), 554-9.

Humbert, M., Sitbon, O., Chaouat, A., Bertocchi, M., Habib, G., Gressin, V., Yaici, A., Weitzenblum, E., Cordier, J. F., Chabot, F., Dromer, C., Pison, C., Reynaud-Gaubert, M., Haloun, A., Laurent, M., Hachulla, E., Cottin, V., Degano, B., Jais, X., Montani, D., Souza, R. and Simonneau, G. (2010) Survival in patients with idiopathic, familial, and anorexigen-associated pulmonary arterial hypertension in the modern management era. *Circulation* 122 (2), 156-63.

Humbert, M., Sitbon, O., Chaouat, A., Bertocchi, M., Habib, G., Gressin, V., Yaici, A., Weitzenblum, E., Cordier, J. F., Chabot, F., Dromer, C., Pison, C., Reynaud-Gaubert, M., Haloun, A., Laurent, M., Hachulla, E. and Simonneau, G. (2006) Pulmonary arterial hypertension in France: results from a national registry. *Am J Respir Crit Care Med* 173 (9), 1023-30.

Hurst, L. A., Dunmore, B. J., Long, L., Crosby, A., Al-Lamki, R., Deighton, J., Southwood, M., Yang, X., Nikolic, M. Z., Herrera, B., Inman, G. J., Bradley, J. R., Rana, A. A., Upton, P. D. and Morrell, N. W. (2017) TNFalpha drives pulmonary arterial hypertension by suppressing the BMP type-II receptor and altering NOTCH signalling. *Nat Commun* 8, 14079.

Ishihara, T., Hayashi, E., Yamamoto, S., Kobayashi, C., Tamura, Y., Sawazaki, R., Tamura, F., Tahara, K., Kasahara, T., Ishihara, T., Takenaga, M., Fukuda, K. and Mizushima, T. (2015) Encapsulation of beraprost sodium in nanoparticles: analysis of sustained release properties, targeting abilities and pharmacological activities in animal models of pulmonary arterial hypertension. *J Control Release* 197, 97-104.

Ito, T., Ando, H., Suzuki, T., Ogura, T., Hotta, K., Imamura, Y., Yamaguchi, Y. and Handa, H. (2010) Identification of a primary target of thalidomide teratogenicity. *Science* 327 (5971), 1345-50.

Ito, T., Okada, T., Miyashita, H., Nomoto, T., Nonaka-Sarukawa, M., Uchibori, R., Maeda, Y., Urabe, M., Mizukami, H., Kume, A., Takahashi, M., Ikeda, U.,

Shimada, K. and Ozawa, K. (2007) Interleukin-10 expression mediated by an adeno-associated virus vector prevents monocrotaline-induced pulmonary arterial hypertension in rats. *Circ Res* 101 (7), 734-41.

Jamur, M. C. and Oliver, C. (2010) Permeabilization of Cell Membranes. In Oliver, C. and Jamur, M. C. (editors) *Immunocytochemical Methods and Protocols.* Totowa, NJ: Humana Press. 63-66.

Jankov, R. P., Kantores, C., Belcastro, R., Yi, S., Ridsdale, R. A., Post, M. and Tanswell, A. K. (2005) A role for platelet-derived growth factor beta-receptor in a newborn rat model of endothelin-mediated pulmonary vascular remodeling. *Am J Physiol Lung Cell Mol Physiol* 288 (6), L1162-70.

Jansa, P., Jarkovsky, J., Al-Hiti, H., Popelova, J., Ambroz, D., Zatocil, T., Votavova, R., Polacek, P., Maresova, J., Aschermann, M., Brabec, P., Dusek, L. and Linhart, A. (2014) Epidemiology and long-term survival of pulmonary arterial hypertension in the Czech Republic: a retrospective analysis of a nationwide registry. *BMC Pulm Med* 14, 45.

Jasiewicz, M., Knapp, M., Waszkiewicz, E., Ptaszynska-Kopczynska, K., Szpakowicz, A., Sobkowicz, B., Musial, W. J. and Kaminski, K. A. (2015) Enhanced IL-6 trans-signaling in pulmonary arterial hypertension and its potential role in disease-related systemic damage. *Cytokine* 76 (2), 187-92.

Jiang, X., Humbert, M. and Jing, Z. (2012) *Idiopathic Pulmonary Arterial Hypertension and Its Prognosis in the Modern Management Era in Developed and Developing Countries.* Pulmonary Vascual Disorders: Karger.

Jin, S., Mutvei, A. P., Chivukula, I. V., Andersson, E. R., Ramskold, D., Sandberg, R., Lee, K. L., Kronqvist, P., Mamaeva, V., Ostling, P., Mpindi, J. P., Kallioniemi, O., Screpanti, I., Poellinger, L., Sahlgren, C. and Lendahl, U. (2013) Non-canonical Notch signaling activates IL-6/JAK/STAT signaling in breast tumor cells and is controlled by p53 and IKKalpha/IKKbeta. *Oncogene* 32 (41), 4892-902.

Jing, Z. C., Parikh, K., Pulido, T., Jerjes-Sanchez, C., White, R. J., Allen, R., Torbicki, A., Xu, K. F., Yehle, D., Laliberte, K., Arneson, C. and Rubin, L. J. (2013) Efficacy and safety of oral treprostinil monotherapy for the treatment of pulmonary arterial hypertension: a randomized, controlled trial. *Circulation* 127 (5), 624-33.

Jonigk, D., Golpon, H., Bockmeyer, C. L., Maegel, L., Hoeper, M. M., Gottlieb, J., Nickel, N., Hussein, K., Maus, U., Lehmann, U., Janciauskiene, S., Welte, T., Haverich, A., Rische, J., Kreipe, H. and Laenger, F. (2011) Plexiform lesions in pulmonary arterial hypertension composition, architecture, and microenvironment. *Am J Pathol* 179 (1), 167-79.

Jorgensen, S. B., O'Neill, H. M., Sylow, L., Honeyman, J., Hewitt, K. A., Palanivel, R., Fullerton, M. D., Oberg, L., Balendran, A., Galic, S., van der Poel, C., Trounce, I. A., Lynch, G. S., Schertzer, J. D. and Steinberg, G. R. (2013) Deletion of skeletal muscle SOCS3 prevents insulin resistance in obesity. *Diabetes* 62 (1), 56-64.

Jostock, T., Mullberg, J., Ozbek, S., Atreya, R., Blinn, G., Voltz, N., Fischer, M., Neurath, M. F. and Rose-John, S. (2001) Soluble gp130 is the natural inhibitor of soluble interleukin-6 receptor transsignaling responses. *Eur J Biochem* 268 (1), 160-7.

Ju, H., Zou, R., Venema, V. J. and Venema, R. C. (1997) Direct interaction of endothelial nitric-oxide synthase and caveolin-1 inhibits synthase activity. *J Biol Chem* 272 (30), 18522-5.

Justus, C. R., Leffler, N., Ruiz-Echevarria, M. and Yang, L. V. (2014) In vitro cell migration and invasion assays. *J Vis Exp* (88).

Kanellakis, P., Ditiatkovski, M., Kostolias, G. and Bobik, A. (2012) A pro-fibrotic role for interleukin-4 in cardiac pressure overload. *Cardiovasc Res* 95 (1), 77-85.

Kayakabe, K., Kuroiwa, T., Sakurai, N., Ikeuchi, H., Kadiombo, A. T., Sakairi, T., Matsumoto, T., Maeshima, A., Hiromura, K. and Nojima, Y. (2012) Interleukin-6 promotes destabilized angiogenesis by modulating angiopoietin expression in rheumatoid arthritis. *Rheumatology (Oxford)* 51 (9), 1571-9.

Kershaw, N. J., Laktyushin, A., Nicola, N. A. and Babon, J. J. (2014) Reconstruction of an active SOCS3-based E3 ubiquitin ligase complex in vitro: identification of the active components and JAK2 and gp130 as substrates. *Growth Factors* 32 (1), 1-10.

Kim, H., Hawley, T. S., Hawley, R. G. and Baumann, H. (1998) Protein tyrosine phosphatase 2 (SHP-2) moderates signaling by gp130 but is not required for the induction of acute-phase plasma protein genes in hepatic cells. *Mol Cell Biol* 18 (3), 1525-33.

Kim, Y. S., Choi, S. J., Tae, Y. M., Lee, B. J., Jeon, S. G., Oh, S. Y., Gho, Y. S., Zhu, Z. and Kim, Y. K. (2010) Distinct roles of vascular endothelial growth factor receptor-1- and receptor-2-mediated signaling in T cell priming and Th17 polarization to lipopolysaccharide-containing allergens in the lung. *J Immunol* 185 (9), 5648-55.

King, A. J., Sun, H., Diaz, B., Barnard, D., Miao, W., Bagrodia, S. and Marshall, M. S. (1998) The protein kinase Pak3 positively regulates Raf-1 activity through phosphorylation of serine 338. *Nature* 396 (6707), 180-3.

Kinjyo, I., Inoue, H., Hamano, S., Fukuyama, S., Yoshimura, T., Koga, K., Takaki, H., Himeno, K., Takaesu, G., Kobayashi, T. and Yoshimura, A. (2006) Loss of SOCS3 in T helper cells resulted in reduced immune responses and hyperproduction of interleukin 10 and transforming growth factor-beta 1. *J Exp Med* 203 (4), 1021-31.

Kooistra, M. R., Corada, M., Dejana, E. and Bos, J. L. (2005) Epac1 regulates integrity of endothelial cell junctions through VE-cadherin. *FEBS Lett* 579 (22), 4966-72.

Kovtun, O., Tillu, V. A., Ariotti, N., Parton, R. G. and Collins, B. M. (2015) Cavin family proteins and the assembly of caveolae. *J Cell Sci* 128 (7), 1269-78.

Krump-Konvalinkova, V., Bittinger, F., Olert, J., Brauninger, W., Brunner, J. and Kirkpatrick, C. J. (2003) Establishment and characterization of an angiosarcoma-derived cell line, AS-M. *Endothelium* 10 (6), 319-28.

Kumar, P., Thudium, E., Laliberte, K., Zaccardelli, D. and Nelsen, A. (2016) A Comprehensive Review of Treprostinil Pharmacokinetics via Four Routes of Administration. *Clin Pharmacokinet* 55 (12), 1495-1505.

Kumar, R., Mickael, C., Chabon, J., Gebreab, L., Rutebemberwa, A., Garcia, A. R., Koyanagi, D. E., Sanders, L., Gandjeva, A., Kearns, M. T., Barthel, L., Janssen, W. J., Mauad, T., Bandeira, A., Schmidt, E., Tuder, R. M. and Graham, B. B.

(2015) The Causal Role of IL-4 and IL-13 in Schistosoma mansoni Pulmonary Hypertension. *Am J Respir Crit Care Med* 192 (8), 998-1008.

Kumari, N., Dwarakanath, B. S., Das, A. and Bhatt, A. N. (2016) Role of interleukin-6 in cancer progression and therapeutic resistance. *Tumour Biol* 37 (9), 11553-11572.

Kuppner, M. C., van Meir, E., Hamou, M. F. and de Tribolet, N. (1990) Cytokine regulation of intercellular adhesion molecule-1 (ICAM-1) expression on human glioblastoma cells. *Clin Exp Immunol* 81 (1), 142-8.

Kurth, I., Horsten, U., Pflanz, S., Timmermann, A., Kuster, A., Dahmen, H., Tacken, I., Heinrich, P. C. and Muller-Newen, G. (2000) Importance of the membrane-proximal extracellular domains for activation of the signal transducer glycoprotein 130. *J Immunol* 164 (1), 273-82.

Kvale, D., Krajci, P. and Brandtzaeg, P. (1992) Expression and regulation of adhesion molecules ICAM-1 (CD54) and LFA-3 (CD58) in human intestinal epithelial cell lines. *Scand J Immunol* 35 (6), 669-76.

Lai, Y. J., Pullamsetti, S. S., Weissmann, N., Ghofrani, H. A., Voswinckel, R., Seeger, W., Grimminger, F. and Schermuly, R. T. (2009) Treprostinil Mediated Activation of Peroxisome Proliferator-Activated Receptors in Pulmonary Hypertension. *American Journal of Respiratory and Critical Care Medicine* 179.

Lamaze, C., Tardif, N., Dewulf, M., Vassilopoulos, S. and Blouin, C. M. (2017) The caveolae dress code: structure and signaling. *Curr Opin Cell Biol* 47, 117-125.

Landsberg, J. W. and Yuan, J. X. (2004) Calcium and TRP channels in pulmonary vascular smooth muscle cell proliferation. *News Physiol Sci* 19, 44-50.

Larabee, J. L., Shakir, S. M., Barua, S. and Ballard, J. D. (2013) Increased cAMP in monocytes augments Notch signaling mechanisms by elevating RBP-J and transducin-like enhancer of Split (TLE). *J Biol Chem* 288 (30), 21526-36.

Lau, E. M. T., Giannoulatou, E., Celermajer, D. S. and Humbert, M. (2017) Epidemiology and treatment of pulmonary arterial hypertension. *Nat Rev Cardiol* 14 (10), 603-614.

Launay, J. M., Herve, P., Peoc'h, K., Tournois, C., Callebert, J., Nebigil, C. G., Etienne, N., Drouet, L., Humbert, M., Simonneau, G. and Maroteaux, L. (2002) Function of the serotonin 5-hydroxytryptamine 2B receptor in pulmonary hypertension. *Nat Med* 8 (10), 1129-35.

Lavelle, A., Sugrue, R., Lawler, G., Mulligan, N., Kelleher, B., Murphy, D. M. and Gaine, S. P. (2009) Sitaxentan-induced hepatic failure in two patients with pulmonary arterial hypertension. *Eur Respir J* 34 (3), 770-1.

Levy, M., Del Cerro, M. J., Nadaud, S., Vadlamudi, K., Colgazier, E., Fineman, J., Bonnet, D. and Adatia, I. (2018) Safety, efficacy and Management of subcutaneous treprostinil infusions in the treatment of severe pediatric pulmonary hypertension. *Int J Cardiol* 264, 153-157.

Lin, W. N., Luo, S. F., Lee, C. W., Wang, C. C., Wang, J. S. and Yang, C. M. (2007) Involvement of MAPKs and NF-kappaB in LPS-induced VCAM-1 expression in human tracheal smooth muscle cells. *Cell Signal* 19 (6), 1258-67.

Ling, Y., Johnson, M. K., Kiely, D. G., Condliffe, R., Elliot, C. A., Gibbs, J. S., Howard, L. S., Pepke-Zaba, J., Sheares, K. K., Corris, P. A., Fisher, A. J., Lordan, J. L., Gaine, S., Coghlan, J. G., Wort, S. J., Gatzoulis, M. A. and Peacock, A. J. (2012) Changing demographics, epidemiology, and survival of incident pulmonary

arterial hypertension: results from the pulmonary hypertension registry of the United Kingdom and Ireland. *Am J Respir Crit Care Med* 186 (8), 790-6.

Liu, E., Cote, J. F. and Vuori, K. (2003) Negative regulation of FAK signaling by SOCS proteins. *EMBO J* 22 (19), 5036-46.

Liu, F., Hata, A., Baker, J. C., Doody, J., Carcamo, J., Harland, R. M. and Massague, J. (1996) A human Mad protein acting as a BMP-regulated transcriptional activator. *Nature* 381 (6583), 620-3.

Liu, L., Brown, D., McKee, M., Lebrasseur, N. K., Yang, D., Albrecht, K. H., Ravid, K. and Pilch, P. F. (2008) Deletion of Cavin/PTRF causes global loss of caveolae, dyslipidemia, and glucose intolerance. *Cell Metab* 8 (4), 310-7.

Liu, L. and Pilch, P. F. (2008) A critical role of cavin (polymerase I and transcript release factor) in caveolae formation and organization. *J Biol Chem* 283 (7), 4314-22.

Liu, S. Y., Deng, S. Y., He, Y. B. and Ni, G. X. (2017) miR-451 inhibits cell growth, migration and angiogenesis in human osteosarcoma via down-regulating IL 6R. *Biochem Biophys Res Commun* 482 (4), 987-993.

Liu, Y., Huang, X., He, X., Zhou, Y., Jiang, X., Chen-Kiang, S., Jaffrey, S. R. and Xu, G. (2015) A novel effect of thalidomide and its analogs: suppression of cereblon ubiquitination enhances ubiquitin ligase function. *FASEB J* 29 (12), 4829-39.

Lo, C. W., Chen, M. W., Hsiao, M., Wang, S., Chen, C. A., Hsiao, S. M., Chang, J. S., Lai, T. C., Rose-John, S., Kuo, M. L. and Wei, L. H. (2011) IL-6 trans-signaling in formation and progression of malignant ascites in ovarian cancer. *Cancer Res* 71 (2), 424-34.

Long, L., MacLean, M. R., Jeffery, T. K., Morecroft, I., Yang, X., Rudarakanchana, N., Southwood, M., James, V., Trembath, R. C. and Morrell, N. W. (2006) Serotonin increases susceptibility to pulmonary hypertension in BMPR2-deficient mice. *Circ Res* 98 (6), 818-27.

Long, L., Ormiston, M. L., Yang, X., Southwood, M., Graf, S., Machado, R. D., Mueller, M., Kinzel, B., Yung, L. M., Wilkinson, J. M., Moore, S. D., Drake, K. M., Aldred, M. A., Yu, P. B., Upton, P. D. and Morrell, N. W. (2015) Selective enhancement of endothelial BMPR-II with BMP9 reverses pulmonary arterial hypertension. *Nat Med* 21 (7), 777-85.

Lust, J. A., Donovan, K. A., Kline, M. P., Greipp, P. R., Kyle, R. A. and Maihle, N. J. (1992) Isolation of an mRNA encoding a soluble form of the human interleukin-6 receptor. *Cytokine* 4 (2), 96-100.

Ma, L. and Chung, W. K. (2017) The role of genetics in pulmonary arterial hypertension. *J Pathol* 241 (2), 273-280.

Ma, L., Roman-Campos, D., Austin, E. D., Eyries, M., Sampson, K. S., Soubrier, F., Germain, M., Tregouet, D. A., Borczuk, A., Rosenzweig, E. B., Girerd, B., Montani, D., Humbert, M., Loyd, J. E., Kass, R. S. and Chung, W. K. (2013) A novel channelopathy in pulmonary arterial hypertension. *N Engl J Med* 369 (4), 351-61.

Machado, R. D., Aldred, M. A., James, V., Harrison, R. E., Patel, B., Schwalbe, E. C., Gruenig, E., Janssen, B., Koehler, R., Seeger, W., Eickelberg, O., Olschewski, H., Elliott, C. G., Glissmeyer, E., Carlquist, J., Kim, M., Torbicki, A., Fijalkowska, A., Szewczyk, G., Parma, J., Abramowicz, M. J., Galie, N., Morisaki, H., Kyotani, S., Nakanishi, N., Morisaki, T., Humbert, M., Simonneau, G., Sitbon, O., Soubrier, F., Coulet, F., Morrell, N. W. and Trembath, R. C. (2006) Mutations of the TGF-

beta type II receptor BMPR2 in pulmonary arterial hypertension. *Hum Mutat* 27 (2), 121-32.

Macias, M. J., Martin-Malpartida, P. and Massague, J. (2015) Structural determinants of Smad function in TGF-beta signaling. *Trends Biochem Sci* 40 (6), 296-308.

Mahony, R., Ahmed, S., Diskin, C. and Stevenson, N. J. (2016) SOCS3 revisited: a broad regulator of disease, now ready for therapeutic use? *Cell Mol Life Sci* 73 (17), 3323-36.

Marcus, J. T., Gan, C. T., Zwanenburg, J. J., Boonstra, A., Allaart, C. P., Gotte, M. J. and Vonk-Noordegraaf, A. (2008) Interventricular mechanical asynchrony in pulmonary arterial hypertension: left-to-right delay in peak shortening is related to right ventricular overload and left ventricular underfilling. *J Am Coll Cardiol* 51 (7), 750-7.

Martin, L. J., Boucher, N., Brousseau, C. and Tremblay, J. J. (2008) The orphan nuclear receptor NUR77 regulates hormone-induced StAR transcription in Leydig cells through cooperation with Ca2+/calmodulin-dependent protein kinase I. *Mol Endocrinol* 22 (9), 2021-37.

Martin, L. J., Boucher, N., El-Asmar, B. and Tremblay, J. J. (2009) cAMP-induced expression of the orphan nuclear receptor Nur77 in MA-10 Leydig cells involves a CaMKI pathway. *J Androl* 30 (2), 134-45.

Mason, N. A., Springall, D. R., Burke, M., Pollock, J., Mikhail, G., Yacoub, M. H. and Polak, J. M. (1998) High expression of endothelial nitric oxide synthase in plexiform lesions of pulmonary hypertension. *J Pathol* 185 (3), 313-8.

Masri, F. A., Xu, W., Comhair, S. A., Asosingh, K., Koo, M., Vasanji, A., Drazba, J., Anand-Apte, B. and Erzurum, S. C. (2007) Hyperproliferative apoptosis-resistant endothelial cells in idiopathic pulmonary arterial hypertension. *Am J Physiol Lung Cell Mol Physiol* 293 (3), L548-54.

Massague, J., Seoane, J. and Wotton, D. (2005) Smad transcription factors. *Genes Dev* 19 (23), 2783-810.

Maston, L. D., Jones, D. T., Giermakowska, W., Resta, T. C., Ramiro-Diaz, J., Howard, T. A., Jernigan, N. L., Herbert, L., Maurice, A. A. and Gonzalez Bosc, L. V. (2018) Interleukin-6 trans-signaling contributes to chronic hypoxia-induced pulmonary hypertension. *Pulm Circ* 8 (3), 2045894018780734.

Mathai, S. C., Puhan, M. A., Lam, D. and Wise, R. A. (2012) The minimal important difference in the 6-minute walk test for patients with pulmonary arterial hypertension. *Am J Respir Crit Care Med* 186 (5), 428-33.

Matsumura, F. and Hartshorne, D. J. (2008) Myosin phosphatase target subunit: Many roles in cell function. *Biochem Biophys Res Commun* 369 (1), 149-56.

Matsuno, Y., Kiwamoto, T., Morishima, Y., Ishii, Y., Hizawa, N. and Hogaboam, C. M. (2018) Notch signaling regulates cell density-dependent apoptosis of NIH 3T3 through an IL-6/STAT3 dependent mechanism. *Eur J Cell Biol* 97 (7), 512-522.

Matura, L. A., Ventetuolo, C. E., Palevsky, H. I., Lederer, D. J., Horn, E. M., Mathai, S. C., Pinder, D., Archer-Chicko, C., Bagiella, E., Roberts, K. E., Tracy, R. P., Hassoun, P. M., Girgis, R. E. and Kawut, S. M. (2015) Interleukin-6 and tumor necrosis factor-alpha are associated with quality of life-related symptoms in pulmonary arterial hypertension. *Ann Am Thorac Soc* 12 (3), 370-5.

Mauritz, G. J., Rizopoulos, D., Groepenhoff, H., Tiede, H., Felix, J., Eilers, P., Bosboom, J., Postmus, P. E., Westerhof, N. and Vonk-Noordegraaf, A. (2011) Usefulness

of serial N-terminal pro-B-type natriuretic peptide measurements for determining prognosis in patients with pulmonary arterial hypertension. *Am J Cardiol* 108 (11), 1645-50.

McCord, J., Mundy, B. J., Hudson, M. P., Maisel, A. S., Hollander, J. E., Abraham, W. T., Steg, P. G., Omland, T., Knudsen, C. W., Sandberg, K. R., McCullough, P. A. and Breathing Not Properly Multinational Study, I. (2004) Relationship between obesity and B-type natriuretic peptide levels. *Arch Intern Med* 164 (20), 2247-52.

McGoon, M. D., Frost, A. E., Oudiz, R. J., Badesch, D. B., Galie, N., Olschewski, H., McLaughlin, V. V., Gerber, M. J., Dufton, C., Despain, D. J. and Rubin, L. J. (2009) Ambrisentan therapy in patients with pulmonary arterial hypertension who discontinued bosentan or sitaxsentan due to liver function test abnormalities. *Chest* 135 (1), 122-9.

McMahon, K. A., Zajicek, H., Li, W. P., Peyton, M. J., Minna, J. D., Hernandez, V. J., Luby-Phelps, K. and Anderson, R. G. (2009) SRBC/cavin-3 is a caveolin adapter protein that regulates caveolae function. *EMBO J* 28 (8), 1001-15.

Medford, A. R., Douglas, S. K., Godinho, S. I., Uppington, K. M., Armstrong, L., Gillespie, K. M., van Zyl, B., Tetley, T. D., Ibrahim, N. B. and Millar, A. B. (2009) Vascular Endothelial Growth Factor (VEGF) isoform expression and activity in human and murine lung injury. *Respir Res* 10, 27.

Melian, E. B. and Goa, K. L. (2002) Beraprost: a review of its pharmacology and therapeutic efficacy in the treatment of peripheral arterial disease and pulmonary arterial hypertension. *Drugs* 62 (1), 107-33.

Meloche, J., Lampron, M. C., Nadeau, V., Maltais, M., Potus, F., Lambert, C., Tremblay, E., Vitry, G., Breuils-Bonnet, S., Boucherat, O., Charbonneau, E., Provencher, S., Paulin, R. and Bonnet, S. (2017) Implication of Inflammation and Epigenetic Readers in Coronary Artery Remodeling in Patients With Pulmonary Arterial Hypertension. *Arterioscler Thromb Vasc Biol* 37 (8), 1513-1523.

Meloche, J., Potus, F., Vaillancourt, M., Bourgeois, A., Johnson, I., Deschamps, L., Chabot, S., Ruffenach, G., Henry, S., Breuils-Bonnet, S., Tremblay, E., Nadeau, V., Lambert, C., Paradis, R., Provencher, S. and Bonnet, S. (2015) Bromodomain-Containing Protein 4: The Epigenetic Origin of Pulmonary Arterial Hypertension. *Circ Res* 117 (6), 525-35.

Mercurio, A., Adriani, G., Catalano, A., Carocci, A., Rao, L., Lentini, G., Cavalluzzi, M. M., Franchini, C., Vacca, A. and Corbo, F. (2017) A Mini-Review on Thalidomide: Chemistry, Mechanisms of Action, Therapeutic Potential and Anti-Angiogenic Properties in Multiple Myeloma. *Curr Med Chem* 24 (25), 2736-2744.

Merklinger, S. L., Jones, P. L., Martinez, E. C. and Rabinovitch, M. (2005) Epidermal growth factor receptor blockade mediates smooth muscle cell apoptosis and improves survival in rats with pulmonary hypertension. *Circulation* 112 (3), 423-31.

Midgett, C., Stitham, J., Martin, K. and Hwa, J. (2011) Prostacyclin receptor regulation--from transcription to trafficking. *Curr Mol Med* 11 (7), 517-28.

Migneault, A., Sauvageau, S., Villeneuve, L., Thorin, E., Fournier, A., Leblanc, N. and Dupuis, J. (2005) Chronically elevated endothelin levels reduce pulmonary vascular reactivity to nitric oxide. *Am J Respir Crit Care Med* 171 (5), 506-13.

Millauer, B., Wizigmann-Voos, S., Schnurch, H., Martinez, R., Moller, N. P., Risau, W. and Ullrich, A. (1993) High affinity VEGF binding and developmental expression suggest Flk-1 as a major regulator of vasculogenesis and angiogenesis. *Cell* 72 (6), 835-46.

Milocco, L. H., Haslam, J. A., Rosen, J. and Seidel, H. M. (1999) Design of conditionally active STATs: insights into STAT activation and gene regulatory function. *Mol Cell Biol* 19 (4), 2913-20.

Minai, O. A., Gudavalli, R., Mummadi, S., Liu, X., McCarthy, K. and Dweik, R. A. (2012) Heart rate recovery predicts clinical worsening in patients with pulmonary arterial hypertension. *Am J Respir Crit Care Med* 185 (4), 400-8.

Mischak, H., Seitz, T., Janosch, P., Eulitz, M., Steen, H., Schellerer, M., Philipp, A. and Kolch, W. (1996) Negative regulation of Raf-1 by phosphorylation of serine 621. *Mol Cell Biol* 16 (10), 5409-18.

Miyamoto, S., Nagaya, N., Satoh, T., Kyotani, S., Sakamaki, F., Fujita, M., Nakanishi, N. and Miyatake, K. (2000) Clinical correlates and prognostic significance of six-minute walk test in patients with primary pulmonary hypertension. Comparison with cardiopulmonary exercise testing. *Am J Respir Crit Care Med* 161 (2 Pt 1), 487-92.

Miyata, M., Ueno, Y., Sekine, H., Ito, O., Sakuma, F., Koike, H., Nishio, S., Nishimaki, T. and Kasukawa, R. (1996) Protective effect of beraprost sodium, a stable prostacyclin analogue, in development of monocrotaline-induced pulmonary hypertension. *J Cardiovasc Pharmacol* 27 (1), 20-6.

Mizuno, S., Farkas, L., Al Husseini, A., Farkas, D., Gomez-Arroyo, J., Kraskauskas, D., Nicolls, M. R., Cool, C. D., Bogaard, H. J. and Voelkel, N. F. (2012) Severe pulmonary arterial hypertension induced by SU5416 and ovalbumin immunization. *Am J Respir Cell Mol Biol* 47 (5), 679-87.

Moncada, S., Gryglewski, R., Bunting, S. and Vane, J. R. (1976) An enzyme isolated from arteries transforms prostaglandin endoperoxides to an unstable substance that inhibits platelet aggregation. *Nature* 263 (5579), 663-5.

Montani, D., Seferian, A., Savale, L., Simonneau, G. and Humbert, M. (2013) Drug-induced pulmonary arterial hypertension: a recent outbreak. *Eur Respir Rev* 22 (129), 244-50.

Moon, H., Lee, C. S., Inder, K. L., Sharma, S., Choi, E., Black, D. M., Le Cao, K. A., Winterford, C., Coward, J. I., Ling, M. T., Australian Prostate Cancer, B., Craik, D. J., Parton, R. G., Russell, P. J. and Hill, M. M. (2014) PTRF/cavin-1 neutralizes non-caveolar caveolin-1 microdomains in prostate cancer. *Oncogene* 33 (27), 3561-70.

Mori, H., Hanada, R., Hanada, T., Aki, D., Mashima, R., Nishinakamura, H., Torisu, T., Chien, K. R., Yasukawa, H. and Yoshimura, A. (2004) Socs3 deficiency in the brain elevates leptin sensitivity and confers resistance to diet-induced obesity. *Nat Med* 10 (7), 739-43.

Morrell, N. W., Adnot, S., Archer, S. L., Dupuis, J., Jones, P. L., MacLean, M. R., McMurtry, I. F., Stenmark, K. R., Thistlethwaite, P. A., Weissmann, N., Yuan, J. X. and Weir, E. K. (2009) Cellular and molecular basis of pulmonary arterial hypertension. *J Am Coll Cardiol* 54 (1 Suppl), S20-31.

Morrell, N. W., Aldred, M. A., Chung, W. K., Elliott, C. G., Nichols, W. C., Soubrier, F., Trembath, R. C. and Loyd, J. E. (2019) Genetics and genomics of pulmonary arterial hypertension. *Eur Respir J* 53 (1).

Morrell, N. W., Bloch, D. B., ten Dijke, P., Goumans, M. J., Hata, A., Smith, J., Yu, P. B. and Bloch, K. D. (2016) Targeting BMP signalling in cardiovascular disease and anaemia. *Nat Rev Cardiol* 13 (2), 106-20.

Mullberg, J., Schooltink, H., Stoyan, T., Gunther, M., Graeve, L., Buse, G., Mackiewicz, A., Heinrich, P. C. and Rose-John, S. (1993) The soluble interleukin-6 receptor is generated by shedding. *Eur J Immunol* 23 (2), 473-80.

Munro, K. M. (2016a) *Stabilising Suppressor of Cytokine Signalling 3 (SOCS3) Protein Levels to Limit Neointimal Hyperplasia*. Doctor of Philosophy. Glasgow: University of Glasgow.

Munro, K. M. (2016b) *Stabilising suppressor of cytokine signalling 3 (SOCS3) protein levels to limit neointimal hyperplasia*. Ph.D. Glasgow: University of Glasgow.

Murai, T., Muraoka, K., Saga, K., Sakai, A., Sato, N., Amemiya, K., Yajima, M., Murata, T., Umetsu, T. and Nishio, S. (1989) Effect of beraprost sodium on peripheral circulation insufficiency in rats and rabbits. *Arzneimittelforschung* 39 (8), 856-9.

Murakami, M., Hibi, M., Nakagawa, N., Nakagawa, T., Yasukawa, K., Yamanishi, K., Taga, T. and Kishimoto, T. (1993) IL-6-induced homodimerization of gp130 and associated activation of a tyrosine kinase. *Science* 260 (5115), 1808-10.

Murata, T., Lin, M. I., Huang, Y., Yu, J., Bauer, P. M., Giordano, F. J. and Sessa, W. C. (2007) Reexpression of caveolin-1 in endothelium rescues the vascular, cardiac, and pulmonary defects in global caveolin-1 knockout mice. *J Exp Med* 204 (10), 2373-82.

Murata, T., Ushikubi, F., Matsuoka, T., Hirata, M., Yamasaki, A., Sugimoto, Y., Ichikawa, A., Aze, Y., Tanaka, T., Yoshida, N., Ueno, A., Oh-ishi, S. and Narumiya, S. (1997) Altered pain perception and inflammatory response in mice lacking prostacyclin receptor. *Nature* 388 (6643), 678-82.

Naka, T., Narazaki, M., Hirata, M., Matsumoto, T., Minamoto, S., Aono, A., Nishimoto, N., Kajita, T., Taga, T., Yoshizaki, K., Akira, S. and Kishimoto, T. (1997) Structure and function of a new STAT-induced STAT inhibitor. *Nature* 387 (6636), 924-9.

Namba, T., Oida, H., Sugimoto, Y., Kakizuka, A., Negishi, M., Ichikawa, A. and Narumiya, S. (1994) cDNA cloning of a mouse prostacyclin receptor. Multiple signaling pathways and expression in thymic medulla. *J Biol Chem* 269 (13), 9986-92.

Narazaki, M., Yasukawa, K., Saito, T., Ohsugi, Y., Fukui, H., Koishihara, Y., Yancopoulos, G. D., Taga, T. and Kishimoto, T. (1993) Soluble forms of the interleukin-6 signal-transducing receptor component gp130 in human serum possessing a potential to inhibit signals through membrane-anchored gp130. *Blood* 82 (4), 1120-6.

Nasim, M. T., Ogo, T., Ahmed, M., Randall, R., Chowdhury, H. M., Snape, K. M., Bradshaw, T. Y., Southgate, L., Lee, G. J., Jackson, I., Lord, G. M., Gibbs, J. S., Wilkins, M. R., Ohta-Ogo, K., Nakamura, K., Girerd, B., Coulet, F., Soubrier, F., Humbert, M., Morrell, N. W., Trembath, R. C. and Machado, R. D. (2011)

Molecular genetic characterization of SMAD signaling molecules in pulmonary arterial hypertension. *Hum Mutat* 32 (12), 1385-9.

Nasim, M. T., Ogo, T., Chowdhury, H. M., Zhao, L., Chen, C. N., Rhodes, C. and Trembath, R. C. (2012) BMPR-II deficiency elicits pro-proliferative and anti-apoptotic responses through the activation of TGFbeta-TAK1-MAPK pathways in PAH. *Hum Mol Genet* 21 (11), 2548-58.

Nedvetsky, P. I., Zhao, X., Mathivet, T., Aspalter, I. M., Stanchi, F., Metzger, R. J., Mostov, K. E. and Gerhardt, H. (2016) cAMP-dependent protein kinase A (PKA) regulates angiogenesis by modulating tip cell behavior in a Notch-independent manner. *Development* 143 (19), 3582-3590.

Nickel, N., Jonigk, D., Kempf, T., Bockmeyer, C. L., Maegel, L., Rische, J., Laenger, F., Lehmann, U., Sauer, C., Greer, M., Welte, T., Hoeper, M. M. and Golpon, H. A. (2011) GDF-15 is abundantly expressed in plexiform lesions in patients with pulmonary arterial hypertension and affects proliferation and apoptosis of pulmonary endothelial cells. *Respir Res* 12, 62.

Nickel, N. P., O'Leary, J. M., Brittain, E. L., Fessel, J. P., Zamanian, R. T., West, J. D. and Austin, E. D. (2017) Kidney dysfunction in patients with pulmonary arterial hypertension. *Pulm Circ* 7 (1), 38-54.

Nicolls, M. R., Mizuno, S., Taraseviciene-Stewart, L., Farkas, L., Drake, J. I., Al Husseini, A., Gomez-Arroyo, J. G., Voelkel, N. F. and Bogaard, H. J. (2012) New models of pulmonary hypertension based on VEGF receptor blockade-induced endothelial cell apoptosis. *Pulm Circ* 2 (4), 434-42.

Nishikawa, K., Yoshida, M., Kusuhara, M., Ishigami, N., Isoda, K., Miyazaki, K. and Ohsuzu, F. (2006) Left ventricular hypertrophy in mice with a cardiac-specific overexpression of interleukin-1. *Am J Physiol Heart Circ Physiol* 291 (1), H176-83.

Nishimura, R., Hata, K., Ikeda, F., Matsubara, T., Yamashita, K., Ichida, F. and Yoneda, T. (2003) The role of Smads in BMP signaling. *Front Biosci* 8, s275-84.

Nishimura, R., Kato, Y., Chen, D., Harris, S. E., Mundy, G. R. and Yoneda, T. (1998) Smad5 and DPC4 are key molecules in mediating BMP-2-induced osteoblastic differentiation of the pluripotent mesenchymal precursor cell line C2C12. *J Biol Chem* 273 (4), 1872-9.

Niu, G., Wright, K. L., Huang, M., Song, L., Haura, E., Turkson, J., Zhang, S., Wang, T., Sinibaldi, D., Coppola, D., Heller, R., Ellis, L. M., Karras, J., Bromberg, J., Pardoll, D., Jove, R. and Yu, H. (2002) Constitutive Stat3 activity up-regulates VEGF expression and tumor angiogenesis. *Oncogene* 21 (13), 2000-8.

Nogueira-Ferreira, R., Vitorino, R., Ferreira, R. and Henriques-Coelho, T. (2015) Exploring the monocrotaline animal model for the study of pulmonary arterial hypertension: A network approach. *Pulm Pharmacol Ther* 35, 8-16.

Novak, U., Ji, H., Kanagasundaram, V., Simpson, R. and Paradiso, L. (1998) STAT3 forms stable homodimers in the presence of divalent cations prior to activation. *Biochem Biophys Res Commun* 247 (3), 558-63.

O'Connell, C., Amar, D., Boucly, A., Savale, L., Jais, X., Chaumais, M. C., Montani, D., Humbert, M., Simonneau, G. and Sitbon, O. (2016) Comparative Safety and Tolerability of Prostacyclins in Pulmonary Hypertension. *Drug Saf* 39 (4), 287-94.

Ogawa, A., Satoh, T., Tamura, Y., Fukuda, K. and Matsubara, H. (2017) Survival of Japanese Patients With Idiopathic/Heritable Pulmonary Arterial Hypertension. *Am J Cardiol* 119 (9), 1479-1484.

Ogo, T., Chowdhury, H. M., Yang, J., Long, L., Li, X., Torres Cleuren, Y. N., Morrell, N. W., Schermuly, R. T., Trembath, R. C. and Nasim, M. T. (2013) Inhibition of overactive transforming growth factor-beta signaling by prostacyclin analogs in pulmonary arterial hypertension. *Am J Respir Cell Mol Biol* 48 (6), 733-41.

Oguz, M. M., Oguz, A. D., Sanli, C. and Cevik, A. (2014) Serum levels of soluble ICAM-1 in children with pulmonary artery hypertension. *Tex Heart Inst J* 41 (2), 159-64.

Ortiz-Munoz, G., Lopez-Parra, V., Lopez-Franco, O., Fernandez-Vizarra, P., Mallavia, B., Flores, C., Sanz, A., Blanco, J., Mezzano, S., Ortiz, A., Egido, J. and Gomez-Guerrero, C. (2010) Suppressors of cytokine signaling abrogate diabetic nephropathy. *J Am Soc Nephrol* 21 (5), 763-72.

Oton, T., Loza, E., Sanmarti, R. and Tornero Molina, J. (2018) AB0469 Efficacy and safety of interleukin 6 inhibitors in rheumatoid arthritis: a systematic literature review. *Annals of the Rheumatic Diseases* 77 (Suppl 2), 1396-1396.

Oudiz, R. J., Galie, N., Olschewski, H., Torres, F., Frost, A., Ghofrani, H. A., Badesch, D. B., McGoon, M. D., McLaughlin, V. V., Roecker, E. B., Harrison, B. C., Despain, D., Dufton, C., Rubin, L. J. and Group, A. S. (2009) Long-term ambrisentan therapy for the treatment of pulmonary arterial hypertension. *J Am Coll Cardiol* 54 (21), 1971-81.

Pagan, R. J., Lee, A. S., Austin, C. O. and Burger, C. D. (2014) Screening for connective tissue disease in pulmonary arterial hypertension. *South Med J* 107 (10), 666-9.

Pant, S., Jones, S. F., Kurkjian, C. D., Infante, J. R., Moore, K. N., Burris, H. A., McMeekin, D. S., Benhadji, K. A., Patel, B. K. R., Frenzel, M. J., Kursar, J. D., Zamek-Gliszczynski, M. J., Yuen, E. S. M., Chan, E. M. and Bendell, J. C. (2016) A first-in-human phase I study of the oral Notch inhibitor, LY900009, in patients with advanced cancer. *Eur J Cancer* 56, 1-9.

Paonessa, G., Graziani, R., De Serio, A., Savino, R., Ciapponi, L., Lahm, A., Salvati, A. L., Toniatti, C. and Ciliberto, G. (1995) Two distinct and independent sites on IL-6 trigger gp 130 dimer formation and signalling. *EMBO J* 14 (9), 1942-51.

Papaioannou, A. I., Zakynthinos, E., Kostikas, K., Kiropoulos, T., Koutsokera, A., Ziogas, A., Koutroumpas, A., Sakkas, L., Gourgoulianis, K. I. and Daniil, Z. D. (2009) Serum VEGF levels are related to the presence of pulmonary arterial hypertension in systemic sclerosis. *BMC Pulm Med* 9, 18.

Pappano, A. J. and Gil Wier, W. (2013) 8 - The Microcirculation and Lymphatics. In Pappano, A. J. and Gil Wier, W. (editors) *Cardiovascular Physiology (Tenth Edition).* Philadelphia: Content Repository Only! 153-170.

Parpaleix, A., Amsellem, V., Houssaini, A., Abid, S., Breau, M., Marcos, E., Sawaki, D., Delcroix, M., Quarck, R., Maillard, A., Couillin, I., Ryffel, B. and Adnot, S. (2016) Role of interleukin-1 receptor 1/MyD88 signalling in the development and progression of pulmonary hypertension. *Eur Respir J* 48 (2), 470-83.

Partovian, C., Adnot, S., Eddahibi, S., Teiger, E., Levame, M., Dreyfus, P., Raffestin, B. and Frelin, C. (1998) Heart and lung VEGF mRNA expression in rats with

monocrotaline- or hypoxia-induced pulmonary hypertension. *Am J Physiol* 275 (6), H1948-56.

Patel, J. A., Shen, L., Hall, S. M., Benyahia, C., Norel, X., McAnulty, R. J., Moledina, S., Silverstein, A. M., Whittle, B. J. and Clapp, L. H. (2018) Prostanoid EP(2) Receptors Are Up-Regulated in Human Pulmonary Arterial Hypertension: A Key Anti-Proliferative Target for Treprostinil in Smooth Muscle Cells. *Int J Mol Sci* 19 (8).

Patel, R., Aronow, W. S., Patel, L., Gandhi, K., Desai, H., Kaul, D. and Sahgal, S. P. (2012) Treatment of pulmonary hypertension. *Med Sci Monit* 18 (4), RA31-9.

Peacock, A. J., Crawley, S., McLure, L., Blyth, K. G., Vizza, C. D., Poscia, R., Francone, M., Iacucci, I., Olschewski, H., Kovacs, G., Vonk Noordegraaf, A., Marcus, J. T., van de Veerdonk, M. C. and Oosterveer, F. P. (2014) Changes in right ventricular function measured by cardiac magnetic resonance imaging in patients receiving pulmonary arterial hypertension-targeted therapy: the EURO-MR study. *Circ Cardiovasc Imaging* 7 (1), 107-14.

Pendergrass, S. A., Hayes, E., Farina, G., Lemaire, R., Farber, H. W., Whitfield, M. L. and Lafyatis, R. (2010) Limited systemic sclerosis patients with pulmonary arterial hypertension show biomarkers of inflammation and vascular injury. *PLoS One* 5 (8), e12106.

Peng, H., Sarwar, Z., Yang, X. P., Peterson, E. L., Xu, J., Janic, B., Rhaleb, N., Carretero, O. A. and Rhaleb, N. E. (2015) Profibrotic Role for Interleukin-4 in Cardiac Remodeling and Dysfunction. *Hypertension* 66 (3), 582-9.

Penumatsa, K. C., Warburton, R. R., Hill, N. S. and Fanburg, B. L. (2019) CrossTalk proposal: The mouse SuHx model is a good model of pulmonary arterial hypertension. *J Physiol* 597 (4), 975-977.

Perros, F., Dorfmuller, P., Souza, R., Durand-Gasselin, I., Godot, V., Capel, F., Adnot, S., Eddahibi, S., Mazmanian, M., Fadel, E., Herve, P., Simonneau, G., Emilie, D. and Humbert, M. (2007) Fractalkine-induced smooth muscle cell proliferation in pulmonary hypertension. *Eur Respir J* 29 (5), 937-43.

Perros, F., Montani, D., Dorfmuller, P., Durand-Gasselin, I., Tcherakian, C., Le Pavec, J., Mazmanian, M., Fadel, E., Mussot, S., Mercier, O., Herve, P., Emilie, D., Eddahibi, S., Simonneau, G., Souza, R. and Humbert, M. (2008) Platelet-derived growth factor expression and function in idiopathic pulmonary arterial hypertension. *Am J Respir Crit Care Med* 178 (1), 81-8.

Piao, L., Park, J., Li, Y., Shin, S., Shin, S., Kong, G., Shrestha, R., Tran, Q., Hur, G. M., Kim, J. L. and Park, J. (2014) SOCS3 and SOCS6 are required for the risperidone-mediated inhibition of insulin and leptin signaling in neuroblastoma cells. *Int J Mol Med* 33 (5), 1364-70.

Pietuch, A., Bruckner, B. R. and Janshoff, A. (2013) Membrane tension homeostasis of epithelial cells through surface area regulation in response to osmotic stress. *Biochim Biophys Acta* 1833 (3), 712-22.

Piqueras, L., Reynolds, A. R., Hodivala-Dilke, K. M., Alfranca, A., Redondo, J. M., Hatae, T., Tanabe, T., Warner, T. D. and Bishop-Bailey, D. (2007) Activation of PPARbeta/delta induces endothelial cell proliferation and angiogenesis. *Arterioscler Thromb Vasc Biol* 27 (1), 63-9.

Ponce, M. L. (2009) Tube formation: an in vitro matrigel angiogenesis assay. *Methods Mol Biol* 467, 183-8.

Ponsioen, B., Gloerich, M., Ritsma, L., Rehmann, H., Bos, J. L. and Jalink, K. (2009) Direct spatial control of Epac1 by cyclic AMP. *Mol Cell Biol* 29 (10), 2521-31.

Prewitt, A. R., Ghose, S., Frump, A. L., Datta, A., Austin, E. D., Kenworthy, A. K. and de Caestecker, M. P. (2015) Heterozygous null bone morphogenetic protein receptor type 2 mutations promote SRC kinase-dependent caveolar trafficking defects and endothelial dysfunction in pulmonary arterial hypertension. *J Biol Chem* 290 (2), 960-71.

Prins, K. W., Archer, S. L., Pritzker, M., Rose, L., Weir, E. K., Sharma, A. and Thenappan, T. (2018) Interleukin-6 is independently associated with right ventricular function in pulmonary arterial hypertension. *J Heart Lung Transplant* 37 (3), 376-384.

Puhr, M., Santer, F. R., Neuwirt, H., Susani, M., Nemeth, J. A., Hobisch, A., Kenner, L. and Culig, Z. (2009) Down-regulation of suppressor of cytokine signaling-3 causes prostate cancer cell death through activation of the extrinsic and intrinsic apoptosis pathways. *Cancer Res* 69 (18), 7375-84.

Pullamsetti, S. S., Seeger, W. and Savai, R. (2018) Classical IL-6 signaling: a promising therapeutic target for pulmonary arterial hypertension. *J Clin Invest* 128 (5), 1720-1723.

Puthier, D., Bataille, R. and Amiot, M. (1999) IL-6 up-regulates mcl-1 in human myeloma cells through JAK / STAT rather than ras / MAP kinase pathway. *Eur J Immunol* 29 (12), 3945-50.

Qiagen (2014) *Transfection Protocols & Applications.* *https://www.qiagen.com/au/resources/molecular-biology-methods/transfection/*

Qin, B. Y., Chacko, B. M., Lam, S. S., de Caestecker, M. P., Correia, J. J. and Lin, K. (2001) Structural basis of Smad1 activation by receptor kinase phosphorylation. *Mol Cell* 8 (6), 1303-12.

Quezada Loaiza, C. A., Velazquez Martin, M. T., Jimenez Lopez-Guarch, C., Ruiz Cano, M. J., Navas Tejedor, P., Carreira, P. E., Flox Camacho, A., de Pablo Gafas, A., Delgado Jimenez, J. F., Gomez Sanchez, M. A. and Escribano Subias, P. (2017) Trends in Pulmonary Hypertension Over a Period of 30 Years: Experience From a Single Referral Centre. *Rev Esp Cardiol (Engl Ed)* 70 (11), 915-923.

Quinn, T. P., Peters, K. G., De Vries, C., Ferrara, N. and Williams, L. T. (1993) Fetal liver kinase 1 is a receptor for vascular endothelial growth factor and is selectively expressed in vascular endothelium. *Proc Natl Acad Sci U S A* 90 (16), 7533-7.

Ranchoux, B., Harvey, L. D., Ayon, R. J., Babicheva, A., Bonnet, S., Chan, S. Y., Yuan, J. X. and Perez, V. J. (2018) Endothelial dysfunction in pulmonary arterial hypertension: an evolving landscape (2017 Grover Conference Series). *Pulm Circ* 8 (1), 2045893217752912.

Razani, B., Altschuler, Y., Zhu, L., Pestell, R. G., Mostov, K. E. and Lisanti, M. P. (2000) Caveolin-1 expression is down-regulated in cells transformed by the human papilloma virus in a p53-dependent manner. Replacement of caveolin-1 expression suppresses HPV-mediated cell transformation. *Biochemistry* 39 (45), 13916-24.

Razani, B., Zhang, X. L., Bitzer, M., von Gersdorff, G., Bottinger, E. P. and Lisanti, M. P. (2001) Caveolin-1 regulates transforming growth factor (TGF)-beta/SMAD

signaling through an interaction with the TGF-beta type I receptor. *J Biol Chem* 276 (9), 6727-38.

Rehmann, H., Das, J., Knipscheer, P., Wittinghofer, A. and Bos, J. L. (2006) Structure of the cyclic-AMP-responsive exchange factor Epac2 in its auto-inhibited state. *Nature* 439 (7076), 625-8.

Rehmann, H., Schwede, F., Doskeland, S. O., Wittinghofer, A. and Bos, J. L. (2003) Ligand-mediated activation of the cAMP-responsive guanine nucleotide exchange factor Epac. *J Biol Chem* 278 (40), 38548-56.

Reynolds, A. M., Holmes, M. D., Danilov, S. M. and Reynolds, P. N. (2012) Targeted gene delivery of BMPR2 attenuates pulmonary hypertension. *Eur Respir J* 39 (2), 329-43.

Rhodes, C. J., Im, H., Cao, A., Hennigs, J. K., Wang, L., Sa, S., Chen, P. I., Nickel, N. P., Miyagawa, K., Hopper, R. K., Tojais, N. F., Li, C. G., Gu, M., Spiekerkoetter, E., Xian, Z., Chen, R., Zhao, M., Kaschwich, M., Del Rosario, P. A., Bernstein, D., Zamanian, R. T., Wu, J. C., Snyder, M. P. and Rabinovitch, M. (2015) RNA Sequencing Analysis Detection of a Novel Pathway of Endothelial Dysfunction in Pulmonary Arterial Hypertension. *Am J Respir Crit Care Med* 192 (3), 356-66.

Richards, M. and Mellor, H. (2016) In Vitro Coculture Assays of Angiogenesis. *Methods Mol Biol* 1430, 159-66.

Riethmueller, S., Ehlers, J. C., Lokau, J., Dusterhoft, S., Knittler, K., Dombrowsky, G., Grotzinger, J., Rabe, B., Rose-John, S. and Garbers, C. (2016) Cleavage Site Localization Differentially Controls Interleukin-6 Receptor Proteolysis by ADAM10 and ADAM17. *Sci Rep* 6, 25550.

Roberts, O. L. and Dart, C. (2014) cAMP signalling in the vasculature: the role of Epac (exchange protein directly activated by cAMP). *Biochem Soc Trans* 42 (1), 89-97.

Rogers, S., Wells, R. and Rechsteiner, M. (1986) Amino acid sequences common to rapidly degraded proteins: the PEST hypothesis. *Science* 234 (4774), 364-8.

Rojkind, M., Novikoff, P. M., Greenwel, P., Rubin, J., Rojas-Valencia, L., de Carvalho, A. C., Stockert, R., Spray, D., Hertzberg, E. L. and Wolkoff, A. W. (1995) Characterization and functional studies on rat liver fat-storing cell line and freshly isolated hepatocyte coculture system. *Am J Pathol* 146 (6), 1508-20.

Romano, M., Sironi, M., Toniatti, C., Polentarutti, N., Fruscella, P., Ghezzi, P., Faggioni, R., Luini, W., van Hinsbergh, V., Sozzani, S., Bussolino, F., Poli, V., Ciliberto, G. and Mantovani, A. (1997) Role of IL-6 and its soluble receptor in induction of chemokines and leukocyte recruitment. *Immunity* 6 (3), 315-25.

Rose-John, S. (2012) IL-6 trans-signaling via the soluble IL-6 receptor: importance for the pro-inflammatory activities of IL-6. *Int J Biol Sci* 8 (9), 1237-47.

Ross, R., Glomset, J., Kariya, B. and Harker, L. (1974) A platelet-dependent serum factor that stimulates the proliferation of arterial smooth muscle cells in vitro. *Proc Natl Acad Sci U S A* 71 (4), 1207-10.

Rubens, C., Ewert, R., Halank, M., Wensel, R., Orzechowski, H. D., Schultheiss, H. P. and Hoeffken, G. (2001) Big endothelin-1 and endothelin-1 plasma levels are correlated with the severity of primary pulmonary hypertension. *Chest* 120 (5), 1562-9.

Rubin, L. J., Badesch, D. B., Barst, R. J., Galie, N., Black, C. M., Keogh, A., Pulido, T., Frost, A., Roux, S., Leconte, I., Landzberg, M. and Simonneau, G. (2002) Bosentan therapy for pulmonary arterial hypertension. *N Engl J Med* 346 (12), 896-903.

Rubin, L. J., Badesch, D. B., Fleming, T. R., Galie, N., Simonneau, G., Ghofrani, H. A., Oakes, M., Layton, G., Serdarevic-Pehar, M., McLaughlin, V. V., Barst, R. J. and Group, S.-S. (2011) Long-term treatment with sildenafil citrate in pulmonary arterial hypertension: the SUPER-2 study. *Chest* 140 (5), 1274-83.

Rubin, L. J., Mendoza, J., Hood, M., McGoon, M., Barst, R., Williams, W. B., Diehl, J. H., Crow, J. and Long, W. (1990) Treatment of primary pulmonary hypertension with continuous intravenous prostacyclin (epoprostenol). Results of a randomized trial. *Ann Intern Med* 112 (7), 485-91.

Rubin, L. J. and Roux, S. (2002) Bosentan: a dual endothelin receptor antagonist. *Expert Opin Investig Drugs* 11 (7), 991-1002.

Ryan, J. J. and Archer, S. L. (2014) The right ventricle in pulmonary arterial hypertension: disorders of metabolism, angiogenesis and adrenergic signaling in right ventricular failure. *Circ Res* 115 (1), 176-88.

Sachithanandan, N., Fam, B. C., Fynch, S., Dzamko, N., Watt, M. J., Wormald, S., Honeyman, J., Galic, S., Proietto, J., Andrikopoulos, S., Hevener, A. L., Kay, T. W. and Steinberg, G. R. (2010) Liver-specific suppressor of cytokine signaling-3 deletion in mice enhances hepatic insulin sensitivity and lipogenesis resulting in fatty liver and obesity. *Hepatology* 52 (5), 1632-42.

Sakao, S., Taraseviciene-Stewart, L., Lee, J. D., Wood, K., Cool, C. D. and Voelkel, N. F. (2005) Initial apoptosis is followed by increased proliferation of apoptosis-resistant endothelial cells. *FASEB J* 19 (9), 1178-80.

Saleby, J., Bouzina, H., Lundgren, J. and Radegran, G. (2017) Angiogenic and inflammatory biomarkers in the differentiation of pulmonary hypertension. *Scand Cardiovasc J* 51 (5), 261-270.

Sanchez, O., Marcos, E., Perros, F., Fadel, E., Tu, L., Humbert, M., Dartevelle, P., Simonneau, G., Adnot, S. and Eddahibi, S. (2007) Role of endothelium-derived CC chemokine ligand 2 in idiopathic pulmonary arterial hypertension. *Am J Respir Crit Care Med* 176 (10), 1041-7.

Sands, W. A., Woolson, H. D., Milne, G. R., Rutherford, C. and Palmer, T. M. (2006) Exchange protein activated by cyclic AMP (Epac)-mediated induction of suppressor of cytokine signaling 3 (SOCS-3) in vascular endothelial cells. *Mol Cell Biol* 26 (17), 6333-46.

Sasaki, A., Inagaki-Ohara, K., Yoshida, T., Yamanaka, A., Sasaki, M., Yasukawa, H., Koromilas, A. E. and Yoshimura, A. (2003) The N-terminal truncated isoform of SOCS3 translated from an alternative initiation AUG codon under stress conditions is stable due to the lack of a major ubiquitination site, Lys-6. *J Biol Chem* 278 (4), 2432-6.

Satoh, K., Kikuchi, N., Satoh, T., Kurosawa, R., Sunamura, S., Siddique, M. A. H., Omura, J., Yaoita, N. and Shimokawa, H. (2018) Identification of Novel Therapeutic Targets for Pulmonary Arterial Hypertension. *Int J Mol Sci* 19 (12).

Sauvageau, S., Thorin, E., Caron, A. and Dupuis, J. (2007) Endothelin-1-induced pulmonary vasoreactivity is regulated by ET(A) and ET(B) receptor interactions. *J Vasc Res* 44 (5), 375-81.

Savai, R., Pullamsetti, S. S., Kolbe, J., Bieniek, E., Voswinckel, R., Fink, L., Scheed, A., Ritter, C., Dahal, B. K., Vater, A., Klussmann, S., Ghofrani, H. A., Weissmann, N., Klepetko, W., Banat, G. A., Seeger, W., Grimminger, F. and Schermuly, R. T. (2012) Immune and inflammatory cell involvement in the pathology of idiopathic pulmonary arterial hypertension. *Am J Respir Crit Care Med* 186 (9), 897-908.

Savale, L., Tu, L., Rideau, D., Izziki, M., Maitre, B., Adnot, S. and Eddahibi, S. (2009) Impact of interleukin-6 on hypoxia-induced pulmonary hypertension and lung inflammation in mice. *Respir Res* 10, 6.

Savino, R., Ciapponi, L., Lahm, A., Demartis, A., Cabibbo, A., Toniatti, C., Delmastro, P., Altamura, S. and Ciliberto, G. (1994) Rational design of a receptor super-antagonist of human interleukin-6. *EMBO J* 13 (24), 5863-70.

Sawa, Y., Ueki, T., Hata, M., Iwasawa, K., Tsuruga, E., Kojima, H., Ishikawa, H. and Yoshida, S. (2008) LPS-induced IL-6, IL-8, VCAM-1, and ICAM-1 expression in human lymphatic endothelium. *J Histochem Cytochem* 56 (2), 97-109.

Saxena, M., Williams, S., Tasken, K. and Mustelin, T. (1999) Crosstalk between cAMP-dependent kinase and MAP kinase through a protein tyrosine phosphatase. *Nat Cell Biol* 1 (5), 305-11.

Schaper, F. and Rose-John, S. (2015) Interleukin-6: Biology, signaling and strategies of blockade. *Cytokine Growth Factor Rev* 26 (5), 475-87.

Schlosser, K., Taha, M., Deng, Y., Jiang, B., McIntyre, L. A., Mei, S. H. and Stewart, D. J. (2017) Lack of elevation in plasma levels of pro-inflammatory cytokines in common rodent models of pulmonary arterial hypertension: questions of construct validity for human patients. *Pulm Circ* 7 (2), 476-485.

Schmitz, J., Weissenbach, M., Haan, S., Heinrich, P. C. and Schaper, F. (2000) SOCS3 exerts its inhibitory function on interleukin-6 signal transduction through the SHP2 recruitment site of gp130. *J Biol Chem* 275 (17), 12848-56.

Schumacher, N., Meyer, D., Mauermann, A., von der Heyde, J., Wolf, J., Schwarz, J., Knittler, K., Murphy, G., Michalek, M., Garbers, C., Bartsch, J. W., Guo, S., Schacher, B., Eickholz, P., Chalaris, A., Rose-John, S. and Rabe, B. (2015) Shedding of Endogenous Interleukin-6 Receptor (IL-6R) Is Governed by A Disintegrin and Metalloproteinase (ADAM) Proteases while a Full-length IL-6R Isoform Localizes to Circulating Microvesicles. *J Biol Chem* 290 (43), 26059-71.

Seamon, K. B., Padgett, W. and Daly, J. W. (1981) Forskolin: unique diterpene activator of adenylate cyclase in membranes and in intact cells. *Proc Natl Acad Sci U S A* 78 (6), 3363-7.

Seferian, A. and Simonneau, G. (2013) Therapies for pulmonary arterial hypertension: where are we today, where do we go tomorrow? *Eur Respir Rev* 22 (129), 217-26.

Segovia-Mendoza, M., Gonzalez-Gonzalez, M. E., Barrera, D., Diaz, L. and Garcia-Becerra, R. (2015) Efficacy and mechanism of action of the tyrosine kinase inhibitors gefitinib, lapatinib and neratinib in the treatment of HER2-positive breast cancer: preclinical and clinical evidence. *Am J Cancer Res* 5 (9), 2531-61.

Segura-Ibarra, V., Wu, S., Hassan, N., Moran-Guerrero, J. A., Ferrari, M., Guha, A., Karmouty-Quintana, H. and Blanco, E. (2018) Nanotherapeutics for Treatment of Pulmonary Arterial Hypertension. *Front Physiol* 9, 890.

Shalaby, F., Rossant, J., Yamaguchi, T. P., Gertsenstein, M., Wu, X. F., Breitman, M. L. and Schuh, A. C. (1995) Failure of blood-island formation and vasculogenesis in Flk-1-deficient mice. *Nature* 376 (6535), 62-6.

Shan, Y., Gnanasambandan, K., Ungureanu, D., Kim, E. T., Hammaren, H., Yamashita, K., Silvennoinen, O., Shaw, D. E. and Hubbard, S. R. (2014) Molecular basis for pseudokinase-dependent autoinhibition of JAK2 tyrosine kinase. *Nat Struct Mol Biol* 21 (7), 579-84.

Shi, H., Tzameli, I., Bjorbaek, C. and Flier, J. S. (2004) Suppressor of cytokine signaling 3 is a physiological regulator of adipocyte insulin signaling. *J Biol Chem* 279 (33), 34733-40.

Shuai, K., Horvath, C. M., Huang, L. H., Qureshi, S. A., Cowburn, D. and Darnell, J. E., Jr. (1994) Interferon activation of the transcription factor Stat91 involves dimerization through SH2-phosphotyrosyl peptide interactions. *Cell* 76 (5), 821-8.

Siewert, E., Muller-Esterl, W., Starr, R., Heinrich, P. C. and Schaper, F. (1999) Different protein turnover of interleukin-6-type cytokine signalling components. *Eur J Biochem* 265 (1), 251-7.

Simonneau, G., Barst, R. J., Galie, N., Naeije, R., Rich, S., Bourge, R. C., Keogh, A., Oudiz, R., Frost, A., Blackburn, S. D., Crow, J. W., Rubin, L. J. and Treprostinil Study, G. (2002) Continuous subcutaneous infusion of treprostinil, a prostacyclin analogue, in patients with pulmonary arterial hypertension: a double-blind, randomized, placebo-controlled trial. *Am J Respir Crit Care Med* 165 (6), 800-4.

Simonneau, G., Gatzoulis, M. A., Adatia, I., Celermajer, D., Denton, C., Ghofrani, A., Gomez Sanchez, M. A., Krishna Kumar, R., Landzberg, M., Machado, R. F., Olschewski, H., Robbins, I. M. and Souza, R. (2013) Updated clinical classification of pulmonary hypertension. *J Am Coll Cardiol* 62 (25 Suppl), D34-41.

Simonneau, G., Torbicki, A., Hoeper, M. M., Delcroix, M., Karlocai, K., Galie, N., Degano, B., Bonderman, D., Kurzyna, M., Efficace, M., Giorgino, R. and Lang, I. M. (2012) Selexipag: an oral, selective prostacyclin receptor agonist for the treatment of pulmonary arterial hypertension. *Eur Respir J* 40 (4), 874-80.

Singhal, S., Mehta, J., Desikan, R., Ayers, D., Roberson, P., Eddlemon, P., Munshi, N., Anaissie, E., Wilson, C., Dhodapkar, M., Zeddis, J. and Barlogie, B. (1999) Antitumor activity of thalidomide in refractory multiple myeloma. *N Engl J Med* 341 (21), 1565-71.

Sinha, B., Koster, D., Ruez, R., Gonnord, P., Bastiani, M., Abankwa, D., Stan, R. V., Butler-Browne, G., Vedie, B., Johannes, L., Morone, N., Parton, R. G., Raposo, G., Sens, P., Lamaze, C. and Nassoy, P. (2011) Cells respond to mechanical stress by rapid disassembly of caveolae. *Cell* 144 (3), 402-13.

Sitbon, O., Channick, R., Chin, K. M., Frey, A., Gaine, S., Galie, N., Ghofrani, H. A., Hoeper, M. M., Lang, I. M., Preiss, R., Rubin, L. J., Di Scala, L., Tapson, V., Adzerikho, I., Liu, J., Moiseeva, O., Zeng, X., Simonneau, G., McLaughlin, V. V. and Investigators, G. (2015) Selexipag for the Treatment of Pulmonary Arterial Hypertension. *N Engl J Med* 373 (26), 2522-33.

Sitbon, O., Humbert, M., Nunes, H., Parent, F., Garcia, G., Herve, P., Rainisio, M. and Simonneau, G. (2002) Long-term intravenous epoprostenol infusion in

primary pulmonary hypertension: prognostic factors and survival. *J Am Coll Cardiol* 40 (4), 780-8.

Sobota, R. M., Muller, P. J., Heinrich, P. C. and Schaper, F. (2008) Prostaglandin E1 inhibits IL-6-induced MCP-1 expression by interfering specifically in IL-6-dependent ERK1/2, but not STAT3, activation. *Biochem J* 412 (1), 65-72.

Somers, W., Stahl, M. and Seehra, J. S. (1997) 1.9 A crystal structure of interleukin 6: implications for a novel mode of receptor dimerization and signaling. *EMBO J* 16 (5), 989-97.

Soon, E., Crosby, A., Southwood, M., Yang, P., Tajsic, T., Toshner, M., Appleby, S., Shanahan, C. M., Bloch, K. D., Pepke-Zaba, J., Upton, P. and Morrell, N. W. (2015) Bone morphogenetic protein receptor type II deficiency and increased inflammatory cytokine production. A gateway to pulmonary arterial hypertension. *Am J Respir Crit Care Med* 192 (7), 859-72.

Soon, E., Holmes, A. M., Treacy, C. M., Doughty, N. J., Southgate, L., Machado, R. D., Trembath, R. C., Jennings, S., Barker, L., Nicklin, P., Walker, C., Budd, D. C., Pepke-Zaba, J. and Morrell, N. W. (2010) Elevated levels of inflammatory cytokines predict survival in idiopathic and familial pulmonary arterial hypertension. *Circulation* 122 (9), 920-7.

Soto-Velasquez, M., Alpsoy, A., Dykhuizen, E. C. and Watts, V. J. (2018) A Novel CRISPR/Cas9-Based Cellular Model to Explore Adenylyl Cyclase and Cyclic AMP Signaling. *Faseb Journal* 32 (1).

Sowa, G., Pypaert, M. and Sessa, W. C. (2001) Distinction between signaling mechanisms in lipid rafts vs. caveolae. *Proc Natl Acad Sci U S A* 98 (24), 14072-7.

Spiekerkoetter, E. (2016) *FK506 (Tacrolimus) in Pulmonary Arterial Hypertension (TransformPAH).* [Study record] October 5, 2016. https://clinicaltrials.gov/ct2/show/results/NCT01647945

Spiekerkoetter, E., Sung, Y. K., Sudheendra, D., Bill, M., Aldred, M. A., van de Veerdonk, M. C., Vonk Noordegraaf, A., Long-Boyle, J., Dash, R., Yang, P. C., Lawrie, A., Swift, A. J., Rabinovitch, M. and Zamanian, R. T. (2015) Low-Dose FK506 (Tacrolimus) in End-Stage Pulmonary Arterial Hypertension. *Am J Respir Crit Care Med* 192 (2), 254-7.

Spiekerkoetter, E., Tian, X., Cai, J., Hopper, R. K., Sudheendra, D., Li, C. G., El-Bizri, N., Sawada, H., Haghighat, R., Chan, R., Haghighat, L., de Jesus Perez, V., Wang, L., Reddy, S., Zhao, M., Bernstein, D., Solow-Cordero, D. E., Beachy, P. A., Wandless, T. J., Ten Dijke, P. and Rabinovitch, M. (2013) FK506 activates BMPR2, rescues endothelial dysfunction, and reverses pulmonary hypertension. *J Clin Invest* 123 (8), 3600-13.

Srinivasan, B., Kolli, A. R., Esch, M. B., Abaci, H. E., Shuler, M. L. and Hickman, J. J. (2015) TEER measurement techniques for in vitro barrier model systems. *J Lab Autom* 20 (2), 107-26.

Stahl, N., Farruggella, T. J., Boulton, T. G., Zhong, Z., Darnell, J. E., Jr. and Yancopoulos, G. D. (1995) Choice of STATs and other substrates specified by modular tyrosine-based motifs in cytokine receptors. *Science* 267 (5202), 1349-53.

Star, G. P., Giovinazzo, M. and Langleben, D. (2013) ALK2 and BMPR2 knockdown and endothelin-1 production by pulmonary microvascular endothelial cells. *Microvasc Res* 85, 46-53.

Stearman, R. S., Cornelius, A. R., Lu, X., Conklin, D. S., Del Rosario, M. J., Lowe, A. M., Elos, M. T., Fettig, L. M., Wong, R. E., Hara, N., Cogan, J. D., Phillips, J. A., 3rd, Taylor, M. R., Graham, B. B., Tuder, R. M., Loyd, J. E. and Geraci, M. W. (2014) Functional prostacyclin synthase promoter polymorphisms. Impact in pulmonary arterial hypertension. *Am J Respir Crit Care Med* 189 (9), 1110-20.

Steiner, M. K., Syrkina, O. L., Kolliputi, N., Mark, E. J., Hales, C. A. and Waxman, A. B. (2009) Interleukin-6 overexpression induces pulmonary hypertension. *Circ Res* 104 (2), 236-44, 28p following 244.

Stenmark, K. R., Fagan, K. A. and Frid, M. G. (2006) Hypoxia-induced pulmonary vascular remodeling: cellular and molecular mechanisms. *Circ Res* 99 (7), 675-91.

Strange, G., Lau, E. M., Giannoulatou, E., Corrigan, C., Kotlyar, E., Kermeen, F., Williams, T., Celermajer, D. S., Dwyer, N., Whitford, H., Wrobel, J. P., Feenstra, J., Lavender, M., Whyte, K., Collins, N., Steele, P., Proudman, S., Thakkar, V., Keating, D., Keogh, A. and Registry, P. (2018) Survival of Idiopathic Pulmonary Arterial Hypertension Patients in the Modern Era in Australia and New Zealand. *Heart Lung Circ* 27 (11), 1368-1375.

Suessmuth, Y., Elliott, J., Percy, M. J., Inami, M., Attal, H., Harrison, C. N., Inokuchi, K., McMullin, M. F. and Johnston, J. A. (2009) A new polycythaemia vera-associated SOCS3 SH2 mutant (SOCS3F136L) cannot regulate erythropoietin responses. *Br J Haematol* 147 (4), 450-8.

Sui, X. F., Kiser, T. D., Hyun, S. W., Angelini, D. J., Del Vecchio, R. L., Young, B. A., Hasday, J. D., Romer, L. H., Passaniti, A., Tonks, N. K. and Goldblum, S. E. (2005) Receptor protein tyrosine phosphatase micro regulates the paracellular pathway in human lung microvascular endothelia. *Am J Pathol* 166 (4), 1247-58.

Sun, D., Li, Z., Rew, Y., Gribble, M., Bartberger, M. D., Beck, H. P., Canon, J., Chen, A., Chen, X., Chow, D., Deignan, J., Duquette, J., Eksterowicz, J., Fisher, B., Fox, B. M., Fu, J., Gonzalez, A. Z., Gonzalez-Lopez De Turiso, F., Houze, J. B., Huang, X., Jiang, M., Jin, L., Kayser, F., Liu, J. J., Lo, M. C., Long, A. M., Lucas, B., McGee, L. R., McIntosh, J., Mihalic, J., Oliner, J. D., Osgood, T., Peterson, M. L., Roveto, P., Saiki, A. Y., Shaffer, P., Toteva, M., Wang, Y., Wang, Y. C., Wortman, S., Yakowec, P., Yan, X., Ye, Q., Yu, D., Yu, M., Zhao, X., Zhou, J., Zhu, J., Olson, S. H. and Medina, J. C. (2014) Discovery of AMG 232, a potent, selective, and orally bioavailable MDM2-p53 inhibitor in clinical development. *J Med Chem* 57 (4), 1454-72.

Sun, N. and Zhao, H. (2013) Transcription activator-like effector nucleases (TALENs): a highly efficient and versatile tool for genome editing. *Biotechnol Bioeng* 110 (7), 1811-21.

Sungprem, K., Khongphatthanayothin, A., Kiettisanpipop, P., Chotivitayatarakorn, P., Poovorawan, Y. and Lertsapcharoen, P. (2009) Serum level of soluble intercellular adhesion molecule-1 correlates with pulmonary arterial pressure in children with congenital heart disease. *Pediatr Cardiol* 30 (4), 472-6.

Suttorp, M., Bornhauser, M., Metzler, M., Millot, F. and Schleyer, E. (2018) Pharmacology and pharmacokinetics of imatinib in pediatric patients. *Expert Rev Clin Pharmacol* 11 (3), 219-231.

Sztuka, K. and Jasinska-Stroschein, M. (2017) Animal models of pulmonary arterial hypertension: A systematic review and meta-analysis of data from 6126 animals. *Pharmacol Res* 125 (Pt B), 201-214.

Tachikawa, M., Morone, N., Senju, Y., Sugiura, T., Hanawa-Suetsugu, K., Mochizuki, A. and Suetsugu, S. (2017) Measurement of caveolin-1 densities in the cell membrane for quantification of caveolar deformation after exposure to hypotonic membrane tension. *Sci Rep* 7 (1), 7794.

Takahashi, M., Galligan, C., Tessarollo, L. and Yoshimura, T. (2009) Monocyte chemoattractant protein-1 (MCP-1), not MCP-3, is the primary chemokine required for monocyte recruitment in mouse peritonitis induced with thioglycollate or zymosan A. *J Immunol* 183 (5), 3463-71.

Takatsuki, S., Wagner, B. D. and Ivy, D. D. (2012) B-type natriuretic peptide and amino-terminal pro-B-type natriuretic peptide in pediatric patients with pulmonary arterial hypertension. *Congenit Heart Dis* 7 (3), 259-67.

Takayama, K., Sukhova, G. K., Chin, M. T. and Libby, P. (2006) A novel prostaglandin E receptor 4-associated protein participates in antiinflammatory signaling. *Circ Res* 98 (4), 499-504.

Taleb, S., Romain, M., Ramkhelawon, B., Uyttenhove, C., Pasterkamp, G., Herbin, O., Esposito, B., Perez, N., Yasukawa, H., Van Snick, J., Yoshimura, A., Tedgui, A. and Mallat, Z. (2009) Loss of SOCS3 expression in T cells reveals a regulatory role for interleukin-17 in atherosclerosis. *J Exp Med* 206 (10), 2067-77.

Tamura, Y., Phan, C., Tu, L., Le Hiress, M., Thuillet, R., Jutant, E. M., Fadel, E., Savale, L., Huertas, A., Humbert, M. and Guignabert, C. (2018) Ectopic upregulation of membrane-bound IL6R drives vascular remodeling in pulmonary arterial hypertension. *J Clin Invest* 128 (5), 1956-1970.

Taniguchi, K., Wu, L. W., Grivennikov, S. I., de Jong, P. R., Lian, I., Yu, F. X., Wang, K., Ho, S. B., Boland, B. S., Chang, J. T., Sandborn, W. J., Hardiman, G., Raz, E., Maehara, Y., Yoshimura, A., Zucman-Rossi, J., Guan, K. L. and Karin, M. (2015) A gp130-Src-YAP module links inflammation to epithelial regeneration. *Nature* 519 (7541), 57-62.

Tapson, V. F., Torres, F., Kermeen, F., Keogh, A. M., Allen, R. P., Frantz, R. P., Badesch, D. B., Frost, A. E., Shapiro, S. M., Laliberte, K., Sigman, J., Arneson, C. and Galie, N. (2012) Oral treprostinil for the treatment of pulmonary arterial hypertension in patients on background endothelin receptor antagonist and/or phosphodiesterase type 5 inhibitor therapy (the FREEDOM-C study): a randomized controlled trial. *Chest* 142 (6), 1383-90.

Taylor, P. C. (2019) Clinical efficacy of launched JAK inhibitors in rheumatoid arthritis. *Rheumatology (Oxford)* 58 (Supplement_1), i17-i26.

Teichert-Kuliszewska, K., Kutryk, M. J., Kuliszewski, M. A., Karoubi, G., Courtman, D. W., Zucco, L., Granton, J. and Stewart, D. J. (2006) Bone morphogenetic protein receptor-2 signaling promotes pulmonary arterial endothelial cell survival: implications for loss-of-function mutations in the pathogenesis of pulmonary hypertension. *Circ Res* 98 (2), 209-17.

ten Dijke, P., Yamashita, H., Ichijo, H., Franzen, P., Laiho, M., Miyazono, K. and Heldin, C. H. (1994a) Characterization of type I receptors for transforming growth factor-beta and activin. *Science* 264 (5155), 101-4.

ten Dijke, P., Yamashita, H., Sampath, T. K., Reddi, A. H., Estevez, M., Riddle, D. L., Ichijo, H., Heldin, C. H. and Miyazono, K. (1994b) Identification of type I receptors for osteogenic protein-1 and bone morphogenetic protein-4. *J Biol Chem* 269 (25), 16985-8.

ThermoFisherSCIENTIFIC (2019) *Factors Influencing Transfection Efficiency.* https://www.thermofisher.com/uk/en/home/references/gibco-cell-culture-basics/transfection-basics/factors-influencing-transfection-efficiency.html

Toms, A. V., Deshpande, A., McNally, R., Jeong, Y., Rogers, J. M., Kim, C. U., Gruner, S. M., Ficarro, S. B., Marto, J. A., Sattler, M., Griffin, J. D. and Eck, M. J. (2013) Structure of a pseudokinase-domain switch that controls oncogenic activation of Jak kinases. *Nat Struct Mol Biol* 20 (10), 1221-3.

Tonelli, A. R., Arelli, V., Minai, O. A., Newman, J., Bair, N., Heresi, G. A. and Dweik, R. A. (2013) Causes and circumstances of death in pulmonary arterial hypertension. *Am J Respir Crit Care Med* 188 (3), 365-9.

Tripathi, S. K., Chen, Z., Larjo, A., Kanduri, K., Nousiainen, K., Aijo, T., Ricano-Ponce, I., Hrdlickova, B., Tuomela, S., Laajala, E., Salo, V., Kumar, V., Wijmenga, C., Lahdesmaki, H. and Lahesmaa, R. (2017) Genome-wide Analysis of STAT3-Mediated Transcription during Early Human Th17 Cell Differentiation. *Cell Rep* 19 (9), 1888-1901.

Tsuboi, K., Sugimoto, Y. and Ichikawa, A. (2002) Prostanoid receptor subtypes. *Prostaglandins Other Lipid Mediat* 68-69, 535-56.

Tsuji, F., Yoshimi, M., Katsuta, O., Takai, M., Ishihara, K. and Aono, H. (2009) Point mutation of tyrosine 759 of the IL-6 family cytokine receptor, gp130, augments collagen-induced arthritis in DBA/1J mice. *BMC Musculoskelet Disord* 10, 23.

Tuder, R. M. (2017) Pulmonary vascular remodeling in pulmonary hypertension. *Cell Tissue Res* 367 (3), 643-649.

Tuder, R. M., Chacon, M., Alger, L., Wang, J., Taraseviciene-Stewart, L., Kasahara, Y., Cool, C. D., Bishop, A. E., Geraci, M., Semenza, G. L., Yacoub, M., Polak, J. M. and Voelkel, N. F. (2001) Expression of angiogenesis-related molecules in plexiform lesions in severe pulmonary hypertension: evidence for a process of disordered angiogenesis. *J Pathol* 195 (3), 367-74.

Tuder, R. M., Cool, C. D., Geraci, M. W., Wang, J., Abman, S. H., Wright, L., Badesch, D. and Voelkel, N. F. (1999) Prostacyclin synthase expression is decreased in lungs from patients with severe pulmonary hypertension. *Am J Respir Crit Care Med* 159 (6), 1925-32.

Tuder, R. M., Groves, B., Badesch, D. B. and Voelkel, N. F. (1994) Exuberant endothelial cell growth and elements of inflammation are present in plexiform lesions of pulmonary hypertension. *Am J Pathol* 144 (2), 275-85.

Ueki, K., Kondo, T. and Kahn, C. R. (2004) Suppressor of cytokine signaling 1 (SOCS-1) and SOCS-3 cause insulin resistance through inhibition of tyrosine phosphorylation of insulin receptor substrate proteins by discrete mechanisms. *Mol Cell Biol* 24 (12), 5434-46.

Ueno, H., Shibasaki, T., Iwanaga, T., Takahashi, K., Yokoyama, Y., Liu, L. M., Yokoi, N., Ozaki, N., Matsukura, S., Yano, H. and Seino, S. (2001) Characterization of the gene EPAC2: structure, chromosomal localization, tissue expression, and identification of the liver-specific isoform. *Genomics* 78 (1-2), 91-8.

van Wolferen, S. A., Marcus, J. T., Boonstra, A., Marques, K. M., Bronzwaer, J. G., Spreeuwenberg, M. D., Postmus, P. E. and Vonk-Noordegraaf, A. (2007) Prognostic value of right ventricular mass, volume, and function in idiopathic pulmonary arterial hypertension. *Eur Heart J* 28 (10), 1250-7.

Vane, J. and Corin, R. E. (2003) Prostacyclin: a vascular mediator. *Eur J Vasc Endovasc Surg* 26 (6), 571-8.

Vane, J. R., Anggard, E. E. and Botting, R. M. (1990) Regulatory functions of the vascular endothelium. *N Engl J Med* 323 (1), 27-36.

Vane, J. R. and Botting, R. M. (1995) Pharmacodynamic profile of prostacyclin. *Am J Cardiol* 75 (3), 3A-10A.

VanRenterghem, B., Browning, M. D. and Maller, J. L. (1994) Regulation of mitogen-activated protein kinase activation by protein kinases A and C in a cell-free system. *J Biol Chem* 269 (40), 24666-72.

Vijay, S. K., Mishra, M., Kumar, H. and Tripathi, K. (2009) Effect of pioglitazone and rosiglitazone on mediators of endothelial dysfunction, markers of angiogenesis and inflammatory cytokines in type-2 diabetes. *Acta Diabetol* 46 (1), 27-33.

Vitali, S. H., Hansmann, G., Rose, C., Fernandez-Gonzalez, A., Scheid, A., Mitsialis, S. A. and Kourembanas, S. (2014) The Sugen 5416/hypoxia mouse model of pulmonary hypertension revisited: long-term follow-up. *Pulm Circ* 4 (4), 619-29.

Voelkel, N. F. and Gomez-Arroyo, J. (2014) The role of vascular endothelial growth factor in pulmonary arterial hypertension. The angiogenesis paradox. *Am J Respir Cell Mol Biol* 51 (4), 474-84.

Voelkel, N. F., Quaife, R. A., Leinwand, L. A., Barst, R. J., McGoon, M. D., Meldrum, D. R., Dupuis, J., Long, C. S., Rubin, L. J., Smart, F. W., Suzuki, Y. J., Gladwin, M., Denholm, E. M., Gail, D. B., National Heart, L., Blood Institute Working Group on, C. and Molecular Mechanisms of Right Heart, F. (2006) Right ventricular function and failure: report of a National Heart, Lung, and Blood Institute working group on cellular and molecular mechanisms of right heart failure. *Circulation* 114 (17), 1883-91.

Waldner, M. J., Wirtz, S., Jefremow, A., Warntjen, M., Neufert, C., Atreya, R., Becker, C., Weigmann, B., Vieth, M., Rose-John, S. and Neurath, M. F. (2010) VEGF receptor signaling links inflammation and tumorigenesis in colitis-associated cancer. *J Exp Med* 207 (13), 2855-68.

Wang, Q., Zuo, X. R., Wang, Y. Y., Xie, W. P., Wang, H. and Zhang, M. (2013) Monocrotaline-induced pulmonary arterial hypertension is attenuated by TNF-alpha antagonists via the suppression of TNF-alpha expression and NF-kappaB pathway in rats. *Vascul Pharmacol* 58 (1-2), 71-7.

Wang, Y. and Fuller, G. M. (1994) Phosphorylation and internalization of gp130 occur after IL-6 activation of Jak2 kinase in hepatocytes. *Mol Biol Cell* 5 (7), 819-28.

Wang, Y. and Fuller, G. M. (1995) Interleukin-6 and ciliary neurotrophic factor trigger janus kinase activation and early gene response in rat hepatocytes. *Gene* 162 (2), 285-9.

Waxman, A. B., McElderry, H. T., Gomberg-Maitland, M., Burke, M. C., Ross, E. L., Bersohn, M. M., Pangarkar, S. S., Tarver, J. H., Zwicke, D. L., Feldman, J. P., Chakinala, M. M., Frantz, R. P., Thompson, G. B., Torres, F., Rauck, R. L., Clagg,

K., Durst, L., Li, P., Morris, M., Southall, K. L., Peterson, L. and Bourge, R. C. (2017) Totally Implantable IV Treprostinil Therapy in Pulmonary Hypertension Assessment of the Implantation Procedure. *Chest* 152 (6), 1128-1134.

Waxman, A. B. and Zamanian, R. T. (2013) Pulmonary arterial hypertension: new insights into the optimal role of current and emerging prostacyclin therapies. *Am J Cardiol* 111 (5 Suppl), 1A-16A; quiz 17A-19A.

Wei, D., Le, X., Zheng, L., Wang, L., Frey, J. A., Gao, A. C., Peng, Z., Huang, S., Xiong, H. Q., Abbruzzese, J. L. and Xie, K. (2003a) Stat3 activation regulates the expression of vascular endothelial growth factor and human pancreatic cancer angiogenesis and metastasis. *Oncogene* 22 (3), 319-29.

Wei, L. H., Chou, C. H., Chen, M. W., Rose-John, S., Kuo, M. L., Chen, S. U. and Yang, Y. S. (2013) The role of IL-6 trans-signaling in vascular leakage: implications for ovarian hyperstimulation syndrome in a murine model. *J Clin Endocrinol Metab* 98 (3), E472-84.

Wei, L. H., Kuo, M. L., Chen, C. A., Chou, C. H., Lai, K. B., Lee, C. N. and Hsieh, C. Y. (2003b) Interleukin-6 promotes cervical tumor growth by VEGF-dependent angiogenesis via a STAT3 pathway. *Oncogene* 22 (10), 1517-27.

Whittle, B. J. and Moncada, S. (1984) Antithrombotic assessment and clinical potential of prostacyclin analogues. *Prog Med Chem* 21, 237-79.

Whittle, B. J., Silverstein, A. M., Mottola, D. M. and Clapp, L. H. (2012) Binding and activity of the prostacyclin receptor (IP) agonists, treprostinil and iloprost, at human prostanoid receptors: treprostinil is a potent DP1 and EP2 agonist. *Biochem Pharmacol* 84 (1), 68-75.

Wiejak, J., Dunlop, J., Mackay, S. P. and Yarwood, S. J. (2013) Flavanoids induce expression of the suppressor of cytokine signalling 3 (SOCS3) gene and suppress IL-6-activated signal transducer and activator of transcription 3 (STAT3) activation in vascular endothelial cells. *Biochem J* 454 (2), 283-93.

Wiejak, J., Dunlop, J. and Yarwood, S. J. (2014) The role of c-Jun in controlling the EPAC1-dependent induction of the SOCS3 gene in HUVECs. *FEBS Lett* 588 (9), 1556-61.

Wiejak, J., van Basten, B., Luchowska-Stanska, U., Hamilton, G. and Yarwood, S. J. (2019) The novel exchange protein activated by cyclic AMP 1 (EPAC1) agonist, I942, regulates inflammatory gene expression in human umbilical vascular endothelial cells (HUVECs). *Biochim Biophys Acta Mol Cell Res* 1866 (2), 264-276.

Williams, J. J. L., Alotaiq, N., Mullen, W., Burchmore, R., Liu, L., Baillie, G. S., Schaper, F., Pilch, P. F. and Palmer, T. M. (2018) Interaction of suppressor of cytokine signalling 3 with cavin-1 links SOCS3 function and cavin-1 stability. *Nat Commun* 9 (1), 168.

Woodrick, R. and Ruderman, E. M. (2010) Anti-interleukin-6 therapy in rheumatoid arthritis. *Bull NYU Hosp Jt Dis* 68 (3), 211-7.

Woodward, D. F., Jones, R. L. and Narumiya, S. (2011) International Union of Basic and Clinical Pharmacology. LXXXIII: classification of prostanoid receptors, updating 15 years of progress. *Pharmacol Rev* 63 (3), 471-538.

Woolson, H. D., Thomson, V. S., Rutherford, C., Yarwood, S. J. and Palmer, T. M. (2009) Selective inhibition of cytokine-activated extracellular signal-regulated

kinase by cyclic AMP via Epac1-dependent induction of suppressor of cytokine signalling-3. *Cell Signal* 21 (11), 1706-15.

Wragg, D., Techer, M. A., Canale-Tabet, K., Basso, B., Bidanel, J. P., Labarthe, E., Bouchez, O., Le Conte, Y., Clemencet, J., Delatte, H. and Vignal, A. (2018) Autosomal and Mitochondrial Adaptation Following Admixture: A Case Study on the Honeybees of Reunion Island. *Genome Biol Evol* 10 (1), 220-238.

Wu, C. X., Xu, A., Zhang, C. C., Olson, P., Chen, L., Lee, T. K., Cheung, T. T., Lo, C. M. and Wang, X. Q. (2017) Notch Inhibitor PF-03084014 Inhibits Hepatocellular Carcinoma Growth and Metastasis via Suppression of Cancer Stemness due to Reduced Activation of Notch1-Stat3. *Mol Cancer Ther* 16 (8), 1531-1543.

Wu, J., Dent, P., Jelinek, T., Wolfman, A., Weber, M. J. and Sturgill, T. W. (1993) Inhibition of the EGF-activated MAP kinase signaling pathway by adenosine 3',5'-monophosphate. *Science* 262 (5136), 1065-9.

Wunderlich, C., Schmeisser, A., Heerwagen, C., Ebner, B., Schober, K., Braun-Dullaeus, R. C., Schwencke, C., Kasper, M., Morawietz, H. and Strasser, R. H. (2008) Chronic NOS inhibition prevents adverse lung remodeling and pulmonary arterial hypertension in caveolin-1 knockout mice. *Pulm Pharmacol Ther* 21 (3), 507-15.

Xia, X. D., Lee, J., Khan, S., Ye, L., Li, Y. and Dong, L. (2016) Suppression of Phosphatidylinositol 3-Kinase/Akt Signaling Attenuates Hypoxia-Induced Pulmonary Hypertension Through the Downregulation of Lysyl Oxidase. *DNA Cell Biol* 35 (10), 599-606.

Xiang, S., Dong, N. G., Liu, J. P., Wang, Y., Shi, J. W., Wei, Z. J., Hu, X. J. and Gong, L. (2013) Inhibitory effects of suppressor of cytokine signaling 3 on inflammatory cytokine expression and migration and proliferation of IL-6/IFN-gamma-induced vascular smooth muscle cells. *J Huazhong Univ Sci Technolog Med Sci* 33 (5), 615-22.

Xu, S., Grande, F., Garofalo, A. and Neamati, N. (2013) Discovery of a novel orally active small-molecule gp130 inhibitor for the treatment of ovarian cancer. *Mol Cancer Ther* 12 (6), 937-49.

Xu, W., Kaneko, F. T., Zheng, S., Comhair, S. A., Janocha, A. J., Goggans, T., Thunnissen, F. B., Farver, C., Hazen, S. L., Jennings, C., Dweik, R. A., Arroliga, A. C. and Erzurum, S. C. (2004) Increased arginase II and decreased NO synthesis in endothelial cells of patients with pulmonary arterial hypertension. *FASEB J* 18 (14), 1746-8.

Xu, Y., Gu, Q., Liu, N., Yan, Y., Yang, X., Hao, Y. and Qu, C. (2017) PPARgamma Alleviates Right Ventricular Failure Secondary to Pulmonary Arterial Hypertension in Rats. *Int Heart J*.

Yamamoto, K. and Ando, J. (2015) Vascular endothelial cell membranes differentiate between stretch and shear stress through transitions in their lipid phases. *Am J Physiol Heart Circ Physiol* 309 (7), H1178-85.

Yamamoto, T., Sekine, Y., Kashima, K., Kubota, A., Sato, N., Aoki, N. and Matsuda, T. (2002) The nuclear isoform of protein-tyrosine phosphatase TC-PTP regulates interleukin-6-mediated signaling pathway through STAT3 dephosphorylation. *Biochem Biophys Res Commun* 297 (4), 811-7.

Yanagisawa, M., Kurihara, H., Kimura, S., Tomobe, Y., Kobayashi, M., Mitsui, Y., Yazaki, Y., Goto, K. and Masaki, T. (1988) A novel potent vasoconstrictor peptide produced by vascular endothelial cells. *Nature* 332 (6163), 411-5.

Yang, X., Long, L., Southwood, M., Rudarakanchana, N., Upton, P. D., Jeffery, T. K., Atkinson, C., Chen, H., Trembath, R. C. and Morrell, N. W. (2005) Dysfunctional Smad signaling contributes to abnormal smooth muscle cell proliferation in familial pulmonary arterial hypertension. *Circ Res* 96 (10), 1053-63.

Yang, Z., Hackshaw, A., Feng, Q., Fu, X., Zhang, Y., Mao, C. and Tang, J. (2017) Comparison of gefitinib, erlotinib and afatinib in non-small cell lung cancer: A meta-analysis. *Int J Cancer* 140 (12), 2805-2819.

Yao, J. S., Zhai, W., Young, W. L. and Yang, G. Y. (2006) Interleukin-6 triggers human cerebral endothelial cells proliferation and migration: the role for KDR and MMP-9. *Biochem Biophys Res Commun* 342 (4), 1396-404.

Yao, Y., Li, H., Da, X., He, Z., Tang, B., Li, Y., Hu, C., Xu, C., Chen, Q. and Wang, Q. K. (2019) SUMOylation of Vps34 by SUMO1 promotes phenotypic switching of vascular smooth muscle cells by activating autophagy in pulmonary arterial hypertension. *Pulm Pharmacol Ther* 55, 38-49.

Yarwood, S. J., Borland, G., Sands, W. A. and Palmer, T. M. (2008) Identification of CCAAT/enhancer-binding proteins as exchange protein activated by cAMP-activated transcription factors that mediate the induction of the SOCS-3 gene. *J Biol Chem* 283 (11), 6843-53.

Yasukawa, H., Ohishi, M., Mori, H., Murakami, M., Chinen, T., Aki, D., Hanada, T., Takeda, K., Akira, S., Hoshijima, M., Hirano, T., Chien, K. R. and Yoshimura, A. (2003) IL-6 induces an anti-inflammatory response in the absence of SOCS3 in macrophages. *Nat Immunol* 4 (6), 551-6.

Yeow, I., Howard, G., Chadwick, J., Mendoza-Topaz, C., Hansen, C. G., Nichols, B. J. and Shvets, E. (2017) EHD Proteins Cooperate to Generate Caveolar Clusters and to Maintain Caveolae during Repeated Mechanical Stress. *Curr Biol* 27 (19), 2951-2962 e5.

Yin, Y., Liu, W., Ji, G. and Dai, Y. (2013) The essential role of p38 MAPK in mediating the interplay of oxLDL and IL-10 in regulating endothelial cell apoptosis. *Eur J Cell Biol* 92 (4-5), 150-9.

Yokoyama, C., Yabuki, T., Shimonishi, M., Wada, M., Hatae, T., Ohkawara, S., Takeda, J., Kinoshita, T., Okabe, M. and Tanabe, T. (2002) Prostacyclin-deficient mice develop ischemic renal disorders, including nephrosclerosis and renal infarction. *Circulation* 106 (18), 2397-403.

Yu, J., Taylor, L., Wilson, J., Comhair, S., Erzurum, S. and Polgar, P. (2013) Altered expression and signal transduction of endothelin-1 receptors in heritable and idiopathic pulmonary arterial hypertension. *J Cell Physiol* 228 (2), 322-9.

Yu, P. B., Deng, D. Y., Beppu, H., Hong, C. C., Lai, C., Hoyng, S. A., Kawai, N. and Bloch, K. D. (2008) Bone morphogenetic protein (BMP) type II receptor is required for BMP-mediated growth arrest and differentiation in pulmonary artery smooth muscle cells. *J Biol Chem* 283 (7), 3877-88.

Zaiman, A. L., Podowski, M., Medicherla, S., Gordy, K., Xu, F., Zhen, L., Shimoda, L. A., Neptune, E., Higgins, L., Murphy, A., Chakravarty, S., Protter, A., Sehgal, P. B., Champion, H. C. and Tuder, R. M. (2008) Role of the TGF-beta/Alk5 signaling

pathway in monocrotaline-induced pulmonary hypertension. *Am J Respir Crit Care Med* 177 (8), 896-905.

Zakrzewicz, A., Kouri, F. M., Nejman, B., Kwapiszewska, G., Hecker, M., Sandu, R., Dony, E., Seeger, W., Schermuly, R. T., Eickelberg, O. and Morty, R. E. (2007) The transforming growth factor-beta/Smad2,3 signalling axis is impaired in experimental pulmonary hypertension. *Eur Respir J* 29 (6), 1094-104.

Zegeye, M. M., Lindkvist, M., Falker, K., Kumawat, A. K., Paramel, G., Grenegard, M., Sirsjo, A. and Ljungberg, L. U. (2018) Activation of the JAK/STAT3 and PI3K/AKT pathways are crucial for IL-6 trans-signaling-mediated pro-inflammatory response in human vascular endothelial cells. *Cell Commun Signal* 16 (1), 55.

Zeng, Z., Yao, J., Li, Y., Xue, Y., Zou, Y., Shu, Z. and Jiao, Z. (2018) Anti-apoptosis endothelial cell-secreted microRNA-195-5p promotes pulmonary arterial smooth muscle cell proliferation and migration in pulmonary arterial hypertension. *J Cell Biochem* 119 (2), 2144-2155.

Zhang, B., Qiangba, Y., Shang, P., Lu, Y., Yang, Y., Wang, Z. and Zhang, H. (2016a) Gene expression of vascular endothelial growth factor A and hypoxic adaptation in Tibetan pig. *J Anim Sci Biotechnol* 7, 21.

Zhang, D., Sun, M., Samols, D. and Kushner, I. (1996) STAT3 participates in transcriptional activation of the C-reactive protein gene by interleukin-6. *J Biol Chem* 271 (16), 9503-9.

Zhang, D., Wang, G., Han, D., Zhang, Y., Xu, J., Lu, J., Li, S., Xie, X., Liu, L., Dong, L. and Li, M. (2014) Activation of PPAR-gamma ameliorates pulmonary arterial hypertension via inducing heme oxygenase-1 and p21(WAF1): an in vivo study in rats. *Life Sci* 98 (1), 39-43.

Zhang, H., Li, X., Huang, J., Li, H., Su, Z. and Wang, J. (2016b) Comparative Efficacy and Safety of Prostacyclin Analogs for Pulmonary Arterial Hypertension: A Network Meta-Analysis. *Medicine (Baltimore)* 95 (4), e2575.

Zhang, S., Fantozzi, I., Tigno, D. D., Yi, E. S., Platoshyn, O., Thistlethwaite, P. A., Kriett, J. M., Yung, G., Rubin, L. J. and Yuan, J. X. (2003) Bone morphogenetic proteins induce apoptosis in human pulmonary vascular smooth muscle cells. *Am J Physiol Lung Cell Mol Physiol* 285 (3), L740-54.

Zhang, X. H., Zhou, S. Y., Feng, R., Wang, Y. Z., Kong, Y., Zhou, Y., Zhang, J. M., Wang, M., Zhao, J. Z., Wang, Q. M., Feng, F. E., Zhu, X. L., Wang, F. R., Wang, J. Z., Han, W., Chen, H., Xu, L. P., Liu, Y. R., Liu, K. Y. and Huang, X. J. (2016c) Increased prostacyclin levels inhibit the aggregation and activation of platelets via the PI3K-AKT pathway in prolonged isolated thrombocytopenia after allogeneic hematopoietic stem cell transplantation. *Thromb Res* 139, 1-9.

Zhang, Y., Musci, T. and Derynck, R. (1997) The tumor suppressor Smad4/DPC 4 as a central mediator of Smad function. *Curr Biol* 7 (4), 270-6.

Zhao, G., Zhu, G., Huang, Y., Zheng, W., Hua, J., Yang, S., Zhuang, J. and Ye, J. (2016) IL-6 mediates the signal pathway of JAK-STAT3-VEGF-C promoting growth, invasion and lymphangiogenesis in gastric cancer. *Oncol Rep* 35 (3), 1787-95.

Zhao, Y. Y., Liu, Y., Stan, R. V., Fan, L., Gu, Y., Dalton, N., Chu, P. H., Peterson, K., Ross, J., Jr. and Chien, K. R. (2002) Defects in caveolin-1 cause dilated cardiomyopathy and pulmonary hypertension in knockout mice. *Proc Natl Acad Sci U S A* 99 (17), 11375-80.

Zhao, Y. Y., Zhao, Y. D., Mirza, M. K., Huang, J. H., Potula, H. H., Vogel, S. M., Brovkovych, V., Yuan, J. X., Wharton, J. and Malik, A. B. (2009) Persistent eNOS activation secondary to caveolin-1 deficiency induces pulmonary hypertension in mice and humans through PKG nitration. *J Clin Invest* 119 (7), 2009-18.

Zheng, X., Zhang, W. and Hu, X. (2018) Different concentrations of lipopolysaccharide regulate barrier function through the PI3K/Akt signalling pathway in human pulmonary microvascular endothelial cells. *Sci Rep* 8 (1), 9963.

Zhou, C., Francis, C. M., Xu, N. and Stevens, T. (2018) The role of endothelial leak in pulmonary hypertension (2017 Grover Conference Series). *Pulm Circ* 8 (4), 2045894018798569.

Zhou, C., Townsley, M. I., Alexeyev, M., Voelkel, N. F. and Stevens, T. (2016) Endothelial hyperpermeability in severe pulmonary arterial hypertension: role of store-operated calcium entry. *Am J Physiol Lung Cell Mol Physiol* 311 (3), L560-9.

Zhuo, Y., Zeng, Q., Zhang, P., Li, G., Xie, Q. and Cheng, Y. (2017) VEGF Promoter Polymorphism Confers an Increased Risk of Pulmonary Arterial Hypertension in a Chinese Population. *Yonsei Med J* 58 (2), 305-311.

Zuckerbraun, B. S., George, P. and Gladwin, M. T. (2011) Nitrite in pulmonary arterial hypertension: therapeutic avenues in the setting of dysregulated arginine/nitric oxide synthase signalling. *Cardiovasc Res* 89 (3), 542-52.

Zuckerbraun, B. S., Stoyanovsky, D. A., Sengupta, R., Shapiro, R. A., Ozanich, B. A., Rao, J., Barbato, J. E. and Tzeng, E. (2007) Nitric oxide-induced inhibition of smooth muscle cell proliferation involves S-nitrosation and inactivation of RhoA. *Am J Physiol Cell Physiol* 292 (2), C824-31.

10. Appendices

10.1 Appendix 1: Vector summary for pLV[shRNA]-mCherry:T2A:Puro-U6>hSOCS3[shRNA#1]

Vector Summary

Vector ID	VB180808-1176mwy
Vector Name	pLV[shRNA]-mCherry:T2A:Puro-U6>hSOCS3[shRNA#1]
Date Created (Pacific Time)	2018-08-08
Vector Size	8338 bp
Vector Type	Mammalian shRNA Knockdown Lentiviral Vector
Inserted shRNA	hSOCS3[shRNA#1]
Target Sequence	CCACCTGGACTCCTATGAGAA
Inserted Marker	mCherry:T2A:Puro
Plasmid Copy Number	High
Antibiotic Resistance	Ampicillin
Cloning Host	Stbl3 (or alternative strain)

Vector Map

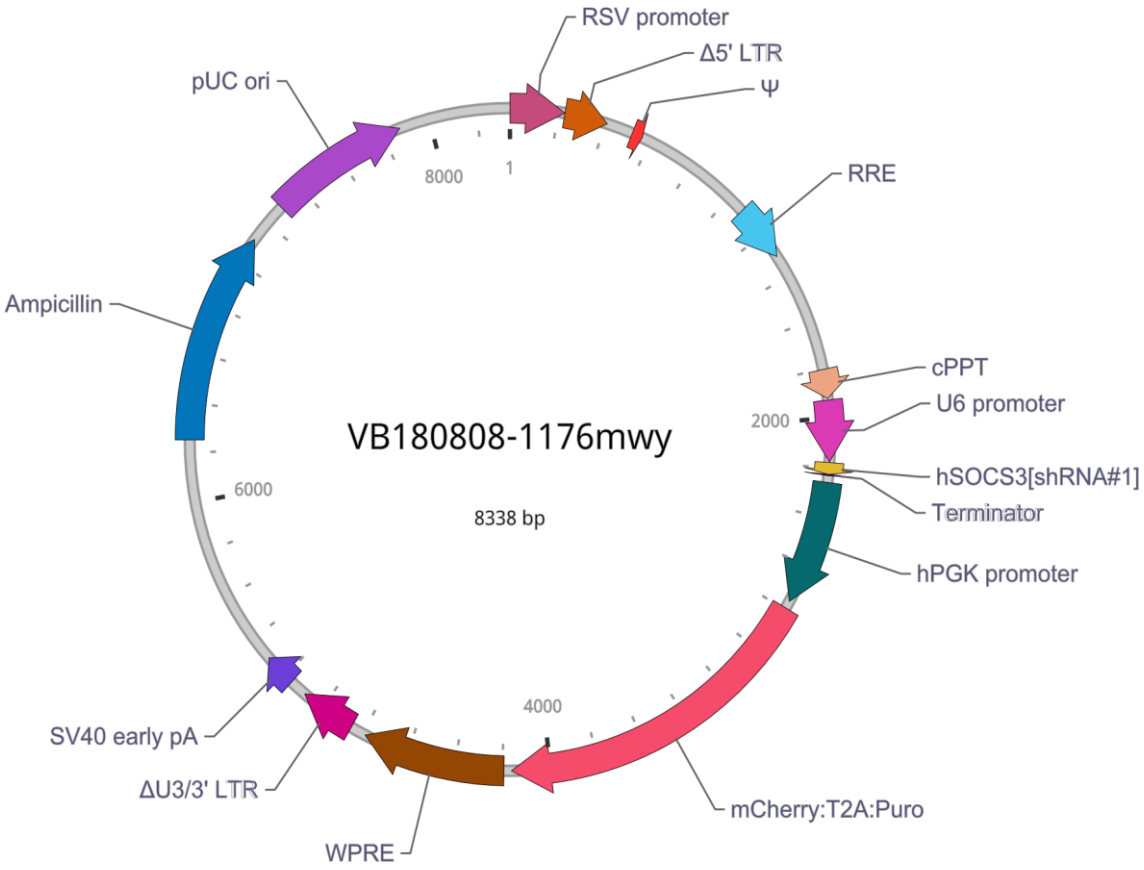

Vector Components

Name	Position	Size (bp)	Type	Description	Application notes
RSV promoter	1-229	229	Promoter	Rous sarcoma virus enhancer/promoter	Strong promoter; drives transcription of viral RNA in packaging cells.
Δ5' LTR	230-410	181	LTR	Truncated HIV-1 5' long terminal repeat	Allows transcription of viral RNA and its packaging into virus.
Ψ	521-565	45	Miscellaneous	HIV-1 packaging signal	Allows packaging of viral RNA into virus.

RRE	1075-1308	234	Miscellaneous	HIV-1 Rev response element	Rev protein binding site that allows Rev-dependent nuclear export of viral RNA during viral packaging.
cPPT	1803-1920	118	Miscellaneous	Central polypurine tract	Facilitates the nuclear import of HIV-1 cDNA through a central DNA flap.
U6 promoter	1927-2175	249	Promoter	Human U6 small nuclear 1 promoter	Pol III promoter; drives expression of small RNAs.
hSOCS3[shRNA#1]	2178-2225	48	shRNA	None	None
Terminator	2226-2230	5	terminator	Pol III transcription terminator	Allows transcription termination of small RNA transcribed by Pol III RNA polymerase.
hPGK promoter	2258-2762	505	Promoter	Human phosphoglycerate kinase 1 promoter	Medium-strength promoter.
mCherry:T2A:Puro	2793-4163	1371	ORF	mCherry and Puro linked by T2A	Allows cells to be visualized by red fluorescence and resistant to puromycin.
WPRE	4195-4792	598	Miscellaneous	Woodchuck hepatitis virus posttranscriptional regulatory element	Enhances viral RNA stability in packaging cells, leading to higher titer of packaged virus.

ΔU3/3' LTR	4858-5092	235	LTR	Truncated HIV-1 3' long terminal repeat	Allows packaging of viral RNA into virus; selfinactivates the 5' LTR by a copying mechanism during viral genome integration; contains polyadenylation signal for transcription termination.
SV40 early pA	5165-5299	135	PolyA_signal	Simian virus 40 early polyadenylation signal	Allows transcription termination and polyadenylation of mRNA transcribed by Pol II RNA polymerase.
Ampicillin	6253-7113	861	ORF	Ampicillin resistance gene	Allows E. coli to be resistant to ampicillin.
pUC ori	7284-7872	589	Rep_origin	pUC origin of replication	Facilitates plasmid replication in E. coli; regulates high-copy plasmid number (500-700).

Note: Components added by user are listed in bold red text.

Vector Sequence

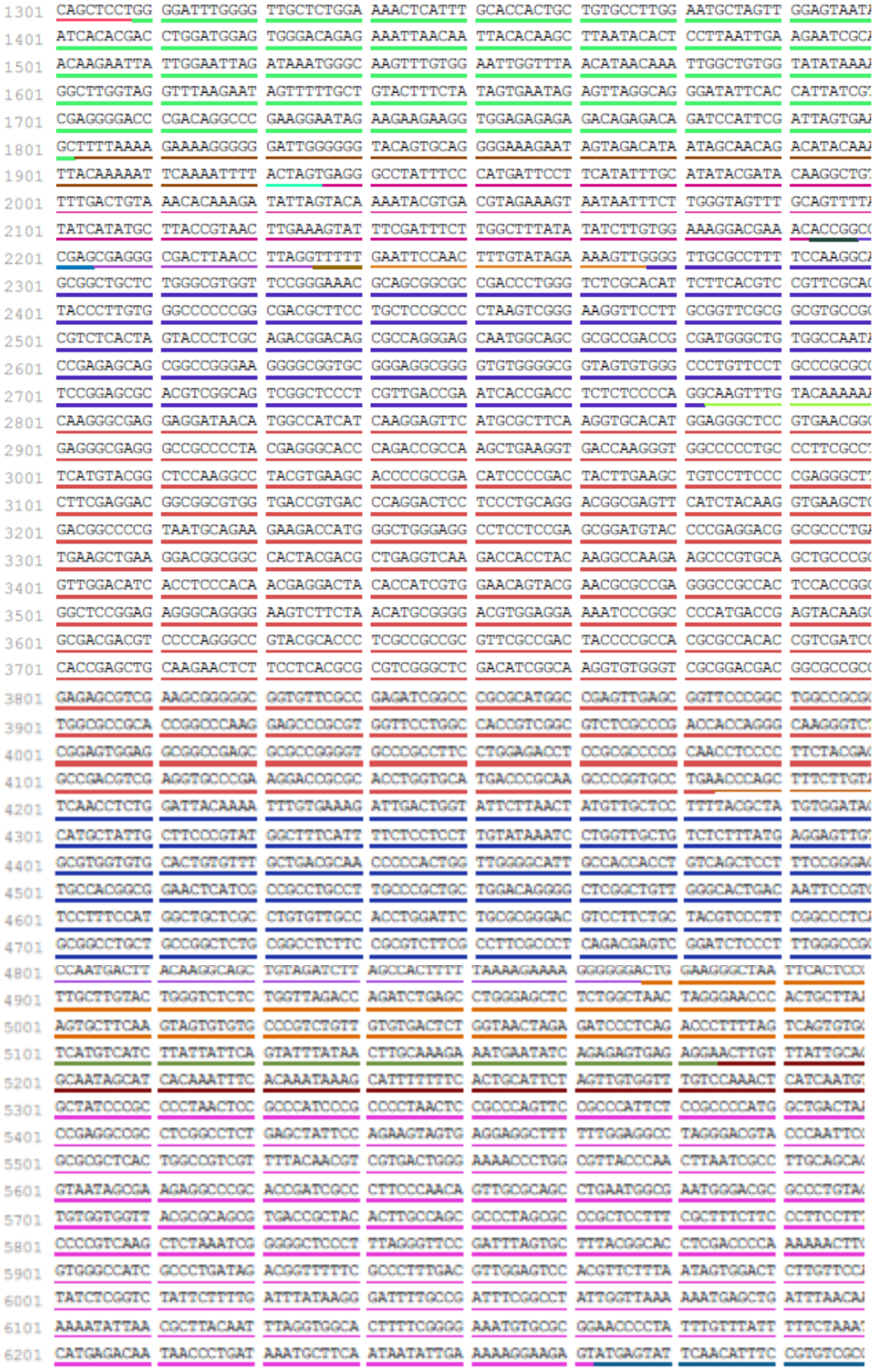

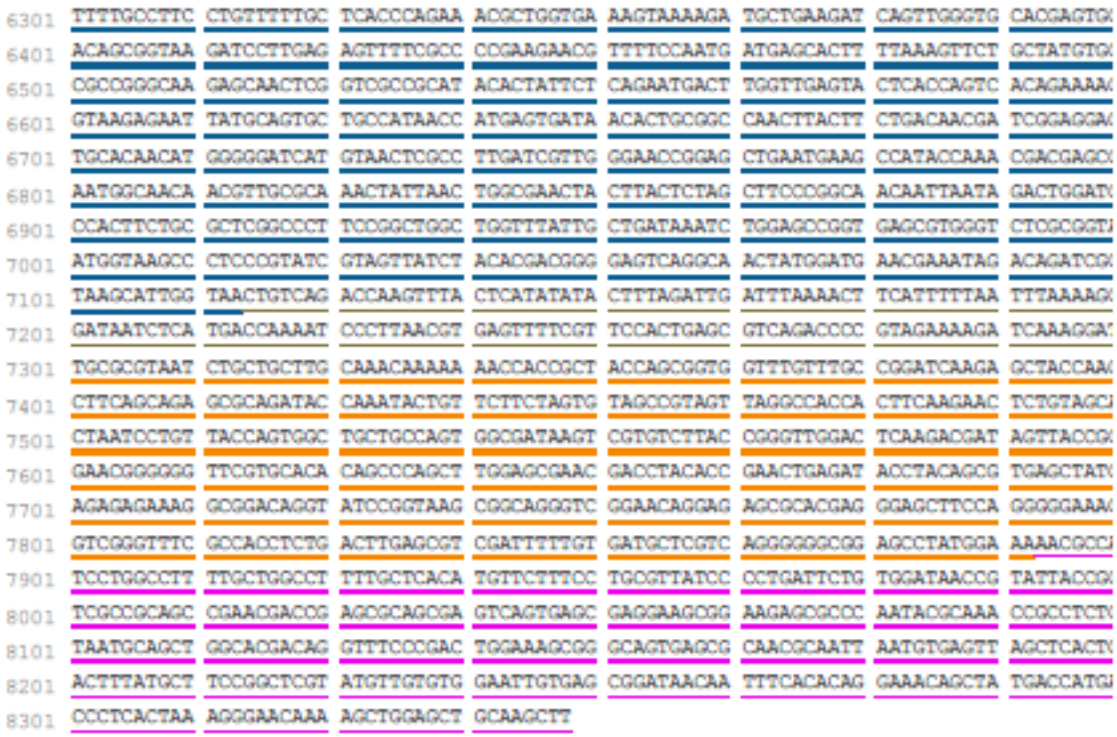

Validation by Restriction Enzyme Digestion

Restriction Enzymes	Cutting Sites	DNA Fragments (bp)
XhoI	2200	8338
ApaLI	2854, 4409, 6369, 7615	1555, 1960, 1246, 3577
ApaLI+XhoI	2200, 2854, 4409, 6369, 7615	654, 1555, 1960, 1246, 2923

10.2 Appendix 2: Vector summary for pLV[shRNA]-mCherry/Puro-U6>Scramble_shRNA

Vector Summary

Vector ID	VB151104-10082
Vector Name	pLV[shRNA]-mCherry/Puro-U6>Scramble_shRNA
Date Created (Pacific Time)	2017-05-08
Vector Size	8338 bp
Vector Type	Lentivirus shRNA knockdown vector (3rd generation)
Cloning Host	VB UltraStable (or alternative strain)

Vector Map

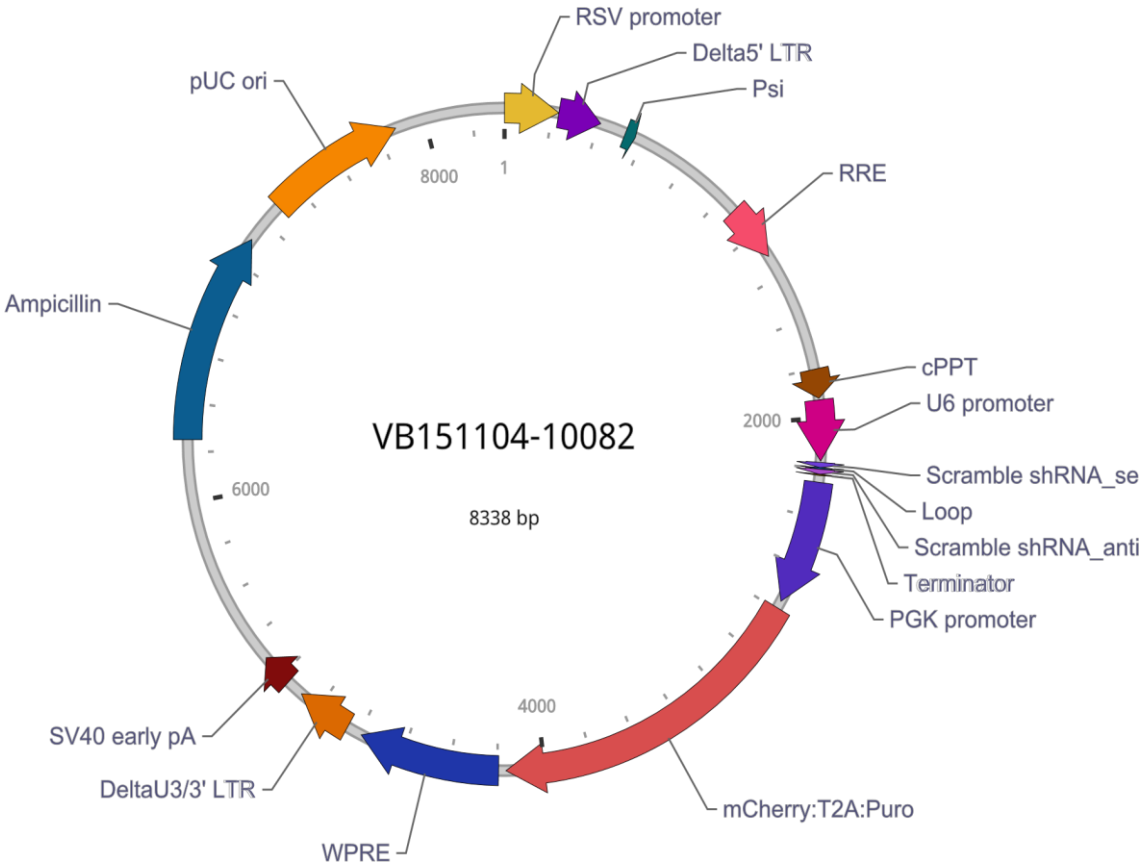

Vector Components

Name	Position	Size (bp)	Type	Description	Application notes
RSV promoter	1-229	229	promoter	Rous sarcoma virus enhancer/promoter	None
Delta5' LTR	230-410	181	LTR	Truncated HIV-1 5' long terminal repeat	None
Psi	521-565	45	misc_feature	HIV-1 packaging signal	None
RRE	1075-1308	234	misc_feature	HIV-1 Rev response element	None
cPPT	1803-1920	118	misc_feature	Central polypurine tract	None
U6 promoter	1927-2172	246	promoter	Human U6 small nuclear 1 promoter	None
Scramble shRNA_sense	2178-2198	21	sense	Component entered by user	None
Loop	2199-2204	6	loop	Loop region of shRNA	None
Scramble shRNA_antisense	2205-2225	21	antisense	Component entered by user	None
Terminator	2226-2230	5	terminator	Pol III transcription terminator	None
PGK promoter	2258-2762	505	promoter	Human phosphoglycerate kinase 1 promoter	None
mCherry:T2A:Puro	2793-4163	1371	ORF	mCherry and Puro linked by T2A	None
WPRE	4195-4792	598	misc_feature	Woodchuck hepatitis virus posttranscriptional regulatory element	None
DeltaU3/3' LTR	4858-5092	235	LTR	Truncated HIV-1 3' long terminal repeat	None
SV40 early pA	5165-5299	135	PolyA_signal	Simian virus 40 early polyadenylation signal	None
Ampicillin	6253-7113	861	ORF	Ampicillin resistance gene	None
pUC ori	7284-7872	589	rep_origin	pUC origin of replication	None

Note: Components added by user are listed in bold red text.

Vector Sequence

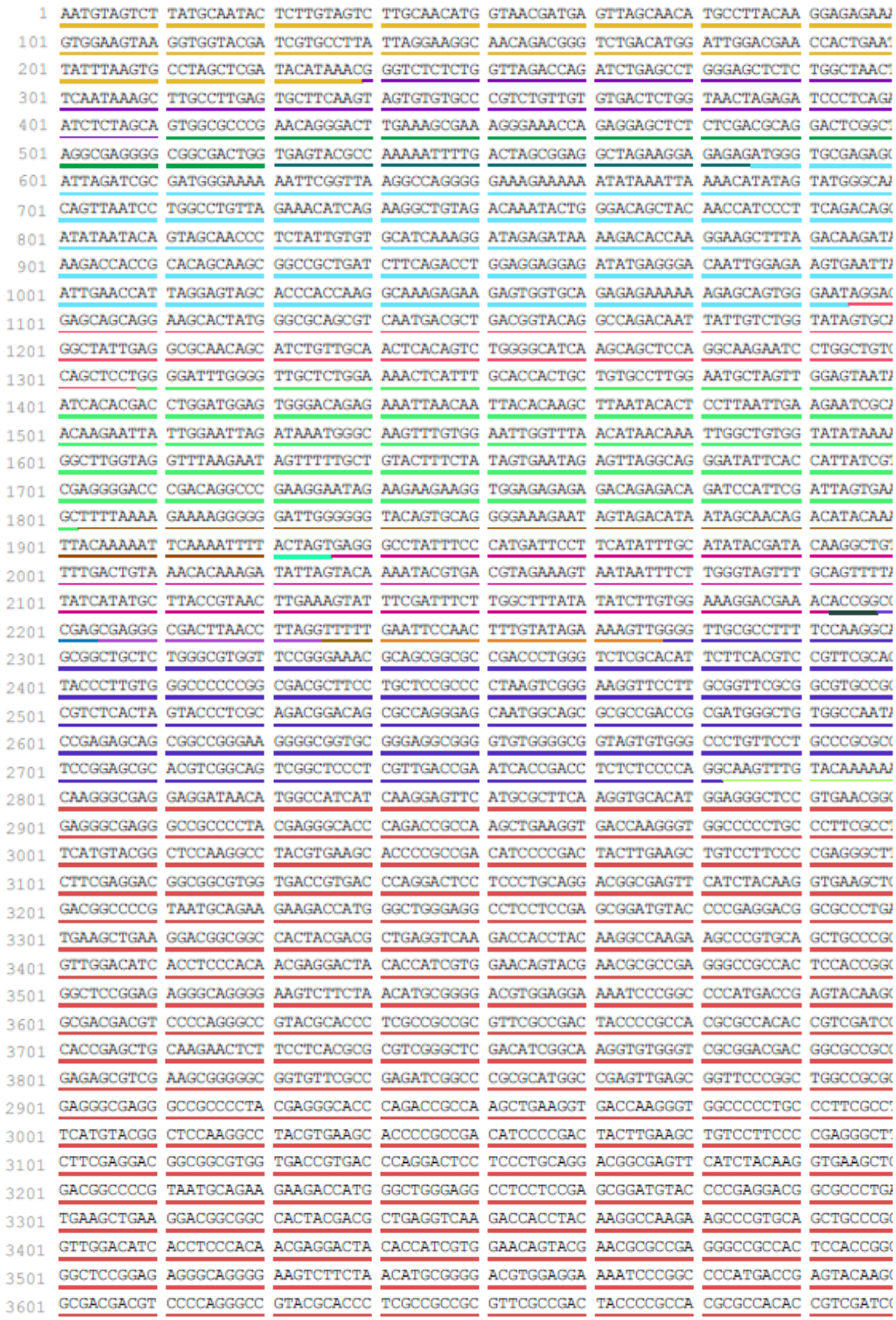

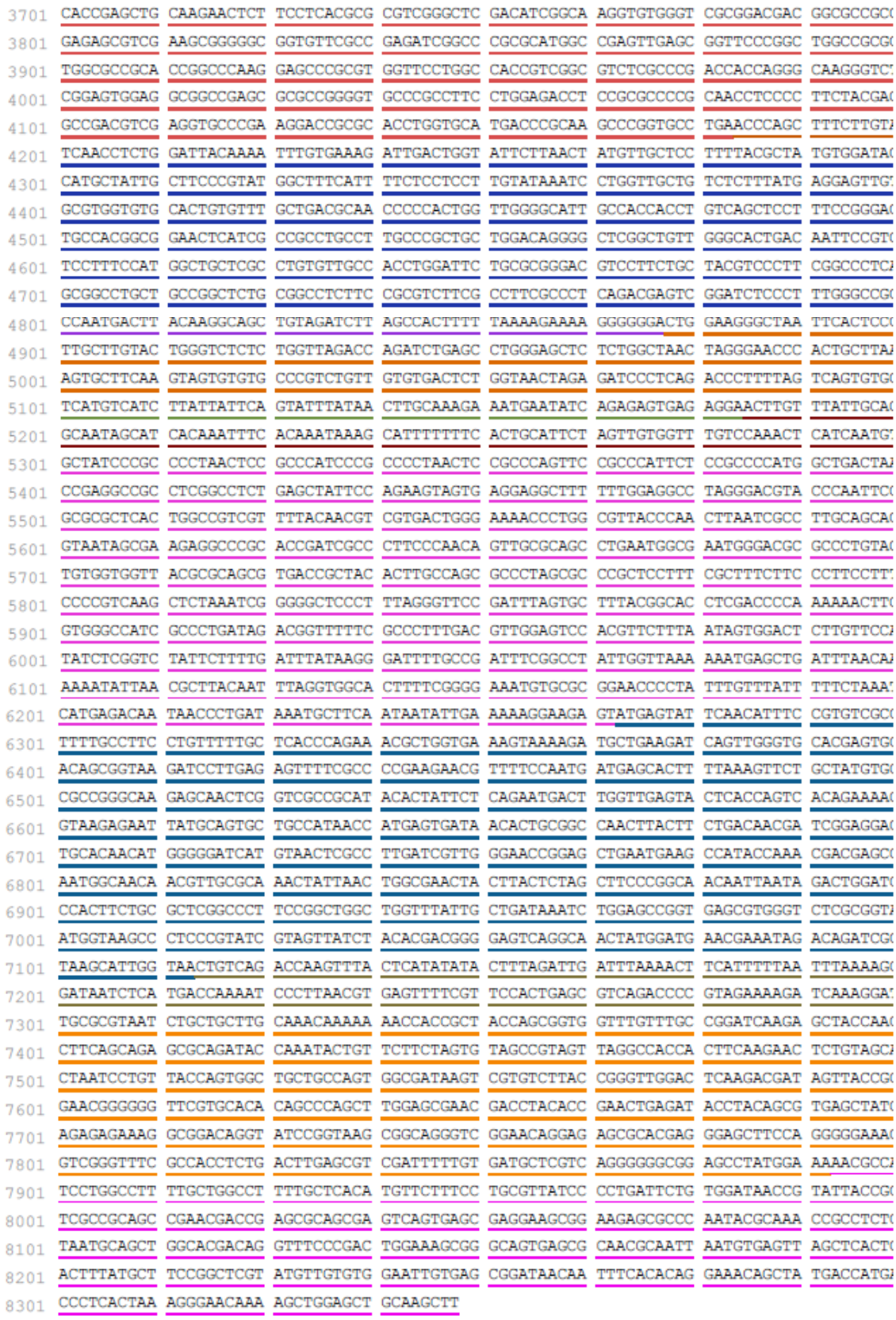
3701 CACCGAGCTG CAAGAACTCT TCCTCACGCG CGTCGGGCTC GACATCGGCA AGGTGTGGGT CGCGGACGAC GGCGCCGC
3801 GAGAGCGTCG AAGCGGGGGC GGTGTTCGCC GAGATCGGCC CGCGCATGGC CGAGTTGAGC GGTTCCCGGC TGGCCGCG
3901 TGGCGCCGCA CCGGCCCAAG GAGCCCGCGT GGTTCCTGGC CACCGTCGGC GTCTCGCCCG ACCACCAGGG CAAGGGTC
4001 CGGAGTGGAG GCGGCCGAGC GCGCCGGGGT GCCCGCCTTC CTGGAGACCT CCGCGCCCCG CAACCTCCCC TTCTACGA
4101 GCCGACGTCG AGGTGCCCGA AGGACCGCGC ACCTGGTGCA TGACCCGCAA GCCCGGTGCC TGAACCCAGC TTTCTTGT
4201 TCAACCTCTG GATTACAAAA TTTGTGAAAG ATTGACTGGT ATTCTTAACT ATGTTGCTCC TTTTACGCTA TGTGGATA
4301 CATGCTATTG CTTCCCGTAT GGCTTTCATT TTCTCCTCCT TGTATAAATC CTGGTTGCTG TCTCTTTATG AGGAGTTG
4401 GCGTGGTGTG CACTGTGTTT GCTGACGCAA CCCCCACTGG TTGGGGCATT GCCACCACCT GTCAGCTCCT TTCCGGGA
4501 TGCCACGGCG GAACTCATCG CCGCCTGCCT TGCCCGCTGC TGGACAGGGG CTCGGCTGTT GGGCACTGAC AATTCCGT
4601 TCCTTTCCAT GGCTGCTCGC CTGTGTTGCC ACCTGGATTC TGCGCGGGAC GTCCTTCTGC TACGTCCCTT CGGCCCTC
4701 GCGGCCTGCT GCCGGCTCTG CGGCCTCTTC CGCGTCTTCG CCTTCGCCCT CAGACGAGTC GGATCTCCCT TTGGGCCG
4801 CCAATGACTT ACAAGGCAGC TGTAGATCTT AGCCACTTTT TAAAAGAAAA GGGGGGACTG GAAGGGCTAA TTCACTCC
4901 TTGCTTGTAC TGGGTCTCTC TGGTTAGACC AGATCTGAGC CTGGGAGCTC TCTGGCTAAC TAGGGAACCC ACTGCTTA
5001 AGTGCTTCAA GTAGTGTGTG CCCGTCTGTT GTGTGACTCT GGTAACTAGA GATCCCTCAG ACCCTTTTAG TCAGTGTG
5101 TCATGTCATC TTATTATTCA GTATTTATAA CTTGCAAAGA AATGAATATC AGAGAGTGAG AGGAACTTGT TTATTGCA
5201 GCAATAGCAT CACAAATTTC ACAAATAAAG CATTTTTTTC ACTGCATTCT AGTTGTGGTT TGTCCAAACT CATCAATG
5301 GCTATCCCGC CCCTAACTCC GCCCATCCCG CCCCTAACTC CGCCCAGTTC CGCCCATTCT CCGCCCCATG GCTGACTA
5401 CCGAGGCCGC CTCGGCCTCT GAGCTATTCC AGAAGTAGTG AGGAGGCTTT TTTGGAGGCC TAGGGACGTA CCCAATTC
5501 GCGCGCTCAC TGGCCGTCGT TTTACAACGT CGTGACTGGG AAAACCCTGG CGTTACCCAA CTTAATCGCC TTGCAGCA
5601 GTAATAGCGA AGAGGCCCGC ACCGATCGCC CTTCCCAACA GTTGCGCAGC CTGAATGGCG AATGGGACGC GCCCTGTA
5701 TGTGGTGGTT ACGCGCAGCG TGACCGCTAC ACTTGCCAGC GCCCTAGCGC CCGCTCCTTT CGCTTTCTTC CCTTCCTT
5801 CCCCGTCAAG CTCTAAATCG GGGGCTCCCT TTAGGGTTCC GATTTAGTGC TTTACGGCAC CTCGACCCCA AAAAACTT
5901 GTGGGCCATC GCCCTGATAG ACGGTTTTTC GCCCTTTGAC GTTGGAGTCC ACGTTCTTTA ATAGTGGACT CTTGTTCC
6001 TATCTCGGTC TATTCTTTTG ATTTATAAGG GATTTTGCCG ATTTCGGCCT ATTGGTTAAA AAATGAGCTG ATTTAACA
6101 AAAATATTAA CGCTTACAAT TTAGGTGGCA CTTTTCGGGG AAATGTGCGC GGAACCCCTA TTTGTTTATT TTTCTAAA
6201 CATGAGACAA TAACCCTGAT AAATGCTTCA ATAATATTGA AAAAGGAAGA GTATGAGTAT TCAACATTTC CGTGTCGC
6301 TTTTGCCTTC CTGTTTTTGC TCACCCAGAA ACGCTGGTGA AAGTAAAAGA TGCTGAAGAT CAGTTGGGTG CACGAGTG
6401 ACAGCGGTAA GATCCTTGAG AGTTTTCGCC CCGAAGAACG TTTTCCAATG ATGAGCACTT TTAAAGTTCT GCTATGTG
6501 CGCCGGGCAA GAGCAACTCG GTCGCCGCAT ACACTATTCT CAGAATGACT TGGTTGAGTA CTCACCAGTC ACAGAAAA
6601 GTAAGAGAAT TATGCAGTGC TGCCATAACC ATGAGTGATA ACACTGCGGC CAACTTACTT CTGACAACGA TCGGAGGA
6701 TGCACAACAT GGGGGATCAT GTAACTCGCC TTGATCGTTG GGAACCGGAG CTGAATGAAG CCATACCAAA CGACGAGC
6801 AATGGCAACA ACGTTGCGCA AACTATTAAC TGGCGAACTA CTTACTCTAG CTTCCCGGCA ACAATTAATA GACTGGAT
6901 CCACTTCTGC GCTCGGCCCT TCCGGCTGGC TGGTTTATTG CTGATAAATC TGGAGCCGGT GAGCGTGGGT CTCGCGGT
7001 ATGGTAAGCC CTCCCGTATC GTAGTTATCT ACACGACGGG GAGTCAGGCA ACTATGGATG AACGAAATAG ACAGATCG
7101 TAAGCATTGG TAACTGTCAG ACCAAGTTTA CTCATATATA CTTTAGATTG ATTTAAAACT TCATTTTTAA TTTAAAAG
7201 GATAATCTCA TGACCAAAAT CCCTTAACGT GAGTTTTCGT TCCACTGAGC GTCAGACCCC GTAGAAAAGA TCAAAGGA
7301 TGCGCGTAAT CTGCTGCTTG CAAACAAAAA AACCACCGCT ACCAGCGGTG GTTTGTTTGC CGGATCAAGA GCTACCAA
7401 CTTCAGCAGA GCGCAGATAC CAAATACTGT TCTTCTAGTG TAGCCGTAGT TAGGCCACCA CTTCAAGAAC TCTGTAGC
7501 CTAATCCTGT TACCAGTGGC TGCTGCCAGT GGCGATAAGT CGTGTCTTAC CGGGTTGGAC TCAAGACGAT AGTTACCG
7601 GAACGGGGGG TTCGTGCACA CAGCCCAGCT TGGAGCGAAC GACCTACACC GAACTGAGAT ACCTACAGCG TGAGCTAT
7701 AGAGAGAAAG GCGGACAGGT ATCCGGTAAG CGGCAGGGTC GGAACAGGAG AGCGCACGAG GGAGCTTCCA GGGGGAAA
7801 GTCGGGTTTC GCCACCTCTG ACTTGAGCGT CGATTTTTGT GATGCTCGTC AGGGGGGCGG AGCCTATGGA AAAACGCC
7901 TCCTGGCCTT TTGCTGGCCT TTTGCTCACA TGTTCTTTCC TGCGTTATCC CCTGATTCTG TGGATAACCG TATTACCG
8001 TCGCCGCAGC CGAACGACCG AGCGCAGCGA GTCAGTGAGC GAGGAAGCGG AAGAGCGCCC AATACGCAAA CCGCCTCT
8101 TAATGCAGCT GGCACGACAG GTTTCCCGAC TGGAAAGCGG GCAGTGAGCG CAACGCAATT AATGTGAGTT AGCTCACT
8201 ACTTTATGCT TCCGGCTCGT ATGTTGTGTG GAATTGTGAG CGGATAACAA TTTCACACAG GAAACAGCTA TGACCATG
8301 CCCTCACTAA AGGGAACAAA AGCTGGAGCT GCAAGCTT

Validation by Restriction Enzyme Digestion

Restriction Enzymes	Cutting Sites	DNA Fragments (bp)
XhoI	2200	8338
ApaLI	2854, 4409, 6369, 7615	1555, 1960, 1246, 3577
ApaLI+XhoI	2200, 2854, 4409, 6369, 7615	654, 1555, 1960, 1246, 2923

10.3 Appendix 3: 8%, 10% and 12% acrylamide resolving gels and stacking gel recipes

	8%		10%		12%		stacking gel	
	Vol	Final Conc. (v/v)	Vol	Final Conc. (v/v)	Vol	Final Conc. (v/v)	Vol	Final Conc. (v/v)
Resolving gel buffer; 1.5M Tris-HCl pH 8.8 at room temp, 0.4% (w/v) SDS	2.5 ml	25%	2.5 ml	25%	2.5 ml	25%	-	-
Stacking gel buffer; 0.5M Tris-HCL pH 6.8 at room temp, 0.4% (w/v) SDS	-	-	-	-	-	-	1.34 ml	25%
50% (v/v) glycerol	0.65 ml	6.5%	0.65 ml	6.5%	0.65 ml	6.5%	-	
30% (w/v) APS	32 µl	0.32%	32 µl	0.32%	32 µl	0.32%	54 µl	1%
TEMED	8 µl	0.08%	8 µl	0.08%	8 µl	0.08%	7 µl	0.1%
Acrylamide; 30% (w/v) acrylamide, 0.8% (w/v) bisacylamide	2.64 ml	26.7%	3.3 ml	33.4%	3.96 ml	40%	0.63 ml	12%
Distilled H_2O	4.07 ml	41%	3.4 ml	34%	2.74 ml	28%	3.4 ml	62%

HCl; hydrochloride, SDS; sodium dodecyl sulphate, APS; ammonium persulphate, TEMED; N,N,N',N' tetramethylethylenediamine.

10.4: Appendix 4: 1%, 1.5% and 2% agarose gel recipes

Agarose gel concentration	**1%**	**1.5%**	**2%**
Agarose	1.6g	2.4g	3.2g
1x TAE buffer (40mM Tris, 20mM acetate, 1mM EDTA, pH8.6)	160ml	160ml	160ml
SYBR safe	10µl	10µl	10µl

EDTA, ethylenediamine tetraacetic acid, Tris; Tris base, acetic acid and EDTA.